Implementation of CRISPR based genetic circuits in the yeast *S. cerevisiae*

Wie alles sich zum Ganzen webt,

eins in dem andern wirkt und lebt!

Johann Wolfgang von Goethe, 1749-1832
Aus: Faust I, Vers 447 f.; Faust
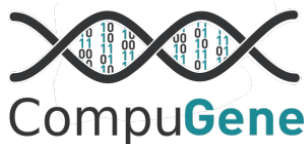
Die vorliegende Arbeit wurde unter der Leitung von Herrn Prof. Dr. Harald Kolmar am Clemens-Schöpf-Institut für Organische Chemie und Biochemie der Technischen Universität Darmstadt im Zeitraum vom Oktober 2016 bis Dezember 2019 angefertigt.

Parts of this work have been published in:

Hofmann, A., Falk, J., Prangemeier, T., Happel, D., Köber, A., Christmann, A., Koeppl, H. and Kolmar, H. (2019) A tightly regulated and adjustable CRISPR-dCas9 based AND gate in yeast, Nucleic acids research, 47, 509–520.

Index

1. Abstract

1.1. Zusammenfassung

Über die letzten Jahre wurde eine große Anzahl verschiedener Verfahren entwickelt, die eine gezielte und induzierbare Genexpression ermöglichen. Diese Systeme kommen in einer Vielzahl von Feldern zur Anwendung. Hierzu gehören unter anderem die Bereiche akademische Forschung sowie industrielle Produktion. Ein beliebter Modellorganismus ist die Bäckerhefe *Saccharomyces cerevisiae* (*S. cerevisiae*). Obwohl der Einzeller *S. cerevisiae* bereits seit vielen Jahren erfolgreich verwendet wird, besteht immer noch ein großer Bedarf an öffentlich zugänglichen und gut charakterisierten genetischen Schaltern. Besonders im Bereich der Expressionskontrolle besteht weiterer Forschungsbedarf, denn viele etablierte Systeme erlauben keine konzentrationsabhängige Induktion, sind in einem gewissen Maße toxisch für den Organismus oder weisen eine hohe basale Expression auf.

Die vorliegende Arbeit beschäftigt sich daher mit dem Design, der Implementierung und der Charakterisierung modularer Schalter in *S. cerevisiae*. Hierfür dient ein modifiziertes CRISPR/dCas9 System als Grundlage. Die dabei verwendete scaffold RNA (scRNA) ist um ein RNA-Bindemodul verlängert, welches von dem RNA-bindenden Fusionsprotein MCP-VP64 erkannt wird und nach Bindung eine Transkriptionsinitiation auslöst. Das verwendete CRISPR/dCas9 ermöglicht also die modulare Expressionskontrolle der drei Komponenten dCas9, MCP-VP64 und scRNA. Ziel dieser Arbeit war es, alle drei CRISPR/dCas9 Komponenten unabhängig voneinander induzieren zu können und im Anschluss die einzelnen Komponenten zu einem UND-Gatter zu kombinieren.

Um einen ersten Schalter zu generieren, wurde die Expression des dCAS9-Proteins unter Kontrolle des *GAL* Promotors gebracht, was zu einer Galactose-abhängigen Induktion der Expression des fluoreszierenden Reporterproteins Venus führte. Der Galactose-Schalter ermöglichte hohe Expressionsraten, was jedoch auch eine verhältnismäßig hohe basale Expression mit sich brachte. Daher wurde ein funktionelles logisches UND-Gatter entworfen, bei dem MCP-VP64 unter die Kontrolle von β-Estradiol (ES) gebracht wurde. Nur bei Anwesenheit beider Induktoren wurde eine Expression des Reportergens gemessen. Dies zeigt, dass ein streng reguliertes, sowie konzentrationsabhängiges UND-Gatter entwickelt wurde. Zusätzlich zu Venus als Reportergen wurde ein zweites Reporter-Konstrukt zur regulierten Expression von Proteinen mit biotechnologischer Relevanz evaluiert. Hierfür wurde das Zielgen durch ein so genanntes T2A Peptid mit dem Fluorophor tGFP verbunden, wodurch die Expression beider Gene in einem mRNA Transkript, sowie die direkte Detektion der Expression ermöglicht wurde. Um die Möglichkeiten der Toolbox zu erweitern, wurde zusätzlich ein positiver Feedback Mechanismus untersucht.

Das verwendete System wurde außerdem um eine induzierbare scRNA erweitert. Hierfür wurde ein Ribozym-scRNA-Ribozym Konstrukt implementiert und sowohl mit einem konstitutiven als auch mit dem ES-induzierbaren Promotor getestet. Alle verwendeten Schalter und Gatter wurden auf ihr Expressionslevel, ihre basale Expression und Konzentrationsabhängigkeit getestet. Um ein besseres Verständnis der zugrunde liegenden Prinzipien und der Funktionsweise des UND-Gatter Designs zu erhalten, wurden die experimentellen Ergebnisse durch die Entwicklung eines mathematischen Modells und einer Einzelzellanalyse erweitert. Mit dieser Arbeit wurde ein vorhersehbares, modulares und vielseitig einsetzbares Expressionskontrollsystem entwickelt.

1.2. Abstract

Many different routes for targeted gene expression are available and with the help of Synthetic Biology (SynBio), more and more controlled expression systems are developed every year aimed at robustly and precisely switching one or more genes on and off (1). Targeted repression and expression are essential for basic research, as well as for many industrial applications. In this context the unicellular eukaryote *S. cerevisiae* is one of the oldest and most commonly used hosts (2,3). Despite the fact, that *S. cerevisiae* has been investigated extensively for many years, researchers are still lacking easy-to-implement and well-organized toolboxes (3). In addition, many frequently used regulatory systems influence the viability of the host cell, show high basal expression or enable only the overexpression of the target gene without the possibility of fine regulation (4).

Within this work, a modular system for targeted gene expression was designed, implemented and extensively characterized to overcome these limitations. Additionally, it was aimed to contribute to and therefore improve the already existing publicly available yeast toolbox. A scaffold RNA (scRNA) CRISPR/dCas9 system served as a modular expression platform (5). This is based on three components namely dCas9, the RNA-binding protein MCP fused to the transcriptional activation domain VP64 and a scRNA encoding the desired locus and action. A scRNA specifically targeting a *tet*O binding sequence was used, resulting in Venus reporter gene expression. The functionality of the reporter gene setup was demonstrated by the expression of the reporter gene Venus.

A natural switch was integrated based on the well-established Gal10 expression cassette by implementation of a *GAL* promoter in front of dCas9. High expression levels were achieved, but comparatively high basal expression was observed. Hence, a second switch based on the synthetic LexA-ER-AD heterologous transcription factor was added. A functional AND gate was achieved by implementing four β-estradiol (ES) inducible *lexA* boxes in front of MCP-VP64. The AND gate was demonstrated to achieve high expression rates in presence of galactose and ES

while being tightly regulated in their absence. Additionally, a reporter gene setup was implemented combining a gene of interest (GOI) with the fluorophore tGFP by the ribosomal skipping T2A sequence. This setup allows to adapt the system to any gene of interest without losing reporter function. To extend the possibilities for applications, a positive feedback loop was designed and verified as functional.

The modularity of the system was demonstrated by the construction of a second AND gate, in which the scRNA was placed under the control of ES. For this purpose, a ribozyme-scRNA-ribozyme construct was introduced and its functionality verified for both, a constitutive promoter and an ES inducible promoter. The established switches and AND gates were characterized in detail for their expression levels, basal activity and their dose-dependency. A better understanding of the underlying principles and the functioning of the AND gate design was achieved by backing up of the experimental findings with the development of a mathematical model and single-cell analysis. In summary, a predictable and modular, as well as versatile expression control system was developed.

2. Introduction

2.1. Synthetic biology

Synthetic biology (SynBio) is an interdisciplinary approach combining both the investigative nature of biology and the constructive nature of engineering in order to protect and expand our planets habitability and resources (1,6,7). The term synthetic biology was first introduced by the French chemist Stéphane Leduc in 1912 (8,9). The field of recombinant DNA technologies and genetic engineering, which emerged in the 1970s, is considered as the logical precursor of SynBio (10). In the 1980s synthetic human insulin was the first commercially available health care product manufactured by recombinant DNA technology. Due to the high demand for human insulin, a cost-intense biotechnological process of cloning, expression and up-scaling was started by a collaboration of multiple companies (10–12). Conventional genetic engineering focuses on approaches to solve complex problems by concentrating only on one or few genes. SynBio instead aims for a more comprehensive solution, combining adapted existing cellular architectures with novel systems build from ground up (7). Thus, when SynBio launched in the early 2000s, one of the main advantages had been the possibility to enable the overarching theoretical and practical construction of organisms solving various problems in multiple disciplines. These organisms cover a brought range, such as bacteria cleaning hazardous waste in inaccessible places (13), plants that are able to detect and report chemicals due to a de-greening circuit (14), algae that produce biofuel in an efficient and sustainable fashion (15) and human cell lines recognizing and fighting specific diseases like cancer (16).

During the so-called "first wave of SynBio" researchers focused on creating and perfecting basic genetic elements like promoters or repressors, which improved the understanding of biological processes and allowed to establish first principles for the design of small modules. As a result, multiple well characterized small modules could be combined to build up a toolbox for targeted genetic engineering in order to regulate gene expression or to tune biomolecules or biosynthetic mechanisms (7,17). The resulting toolbox includes, among others simple switches, pulse generators and oscillators (7,18,19). It has been shown, that, in order to achieve a certain goal, the manipulation of both well-established and novel elements is still troublesome. Hence, the duty of the ongoing "second wave of SynBio" is not only to effectively assemble elements and modules into functional, customizable large-scale systems, but also to formulate new and effective bioengineering design principles (7,17,20). To achieve this goal, the approaches of genetic engineering have to be combined with the basic principles of chemistry, biology, mathematics, biophysics and many more. Especially important is the implementation of computational engineering and mathematical models, which play a key role in industrial up-scaling. Before SynBio, bio-derived materials, like the polysaccharide cellulose, could only be produced in small scales, with yields sufficient for research purposes. Due to SynBio nowadays

the large-scale production of cellulose in bacteria is possible, which allowed multiple applications in the field of optoelectronics, medicine and others (1,17,21,22). Only this holistic approach allows scientists to think big, to really understand the underlying biological principles and to design and implement whole functioning systems (10,20,23).

In order to optimize production of bio-derived materials, choosing an appropriate host is of utmost importance. Prokaryotes as *Escherichia coli* (*E. coli*) are the best understood hosts, due to their easy excess and handling, as well as for the long history of research (10,20,24). Besides prokaryotes, yeast strains like *Saccharomyces cerevisiae* (*S. cerevisiae*) or *Yarrowia lipolytica* and mammalian cell lines like Chinese hamster ovary cells (CHO) have been established for industrial production of pharmaceuticals or other bio-derived materials (16,25–27). In order to enhance productivity, the nature of SynBio allows to also take advantage of less traditional hosts showing promising characteristics. For example, an extremophilic *Halomonas* strain, which can be cultivated under high osmotic pressure and pH, was engineered to produce microbial polyesters in saltwater only by using an open fermenter without the need of further ingredients, which leads to a significant reduction of production costs (1,17,28).

Nowadays SynBio is expanding as part of the fourth industrial revolution, generating novel and sustainable innovations in the fields of agriculture, healthcare and environmental issues (1,29). Even though SynBio will have a decisive influence on our future, there are some basic problems that have to be addressed:

- many of the utilized systems are not fully understood, which makes the targeted manipulation more challenging
- biological systems always produce a certain amount of noise, which has to be especially taken into account for models
- most synthetic systems have been studied in a laboratory setup, but might have a severe impact in a living organism or a wider ecological system (7)

Nevertheless, it is expected, that the impact of SynBio will further increase and that its only limitation will be the imagination of researchers and the acceptance by the society. After all, science, politics and industry have to openly calculate risks and benefits to build up a culture of trust, so that society will get a better understanding of the advantages achievable through SynBio (1,7,30).

2.1.1. *Saccharomyces cerevisiae* as a model organism for synthetic biology

The decision for a host is a crucial step for both, scientific research and biotechnological production of bio-derived materials. The baker yeast *S. cerevisiae* is the most intensely studied unicellular eukaryote and one of the oldest and most frequently used microorganisms in biotechnological applications. *S. cerevisiae* has been successfully used for the production of fine and bulk chemicals like ethanol, butanol or lactic acid (2,3) and it is especially valuable as a cell factory, due to the properties of:

- fast growth on cheap media containing only a carbon source, vitamins and salt
- tools for genetic manipulations are well-developed and -established
- robustness in large-scale set ups
- growth at low pH is possible, which reduces the risk of bacterial contaminations

Additionally, there is a large genetic knock-out collection available and new mutants can be generated and analyzed in a straightforward approach (31,32).

At the moment one of the biggest disadvantages of *S. cerevisiae* as a production host is its disability to grow on alternative carbon sources like arabinose or xylose. However, genetic engineering may easily solve this issue. Even more problematic is the fact, that even though over a hundred synthesis routed for chemicals were genetically integrated into yeast successfully, only a few reached commercial-scale productions. Though metabolic engineering had already been established in the 1990s, the engineering of product strains is still disproportionately time and resource consuming (33,34). Thus, for biotechnological applications the integrative usage of metabolic engineering and SynBio is a really promising approach, which has already led to (35,36) and will lead to more efficient ways of product-strain construction in the future (2). The synergy consists of metabolic engineering, which defines the direction of manipulation, and SynBio, which provides the tools to establish these tasks. Even though SynBio is still in its infancy, many technical challenges were solved, like the ever-decreasing costs in DNA-sequencing and synthesis allowing in-depth knowledge about the genome of a manipulated host, as well as the *de novo* synthesis of whole modules. At the same time the standardization of DNA assembly and the generation of well-characterized elements and modules is expected to lead the way for industrial plug-and-play strains, which can be easily modified towards the high-level production of a desired product (2,3,33,37).

The potential to build up a powerful host from *S. cerevisiae* and SynBio tools has been demonstrated not only by basic research, namely the *de novo* synthesis of a complete chromosome (38), but also by application-oriented engineering, which successfully manufactured the complex pathway of vanillin (3,39). For a true benefit in the long run, both academia and industry have to communicate openly about general bioprocess bottlenecks,

about basic growth and cultivation conditions, as well as about the tools and hosts that are actually required (2). Therefore, the established method of "rational engineering" may be complemented or even replaced by the cost-effective and more rational method of "predictable engineering" (see Figure 1).
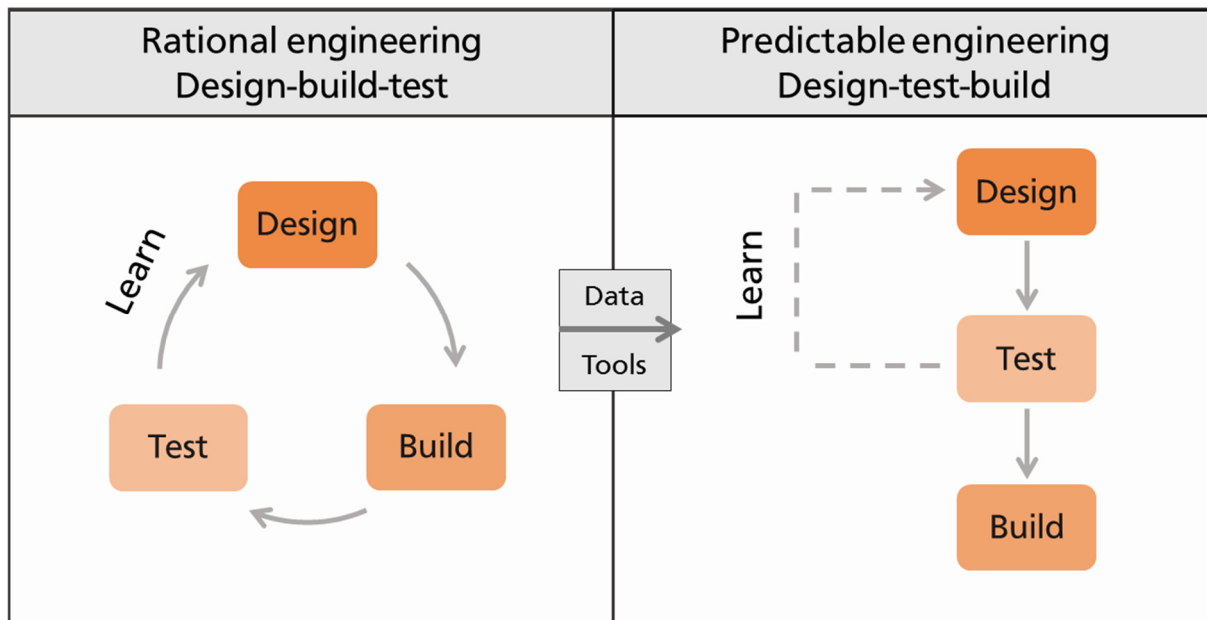
Figure 1 Schematic representation of models for genetic engineering.

Transformation of a trial-and-error design-test-build circle to a predictable design-test-build workflow by using high-throughput screens and multidimensional data analysis. (Figure adapted after (2))

First an iterative design-build-test cycle is used (34), where one or multiple cell-factory variants are designed, built and screened using high-throughput methods. The most promising candidates are characterized in detail und used for another circle of design and building. In order to achieve a new generation of cell factories, the obtained knowledge from the design-build-test cycle is used to start a computer-aided approach leading to the design-test-build workflow. Hopefully, the usage of the design-test-build workflow causes a significant decrease of the efforts and resources of development (2,33,40,41).

2.2. Multiple switches established in the yeast *Saccharomyces cerevisiae*

Despite the great popularity of *S. cerevisiae*, research and applications are still lagging behind other organisms. Especially in comparison to the omnipresent host *E. coli.*, the collection of well characterized biological parts and the standardized assembling methods as part of a toolbox in *S. cerevisiae* are still limited (3).

Nevertheless, there is a wide and constantly increasing platform of resources and literature about the available elements for *S. cerevisiae*. Just recently Lee *et al.* published one of the first

well characterized publicly available toolboxes for *S. cerevisiae* (42). Since most regulations take place on the transcriptional level, the choice of the right promoter(s) is particularly important for the design of every system or pathway (43). Most endogenous yeast promoters respond to the concentration or type of a carbon source. Regulation systems based on the induction of these natural promotors, like the *Gal1* promotor, inducible by galactose, influence cell growth and depend on host cell genes for correct performance (2.2.1). Other inducible systems, like the copper sensitive *CUP1* promotor or the tetON and tetOFF system, which are inducible by the antibiotic tetracycline (2.2.2), are even toxic to the host (44,45).

To overcome these limitations of natural transcription factors (nTF), heterologous transcription factors (hTF) consisting of a DNA-binding domain, an activation domain (AD) and a regulatory domain have been implemented (2.2.3). Such transcription factors should theoretically not influence the host metabolism and generally allow the inducible and concentration-dependent activation of transcription. For example, a heterologous transcription factor based on the estrogenic hormone ß-estradiol (ES) combined with a transcription activator like VP16, an activation domain of the Herpes simplex virus, already showed promising results (45–48).

2.2.1. Switches based on the carbon source

To express a desired protein, one can choose between inducible or constitutive promoters. Constitutive induction leads to high product yields, which is not always desirable; for example, in cases where the product has a toxic effect on the host. Hence, the majority of promoters used for protein expression in yeast are inducible promoters, sensitive to environmental conditions, such as stress or ion concentration inside the cells (49,50). In yeast, the best understood and most intensely used set of controllable promoters depends on a certain carbon source, where the carbon source either leads to a repression or induction of target gene expression. The main advantage of the carbon-source-dependent promoters is to allow growth before the initiation of a potentially burdening expression phase (43). Depending on factors like the available carbon source, the amount of glucose in the growth media and the promoter itself, there are different pathways of induction and repression.

Since glucose is the favored carbon- and energy-source of *S. cerevisiae*, it plays a key role in the repression and derepression of certain genes. To be precise, glucose interacts in a repressing way with genes involved in the oxidative metabolism, in the usage of alternative carbon sources, in the gluconeogenesis or the tricarboxylic acid cycle (51,52). This interaction either leads to a decrease in transcription or translation on the gene level or to enhanced protein degradation on protein level, while mainly relying on the protein kinase Snf1 (53,54). Only after glucose is depleted, Snf1 builds a specific complex, which enters the nucleus to initiate derepression (54).

Another set of promoters is derepressed by carbon source depletion. Hence, these promoters get induced at low glucose levels. A considerable disadvantage of these promoters is the lack of a proper induction for activity. Nevertheless, this ability is also a substantial advantage when used for biotechnological application, where the expression of the protein of interest does only start after cell growth, when the carbon source is typically depleted. So, the gene expression can *de facto* be regulated or even be called inducible in highly monitored environments like fed-batches – at least to a certain degree (43). The Adh2 promoter is a popular promoter controlling the alcohol dehydrogenase II. This strong promoter is strictly repressed by glucose and only derepressed when glucose is depleted, which causes the cells to switch to ethanol growth (55). Another class of carbon dependent promoter is the carbohydrate-inducible one. The best characterized and most used carbon-inducible promoters are controlling the *Gal* genes, where galactose is acting as the main inducer (Figure 2A). In the presence of glucose these promoters are strongly regulated by cis-acting elements (Figure 2B) (56). In *S. cerevisiae*, the P_{GAL1} and P_{GAL10} are widely used for recombinant protein production. The best results for galactose-induced protein production can be expected if a low glucose level is maintained. However, it should be noted that due to the nature of the glucose/galactose pathway, a certain leakiness must be expected (57).

2.2.2. Switches based on tetracyclines - the Tet-On and Tet-Off approach

During the last two decades, scientists were searching for systems, allowing stringent and inducible transcription control of a gene of interest (GOI), especially in complex genetic environments such as mammalian cells (58). A first attempt was started to control gene expression by endogenous eukaryotic promoters, which can be induced for example by heat shock. This attempt was insufficient since it suffered from a broad range of secondary effects like the pleiotropic effect of elevated temperatures (59). Hence, scientists embarked on the search for non-endogenous systems. The already relatively well characterized bacterial regulatory elements seemed to deliver promising elements to start with. One of the first elements tested for its functionality in eukaryotic cells was the bacterial *lac* system (originally from *E. coli*), which is inducible by isopropyl β-d-1-thiogalactopyranoside (IPTG) (60,61). IPTG has been proven to be rapidly taken up and intracellularly stable, nevertheless, it showed a rather slow and ineffective transcriptional regulation, leading to low induction levels (58,62). In contrast, the *tet* system, based on the Tn*10*-specified tetracycline-resistance operon of *E. coli*, has proven to be functional in different eukaryotic organism such as yeast or mammalian cells. The success of the *tet* system is based on a rapid uptake of the inducer tetracycline (or derivates) and a corresponding rapid induction of target gene expression (58,63).
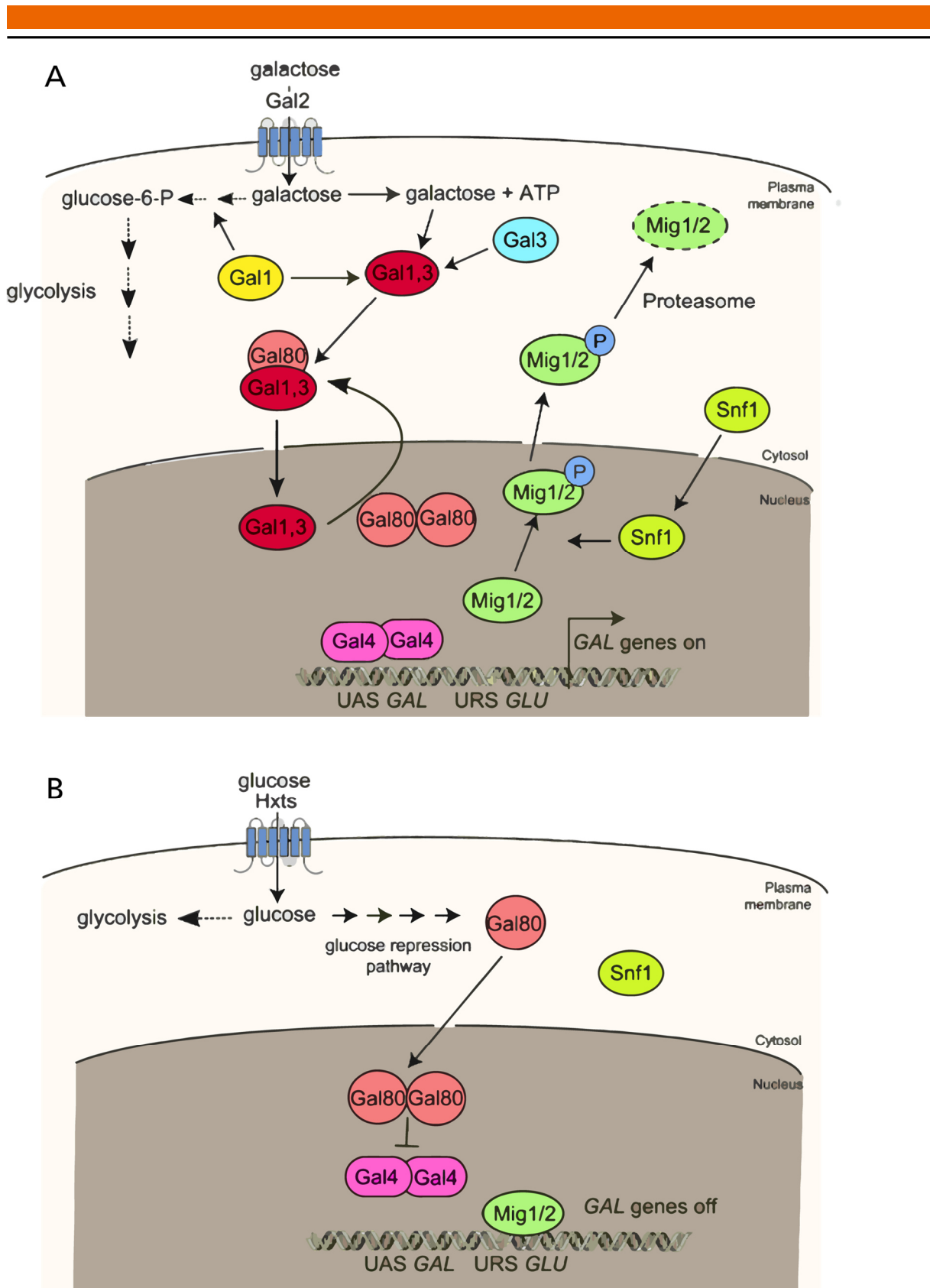
Figure 2 Reaction of the *GAL* genes to glucose and galactose.

(A) In the absence of glucose and the presence of galactose a complex pathway leads to the induction of the *Gal* genes. (B) In contrast, in the presence of glucose the *Gal* gene expression is repressed independently from the absence or presence of galactose. (Figure adapted after (54))

Originally the *tet* system serves Gram-negative bacteria as a defense mechanism against tetracyclines (tc) mediated by the resistance gene *tetA*. TetA is a tetracycline/metal-proton antiporter located in the cytoplasmic membrane (64). When overexpressed, TetA is lethal for its host (65), hence the *tetA* genes are strictly regulated on the transcriptional level by the tc-responsive Tet repressor (TetR). The genes for TetA and TetR are oriented with divergent polarity around a regulatory region with overlapping promoters and operons called *tet* operator (*tet*O) (66). In the absence of tc, TetR dimers bind to the operators *tet*O$_1$ and *tet*O$_2$ silencing the genes *tetA* and *tetR*. As soon as tc enters the cell, it binds TetR with high affinity; about nine orders of magnitudes higher than the binding affinity to *tet*O (67,68). A conformational change of TetR leads to the dissociation from *tet*O (67,69), which in turn leads to a burst-like expression of TetA and TetR followed by a rapid reduction of free tc in the cytoplasm. The lack of tc then leads to the shutdown of the expression of *tetA* and *tetR* (70). During the presence of tc, the expression of TetA is fine-tuned, so the tc-concentration in the media cannot reach a level where it slows down or even stops translation. To start the whole process, only nanomolar concentrations of tc are necessary, especially since tc efficiently penetrates most cell types (66,71).

For the control of gene expression at first a relatively simple tet system was utilized. Therefore, the so-called tetracycline response element (TRE), consisting of 7 repeats of the 19 nucleotide *tet*O$_2$ sequence separated by a 41 bp spacer, is placed upstream of a minimal promoter and a GOI. Additionally, *tetR* is expressed from a strong constitutive promoter. In the absence of tc, TetR binds to *tet*O and gene expression is silenced by sterical interference. When tc is added to the media, TetR will bind tc instead of *tet*O and therefore gene transcription is permitted (72,73).

In 1992, Gossen and Bujard established an improved *tet* expression system, where they fused TetR with the *C*-terminal domain of VP16. This tetracycline-controlled transactivator (tTA) binds to the TRE in the absence of tc, and the activation domain VP16 initiates gene expression. As soon as tc is added, it binds to tTA with high affinity. The tTA complex is removed from the activation site, which leads to a delayed decrease of gene expression (58,74). This tTA-dependent system is also called the Tet-Off system (Figure 3A).

For more precise control of the expression time and to prevent prolonged exposure of the targeted organisms to tc, a reverse Tet-On system has been established. Random mutagenisis was used to identify a TetR-variant showing a reversed phenotype. This reverse TetR (rTetR) only binds to DNA in the presence of tetracycline. Hence, after rTetR was fused to the activation domain VP16 to build the reverse tetracycline-controlled transactivator (rtTA), the GOI behind a TRE is only expressed in the presence of tc and expression decreases in its absence (69,74,75) (Figure 3B).
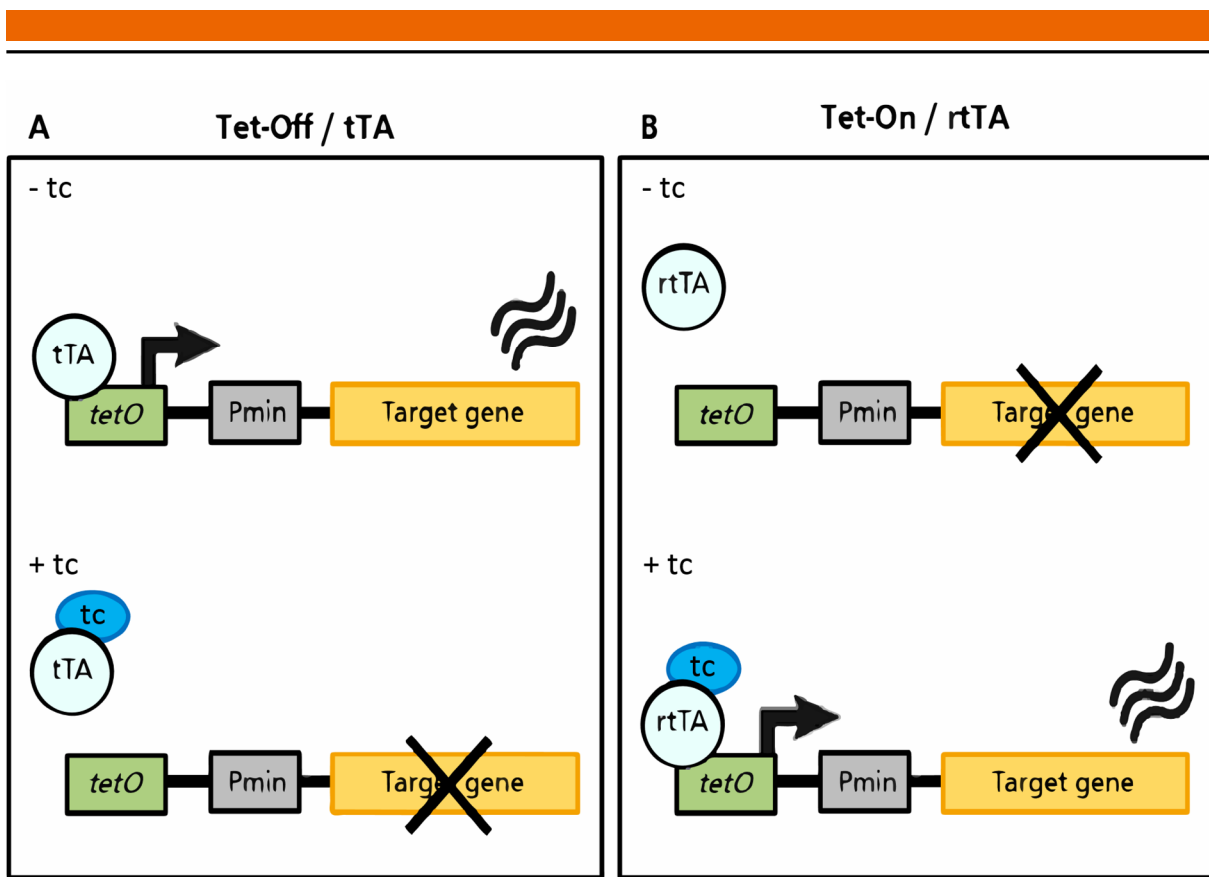
Figure 3 Regulation of gene expression by the tet regulators tTA and rtTA.

The *tet*O binding region is shown in green boxes, the minimal promotor in grey and the target gene in yellow. The transregulators rTA and rtTA are shown in light blue circles and dox in a bright blue one. Target gene expression is displayed by an arrow and waves, silenced transcriptions as a X. (Figure adapted after (73))

Interestingly tTA and rtTA have shown a different sensitivity to tetracycline and its derivates. Doxycycline (dox) is the most widely used derivative, on account of a high affinity to both systems, a good tissue distribution, low toxicity, a half life of 24 h and low cost. Additionally, in 2015 it was shown, that dox has no effect on the global gene expression of *S. cerevisiae* (76). Over the years, many different tc-dependent systems have been invented, showing less background expression, a higher affinity to dox or enhanced transcriptional activity (77,78). Hence, the *tet* system is one of the most widely used routes for regulated gene expression in many different organisms. Both Tet-On and Tet-Off are well characterized and have proven themselves to be functional in *S. cerevisiae* (73,79,80).

2.2.3. Hormonal switches for tightly regulated gene expression

One of the major advantages of TetR-based systems is their high binding constant of TetR to tc ($K_a \sim 10^9$ M^{-1} (68), in comparison for IPTG, which is commonly used for induction of the lac operator in *E. coli* ($K_a \sim 10^6$ M^{-1} (81)). Hence, low tc-concentrations are necessary for induction or repression of gene expression. The Tet-On system shows substantial basal activity, which is why the Tet-Off system is still preferred. However, the main disadvantages of the Tet-Off system

are the need to constantly add tc and that after removal of tc the system relies on protein dilution and degradation to reduce target protein levels (46,79).

To overcome those limitations, heterologous gene expression controls based on steroid hormones were invented. Steroid hormone receptors are (partially) highly conserved intracellular receptors, which, upon steroid binding, activate or repress the transcription of specific genes (82,83). Naturally occurring steroid hormone receptors regulate gene expression due to four main reactions:

- specific binding to the corresponding response elements
- formation of stable complexes at the response elements
- allosteric receptor activation due to the corresponding ligand
- initiation of target gene expression due to the recruitment of TF and RNA polymerases

Additionally, for some receptors, like the estrogen receptor, the binding to heat shock proteins like hp90 plays a key role. Unoccupied receptors are thought to bind with cellular heat shock proteins to form a complex that is unable to bind DNA. Addition of the ligand leads to the dissociation of the heat shock proteins, which restores the DNA binding ability and allows target gene expression (83,84) . It can be assumed that the steroid binding domain has the ability to function as an autonomous regulator, which makes them a valuable tool to build novel transcription factors.

In the 80s and 90s of the last century, the combination of a steroid binding domain with an activation domain to an chimeric TF (cTF) has proven to successfully allow hormone induced target gene expression in vertebrate cells (47,85). Since several steroid receptors from vertebrates have shown to be functional in yeast as well (86), Louvion *et al.* implemented 1993 a first steroid hormone dependent regulator in *S. cerevisiae* cells. They fused the steroid binding domain of the human estrogen receptor (ER) to the DNA binding domain (dbd) of Gal4 and the activation domain (AD) VP16. This first cTF based on the inducer ES allowed the hormone-inducible expression of target genes under the control of the *GAL1-10* promoters in yeast (47). Among others, McIsaac *et al.* established a tightly controlled and well characterized gene expression strategy based on the Gal4 dbd, ER and the AD VP16 (46,68,87). The resulting cTF GEV allows a graduated and rapid induction within minutes after addition of ES (Figure 4). It reduces target gene expression in the absence of ES to near background activity and only affects a few genes unintentionally (46).
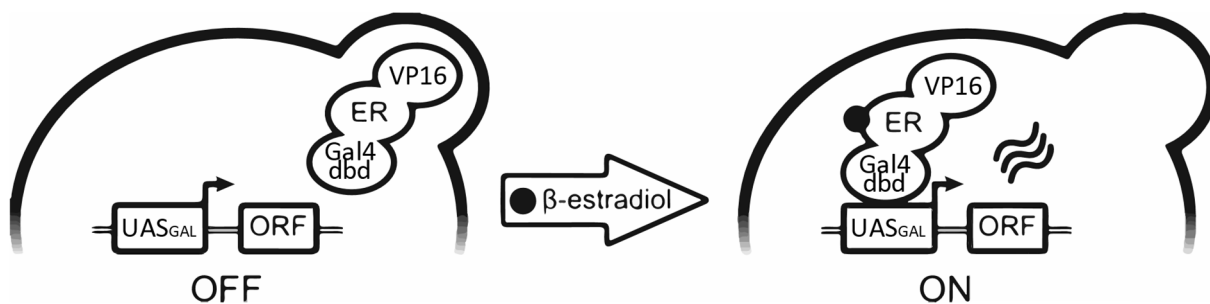
Figure 4 The mechanism of activation of the GEV system.

ORF: open reading frame, Gal4 dbd: Gal4 DNA binding domain, ER: hormone-binding domain of the human estrogen receptor. (Figure adapted after (45))

Even though GEV provides significant advantages like tight regulation over the standard Gal4-based TF, there are still multiple limitations. Since GEV is based on the Gal4 dbd, it binds to the endogenous *GAL* promoter and therefore influences the host cell metabolism and strongly limits the growth in galactose-containing media. Additionally, the system is toxic after induction with ES (45,46). Hence, Ottoz *et al.* devised a gene expression strategy, that does not rely on the Gal4 dbd, but on the bacterial DNA-binding domain of LexA and is therefore assumed to not influence the host organism (45).

2.2.4. A heterologous transcription factor allows regulated gene expression without influencing the host organism

LexA (1-202 aa) is a repressor in *E. coli*, repressing many genes in a phage repressor like manner. The LexA binding region (1-87 aa) binds specifically to the *lexA* operator (*lexA*) as a dimer (88,89). When the cellular DNA is damaged, the LexA hinge region is cleaved and the dimerization is prevented, which results in the loss of operator binding. This leads to the activation of LexA-repressed genes (90). In 1984 Brent and Ptashne demonstrated, that LexA is able to repress a gene, when *lexA* is inserted between the UAS$_G$ of a *Gal1* promoter and the transcription start (88). Building on the assumption, that LexA is able to enter the nucleus and bind to *lexA*, Ma and Ptashne built a first cTF out of LexA and the Gal4 dbd, which was able to induce target gene expression (91). Since the LexA-*lexA* combination serves as an inducer that does not contain yeast analogues (91), it is ideally suited for the combination to a hTF.

A hTF should not interfere with the host's physiology and is defined as a fusion of protein domains from other organisms, consisting of a DNA-binding domain, a regulatory domain and an activation domain (45,92). In Ottoz *et al.* such a hTF was constructed by genetically fusing the bacterial dpd LexA (1-202 aa) (92), the hormone-binding domain of the human estrogen receptor as regulatory domain (47) and different ADs. They used the Gal4 AD (93), the VP16 AD (48) and B42 and B112, two short unstructured acidic peptides originally encoded by DNA fragments of *E. coli* (91,92).
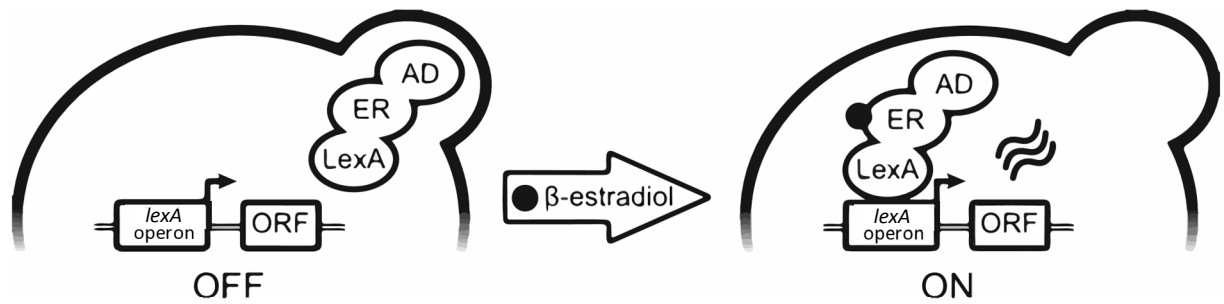
Figure 5 The mechanism of activation of the LexA-ER-AD system.

ORF: open reading frame, ER: hormone-binding domain of the human estrogen receptor, AD: activation domain. (Figure adapted after (42))

Depending on the utilized AD, the range and steepness of target gene expression can be controlled, as well as the toxicity of the genetic switch. For example, the fusion of LexA-ER to the unstructured acidic peptide B112 as AD allowed strong target gene expression (in the range of the strong *TDH3* promoter) and a fine-tuned and therefore precise induction of gene expression, while not showing any toxic effects. Hence, the selection of the AD is important for the performance and targeted control of gene expression (45). Based on the hTF LexA-ER-AD, Ottoz *et al.* established a novel route of gene expression control that operates predictably in different growth media without influencing the host organism. Additionally, all steps were accompanied by detailed modeling, making this tool a perfect example for a SynBio application.

2.3. Genome engineering

Genome engineering is a tool that allows one to dissect and therefore understand complex genetic interactions, as well as building whole new pathways with the help of SynBio. Genome engineering was established in the 1970s, when researchers could demonstrate that it is possible to insert endogenous DNA into a target organism and integrate this DNA in the hosts genome. With the help of homologous recombination (HR), targeted mutation, deletion or integration into a host's genome is possible. Therefore, a plasmid or linear DNA fragment with a homologous region or homologous flanks to a certain site in the genome is delivered into a host cell and integrated by HR at the targeted site (94–97). In 1989, Mario Capecchi generated the first knock-out mouse, successfully manipulated by HR (95). This technology seemed very promising back in the 1980s, but soon turned out to have some main disadvantages:

- HR occurs with a relatively low frequency, which results in a quite low efficiency (98,99)
- integration efficiency depends heavily on the HR properties of the host organism
- HR experiments are time-consuming and labor-intensive, especially when it comes to selection and screening strategies
- there is always potential for mutagenic effects (97,100)

Due to these limitations, new approaches had to be developed to allow targeted manipulation with a much higher efficiency than possible with HR only. It was found, that the efficiency of HR could be greatly enhanced, if endonucleases create a double-strand break (DSB), which are difficult to repair for the host (100,101). The DSB is then repaired by one of the intrinsic repair mechanisms: homology-directed-repair (HDR) or nonhomologous end joining (NHEJ) (102). NHEJ usually occurs after a DSB, when no DNA template is provided. Since NHEJ may repair DNA in an error-prone process, this repair mechanism often leads to inactivating mutations. HDR occurs, when a DNA template, defining the desired genetic modifications, is present. Thus, HDR allows precise genome editing (97,102).

The discovery that the induction of a DSB increases the frequency of cellular repair mechanism dramatically, refocused the field of research into the direction of targeted DNA-binding endonucleases. Chimeric nucleases like zinc-finger nucleases (ZFN) or later Transcription Activator-like Effector Nucleases (TALEN), combining sequence-specific DNA binding domains with a nonspecific DNA cleaving module (100) were established.

2.3.1. CRISPR/Cas – a powerful tool for synthetic biology

When invented, TALEN seemed to be the most promising tool for genome engineering, but when the potential of the novel CRISPR/CRISPR-associated (Cas) approach was discovered, it exceeded the potential of previously established TALEN restriction endonucleases by far (103). Clustered regularly interspaced short palindromic repeats (CRISPR) originally are part of the adaptive immune response of archaea and bacteria (for detailed mechanism and description see 2.3.2) and provide immunity *via* RNA-guided DNA cleavage against invading foreign DNA like phage DNA (104).

Nowadays, due to the simplicity and adaptability, the less time- and cost-consuming production, as well as the precise and scalable DNA targeting, CRISPR is the most popular tool for genome engineering (97). Multiple CRISPR approaches have already been established for applications such as targeted DNA manipulation (2.4.1)(105), transcription control (2.4.4) (106) and many more (2.4.5).

For targeted genome engineering, basically three components are necessary (Figure 6):

- the CRISPR-associated endonuclease Cas9
- a guide RNA directing Cas9 to a specific DNA locus
- a protospacer adjacent motif (PAM), that can be recognized by Cas9 (107)
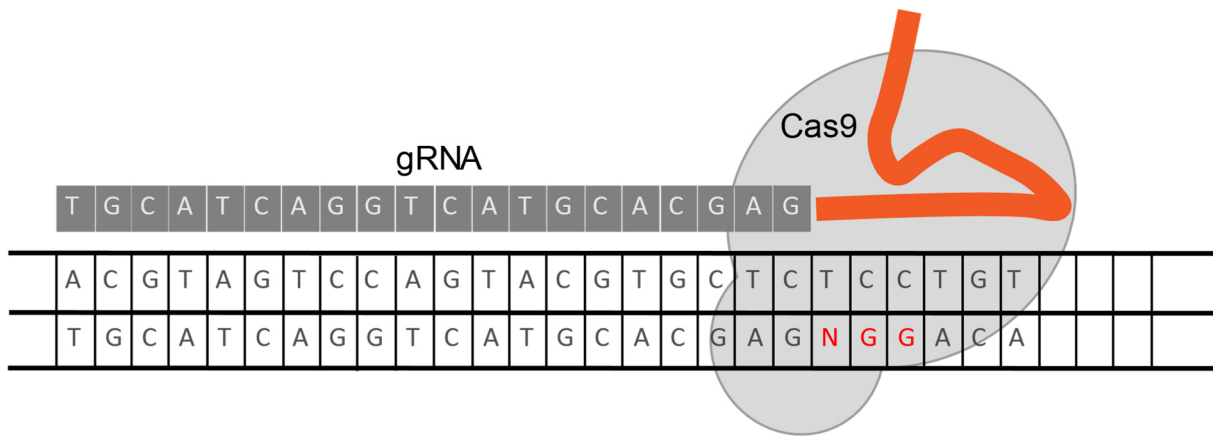
Figure 6 Structure of CRISPR/Cas9 system.

Designed gRNA recruits Cas9 and binds as a complex with DNA. The gRNA specifically targets 20 bp of the DNA, while the Cas9 additionally needs a PAM sequence (marked in red) to allow binding and cleavage of DNA. (Figure adapted after (97,100))

2.3.2. The bacterial adaptive immune response by CRISPR

Since bacteriophages are the most abundant biological entity present in this world, bacteria had to develop strategies to defend themselves from their invasive nature (108). Some strategies like the prevention of DNA injection, focus on keeping the virus out of the cell, whereas other like the CRISPR/Cas system concentrate on the destruction of the DNA that already invaded the cell (109,110). Consequently, more than 90 % of all archaea and 40 % of all bacteria possess CRISPR genes in their genome (111–113). Notably, the different loci of the CRISPR/Cas complexes show a great diversity in sequence and gene arrangement depending on the host organism. With the help of a computational approach two classes, five types and 16 subtypes of CRISPR-Cas complex were identified (114). Type II found in *Streptococcus pyogenes* is one of the simplest and therefore widely used variant only depending on the Cas protein Cas9 for silencing endogenous DNA (105,109).

The defense efficiency of CRISPR/Cas relies on small RNAs which specifically target the foreign DNA to allow silencing/cleaving by Cas proteins. As a first step during the infection, double stranded viral DNA invades the host and is recognized as exogenous DNA. If the host contains one or more CRISPR loci, it responds by digesting the foreign DNA into ~30 bp DNA fragments and integrates them as protospacer into the own genome at the proximal end of the CRISPR array (97,104,105). As a second step during the expression and interference phase, the genomically integrated repeat-spacer elements are transcribed into the precursor CRISPR RNA (pre-crRNA). This pre-crRNA is enzymatically cleaved by Cas proteins to achieve a mature crRNA (115,116). In the third and last step of active immune defense, the crRNA containing a spacer sequence complementary to the invading DNA directs the Cas proteins to the foreign

DNA. The Cas proteins then silence the invading genes (117,118). An adaptive immune response is acquired (Figure 7).
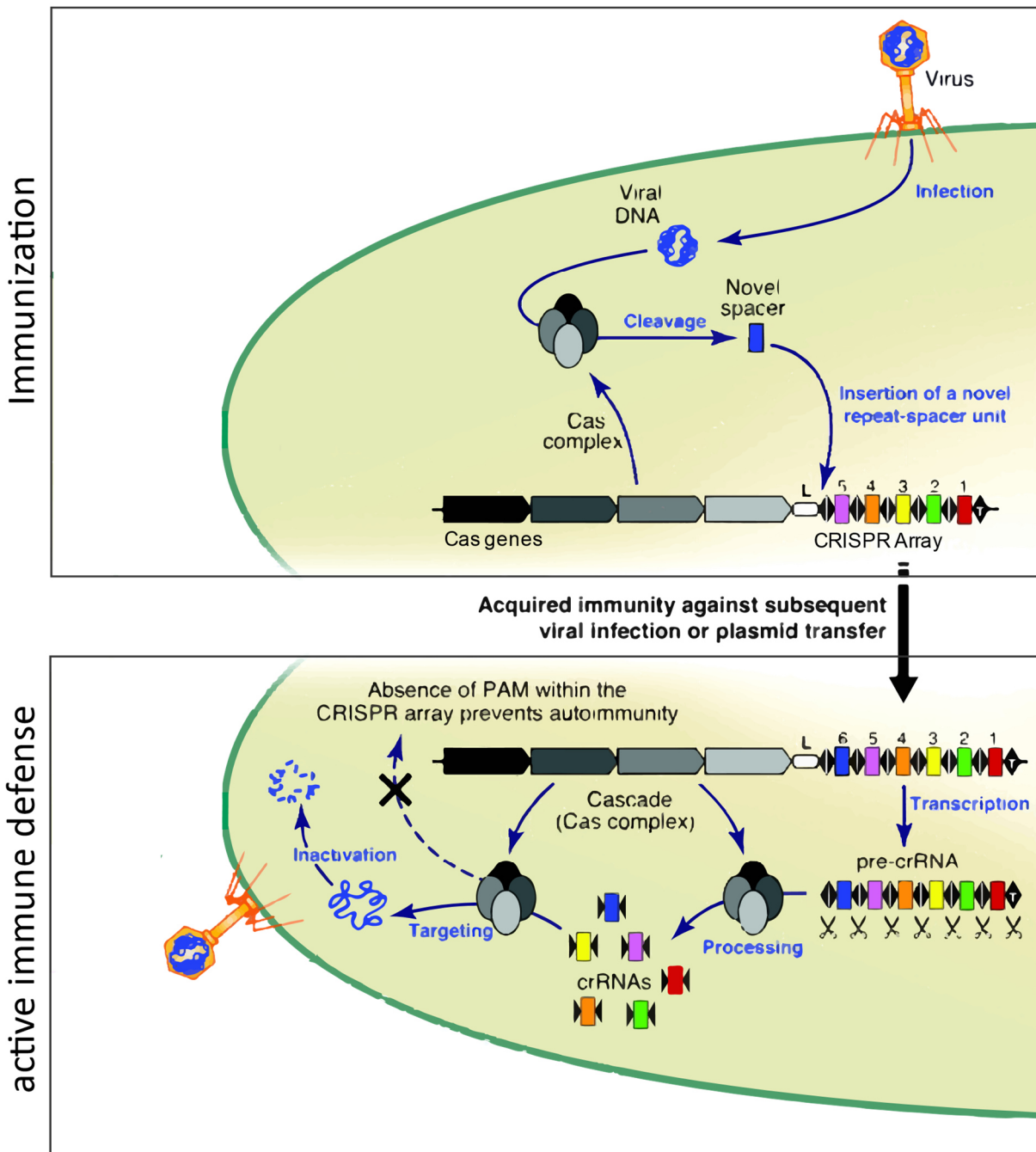
Figure 7 Mechanism of adaptive immune system of bacteria and archaea.

Immunization: foreign DNA, like double-stranded viral DNA, invades the cell and is recognized by the Cas complex. After cleavage of the foreign DNA into small fragment, the Cas complex integrates those fragments as novel repeat-spacer units into the hosts genome at the leader end of the CIRPSR locus. Active immune defense: The repeat-spacer array is transcribed into pre-crRNA and processed into mature crRNA by a Cas complex. The so build crRNA:tracrRNA:Cas complex can now specifically bind to the viral DNA invading the cell and cleave it into harmless fragments. L: CIRSPR leader, triangles: repeats, rectangles: spacers. (Figure adapted after (110))

2.3.3. Components for a CRIPSR/Cas system of type II from *Streptococcus pyogenes*

The CRISPR loci were already described by Ishino *et al*. in 1987 (119), but their function was not understood until 2002 (111). A CRISPR locus typically consists of two main elements. First the CRISPR-associated (*cas*) genes encoding for multiple proteins like nucleases, polymerases, helicases or polynucleotide-binding proteins (120). Second a CRISPR array consisting of several noncontinuous direct repeats separated by variable spacer regions. Each direct repeat together with one adjacent spacer encodes for one crRNA (97). The repeat sequences are 23 to 47 bp long and highly conserved within a given CRISPR locus while having a broad sequence variety across microbial species (110,111). The repeat sequences contain information for the processing of the pre-crRNA into a mature crRNA. The spacer sequences on the other hand are 21 to 72 bp long and each spacer codes for a unique foreign DNA target sequence (110,111).

In type II CRISPR/Cas systems an additional trans-activating crRNA (tracrRNA) is required. The tracrRNA binds to the partially complementary pre-crRNA and initiates the recruitment of RNAse III and Cas9 protein to achieve a mature Cas9:crRNA:tracrRNA complex (see Figure 8A) (105). Hence, only with the help of the tracrRNA, a successful inactivation of exogenous DNA can be achieved (105,116). The Cas9:crRNA:tracrRNA complex can bind to the crRNA target sequence only if a PAM is located directly after the binding region. It should be noted that the PAM sequence strongly depends on the respective system and Cas protein (121). For the type II system the PAM sequence is NGG (116).

For type II CRISPR/Cas Cas9 is the sole protein responsible for cleavage of the exogenous DNA. Therefore, Cas9 contains two endonuclease domains, a HNH nuclease domain in the middle of the protein and a RuvC-like nuclease domain near the amino terminus (122). After binding of the Cas9:crRNA:tracrRNA complex to the foreign DNA, the complementary DNA strand is cleaved three base pairs upstream of the PAM sequence by the Cas9 HNH domain. The noncomplementary DNA strand is cleaved endonucleolytically by the RuvC-like domain and subsequently trimmed by a 3´-5´ exonuclease (105). Through this process, blunt end DNA cleavage of both (supercoiled) plasmid and linear DNA is achieved (105,123).

2.4. Multiple novel CRISPR approaches for targeted genome engineering
2.4.1. Development from a naturally occurring system to a valuable synthetic tool

In 2012, Jinek *et al.* first invented a strategy that allowed for the targeted DNA cleavage *in vivo* with a programmed CRISPR/Cas9 system. Therefore, they developed a chimeric single-guide RNA (gRNA or sgRNA) combining crRNA and tracrRNA to a short synthetic RNA. A gRNA is composed of a fixed scaffold sequence, which is necessary for the binding of Cas9, and an unspecified 20 nucleotide long spacer, which is designed by the user to target a specific

sequence (105,106). Therefore, by changing the 20-nucleotide spacer, the target destination of Cas9 can be easily changed (see Figure 8B).
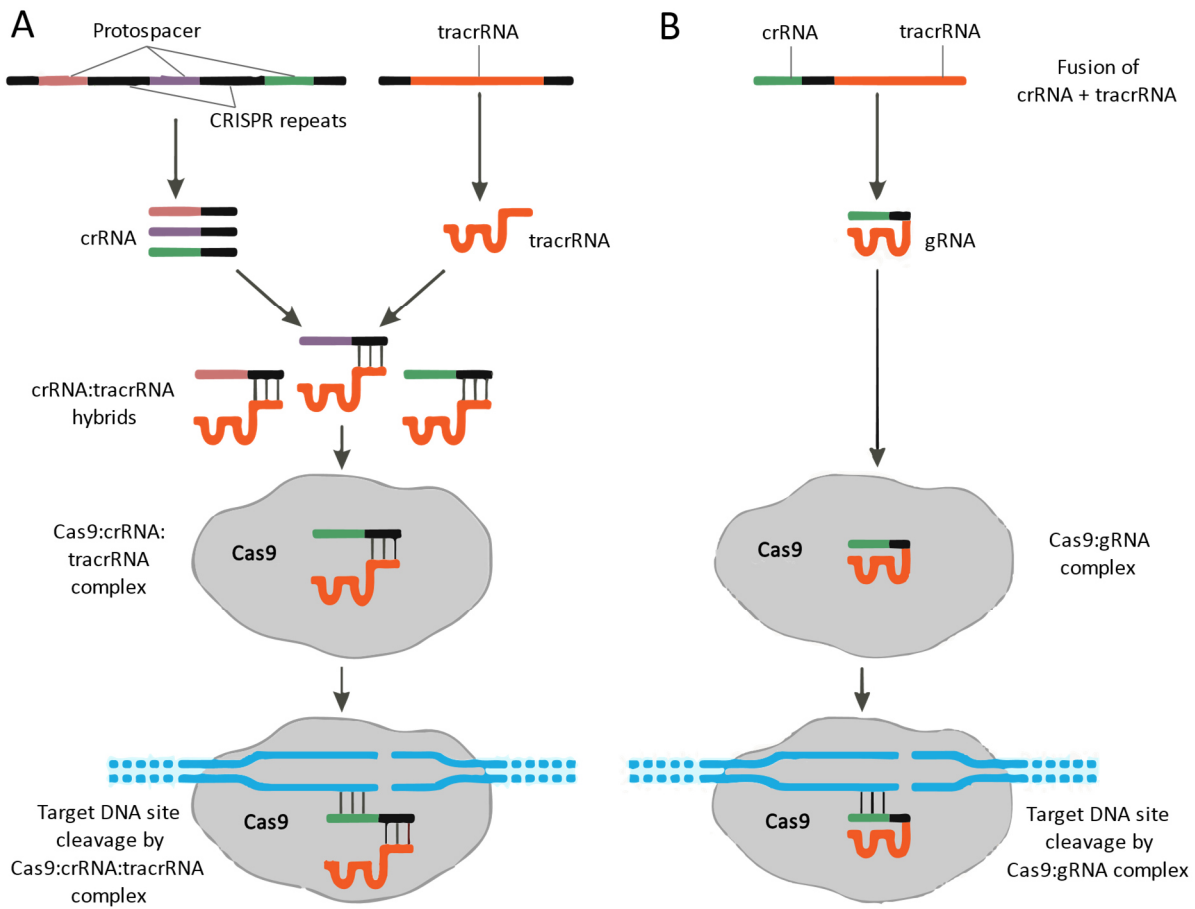
Figure 8 Comparison of naturally occurring (a) and engineered (b) type II CRSPR/Cas9 system. (Figure adapted after (107))

The CRISPR/Cas9 system is directly portable, *e.g.* in human cells. Hence, for targeted genome engineering, it is sufficient to implement the genes for Cas9 and a gRNA, whose spacer is homologous to the target DNA site (103,124). For efficient targeting, a PAM site has to be present in the target DNA immediately adjacent to the gRNA homology region. After successful targeting, the endonuclease domains of Cas9 induce a blunt end DSB 3 bp 5´ of the PAM (125). The DSB is either repaired by error-prone NHEJ or by precise HDR (126). NHEJ often leads to insertions, deletions or frameshifts, which makes it a great tool for genetic knock-outs. When a repair template with homologous arms is provided, DSB repair is performed using HDR. The template will be integrated into the target gene, giving precise information about the desired genetic modification. HDR thus creates a variety of options for targeted genome engineering (127,128).

After the publication of Jinek *et al.* in 2012, in 2013 the first papers about CRISPR-based genome engineering in mammalian cells were published (103,129). Only five years later, 6300 CRISPR-related publications are listed on PubMed, among others demonstrating efficient and precise genome engineering in a brought range of cell lines and organism (for an overview from 2014 check (107)). This demonstrates the importance of CRISPR genome editing strategies, as well as their potential for laboratory research and therapeutic applications (97,100).

2.4.2. CasEMBLR - A practical approach using CRISPR/Cas9 for genomic integration in yeast

Genome engineering, or more precisely chromosomal integration of foreign DNA, was carried out by HR for decades. Even though HR is relatively efficient in *Saccharomyces cerevisiae*, the efficiency of HR is only 10^{-6} to 10^{-4} (130). In order to enhance the efficiency of chromosomal integration, in 2015 Jakociunas *et al.* published a method called CasEMBLR (<u>Cas</u>9-facilitated multiloci integration of ass<u>embl</u>ed DNA parts into *S. cerevisiae* chromosomes, as a reference to the two mutually important methods DNA Assemble<u>r</u> and Cas9-facilitated integration). CasEMBLR allows the marker-free multiloci integration of *in vivo* assembled DNA parts. For CasEMBLR two plasmids have to be transferred into the yeast cell simultaneously with the DNA parts: a plasmid bearing an active Cas9 and a plasmid containing one or more gRNA(s) targeting one or more loci for genomic integration. It is noteworthy that the DNA template does not have to be assembled before transformation. Instead linear DNA parts, each with 50 bp overlap, can simply be co-transformed, are *in vivo* combined by HR and therefore build the new gene of interest (Figure 9)(99).
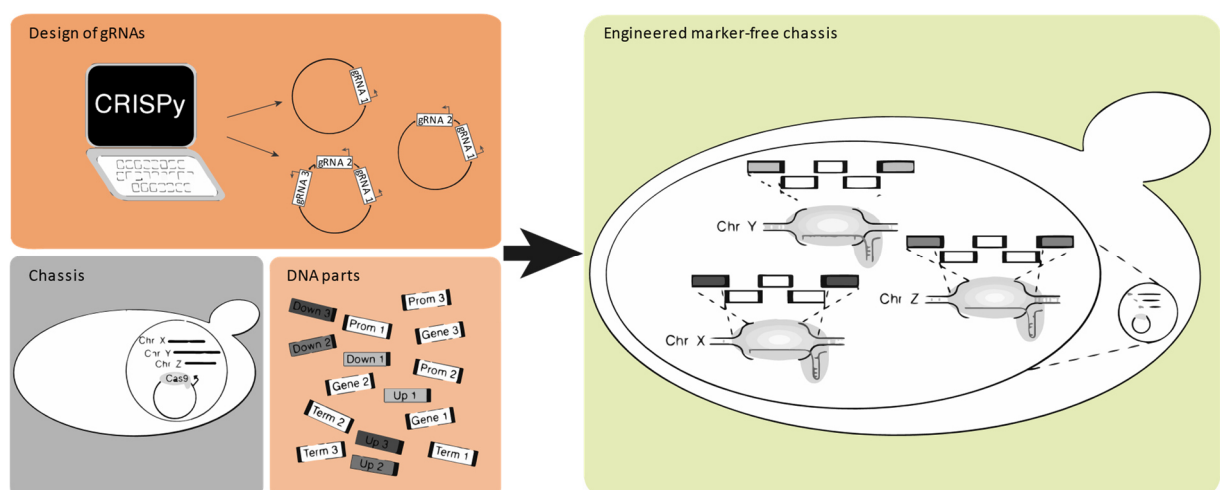
Figure 9 Construction and integration of the CasEMBLR method.

For marker-free multiloci integration *in vivo* a gRNA plasmid containing one gRNA for each integration side needs to be designed and integrated together with linear DNA template fragments. gRNA plasmids and DNA fragments are co-transformed into a yeast cell already containing a Cas9 plasmid. (Figure adapted after (99))

The efficiency of the chromosomal integration depends on the targeted genome locus and the number of simultaneous genomic integrations. According to Jakociunas *et al.* an efficiency of nearly 100 % can be achieved for a single locus, ~ 60 % for two loci and ~30 % for three loci at the same time (99). In order to achieve maximum efficiency, a web-tool named CRISPy was invented for the design of the gRNA target sequence (131). CasEMBLR allowed the simple and straight forward integration of multiple genes in the exemplary genomic sites ADE2, HIS3, and/or URA3 without the need of a marker or the pre-assembly of parts (99). Hence, CasEMBLR delivers a really useful tool for genomic integration and was used for the integration of various switches in the scope of this thesis (4). CasEMBLR is a perfect example for the advantages CRISPR-based systems offer to every-day research, especially with the focus on SynBio applications.

2.4.3. Versatile approaches to optimize the CRISPR/Cas9 target binding specificity

The CRISPR/Cas9 system delivers a simple and modular tool for genome engineering, further it allows to precisely target, cleave and manipulate DNA. Any possible sequence can be targeted, as long as the sequence is unique in the respective genome and a PAM is present immediately adjacent to the targeted site (107).

Unfortunately, depending on the gRNA sequence, partial sequence homologies of a given gRNA throughout the genome will occur. Right from the start the extent of off-target binding/cleavage events was one of the major concerns regarding any genome engineering tool (100). Various studies indicate that off-target effects for the CRISPR/Cas9 system vary in frequency. In 2014, Sander and Joung reported that it is difficult to predict the off-target sites and their influence on the host, especially since it is not completely understood why some sites are cleaved whereas others are not (107). Either way, researchers aim for reducing off-target effects of CRISPR/dCas9, which is extraordinarily important particularly for medical applications (100,107).

A simple approach to reduce off-target effects may be to lower the amount of gRNA and Cas9, which is expressed in the host. It seems, that the reduction of an off-target effect also leads to lower efficiency of the on-target engineering. Hence, this approach is only partially promising (107). Therefore, a more complex approach was envisioned – optimization of the gRNA. Many (web-based) computer tools for targeted gRNA design have been established, which allows one to find a/multiple gRNA(s) fitting exactly to the users' requirements (132,133). Theoretically, these computer-based tools work well, but they do not always live up to the expectations, so that researchers have to repeat experiments with a different gRNA setup (99). Another approach to decrease off-target effects is to use a gRNA shortened at the 5´end of their complementarity region. In 2014 Fu *et al.* demonstrated that a truncated gRNA with only 17 or

18 nucleotides of complementarity generally functions as efficient as full-length gRNAs. At the same time the off-target mutagenic effects are reduced and the sensitivity to mismatches at the gRNA:DNA interference is increased (134).

In addition to the optimization of gRNA, Cas9 can be modified to not only achieve better off-target rates, but also to expand the field of applications. To increase specificity, Le Cong *et al.* engineered Cas9 in a way, that the nuclease was converted into a nickase (129). As mentioned above Cas9 cleaves the DNA using a RuvC-like domain together with an HNH nuclease domain, leading to a DSB inducing either NHEJ or HDR. Le Cong *et al.* performed an aspartate-to-alanine substitution (D10A) in the RuvC-like domain to only nick one DNA strand. Alternatively, to achieve a Cas9 nickase a H840A substitution of the HNH domain is possible. Nicked DNA is typically repaired by either seamless or high-fidelity HDR (105,129). In order to achieve a DSB, two nickases targeting opposite DNA strands can be used together with two gRNAs, each targeting one side of the DNA strand. The gRNAs bind in a distance of 4 to 100 bp, leading to efficient indel mutations or HDR events in the presence of a donor template (135–137). Since it is unlikely that two off-target nicks will occur close enough to cause a DSB, this double nickase setup lowers off-target effects drastically. However, it was shown by several studies, that monomeric nickases themselves can induce indel mutations at certain genomic loci (135–137). A system, where both nickase monomers are strictly co-dependent on each other to induce genome engineering activity, may solve this problem (107). Accordingly, Cas9 nickases do not only reduce off-target effects, but also allow specific nicking of the DNA and, in a dimer-approach increase the occurrence of HDR, while decreasing the one of NHEJ.

Another approach to optimize off-target effects, is the genetic modification of wildtype Cas9 towards a high fidelity enzyme (97). In 2015, the first variants of high fidelity Cas9 endonucleases were published. By rational mutagenesis and structure-guided protein engineering, Slaymaker *et al.* were able to improve the specificity of *Streptococcus pyogenes* Cas9 (SpCas9) to an "enhanced specificity" SpCas9 (eSpCas9). It could be demonstrated by targeted deep sequencing and unbiased whole-genome off-target analysis that eSpCas9 variants reduce off-target effects while maintaining a robust on-target cleavage (138). Even more promising is the evolved Cas9 (evoCas9) variant, published 2018 by Casini *et al.* With the help of a yeast-based assay that enabled simultaneous evaluation of on- and off-target activity, they screened for random mutations in SpCas9. Afterwards they combined four promising mutations into evoCas9. EvoCas9 was demonstrated to maintain near wild type on-target efficiency, while off-target effects are dramatically decreased even in comparison to other rationally designed Cas9 variants like eSpCas9. Even in a long-time experiment over 40 h, nearly no off-target effects were detected (139). These enhanced Cas9 variants provide promising high-fidelity enzymes, which allows genome engineering with high specificity and nearly no off-target effects.

Despite all the advantages of CRISPR, the main disadvantage is still that the target site must always have an appropriate PAM sequence (105). As a result, not every DSB can be made with the desired precision. Thus, Kleinstiver *et al.* demonstrated, that SpCas9 can be modified to specifically recognize altered PAM sequences. Alternatively they describe two smaller-sized Cas9 orthologues from *Streptococcus thermophilus* and *Staphylococcus aureus*, both efficiently working in bacteria and human cells and recognizing altered PAM sequences (121). Other orthogonal Cas9 proteins recognize gRNAs with different Cas9-binding modules (140). The usage of Cas9 proteins which recognize altered PAM sequences or gRNAs will expand the options for specific targeting and allows one to switch between distinct programs by controlling the expression of the Cas9 proteins targeted (for an example see 2.5) (5).

2.4.4. Using inactive Cas9 variants for targeted transcription repression or activation

CRISPR/Cas9 systems are not only a promising tool in terms of genetic modification, but also for genetic regulation of cells by robust and precise targeting of genes for expression or repression. To achieve this aim, a catalytically dead Cas9 (dCas9) was established, containing a silencing mutation (like D10A and H841A) in both nuclease domains of Cas9 (105,141). Qi *et al.* demonstrated in 2013, that a dCas9 can form a complex with a co-expressed gRNA to specifically recognize and bind DNA. This complex can modify the transcription of an arbitrary gene without causing genetic modifications of the target sequence (141). Hence, with CRISPR/dCas9 a platform was generated, allowing RNA-guided DNA recognition and regulation.

The first system established on this platform was called CRISPR interference (CRISPRi). With the help of a specific gRNA, dCas9 binds to a target gene. The complex sterically blocks transcription with an up to 1000-fold repression. Multiple gRNAs can be used in parallel to simultaneously silence multiple genes. Furthermore, CRISPRi can be used to knock down endogenous genes in bacteria, as well as gene expression in mammalian cells (141). The repression effect can even be enhanced by fusing a transcription repressor like KRAB to Cas9 (106). Target gene repression or knock-down is highly specific; off-target effects have not been reported (106,141). Therefore, it is not surprising, that already in 2013, a system called CRISPR activation (CRISPRa) was published. By fusion of transcription activators like VP16 to Cas9, targeted gene expression could be achieved in multiple organisms, among them the yeast *S. cerevisiae* and human cells (106,135).

CRISPRi and CRISPRa can be used for multiplexed control of endogenous and synthetic genes, simply by implementing multiple gRNAs, where the respective dCas9-effector fusions are constrained to only one direction of regulation for all targeted loci which is either activation or repression. To overcome those limitations Zalatan *et al.* invented a strategy, where the gRNA

overtakes both, target specificity and regulatory function (5). Mali *et al.* demonstrated in 2013, that a sgRNA can be extended with a MS2 hairpin loop to recruit an activator to a reporter gene in human cells (135). Zalatan *et al.* expanded this strategy and, with the help of different hairpin loops, directed three orthogonal RNA-binding modules, which are fused to activators or repressors to reporter genes in *S. cerevisiae* and in human cells (Figure 10). They demonstrated that the RNA-binding modules can be used in parallel, without influencing each other. This allowed the successful regulation of multiple genes at the same time to build a highly branched biosynthetic pathway in yeast (5).
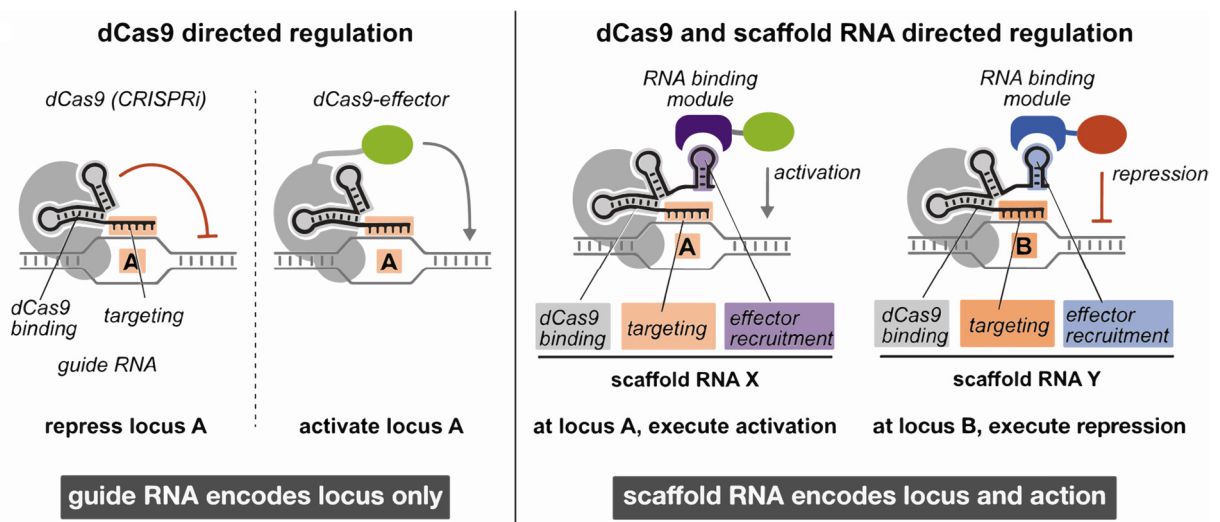
Figure 10 Comparison of regular CRISPR (left) and multi-domain scaffolding RNAs (right).

Left: Repression or activation is regulated by dCas9 only. The gRNA only encodes the locus of action. Right: Repression and activation of target gene transcription is mediated due to dCas9 and scRNA directed regulation. Hence, the scRNA encodes both, locus and action. (Figure adapted after (5))

In summary, the CRISPR/dCas9-scRNA system provides a reversible and straightforward method for the simultaneous ON/OFF regulation of multiply genes and therefore, the design of complex switching programs and pathways. Due to the modular character and the simple application, the CRISPR/dCas9-scRNA system can serve as a basic toolbox to design complex switches, as illustrated in this work.

2.4.5. Further applications for and with CRISPR systems

Like active CRISPR/Cas9, catalytically inactive CRISPR/dCas9 systems only require a dCas9 protein and guide RNAs, which makes them highly flexible and designable. Furthermore, dCas9 can be fused to multiple effector proteins. For example, the fusion of a dCas9 or Cas9 nickase to base editors like the cytidine deaminase APOBEC1, allows precise integration of point mutations (142,143). This is especially useful for medical applications, where accuracy is absolutely critical (144).

Another possibility is to fuse the epigenetic modifier like the catalytic core domain of the human acetyltransferase p300 (145) or the catalytic domain of the DNA methyltransferase 3A (DNMT3A) (146) to dCas9. These fusions allow one to alter gene expression without inducing a DSB due to epigenetic modifications such as histone acetylation. Since the epigenetic modifiers are specific for a particular chromatin and DNA modification, among others they allow for the identification of the effects of a single epigenetic marker (146). This specificity is also their main disadvantage, since they can only be used cell-type and context-dependent (97). A third application for CRIPSR is to fuse an inactive dCas9 to a fluorescent marker like GFP to enable live cell imaging. Researches successfully turned dCas9 into a customizable DNA labeler, allowing among others the visualization of repetitive or nonrepetitive genomic sequences, telomere length change or movement/the dynamics of gene loci (147).

A field, which was revolutionized trough the possibilities of CRISPR/Cas were genome wide screenings (148). Due to large gRNA libraries, large-scale forward genetic screening is possible. This is especially important for the genome-wide studying of diseases or phenotypes, for which the underlying genetic cause is not known (149,150). The goal of those genetic screens is to generate a large population of cells containing multiple mutations or knock-outs in a targeted set of genes. Researches then use these cells to identify the genetic perturbations that result in a desired phenotype (68,151).

2.5. Complex genetic circuits based on CRISPR systems

Collectively, the described techniques and applications establish the CRISPR platform as a powerful tool for modular, scalable, orthogonal, highly specific and practical genome engineering. Some highly complex control systems have already been published, demonstrating the possibilities of CRIPSR to solve problems that previously seemed unsolvable. This paragraph will give two examples for genome engineering tools that solve such problems in the yeast *S. cerevisiae*.

The first problem concerns production of cell factories. Cell factories come to use, when environmentally damaging petro-chemistry productions are to be replaced or when natural bioproduction is not possible (151). Nowadays, the design and establishment of cell factories needs rather extensive multi-step metabolic engineering. Hence a tool is needed, which simplifies and speeds up the generation of cell factories (31). In 2017 Vanegas *et al.* published a CRISPR tool called SWITCH solving the problem at least partially. Due to the integration of two CRISPR tools, one for genetic engineering and one for pathway control, SWITCH allows to iteratively alternate between a genetic engineering state and a pathway control state. They build a whole pathway by integration of the necessary genes in engineering cycles. Each engineering cycle is performed by a different CasX species (151). As the first step of an

engineering cycle, the *casX* genes are integrated into one of the specific loci (152) in the specially designed yeast expression strain. During step two linear parts are combined and integrated into the genome by gRNA mediated genetic engineering. In a third step, by addition of a target gRNA plasmid, the *casX* cassette is either eliminated or by addition of a template replaced by a *dcasX* or *dcasX-effector* cassette. Both possibilities are carried out by recombination trough CasX itself. In the fourth and last step, a new gRNA directs the dCas9/dCas9-effector to a target gene for up- or down-regulation. This cycle can be repeated by the usage of another *casX/dcasX* variants. Therefore, the simple and scalable genome engineering towards a functional cell factory has been established (151).

The second problem concerns the building of novel decision-making regulatory networks (153). It remains difficult to design and implement complex synthetic circuits in eukaryotes, due to arbitrarily interconnections, transcriptionally leaky components or the fact, that mainly analogue response mechanisms are used (154). In 2017, Gander *et al.* established a CRIPSR-based system, that allowed the construction of digital genetic circuits of great complexity as quickly and easily as an electric circuit would be. Therefore, they developed a set of low-variability genetic parts, that have the same programmable input and output signals (same molecular type), as in electronics, allowing them to be wired together. Their system is based on *dCas9-Mxi1* NOR gates (154). *Mxi1* is a chromatin remodelling repression domain that recruits histone deacetylases (155,156). By fusion of *Mxi1* to *dCas9*, a NOR gate with inducible strong repression was achieved showing minimal leakage. The gRNA inputs were directly converted into gRNA outputs, creating a digital output signal. Since the input and output both are gRNAs, multiple NOR gates can be wired together to build large genetic circuits. Hence, Gander *et al.* were able to combine up to seven gRNAs, including repression cascades with up to seven layers. The experimental setup was combined with intense modeling that allowed the authors to predict the circuits behaviors (154). This combination of modeling and experimental research is a perfect example for a successful SynBio application. Based on this conclusion, it can be confirmed that the design and implementation of complex genetic switches according to the idea of SynBio is a really promising approach to solve problems in both areas, basic research and medical applications.

2.6. Objective

Targeted genome engineering and gene regulation play a key role for basic research and industrial applications. Multiple setups have already been established for *e.g.* synthetic production of bio-derived materials in the yeast *S. cerevisiae* (2,3). Nevertheless, there still is a great need for well-defined switching systems and modular genetic circuits in *S. cerevisiae*. The presented work aims to characterize various switches and to assemble them into a modular toolbox. A three component CIRPSR/dCas9 system (5) should be tested to determine whether it is suitable as a basic route for genetic regulation (Figure 11). The genes should be genomically integrated into the yeast *S. cerevisiae* either by simple HR (94–97) or with the help of the method CasEMBLR (99). If the method CasEMBLR turns out to be successful, it should be established in the lab for future genomic integrations.

For targeted gene regulation, the three components of the genetically integrated CRIPSR/dCas9 complex should be individually and independently expressible. It was aimed to use different inducible expression strategies based on different induction mechanisms. As part of this work, three different switches should be tested. The selected switches are either inducible by the carbon source galactose (56), the antibiotic doxycycline (74), or the steroid hormone β-estradiol (45). Promising switches should be combined into an AND gate. Both, the switches and the AND gates should be analyzed regarding their basal activity, expression levels and dose-dependency. Selected AND gates should be further analyzed with the help of collaborations through a model and single-cell microfluidic measurements (4). In addition, a positive feedback-loop should be implemented, which allows the inducer-independent cell growth after a short induction phase.

When successfully expressed, the three CIRSPR/dCas9 components should form a functional complex and bind specifically to the desired binding region. For simple detection *via* flow cytometry, the fluorophore Venus should be utilized as reporter gene. In addition, a setup should be implemented, that allows the verifiable gene expression of virtually every gene of interest. It was aimed to implement the ribosomal skipping peptide T2A (157), which after CRIPSR/dCas9-mediated expression of the GOI also enables the expression of the fluorophore tGFP. As a proof-of-concept two well-detectable GOIs should be used for a GOI-T2A-tGFP setup. The different reporter gene setups should be characterized in combination with the switches and AND gates. In order to demonstrate functionality, targeted gene expression of a reporter gene should be verified.

This work can be seen as a proof-of-concept study for the development and characterization of a new toolbox for yeast.
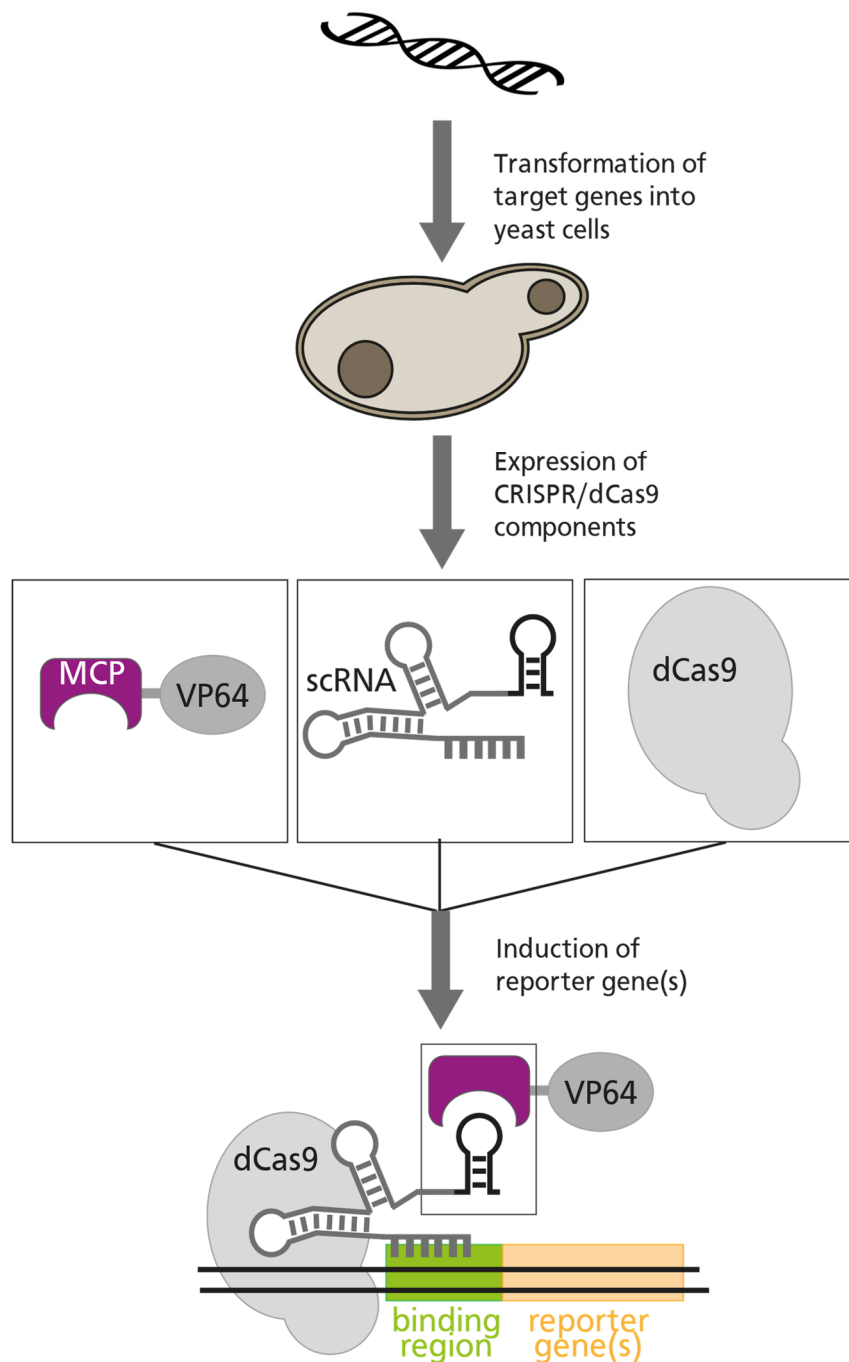
Figure 11 Generation of genetic switches and assembly to genetic circuits.

The target switches will be implemented on DNA level. Therefore, the established DNA will be transformed into *S. cerevisiae* cells. The switches are based on a three component CRISPR/dCas9 system, which will be expressed either constitutively or inducible by various inducers. After all three components are expressed, they will build a complex for targeted binding to the binding region. The transcription activator will enable expression of one or more reporter genes.

3. Material

3.1. Microorganisms

For this study the following microorganisms were utilized.

E. coli strains with the genotype described in Table 1 were used.

Table 1 Purchased bacterial strains.

Bacterial strains	
E. coli DH5α	*F- endA1 glnV44 thi-1 recA1 relA1 gyrA96 deoR nupG Φ80dlacZΔM15 Δ(lacZYA-argF)U169, hdR17(rK- mK+), λ–*
Top10	*mcrA, Δ(mrr-hdRMS-mcrBC), Phi80lacZ(del)M15, ΔlacX74, deoR, recA1, araD139, Δ(ara-leu)7697, galU, galK, rpsL(SmR), endA1, nupG*

S. cerevisiae strains received from the Zalatan lab (*University of Washington*) (5) are described in Table 2. *S. cerevisiae* strains generated in this study are described in Table 3.

Table 2 Purchased yeast strains.

S. cerevisiae strains	
SO992 (W303 derivate)	*MATa ura3 leu2 trp1 his3 can1R ade*
cSLQ.sc002	*SO992 HO::rtTA-msn2_hphR*
cSLQ.sc003	*cSLQ.Sc002 trp1::pTET07-Venus*
yJZC02	*cSLQ.Sc002 trp1::pTET01-Venus*
yJZC03	*cSLQ.Sc002 trp1::pTET02-Venus*
yJZC04	*cSLQ.Sc002 trp1::pTET03-Venus*

Table 3 Yeast strains generated in this study.

Name	Integrated genes	Origin
Ssw, 1x *tet*O	*trp1::TET01-Venus leu2::MCP-VP64_Gal10-dCas9*, scRNA (plasmid)	yJZC02
Ssw, 2x *tet*O	*trp2::TET01-Venus leu2::MCP-VP64_Gal10-dCas9*, scRNA (plasmid)	yJZC03
Ssw, 3x *tet*O	*trp3::TET01-Venus leu2::MCP-VP64_Gal10-dCas9*, scRNA (plasmid)	yJZC04
Ssw, 7x *tet*O	*trp7::TET01-Venus leu2::MCP-VP64_Gal10-dCas9*, scRNA (plasmid)	cSLQ.sc003
dC-VP64, 1x *tet*O	*trp1::TET01-Venus leu2::dCas9-VP64*, gRNA (plasmid)	yJZC02
dC-VP64, 1x *tet*O	*trp1::TET02-Venus leu2::dCas9-VP64*, gRNA (plasmid)	yJZC03
dC-VP64, 1x *tet*O	*trp1::TET03-Venus leu2::dCas9-VP64*, gRNA (plasmid)	yJZC04
dC-VP64, 1x *tet*O	*trp1::TET07-Venus leu2::dCas9-VP64*, gRNA (plasmid)	cSLQ.sc003
AND, 3x *tet*O	*ade2::lexA-MCP-VP64_Gal10-dCas9 his3::TET03-Venus_lexA-ER-B112*, scRNA (plasmid)	cSLQ.sc002
AND, 7x *tet*O	*ade2::lexA-MCP-VP64_Gal10-dCas9 his3::TET07-Venus_lexA-ER-B112*, scRNA (plasmid)	cSLQ.sc002
AND, GO	*ade2::lexA-MCP-VP64 Gal10-dCas9 his3::TET07-app8-Goase-T2A-tGFP_ lexA-ER-B112*, scRNA (plasmid)	cSLQ.sc002

AND, vNAR	*ade2::lexA-MCP-VP64 Gal10-dCas9 his3::TET07-app8-vNAR-His-Tag-T2A-tGFP lexA-ER-B112*, scRNA (plasmid)	cSLQ.sc002
AND, GO, pFL	*ade2::lexA-MCP-VP64 Gal10-dCas9 his3::TET07-app8-Goase-T2A-tGFP_ lexA-ER-B112*, scRNA (plasmid), pFL (plasmid)	AND, GO
Ubi, wt	*ade2::lexA-MCP-VP64 Gal10-dCas9 his3::TET07-UbiY-tGFP_ lexA-ER-B112*	cSLQ.sc002
Ubi, pJZC588	*ade2::lexA-MCP-VP64 Gal10-dCas9 his3::TET07-UbiY-tGFP_ lexA-ER-B112*, scRNA (plasmid)	cSLQ.sc002
Ubi, pJZC588 + AH019	*ade2::lexA-MCP-VP64 Gal10-dCas9 his3::TET07-UbiY-tGFP_ lexA-ER-B112*, scRNA (plasmid), pFL (plasmid)	cSLQ.sc002

3.2. Plasmids

3.2.1. Plasmids for genomic integration into the yeast genome

The plasmids pFRP880 (#58437) (45), pJZC519(#62278) and pJZC638 (#62283, 3.2.1) (5) were received from *addgene*. These plasmids were designed for genetic integration into the yeast genome and do not contain a yeast origin of replication (ori). Instead the plasmids maintain a homology region, which is necessary for the integration by homologous recombination. For genomic integration the plasmids were digested with restriction enzymes. The utilized enzymes, and their digestion sites are marked in the plasmid cards. All plasmids are *E. coli – S. cerevisiae* shuttle vectors, which mediate ampicillin resistance in the bacterial host.
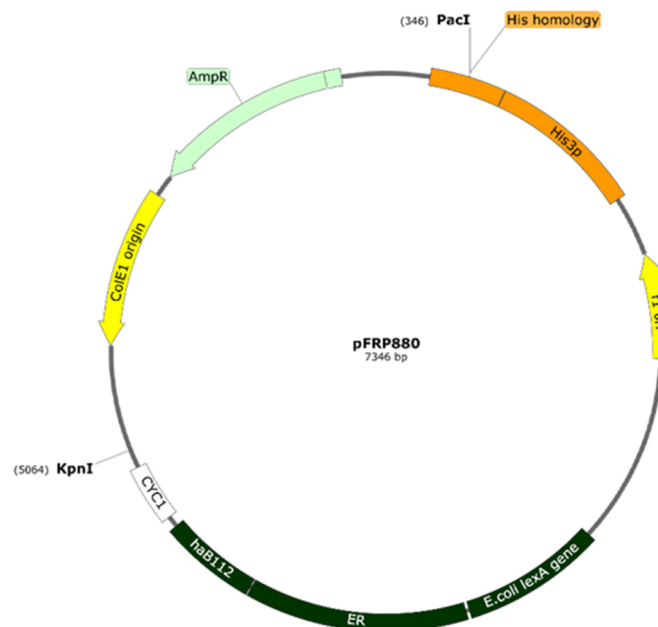
Figure 12 Plasmid map of pFRP880.

The plasmid pFRP880 contains the following genes: **His homology:** region for homologous recombination into the yeast genome, **His3p:** selectable marker, **f1 ori:** origin of replication in T7 phage, *E.coli* **lexA gene:** bacterial LexA DNA-binding protein (88), **ER:** hormone-binding domain of the human estrogen receptor (47), **haB112:** transcriptional activation domain (91), **CYC1:** terminator sequence, **ColE1 origin:** origin of replication in *E. coli*, **AmpR:** gene for β-lactamase, mediating ampicillin resistance in *E. coli*. The plasmid has to be digested for genomic integration at *PacI*/*KpnI*: digestion sites for homologous recombination after linearization.
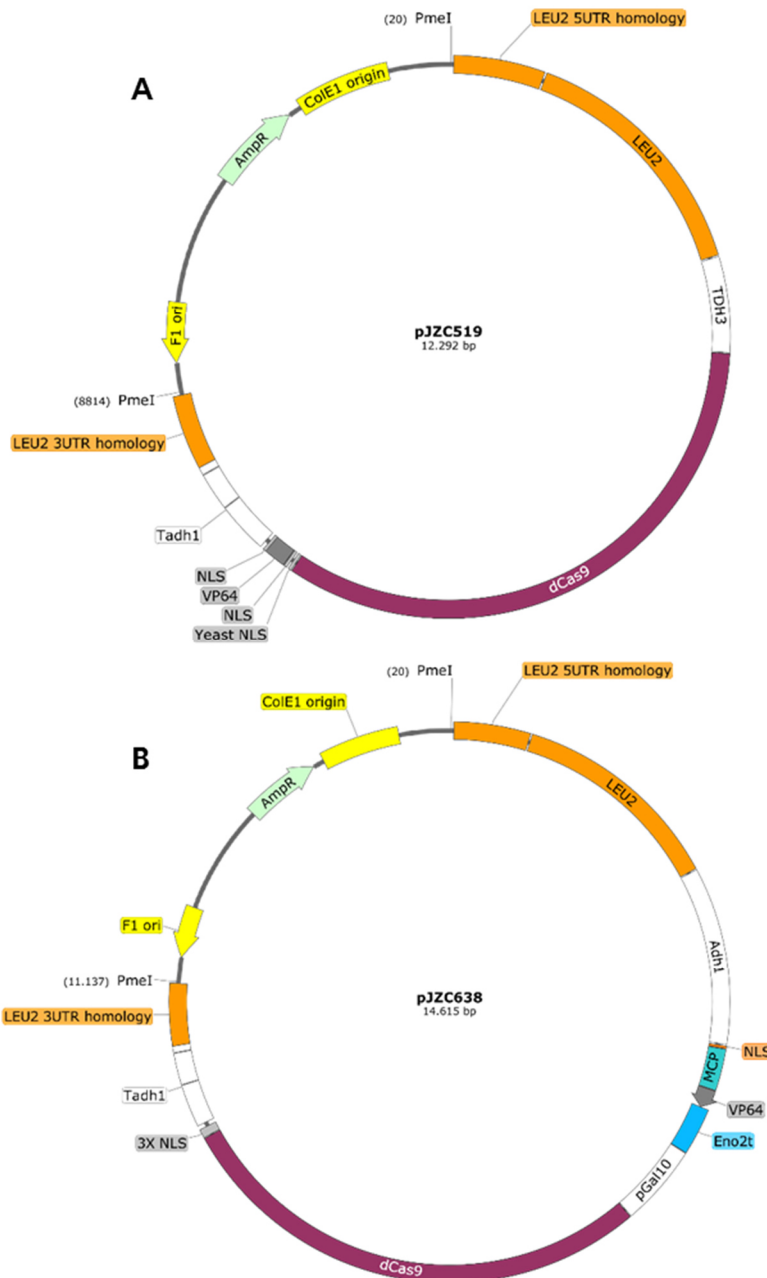
Figure 13 Plasmid map of pJZC519 (#62278) and pJZC638 (#62283).

The plasmids pJZC519 (A) and pJZC638 (B) both contain the following genes: **LEU2 UTR homology:** regions for homologous recombination into the yeast genome, **LEU2:** selectable marker, **dCas9:** catalytically inactive Cas9 *S. Pyogenes* with mutations in the RuvC1 and HNH domains to render it catalytically inactive (105,141), **NLS:** Nuclear localization signal, **Tadh1:** strong terminator derived from *C. albicans*, **f1 ori:** origin of replication in T7 phage, **AmpR:** gene for β-lactamase, mediating ampicillin Amp) resistance in *E. coli*, **ColE1 origin:** origin of replication in *E. coli*. Plasmid pJZC518 contains **TDH3:** strong constitutive promoter, in front of the dCas9 gene, which is genetically fused to **VP64:** transcriptional activation domain, derived from the Large T antigen. Plasmid pJZC638 contains a **ADH1:** strong constitutive promotor, controlling **MCP:** bacteriophage coat protein binding the scRNA MS2 stem loop, that is genetically fused (135) to **VP64:** transcriptional activation domain, derived from the Large T antigen. MCP-VP64 is terminated by the **Eno2t:** strong terminator. The plasmid also contains the dCas9 under control of **pGal10:** Galactose inducible promoter. Both plasmids have to be digested for genomic integration at *Pme*I: digestion sites for homologous recombination after linearization.

3.2.2. CEN/ARS-plasmids for gRNA/scRNA delivery

The plasmid pJZC523 (#62320), pJZC588 (#62315) and pJZC625 (#62321) (5) were received from *addgene*. The plasmids are *E. coli – S. cerevisiae* shuttle vectors. They contain the CEN/ARS motif as yeast origin, the gene for uracil prototrophy in yeast cells and the Amp^R gene to mediate ampicillin resistance in the bacterial host.
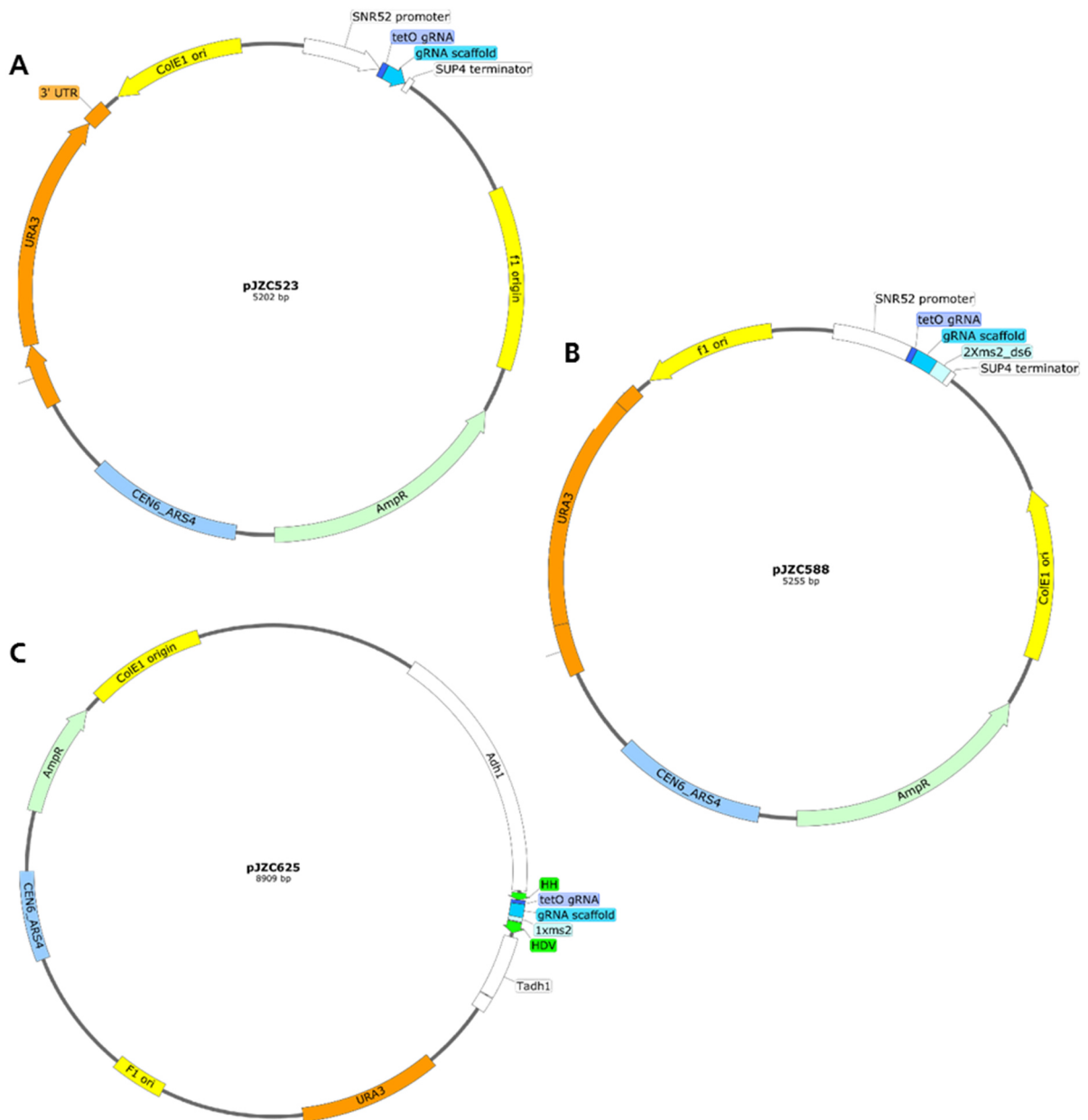
Figure 14 Plasmids cards for gRNA/scRNA plasmids.

All plasmids, namely pJZC523 (A), pJZC588 (B) and pJZC625 (C) contain the following genes: ***tet*O gRNA:** 20 bp long binding region to the tet Operator, **gRNA scaffold:** gRNA with stem loop for dCas9 binding, **f1 ori:** origin of replication in T7 phage, **AmpR:** gene for β-lactamase, mediating ampicillin resistance in *E. coli*, **CEN/ARS:** autonomously replicating sequence (ARS) and yeast centromere. **URA3:** selection marker. **ColE1 origin:** origin of replication in *E. coli*. The plasmid pJZC523 an pJZC588 also contained the genes: **SNR52 promotor:** minimal RNA polymerase III promotor for yeast cells, **SUP4 terminator:** terminator with a T7GT6 sequence for RNA polymerase III. The plasmid pJZC588 also contained the gene: **2xms2_ds6:** two copies of the MS2 stem loop (wt, f6) for MCP binding (5). The plasmid pJZC625 also contained the genes: **ADH1:** strong constitutive promotor for RNA polymerase II, **HH and HDV:** self-cleaving ribozymes (158), **1xms2:** one copy of the MS2 stem loop (wt) for MCP binding (135), **Tadh1:** strong terminator derived from *C. Albicans* for RNA polymerase II.

3.2.3. Plasmids needed for genomic integration by CasEMBLR

The plasmids p414_Cas9, p425-αAde_gRNA and p425-αHis3_2_gRNA (99) were received from the Süß lab (*TU Darmstadt*). All three plasmids are *E. coli – S. cerevisiae* shuttle vectors.
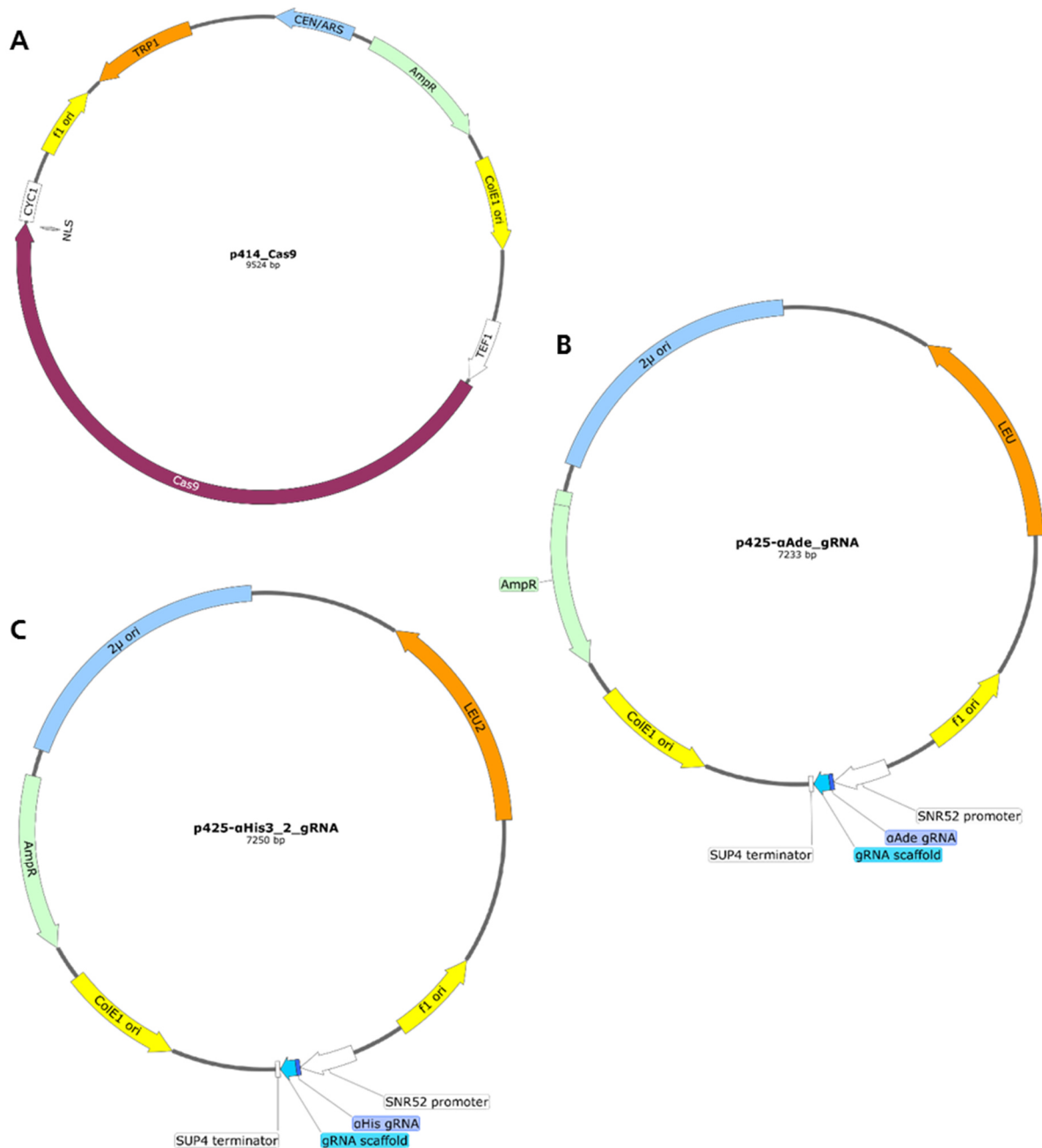
Figure 15 Plasmid map of CasEMBLR plasmids.

All plasmids, namely p414_Cas9 (A), p425-αAde_gRNA (B) and p425-αHis3_2_gRNA (C) contain the *E. coli* genes: **AmpR:** gene for β-lactamase, mediating ampicillin resistance in *E. coli*. **ColE1 origin:** origin of replication in *E. coli*, **f1 ori:** origin of replication in T7 phage. p414_Cas9 also contained the yeast genes: **CEN/ARS:** autonomously replicating sequence (ARS) and yeast centromere (CEN), **TEF1:** strong constitutive promotor for RNA, **Cas9:** catalytically active Cas9, **NLS:** Nuclear localization signal peptide derived from the Large T antigen, **CYC1:** terminator sequence, **TRP1:** selection marker. The plasmids p425-αAde_gRNA (B) and p425-αHis3_2_gRNA also contained the yeast genes: **LEU:** selection marker, **f1 ori:** origin of replication in T7 phage, **SNR52 promotor:** minimal RNA polymerase III promotor for yeast cells (159), **αAde or αHis3_2 gRNA:** 20 bp long binding region to a sequence encoded on the *ade2* gene or *his3* gene in the yeast genome (99), **gRNA scaffold:** gRNA with stem loop for dCas9 binding (105,106), **SUP4 terminator:** terminator with a T7GT6 sequence (159), **ColE1 origin:** origin of replication in *E. coli*, **AmpR:** gene for β-lactamase, mediating ampicillin resistance in *E. coli*, **2μ ori:** origin of replication in yeast.

3.2.4. Additional plasmids utilized for part amplification

For the construction of plasmids and gene constructs, different genes of interest were amplified from certain plasmids. Those plasmids are listed in Table 4. The plasmids pJZC532 and pSLQ1119 were kindly provided by the Zalatan lab. The plasmid pFRP793 (#58434) was received from *addgene*.

Table 4 Plasmids used for GOI part amplification.

Name	Gene of interest
pFRP793	4x *lexA*
pJZC532	3x *tet*O
pSLQ1119	7x *tet*O
pYD_Leu_app8	app8
pET22b	GOase
PCT_2A-GFP	T2A-tGFP
pJZC588/lexA	4x *lexA* in scRNA backbone
pAH013	4x *lexA*_scRNA with ribozymes

3.2.5. Plasmids generated in this study

The plasmids in this chapter are *E. coli* – *S. cerevisiae* shuttle vectors. For the genomic integration into both CasEMBLR loci at the same time, the plasmid pAH006 (5.2) was generated by ligation of the p425-αAde_gRNA and the αHis3_2 gRNA during this study.
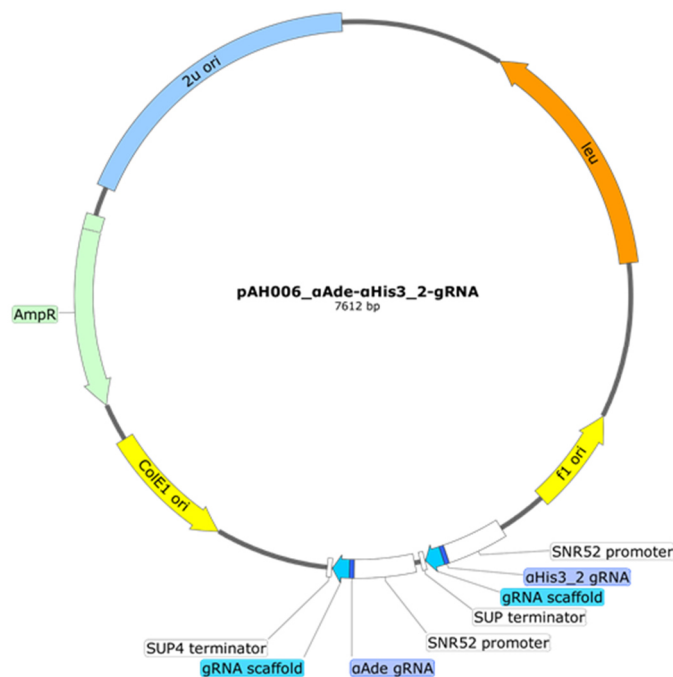
Figure 16 Plasmid map of pAH006.

The plasmid pAH006 contains the following genes: **LEU:** selection marker, **f1 ori:** origin of replication in T7 phage, **SNR52 promotor:** minimal RNA polymerase III promotor for yeast cells, **αAde and αHis3_2 gRNA:** 20 bp long binding region to a sequence encoded on the *ade2* gene or *his3* gene in the yeast genome, **gRNA scaffold:** gRNA with stem loop for dCas9 binding, **SUP4 terminator:** terminator with a T7GT6 sequence, **ColE1 origin:** origin of replication in *E. coli*, **AmpR:** gene for β-lactamase, mediating ampicillin resistance in *E. coli*, **2µ ori:** origin of replication in yeast.

In order to achieve inducibility by ES without the necessity of genetic integration (5.5), the hTF LexA-ER-B112 was integrated on a plasmid named pAH015.
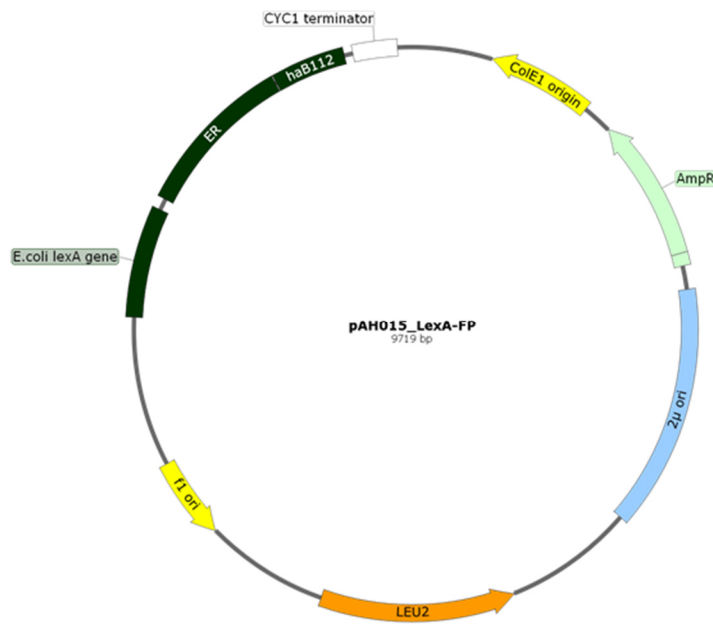
Figure 17 Plasmid map of pAH015.

The plasmid pAH015 contains the following genes: **ColE1 origin:** origin of replication in *E. coli*, **AmpR:** gene for β-lactamase, mediating ampicillin resistance in *E. coli*, **2μ ori:** origin of replication in yeast, **LEU:** selection marker, **f1 ori:** origin of replication in T7 phage, ***E.coli* lexA gene:** bacterial LexA DNA-binding protein, **ER:** hormone-binding domain of the human estrogen receptor, **haB112:** transcriptional activation domain, **CYC1:** terminator sequence.

The plasmid pAH019 contains the genes for a positive feedback loop (5.4).
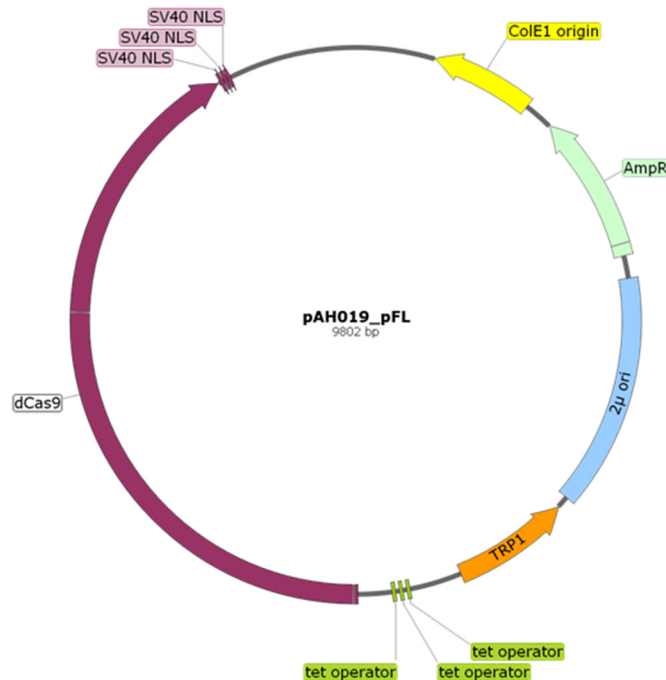
Figure 18 Plasmid map of pAH019.

The plasmid pAH019 contains the following genes: **ColE1 origin:** origin of replication in *E. coli*, **AmpR:** gene for β-lactamase, mediating ampicillin resistance in *E. coli*, **2μ ori:** origin of replication in yeast, **TRP1:** selection marker, ***tet*O:** binding region for scRNA from the Tet-systems (5,58,74), **dCas9:** catalytically inactive Cas9 S. Pyogenes with mutations in the RuvC1 and HNH domains to render it catalytically inactive, **NLS:** Nuclear localization signal.

The plasmid pAH021 contains the genes for an ES inducible scRNA flanked by the ribozymes HH and HDV (5.5). The plasmid is a *E. coli – S. cerevisiae* shuttle vector.
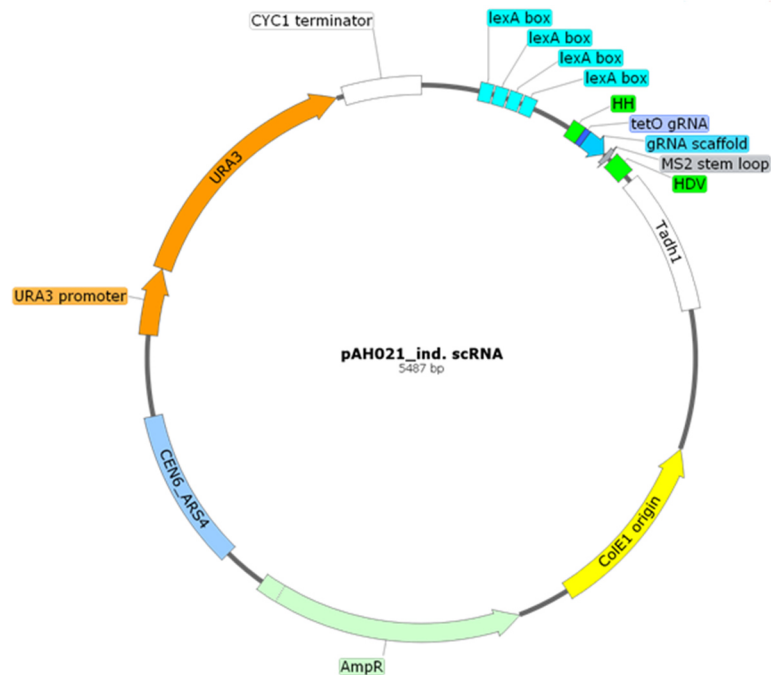
Figure 19 Plasmid map of pAH021.

The plasmid pAH021 contains the following genes: *lexA*: binding region for the hTF LexA-ER-B112 (45), **HH and HDV:** self-cleaving ribozymes, *tet*O gRNA: 20 bp long binding region to the tet Operator, **gRNA scaffold:** gRNA with stem loop for dCas9 binding, **2xms2_ds6:** two copies of the MS2 stem loop (wt, f6) for MCP binding, **Tadh1:** strong terminator derived from *C. Albicans* for RNA polymerase II, **ColE1 origin:** origin of replication in *E. coli*, **AmpR:** gene for β-lactamase, mediating ampicillin resistance in *E. coli*, **CEN/ARS:** autonomously replicating sequence (ARS) and yeast centromere. **URA3:** selection marker.

The plasmids pAH024, pAH025 and pAH026 contain the genes for an ES inducible scRNA, that is either unflanked, flanked by the ribozyme HH or flanked by the ribozyme HDV (5.5). All three plasmids are *E. coli – S. cerevisiae* shuttle vectors.
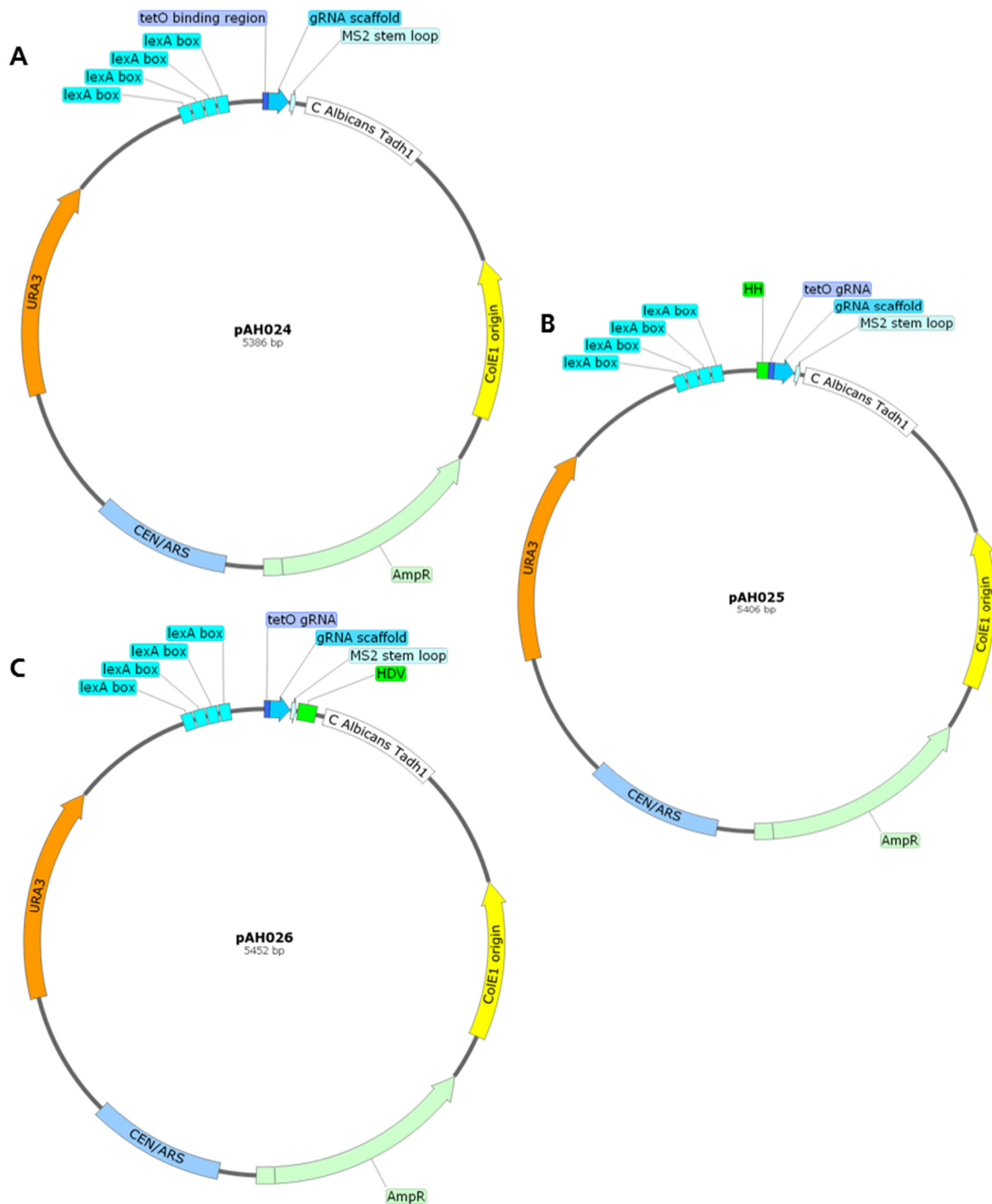
Figure 20 Plasmid maps of *lexA*_scRNA plasmids with different ribozyme setups.

All plasmids, namely pAH024, pAH025 and pAH026 contain the following genes: ***lexA***: binding region for the hTF LexA-ER-B112, ***tet*O gRNA**: 20 bp long binding region to the tet Operator, **gRNA scaffold**: gRNA with stem loop for dCas9 binding, **ms2 stem loop**: MS2 stem loop for MCP binding, **Tadh1**: strong terminator derived from *C. Albicans* for RNA polymerase II, **ColE1 origin**: origin of replication in *E. coli*, **AmpR**: gene for β-lactamase, mediating ampicillin resistance in *E. coli*, **CEN/ARS**: autonomously replicating sequence (ARS) and yeast centromere. **URA3**: selection marker. Depending on the plasmid no ribozyme, only HH or only HDV are present (**HH and HDV**: self-cleaving ribozymes).

3.3. Standard DNA Ladder

DNA size standards

The utilized protein and DNA size standards are listed in Figure 21.
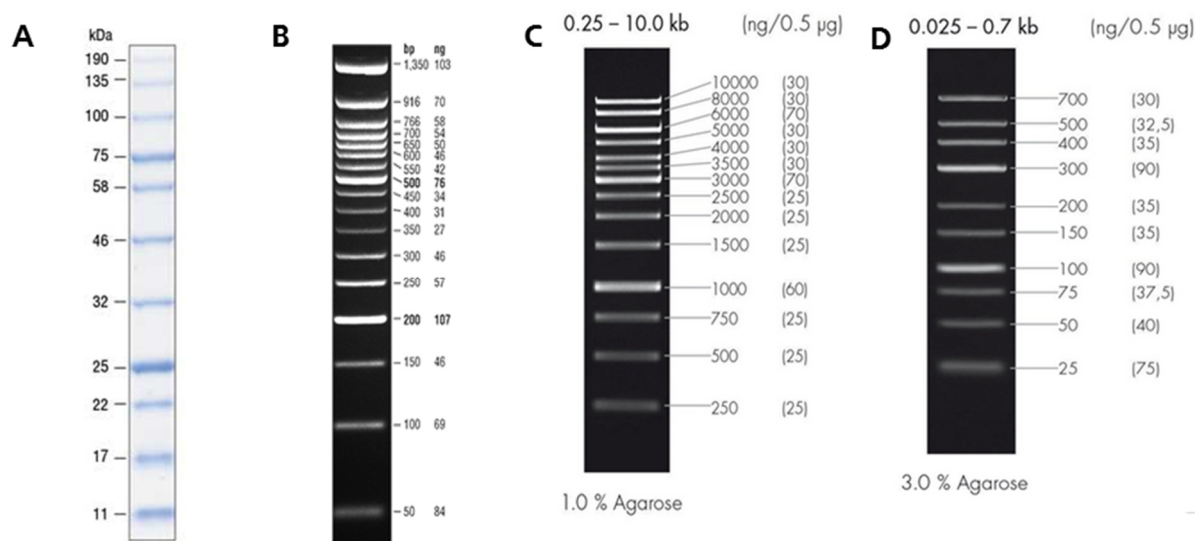
Figure 21 Protein and DNA size standards.

(A) For SDS PAGE, the Blue Prestained Protein Standard, Broad Range (11-190 kDa) (*NEB*) was utilized. For 1 % agarose gels either the 2-Log DNA Ladder (*NEB*) (B) or the 1kb DNA-ladder (*vwr*) (C) were utilized. For 3 % agarose gels the Ultra Low Range DNA-Leiter II, peqGOLD (*vwr*) was utilized.

3.4. Oligonucleotides

The utilized oligonucleotides are listed in Table 5. Oligonucleotides were designed using the SnapGene software (*GSL Biotech*) and synthesized by *Sigma-Aldrich*. Oligonucleotides used for part amplification are marked with a P, oligonucleotides used for colony PCR are marked with a C, oligonucleotides used for sequencing are marked with a S and oligonucleotides used for RNA analysis are marked with a R.

Table 5 List of Oligonucleotides received by *Sigma Aldrich.*

Name	Sequence	Use
A1	GGCATACGATGGAAGAGGTAACTTCGTTGTAAAGAATAAGGAAATGATTC CGGAAGCTTTGGAAGTACTGAAGGATCGTC	P
A3	CTTGAAACTTGAAAACACCGAGTTGATAACCCACACAATTATAAGCAAAG	P
A4	ATTGTACCCCCTTTGCTTATAATTGTGTGGGTTATCAACTCGGTGTTTTC	P
A5	GTTATCCTCCTCGCCCTTGCTCACGCACATCATGGTTGTTTATGTTCGGA	P
A6	TCACATCACATCCGAACATAAACAACCATGATGTGCGTGAGCAAGGGCGA	P
A7	TTTTATTGTCAGTACTGATTATAATTGGCCTTATTGCTCAGCGGTGGCAG	P
A10	AAATGAGCTTCAAATTGAGAAGTGACGCAAGCATCAATGGTATAATGTCCA GAGTTGTGAGGCCTTGGGGCAATTTCGTT	P

A11	GGAAGTACTGAAGGATCGTCCTTTGTACGCCGAAAAATGGGCACCATTTA CTAAAGAATTCGGCCAGTGAATTGTAATAC	P
A12	TGGGCATCTCGAGAGACATTGTATATGAGAGATATCGAATTCCTGCAG	P
A13	GGATCCCCCGGGCTGCAGGAATTCGATATCTCTCATATACAATGTCTCTC	P
A15	AGACGGTAATACTAGATGCTGA	C
A18	ACATACAGAGCACATGCTCT	C
A20	GGCCTTGGGGCAATTTCGTTAATAAGCAATTCCCCTGTTTCTAAATAGAAC ATTTCCACACCCACACAATTATAAGCAAA	P
A25	AGACTATATTTCTTTTCGAGCTCCCTAG	C
A26	AGAAAAGAAAAGTGGGTAGTATGGCTTC	C
A27	AGAAGCCATACTACCCACTTTTCTTTTC	C
A28	TGCATTATGCAATAGACAGCACGAG	C
Cas1	AGCCACGCGGCTCAAAAGAA	C
Cas2	TGCGCAACAGATCTTCTCTG	C
Cas8	CTGATAGGGAGTGGTAAAGGGCCCGGTACCAACGACATTACTATATATAT	P
Cas9	TTCCTATATTATATATATAGTAATGTCGTTGGTACCGGGCCCTTTACCAC	P
Cas10	GATGGCCAGTCCGATAGAATACTTCTTGTCCTCGAGCATCCCGAATTGAT	P
Cas11	AATTACCCGGATCAATTCGGGATGCTCGAGGACAAGAAGTATTCTATCGG	P
Cas12	ATTAACCCTCACTAAAGGGAACAAAAGCTGCACACAATTATAAGCAAAGG	P
Cas13	GATTGTACCCCCTTTGCTTATAATTGTGTGCAGCTTTTGTTCCCTTTAGT	P
Cas14	GCAAATTTCGTCAAAAATGCTAAGAAATAGAGACGAAAGGGCCTCGTGAT	P
Cas15	AAATAGGCGTATCACGAGGCCCTTTCGTCTCTATTTCTTAGCATTTTTGA	P
dCAS_fw_Colony PCR	TGACGAGTACAAGGTGCCCT	C
fw_gene-gene_lexA FP	CCAGGCAACAAGAGGTGTTT	C
fw_genomic int._leu-dCas Plasmid	GTGGAAGCTGAAACGCAAGG	C
fw_lexA+scRNA_ ColonyPCR	TTCTTTTCGAGCTCCCTAGG	C
fw_lexA+scRNA_ ColonyPCR	TTCTTTTCGAGCTCCCTAGG	C, S
gRNA_fw_Colony PCR	GCTCTTCCTGCTCTCAGGTA	C
gRNA_rv_Colony PCR	TAGCGGCTTAACTGTGCCCT	C
gRNA5	GCGCGCGTCGACTCTTTGAAAAGATAATG	P
gRNA6	GCGCGCAAGCTTAGACATAAAAAACAAAAAAAGCACCACCGAC	P
gRNA7	CCCAGTCACGACGTTGTAAAACG	C, S
gRNA8	GGAAACAGCTATGACCATG	C
H1	CGATCTTCCCAGAAAAAGAGGCAGAAGCAGTAGCAGAACAGGCCACACAA TCGCAAGTGATTAACGTCCACACAGGTATA	P
H2	TTAACGTCCACACAGGTATAGGGTTTCTGGACCATATGATACATGCTCTGG CCAAGCATTGGTACCGGGCCCTTTACCAC	P
H3	TTAACGTCCACACAGGTATAGGGTTTCTGGACCATATGATACATGCTCTGG CCAAGCATTGGTACCCGGGCCCTTAATTCGC	P

H6	AAGGCGCAAATCCTGATCCAAACCTTTTTACTCCACGCACGGCCCCTAGGG CCTCTTTAAGAGTGTAAACTGCGAACCTT	P
H7	CGACAACTGCGTACGGCCTGTTCGAAAGATCTACCACCGCTCTGGAAAGT GCCTCATCCAAAGGCGCAAATCCTGATCCA	P
H8	TCCAATTCGCCCTATAGGCGGCCGCTGTTTCGCCAACCAAGTATTTCGG	P
H9	GTTCAGGCACTCCGAAATACTTGGTTGGCGCGCCTATAGGGCGAATTGGA	P
H10	CCCGTTCCTCCATCTCTTTT	C
H11	TGCCAGGTATCGTTTGAACA	C
H12	ACCTTCACCGGAGACAGAAA	C
H14	CGATCCAGTTGCTGAAAGAA	C
H16	AACTGCAGTAAAAAATTGAAGGAAATCTCATCTCGAGCATCCCGAATTGAT	P
H17	AATTACCCGGATCAATTCGGGATGCTCGAGATGAGATTTCCTTCAATTTT	P
H18	CATATGACGACCTTCGATATGGCCGCTGCTTCTTTTATCGAGTTGATACCC	P
H19	AAAGAAGAAGGGGTACAACTCGATAAAAGAAGCAGCGGCCATATCGAAGG	P
H29	TGTCGGTGTTTGTTCAAGCCGTGCGGCCATTCTTTTATCGAGTTGTACCC	P
H30	AAAGAAGAAGGGGTACAACTCGATAAAAGAATGGCCGCACGGCTTGAACA	P
H33	GCCGCAGGTCAGCAGGCTGCCGCGGCCCTCCTGAGTAACGCGAATCGTCG	P
H34	AGTGTGGCTTCGACGATTCGCGTTACTCAGGAGGGCCGCGGCAGCCTGCT	P
H35	GCGGTGGAGCTCCAATTCGCCCTATAGGCGAATTCTCTTAGGATTCGATT	P
H36	GATGAATGTGAATCGAATCCTAAGAGAATTCGCCTATAGGGCGAATTGGA	P
H41	TGCCGCGGCCCTCGTGGTGGTGGTGGTGGTGTTTCACAGTCAGAATGGTC C	P
H42	TCTGACTGTGAAACACCACCACCACCACCACGAGGGCCGCGGCAGCCTGC T	P
H43	AGACACGCAAACACAAATACACACAC	C
H44	ACCATTCAGGGTGCCGGTAATAC	C
lexA FP 7	CGCGTGTACGCATGTAACAT	C
lexA FP 8	GAGGTGTGGAGACAAATGGT	S
lexA FP 13	TCCTTCTAGTGTAGCCGTAG	C
lexA lo1	CCTTATTTTAACTTGCTATTTCTAGCTCTAAAACTATCAGTGATAGAGAAA AGTGATATCGAATTCCTGCAG	P
lexA up	GAATTGTAATACGACTCACTATAGGGCGAATTGGAGCTCACTCGGCGGCC GCAATAATATATAAACCTGTA	P
oAH003	TCATAACTGCAAAGTACACA	C
oAH004	CTGAATCAAAGAGGAGAGCT	C, S
oAH005	GTTTTGGGACGCTCGAAGGCTTTAATTTGCTGTGCTGCAAGGCGATTAAG	P
oAH006	ATTAACCCTCACTAAAGGGAACAAAAGCTGAATTCAGAAACTTTGACAAA	P
oAH007	CAGCTTTTGTTCCCTTTAGT	C
oAH007	CAGCTTTTGTTCCCTTTAGT	C
oAH009	AACTAAAAAACTGTATTATAAGTAAATGCATCATGTAATTAGTTATGTCA	P
oAH010	CGTTACCCAACTTAATCGCCTTGCAGCACAGCAAATTAAAGCCTTCGAGC	P
oAH011	GTGGTCTCTACAGGATCTGA	S
oAH019	CTGATGAGTCCGTGAGGACG	R

oAH020	ACTTTTCTCTATCACTGATAGTTTTAGAGCT	R
oAH021	AAAAGCACATGGGTGATCCT	R
oAH022	GTCCCATTCGCCATGCC	R
oAH025	CTTCTATACTAGTGGATCCCCCGGGCTGCAACTTTTCTCTATCACTGATA	P
oAH026	TATAATTTAGCTATTTGCTTAGAGCTCCACGGGAAGACTCCCCAGTGACT	P
oAH027	CTTCTATACTAGTGGATCCCCCGGGCTGCAGGAAAAGTCTGATGAGTCCG	P
oAH028	TAATTTAGCTATTTGCTTAGAGCTCCACCGAAAAGCACATGGGTGATCCT	P
oAH029	ATAATTTAGCTATTTGCTTAGAGCTCCACCGAGCTCCACCGCGGTGGCGG	P
oAH031	CGCACTCACGTAAACACTTA	C, S
oAH066	TTTACCAGTTAAAGTTTTAACGAAAATCTGCTCGAGCATCCCGAATTGAT	P
oAH067	AATTACCCGGATCAATTCGGGATGCTCGAGCAGATTTTCGTTAAAACTTT	P
oAH068	GGGTGCCGGTAATACGACATTCAATTTCCATTGATCTCTGCATTAAAGAGT	P
oAH069	GCCTTGGCAGACTCTTTAATGCAGAGATCAATGGAAATTGAATGTCGTAT	P
rv_copynumber_dCas-dCas Plasmid	GGTTCTCTTCAAAGAGCTGG	C
rv_gene-gene_lexA FP	TTATCGTTGCCCGGCAGATC	C
rv_genomic int._leu-dCas Plasmid	ATATGCGTCAGGCGACCTCT	C
rv_lexA+scRNA_ColonyPCR	GGGAACGCCTGGTATCTTTA	C, S
scRNA31	TACAGAATAGCAGAATGGGC	C
scRNA32	CTTGCTATTTCTAGCTCTAA	C
scRNA33	TCTATACTAGTGGATCCCCCGGGCTGCAGGAAAAGTCTGATGAGTCCGTG	P
scRNA34	ATTAACCCTCACTAAAGGGAACAAAAGCTGAATTCAGAAACTTTGACAAA	P
204 ura3_in	CAGCCTGCTTTTCTGTAACG	R
205 ura3_out	GGAAGAGATGAAGGTTACG	R

3.5. Enzymes and Proteins

The utilized enzymes and polymerases are listed in Table 6.

Table 6 List of enzymes and polymerases used in this study.

Name	Supplier
Anti-Mouse IgG (whole molecule)-Alkaline Phosphatase antibody (from goat)	*Sigma Aldrich*
*Apa*I	*New England Biolabs*
*Hind*III-HF	*New England Biolabs*
*Kpn*I	*New England Biolabs*
M-MuLV reverse transcriptase	*New England Biolabs*
monoclonal Penta-His antibody (from mouse)	*Quiagen*
One*Taq*®	*New England Biolabs*
Phusion® High-Fidelity DNA Polymerase	*New England Biolabs*
*Pac*I	*New England Biolabs*

*Pme*I	*New England Biolabs*
Q5® High-Fidelity DNA Polymerase	*New England Biolabs*
*Sal*I-HF	*New England Biolabs*
T4 DNA Ligase	*New England Biolabs*
Taq DNA polymerase	*New England Biolabs*
TURBODNase	*Life Technologies, USA*
TURBODNase buffer	*Life Technologies, USA*

3.6. Kits for DNA preparation

The utilized kits are listed in Table 7

Table 7 Kits for DNA preparation utilized in this work.

Name	Supplier
PureYield™ Plasmid Midiprep System Kit	*Promega*
PureYield™ Plasmid Miniprep System Kit	*Promega*
Wizard® SV Gel and PCR-Clean up System	*Promega*
Zymoprep™ Yeast Plasmid Miniprep II	*Zymoresearch*
Frozen-EZ Yeast Transformation II Kit ™	*Zymoresearch*

3.7. Cultivation media

The utilized cultivation media are listed in Table 8. The cultivation media for yeast and bacteria was sterilized for 20 min at 121 °C. In cases where agar plates were prepared, 1.5 % (w/v) agar-agar powder was added. When required, antibiotics were added after sterilisation. The ingredients were solubilized in 9/10 of the total volume and autoclaved for all utilized yeast media. Glucose/galactose, yeast nitrogen base and amino acids were solubilised in 1/10 of the total volume, sterile filtrated and added afterwards. The amino acid drop-out powder was mixed according to the requirements for the drop-out media or plates (Table 9).

Table 8 Composition of cultivation media.

Media	Substances
Double concentrated Yeast Tryptone (dYT) medium	1.0 % (w/v) yeast extract
	1.6 % (w/v) tryptone
	0.5 % (w/v) sodium chloride
	1 L ddH2O
SD media	2.0 % (w/v) glucose
	0.5 % (w/v) ammonium sulfate
	0.17 % (w/v) Yeast Nitrogen Base
	0.13 % (w/v) amino acid powder containing all aa
	0.54 % (w/v) Na2HPO4
	0.86 %(w/v) NaH2PO4 × H2O
SD drop-out media	2.0 % (w/v) glucose

	0.5 % (w/v) ammonium sulfate
	0.17 % (w/v) Yeast Nitrogen Base
	0.13 % (w/v) amino acid drop-out powder
	0.54 % (w/v) Na2HPO4
	0.86 %(w/v) NaH2PO4 × H2O
SG drop-out media	2.0 % (w/v) galactose
	0.5 % (w/v) ammonium sulfate
	0.17 % (w/v) DifcoTM Yeast Nitrogen Base
	0.13 % (w/v) amino acid drop-out powder
	0.54 % (w/v) Na2HPO4
	0.86 % (w/v) NaH2PO4 × H2O
YPD	2.0 % (w/v) glucose
	2.0 % (w/v) Trypton
	1.0 % (w/v) Yeast extract

Table 9 Composition of amino acid drop-out powder.

Substance	Concentration for drop out powder
Adenine hemisulfate	40 mg/L
L-Arginine	20 mg/L
L-Aspartic acid	100 mg/L
L-Glutamic acid	100 mg/L
L-Histidine	20 mg/L
L-Leucine	60 mg/L
L-Lysine	30 mg/L
L-Methionine	20 mg/L
L-Phenylalanine	50 mg/L
L-Serine	375 mg/L
L-Threonine	200 mg/L
L-Tryptophan	40 mg/L
L-Tyrosine	30 mg/L
L-Valine	150 mg/L
Uracil	20 mg/L

3.8. Buffers and Solutions

The utilized buffer and solutions are listed in Table 10.

Table 10 Buffers and Solutions used in this work.

Name	Composition
A	
AE buffer	50 mM NaAc, pH 5.3, 10 mM EDTA
Ammonium acetate solution	7 M ammonium acetate
Ampicillin stock solution (1000x)	100 mg/mL ampicillin (sodium salt)
AP buffer	100 mM TrisHCl (pH 9.1), 50 mM MgCl2 100 mM NaCl
APS stock solution	10 % APS
B	
Buffer E	1.2 g/L Tris, 92.4 g/L Saccharose, 0.2 g/L MgCl2
C	
Chloramphenicol stock (1000x)	25 mg/ml chloramphenicol in 96 % ethanol
Coomassie Brilliant Blue staining	10 % (v/v) solution acetic acid, 40 % (v/v) methanol, 0.25 % (w/v) Coomassie Brilliant Blue R250
Coomassie destaining solution 1	10 % (v/v) Acetic acid, 25 % (v/v) Isopropanol
Coomassie destaining solution 2	10 % (v/v) Acetic acid
D	
DNA-loading dye (6x)	10 mM Tris-HCl (pH 7.6), 0.03 % (w/v) bromo-phenol blue, 0.03% (w/v) xylene cyanol FF, 60 mM EDTA
I	
IMAC buffer A	50 mM Tris-HCl (pH 7.5), 600 mM NaCl, 10 mM Imidazol
IMAC buffer B	50 mM Tris-HCl (pH 7.5), 600 mM NaCl, 1 mM Imidazol
N	
Native PAGE sample buffer (2x)	62.5 mM Tris-HCl pH 6.8, 25 % glycerin, 1 % Bromophenol Blue
Native PAGE running buffer	25 mM Tris, 192 mM glycerin
Native western blot - buffer A	300 mM Tris, 5 % Methanol
Native western blot - buffer B	25 mM Tris, 5 % Methanol
Native western blot - buffer C	25 mM Tris, 40 mM 6-aminocaproic acid, 5 % Methanol
Native western blot - Chloronaphthol	3 mg/mL 4-CN in Ethanol
P	
Phosphate buffered saline (PBS)	140 mM NaCl, 10 mM KCl, 6.4 mM Na2HPO4, 2 mM K2PO4
PBS-B	0.1 % (w/v) BSA in 1x PBS
PBS-T	0.05 % (v/v) Tween® 20 in 1xPBS
PBS-TM	5 % (w/v) milk powder in 1x PBS-T
S	
SDS-PAGE Running buffer	50 mM Tris-HCl pH 8.8, 190 mM glycerin; 1 g/L SDS
T	
TAE buffer (50x)	2M Tris-HCl, 1 M acetic acid (conc.), 50 mM EDTA, pH 8.0
Tris-HCl	1 M Tris, pH 8 with HCl
W	
Western blot transfer buffer	25 mM Tris, 192 mM Glycin, 20 % Methanol

3.9. Chemicals

The utilized chemicals are listed in Table 11.

Table 11 List of chemicals used in this work.

Name	Supplier
A	
α-D(+) glucose	*Carl Roth GmbH & Co. KG*
α-D(+) galactose	*Carl Roth GmbH & Co. KG*
Acrylamide/Bisacrylamide (37,5:1)	*Carl Roth GmbH & Co. KG*
Agar-Agar, Kobe I	*Carl Roth GmbH & Co. KG*
Agarose	*Carl Roth GmbH & Co. KG*
Ammonium acetate	*Carl Roth GmbH & Co. KG*
Ammonium sulfate	*Carl Roth GmbH & Co. KG*
Ammonium persulfate (APS)	*Merck Millipore*
Ampicillin (sodium salt)	*Carl Roth GmbH & Co. KG*
B	
Bacto™ Casamino Acids	*BD (Becton, Dickinson and Company)*
β-Estradiol	*Sigma-Aldrich Co. LLC*
β-Mercaptoethanol	*Carl Roth GmbH & Co. KG*
Bromophenol blue	*Carl Roth GmbH & Co. KG*
5-bromo-4-chloro-3'-indolyphosphate (BCIP)	*Carl Roth GmbH & Co. KG*
C	
Chloramphenicol	*Carl Roth GmbH & Co. KG*
Coomassie Brilliant Blue-R250 and G-250	*Carl Roth GmbH & Co. KG*
CutSmart®-Buffer (10x)	*New England Biolabs*
D	
Difco™ Yeast Nitrogen Base	*BD (Becton, Dickinson and Company)*
Dimethyl sulfoxide (DMSO)	*Carl Roth GmbH & Co. KG*
Dithiothreitol (DTT)	*Carl Roth GmbH & Co. KG*
dNTP mix	*New England Biolabs*
Doxycycline hydrochloride	*Sigma-Aldrich Co. LLC.*
Dry milk powder (DMP)	*Carl Roth GmbH & Co. KG*
E	
EDTA	*Carl Roth GmbH & Co. KG*
Ethanol	*Carl Roth GmbH & Co. KG*
G	
Glycerin	*Carl Roth GmbH & Co. KG*
H	
HCl (conc., 37%)	*Carl Roth GmbH & Co. KGintas*
HD Green Plus DNA stain	*Intas-Science-Imaging Instruments GmbH*
Horseradish peroxidase	*Merck Millipore*
I	
Isopropanol	*Carl Roth GmbH & Co. KG*

M	
Magnesium chloride	*Carl Roth GmbH & Co. KG*
Methanol	*Thermo Fisher Scientific Inc.*
milk powder	*Carl Roth GmbH & Co. KG*
N	
Nitro blue tetrazolium chloride (NBT)	*Carl Roth GmbH & Co. KG*
P	
Phenol (Roti Aqua Phenol)	*Carl Roth GmbH & Co. KG*
Phenol/Chloroform/Isoamyl alcohol, 25:24:1 (PCI)	*Carl Roth GmbH & Co. KG*
5X Phusion HF buffer	*New England Biolabs*
S	
Sodium chloride	*Carl Roth GmbH & Co. KG*
Sodium dodecyl sulfate (SDS)	*Carl Roth GmbH & Co. KG*
R	
Random Hexamer (RHX)	*Sigma-Aldrich Co. LLC.*
T	
Tetramethylethylenediamine (TEMED)	*Sigma-Aldrich Co. LLC.*
ThermoPol buffer (10x)	*New England Biolabs*
Tris(hydroxymethyl)aminomethan (Tris)	*Carl Roth GmbH & Co. KG*
Tryptone/Peptone	*Carl Roth GmbH & Co. KG*
Tween®20	*Carl Roth GmbH & Co. KG*
Y	
Yeast extract	*Carl Roth GmbH & Co. KG*

3.10. Equipment

The utilized equipment is listed in Table 12.

Table 12 List of equipment used in this work.

Equipment	Model	Supplier
A		
Accuri™	C6 Flow Cytometer	*BD (Becton, Dickinson and Company)*
Adhensive foil		*VWR*
ÄKTA Purification System		*Amersham Pharmacia Biotech*
Amicon® Ultra-15 centrifugal filter units	MWCO 3 kDa	*Merck Millipore*
Autoclave	HAST 4-5-6	*Zirbus Technologies*
Autoclave	V-150	*Systec*
C		
Centrifuge	Biofuge pico	*Heraeus*
Centrifuge	Multifuge 3L-R	*Heraeus*
Centrifuge	6K15	*Sigma-Aldrich*
Centrifuge	Centrifuge 5427 R	*Eppendorf*
Countertop centrifuge	ScanSpeed mini	*Eppendorf*

Countertop centrifuge	centrifuge 5415 D	*Eppendorf*
Cover slides	20 x 60 mm	*Carl Roth GmbH & Co. KG*
E		
Electrophoresis Power Supply	301 and 601	*Amersham, Pharmacia Biotech*
Electrophoresis Power Supply	250/2.5	*Bio-Rad*
Electroporation device	Gene Pulser Xcell	*Biorad*
Electroporation vials		*Biorad*
F		
FACS	Influx	*BD (Becton, Dickinson and Company)*
FACS tubes	5 mL	*BD (Becton, Dickinson and Company)*
FACS Laser	Sapphire	*Coherent*
FACS Laser	56CLC100	*CVI Melles Griot*
Falcon™ tubes	15 and 50 mL	*Sarstedt*
Filter (sterile filter)	20 μm pore size	*Millipore*
Freezer (-80°C)	VIP™ Series	*Sanyo*
Freezer (-20°C)	Economic Froster	*Bosch*
G		
Glassware		*Schott; VWR; Merck KGaA*
Gloves (latex and nitrile)		*B. Braun*
Gel analysis software	Gel Jet Imager	*INTAS*
Gel chambers		*Hoefer*
Gel chambers	HU10	*Scie-Plas*
Gel documentation UV	GelDoc-It® 310 imaging system	*UVP INTAS*
H		
Heating block	Thermomixer compact	*Eppendorf*
HisTrap HP column		*GE*
I		
Ice machine	SP125 AS	*NordCap*
Ice machine	AF80	*Scotsman*
IMAC-column		*Quiagen GmbH*
Incubator (shaker)	Certomat BS-1	*Sartorius*
Incubator	Incucell	*Medcenter Einrichuntgen GmbH*
Incubator (shaker)	WiseCube®	*WISD Laboratory Instruments*
Incubator (shaker)	G25	*New Brunswick Scientific Co.*
Incubator (shaker)	Titramax 1000 and Incubator 1000	*Heidolph*
M		
Magnetic stirrer	IKAMAK RCT	*IKA-Labortechnik*
Microfluidic Microscope	Eclipse TI	*Nikon*
Microfluidic camera	ORCA Flash4.0	*Hamamatsu*
Microfluidic light source	SpectraX	*Lumencor*
Microscope slides	76 × 26 mm	*Carl Roth GmbH & Co. KG*
Microwave	Micro700	*Hitachi*
N		

Nanodrop	Biospec Nano™	*Shimadzu Europe GmbH*
Nanodrop	ND-1000 Spekrtophotometer	*PeqLab*
nitrocellulose membrane	0.48 μm	*Amershan™ Protran™*
P		
Parafilm "M" laboratory film	Kimwipes	*Pechiney Plastic Packaging*
Paper towels		*Kimberley-Clark*
Paper towels, green	Mastercycler standard	*Sarstedt*
PCR machine	T100™ *Thermal Cycler*	*Eppendorf*
PCR machine	Multiply®-μStrip	*Bio-Rad*
PCR tubes	PYPF	*Sarstedt*
Petri dishes	BioPhotometer	*Sarstedt*
pH meter	Pipetus R Standard	*Sartorius*
Photometer	Trans-Blot® Turbo™ Transfer System	*Eppendorf*
Pipetting controller		*Hirschmann Laborgeräte*
Protein-Blotting device		Biorad
R		
Reaction tubes	1.5 and 2 mL	*Sarstedt*
S		
Sterile workbench	Unihood	*Clean Air Technik B.V.*
Sterile workbench	Safe2020	*Thermo Fisher Scientific Inc.*
T		
Tecan reader	INFINITE Tecan M-1000	*Tecan*
U		
UV cuvettes		*Sarstedt*
V		
Vortex	Eurolab	*Merck*

3.11. Computer Software

The utilized software is listed in Table 13.

Table 13 Computer software utilized in this work.

Name	Supplier
ApE	*Tangient LLC*
BD FACS Software v1.0	*BD (Becton, Dickinson and Company)*
Fiji	*Fiji team*
Flowing software (version 2.5.1)	*Turku Centre for Biotechnology of Turku*
Inkscape	*The Inkscape Project*
Mathematica II software	*Wolfram*
Matlab	*The MathWorks, Inc*
Microsoft Office Standard 2019	*Microsoft Corporation*
SnapGene software	*GSL Biotech*
T-Coffee	*European Bioinformatics Institute (EMBL-EBI)*

4. Methods

4.1. Microbiological methods

4.1.1. Cultivation and storage of *E. coli* cells

E. coli cells were grown either in liquid dYT media or on dYT agar plates. *E. coli* cells were incubated at 37 °C for up to 24 h and stored a 4 °C. Liquid *E. coli* cultures were shaken at 180 rpm. The optical density was controlled spectrophotometrically at OD_{600}. For long term storage the cell suspension was stored at -80 °C after addition of 10 % DMSO (v/v).

4.1.2. Generation and transformation of electrocompetent *E. coli* cells

Two different strains were used for *E. coli* transformation: DH5α or TOP10 (preferred for large plasmids >8000 bp). Therefore, 50 mL dYT media were inoculated with cells of an overnight culture towards an OD_{600} of 0.1 and grown at 37 °C until an OD_{600} of 0.5-0.7 was reached. Subsequently the cell suspension was transferred into a 50 mL Falcon™ tube and centrifuged at 4000 rpm at 4 °C for 10 min. Afterwards the cells were washed with decreasing volumes of ice-cold ddH_2O (50 mL, 20 mL, 10 mL) and the pellet was suspended in 1 mL ice-cold ddH_2O. For transformation 100 μL of the prepared cell suspension were incubated with $0.1 - 3\,\mu g$ DNA for up to 10 min on ice. 1μL was used for bacterial plasmid DNA and 3 μL were used for yeast plasmid DNA. The transformation was performed in a pre-chilled electroporation cuvette *via* electroporation at room temperature for 4 ms at 200 Ω, 2.5 kV and 25 μF. 1 mL dYT media was immediately added. Following the cell suspension was transferred to a new reaction tube and incubation was performed at 37 °C for 1 h. After incubation, cells were transferred to dYT plates containing the corresponding antibiotics and incubated overnight at 37 °C.

4.1.3. Isolation of plasmid DNA from *E. coli*

For isolation of plasmid DNA from *E. coli*, cells were grown shaking at 37 °C overnight. The *PureYield*™ Plasmid Miniprep System Kit (*Promega*) was used for the isolation of plasmid DNA out of 5 mL of the fresh *E. coli* cultures, whereas the *PureYield*™ Plasmid Midiprep System Kit (*Promega*) was used for 50 mL *E. coli* culture. The concentration of the isolated plasmid DNA was measured at 260 nm using the BioSpec Nano™ photometer (*Shimadzu*). The plasmid DNA storage temperature was -20 °C.

4.1.4. Cultivation and storage of *Saccharomyces cerevisiae* cells

Cultivation of *S. cerevisiae* was performed in liquid YPD or SD media at 30 °C and 180 rpm until an appropriate optical density was reached. Cultivation on YPD agar plates or SD agar plates was performed for 48 h at 30 °C. In case of short-term storage cells were kept at 4 °C. For long-

term storage cells were pelleted for 5 min at 4000 rpm, suspended in PBS, mixed 1:1 with 50 % glycerol (v/v) and stored at -80 °C.

4.1.5. Generation and transformation of electrocompetent *S. cerevisiae* cells

Cells of an overnight culture of the corresponding strain were used to inoculate 50 mL of YPD or SD drop-out media towards an OD_{600} of 0.3. Cells were grown at 30 °C until they reached an OD_{600} of 1.3-1.5 and were subsequently incubated with 500 μL of 0.39 g/mL DTT dissolved in Tris-HCl for 15 min at 30 °C and 180 rpm. Afterwards the cell suspension was transferred into a 50 mL Falcon™ tube and centrifuged at 4000 rpm at 4 °C for 5 min. The cells were washed with decreasing volumes of ice-cold buffer E (40 mL, 15 mL, 1 mL). After the final centrifugation step, the pellet was suspended in 1 mL of ice-cold buffer E. 100 μL of the prepared cell suspension were used for each transformation. Cells were incubated with 0.5 – 2 μg DNA for up to 10 min on ice. Transformation was performed *via* electroporation in a pre-chilled electroporation cuvette at room temperature for 4 ms at 200 Ω, 2.5 kV and 25 μF. Subsequently, 1 mL of YPD media was added and the cell suspension was transferred to a new reaction tube. Cells were grown at 30 °C for 1 h, transferred to the corresponding SD drop-out-plates and incubated for 48 – 120 h at 30 °C.

4.1.6. Generation and transformation of chemo competent *S. cerevisiae* cells

Chemo competent cells were obtained, following the instructions of the *Frozen-EZ Yeast Transformation II Kit™* from *Zymoresearch*. Therefore, cells of an overnight culture of the corresponding strain were used to inoculate 15 mL of YPD or SD media towards an OD_{600} of 0.3. All transformation steps were performed following the manual. 5 μL of precipitated DNA were added for transformation. Cells were grown for two hours after transformation. Afterwards the samples were centrifuged to remove most of the supernatant. Cells were suspended in the remaining supernatant, transferred to the corresponding SD drop-out-plates and incubated for 48 – 120 h at 30 °C.

4.1.7. Gap repair by HR in *S. cerevisiae* for plasmid generation

Gap repair is a fast and efficient method that uses the capacity of *S. cerevisiae* to perform homologous recombination in order to assemble recombinant DNA fragments or parts *in vivo*. For most gap repair approaches a plasmid backbone carrying an ori and selection marker is assembled with one or more linear DNA fragments (160).

In this work, gap repair was used to assemble various plasmids (3.2.5). Therefore, the DNA fragments were amplified by PCR and purified using the *Wizard®* SV Gel and PCR-Clean up System (*Promega*). The DNA concentration was determined at 260 nm using the

BioSpec Nano™ photometer (*Shimadzu*) and 4 pM of each insert fragment was mixed with 1 μg backbone DNA., which was concentrated by ammonium acetate-ethanol precipitation (0) and resuspended in 5 μl of ddH$_2$O. For transformation the chemical competent cSLQ.sc002 cells (4.1.6) were used. After transformation the cells were grown on the corresponding SD drop-out agar plates at 30 °C for 48 h.

4.1.8. Isolation of plasmid DNA from *S. cerevisiae* cells

For isolation of plasmid DNA from *S. cerevisiae*, cells were grown shaking at 30 °C overnight. Usually, 2 mL of the fresh yeast culture were used for the isolation of plasmid DNA with the *Zymoprep*™ Yeast Plasmid Miniprep II Kit (*Zymoresearch*). 3 μL of the isolated plasmid DNA were directly used for transformation into freshly prepared electrocompetent *E. coli* cells. The remaining plasmid DNA was stored at -20 °C.

4.2. Molecular biological methods

4.2.1. Polymerase chain reaction (PCR)

When the amplification or modification of DNA *in vitro* was demanded, polymerase chain reaction (PCR) was accomplished (161). For DNA amplification the commercially available Phusion® High-Fidelity DNA Polymerase (*New England Biolabs*), Q5® High-Fidelity DNA Polymerase (*New England Biolabs*) or Taq/OneTaq® DNA polymerase (*New England Biolabs*) were used. A representative reaction mixture for each polymerase can be seen in Table 14. Primers were ordered in a concentration of 0.025 μmole from *Sigma Aldrich* in form of powder. The protocol for the PCR reactions regarding the utilized polymerase are listed in Table 15. The annealing temperature was adjusted to the primers according to the Tm calculator from *New England Biolabs* (162).

Table 14 Reaction mixtures for PCR utilized in this work, depending on polymerase.

Substance	Phusion®	Q5®	Taq/One*Taq*®
Template DNA (1ng-1μg)	1 μL	1 μL	1 μL
Primer forward (10 μM)	2.5 μL	2.5 μL	1 μL
Primer reverse (10 μM)	2.5 μL	2.5 μL	1 μL
dNTP-Mix (10 mM)	1 μL	1 μL	1 μL
Reaction buffer (5x)	10 μL	10 μL	10 μL
Polymerase	0.5 μL	0.5 μL	0,25 μL
ddH2O	33 μL	33 μL	36 μL
Total volume	50 μL	50 μL	50 μL

Table 15 Protocol for a standard PCR prepared with Phusion® HF DNA Polymerase, Q5® High-Fidelity DNA Polymerase or Taq/One*Taq*® DNA polymerase DNA polymerase.

	Phusion®		Q5®		Taq/One*Taq*®		
Step	Temperature	Duration	Temperature	Duration	Temperature	Duration	Repeats
Initial denaturation	98 °C	30 sec	98 °C	30 sec	94 °C	30 sec	1
Denaturation	98 °C	10 sec	98 °C	10 sec	94 °C	30 sec	30
Annealing	45-72 °C	30 sec	50-72 °C	30 sec	45-68 °C	30 sec	30
Elongation	72 °C	15-30 sec/kb	72 °C	20-30 sec/kb	68 °C	1 min/kb	30
Final Extension	72 °C	5-10 min	72 °C	2 min	68 °C	5 min	1
Hold	10 °C	∞	10 °C	∞	10 °C	∞	

RT PCR

Roof tile PCR was performed, when 120 bp were added to one side of a DNA part in order to allow *in vivo* assembly and genomic integration by CasEMBLR (2.4.2) (99). Since the efficiency and accuracy of PCR is reduced due to the usage of relatively long primers, the 120 bp were added in a two-step PCR with an elongation of 60 bp each round. In the first step, the inner primers were diluted 1/10 and only 10 cycles of denaturation, annealing and elongation were performed. The second step was performed immediately, using the PCR mix of step one. The outer primers were added undiluted and 30 cycles were run for denaturation, annealing and elongation. Either Phusion® High-Fidelity DNA Polymerase (*New England Biolabs*) or Q5® High-Fidelity DNA Polymerase (*New England Biolabs*) were used as polymerase.

Colony PCR

Colony PCR was performed to verify correct transformation. For *S. cerevisiae* colony PCR, fresh yeast colonies were used. Cell material of a single colony was added with a pipette tip into a PCR tube filled with 20 μL of 0,02 M NaOH. To break the cells and release the DNA for following amplification, the cell suspension was heated for 20 min at 98 °C. For *E. Coli* colony PCR cell material of a single colony was added with a pipette tip into a PCR tube filled with 10 μL of ddH2O and boiled for 10 min. After boiling, 1 μL of the boiled cell suspension served as template for the colony PCR and was added to the premixed PCR mixture. The commercially available OneTaq® DNA polymerase (*New England Biolabs*) was used as polymerase.

4.2.2. Restriction digestion

Restriction digestion was prepared for two reasons, first to verify the correct size of a plasmid and second to linearize a plasmid for cloning experiments. The digestion mixtures can be found

in Table 16 named as small digestion mixture for simple size validation or pre-experiments and large digestion mixture for actual cloning experiments. The digestion was accomplished for one to four hours at 37 °C.

For further usage the enzymes were heat inactivated at 65 °C or 80 °C, if possible. The digested plasmids were purified using the *Wizard®* SV Gel and PCR-Clean up System (*Promega*) (4.2.5).

Table 16 Mixtures for restriction digestion utilized in this work.

Substance	Small digestion mixture	Large digestion mixture
Plasmid DNA	2 μL	20 μg
Buffer (CutSmart®-Buffer (1x))	2 μL	5 μL
Restriction enzyme	0.5 μL	2 μL
(Restriction enzyme 2)	(0.5 μL)	(2 μL)
ddH2O	Add to 20 μL	add to 50 μL

4.2.3. DNA Ligation

For ligation, two DNA fragments were used that were digested with the required restriction enzymes. The amounts of the backbone and the insert used for ligation were estimated via agarose gel. The insert was used at a five times higher concentration than the backbone. For ligation, the T4 DNA ligase was used as described in Table 17. Ligation was performed at room temperature for at least 30 min. The DNA was purified by ammonium acetate-ethanol precipitation (0) and suspended in 20 μL ddH$_2$O. 5 μL of this DNA suspension were directly used for transformation into freshly made competent *E. coli* cells. The remaining DNA suspension was stored at -20 °C.

Table 17 Ligation mixture for two fragment ligation with T4 DNA ligase.

Substance	Volume
Backbone	~ 4 μL
Insert	~ 4 μL
T4-DNA-Ligase buffer (10 x)	2 μL
Wasser	10 μL
T4-DNA-Ligase	0,5 μL

4.2.4. Ammonium acetate-ethanol precipitation of DNA

Ammonium acetate-ethanol precipitation was performed for DNA purification after ligation and DNA concentration. Therefore, the DNA solution was mixed with 1/10 volume of 7 M ammonium acetate and three times the volume of DNA + ammonium acetate of 99% ethanol. Precipitation was performed at -20 °C for at least 1 h or ideally overnight. The mixture was

centrifuged at 13000 rpm for at least 20 min at 4 °C. The supernatant was carefully removed and the pellet dried at 37 °C for at least 10 min to remove remaining ethanol. The precipitated DNA was dissolved in 20 μL ddH$_2$O for ligation purification and in 5 μL for concentration.

4.2.5. Clean-up of DNA

After PCR amplification or restriction digestion the DNA was purified using the *Wizard®* SV Gel and PCR-Clean up System (*Promega*). Purification was accomplished according to the user manual. After purification the eluation was performed using 55 μL of nuclease-free water. The concentration of the purified DNA was measured at 260 nm using the BioSpec Nano™ photometer (*Shimadzu*). The DNA was either directly used for transformation or stored at -20 °C.

4.2.6. Agarose gel electrophoresis

A solution of 1 % to 3 % agarose (w/v) in 1x TAE-buffer was prepared depending on the size of the DNA fragment analysed. To perform agarose gel electrophoresis, 5 μL of HD Green Plus DNA stain Master Mix (*intas*) were added to 20 mL of the agarose solution. DNA samples were mixed with DNA-loading dye (6x) (not necessary for prestained One*Taq*® Quick-Load® Buffer) and applied to the polymerized gel. If not described differently, 2.5 μL of the 2-log DNA ladder (*New England Biolabs*) was used as size standard. Electrophoresis was carried out for 20-40 min at 115 V. The gel was analysed using the GelDoc-It® 310 imaging system (*UVP*) or a gel documentation system from *INTAS*.

4.2.7. Sequencing of DNA

For precise analysis of DNA, isolated plasmids or PCR amplified DNA was sent to Sequence Laboratories (*SeqLab*) in Göttingen. Therefore, 12 μL DNA with a concentration of at least 80 ng/μL was mixed with 3 μL of a selected primer. The oligonucleotides used for sequencing are listed in 3.4.

4.2.8. Generation of parts for CasEMBLR

The generation of DNA parts was performed for the *in vivo* assembly by CasEMBLR (2.4.2) (99). For plasmid preparation, the *E. coli* strains DH5α or TOP10 were used. These plasmids were used for part amplification via PCR, which was performed following the manufacturer's instructions using either Q5®High-Fidelity DNA Polymerase or Phusion® High-Fidelity DNA Polymerase (*New England Biolabs*.) (4.2.1). To allow assembly and integration via homologous recombination *in vivo* PCR was used to create 30 bp overlaps to the ends of each part in case of combination with another part and 120 bp in case of combination with the yeast genome. In

case 120 bp should be added by PCR, RT PCR was performed (4.2.1). All utilized oligonucleotides are listed in 3.4. The correct DNA part size was confirmed by agarose gel electrophoresis, followed by purification using Wizard® SV Gel and PCR Clean-Up System (*Promega*). To perform *in vivo* one-step assembly and genomic integration via homologous recombination, 4 pM of each part were mixed. For large parts, 1 μg DNA was used instead. For CasEMBLR integration into one locus, 2 μg of the corresponding gRNA plasmid was used, whereas for integration in multiple loci 1 μg of each gRNA plasmid were added. Plasmids are listed in 3.2.3. The mixture of DNA parts and CasEMBLR plasmids was concentrated by ammonium acetate-ethanol precipitation (0) of DNA and resuspended in 5 μl of ddH$_2$O.

4.3. RNA-related techniques

4.3.1. RNA-Isolation from yeast cells

For RNA extraction from yeast cells, the corresponding strains were grown over night in YPD or SD drop-out media. These cells were used to inoculate 5 mL of YPD, SD drop-out media or induction media (see 3.7) for RNA extraction. After growth for 20 h, the cells were incubated on ice for 5 min, before they were harvested by centrifugation at 4000 xg for 5 min. All following centrifugation steps were performed at 4 °C. The supernatant was removed, the pellet was resuspended in 400 μL AE buffer and transferred into a new 1.5 mL reaction tube. 40 μL of a 10 % SDS solution were added and the sample vigorously mixed. 400 μL phenol were added subsequently and the samples mixed vigorously followed by incubation at 65 °C and vigorous mixing. The samples were put on ice for 10 min, before they were centrifuged at 13000 x g for 10 min. The liquid phase was transferred into a new tube and 400 μL PCI was added. The samples were vigorously mixed and incubated at room temperature for 5 min. The phases were separated by centrifugation at 13.000 x g for 10 min. The liquid phase was transferred into a new 1.5 mL reaction tube. To precipitate the nucleic acids, 40 μL of a 3 M Sodium acetate solution (pH 5.3) and 1 mL 100 % EtOH were added and mixed by inverting several times. The nucleic acids were sedimented by centrifugation at 13.000 x g for 10 min and the pellet washed with 500 μL 70 % EtOH. The pellet was dried for 5 min at room temperature, before it was suspended in 35 μL of ddH$_2$O. Afterwards the DNA/RNA concentration was measured by ND-1000 Spectrophotometer.

According to the measured concentrations, a working solution of 10 μg in 40 μL ddH$_2$0 was prepared. For digestion of DNA, 4 μL TURBO-DNase buffer and 2 μL TURBO-DNase (*New England Biolab*) were added. After incubation at 37 °C for 30 min, 2 μL TURBO-DNase were added followed by further incubation at 37 °C for 30 min. For enzyme removal 4 μL of a 3M Sodium acetate solution (pH 6.5) and 100 μL 100 % EtOH were added for precipitation. The samples were stored at -20 °C for at least 30 min and subsequently sedimented at 17.000 xg.

The supernatant was removed and the pellet washed with 500 μL 70 % EtOH. Afterwards the pellet was dried at room temperature for 5 min and suspended in 20 μL ddH$_2$O and the RNA concentration measured by ND-1000 Spectrophotometer. The concentration was adjusted to 100 ng/μL. For quality control, 500 ng RNA were applied on a 3 % agarose gel. The prepared RNA was stored at -20 °C.

4.3.2. cDNA synthesis

For RNA into cDNA transcription, 10 μg of the isolated RNA (see 4.3.1) were mixed with 4 μL dNTPs (10 nmol), 1 μL Hexamer (RHX, 0,2 μg) and 2 μL ddH$_2$O. The mixture was heated to 65 °C for 5 min, before 2 μL of the corresponding buffer was added and the sample incubated at 25 °C for 2 min. Afterwards 1 μL of the reverse transcriptase M-MuLV (*New England Biolabs*) was added. The sample was incubated at 25 °C for 10 min, followed by an incubation at 42 °C for 60 min. The enzyme was inactivated at 68 °C for 10 min. For the reverse transcription a thermo cycler was utilized. The synthesized cDNA was used as template for a PCR using *Taq* polymerase (*New England Biolabs*) (see 4.2.1).

4.4. Cell biological techniques

4.4.1. Induction of reporter gene expression

The induction of the reporter gene constructs was performed in two different set ups, single sample analysis after growth in a flask/tube or multiple sample analysis in a 96-deep-well plate, both described below. The induction media was adapted to the utilized strain and the experimental setup. The induction media is described in the corresponding results paragraph. The sample fluorescence was measured by Accuri™ C6 (*BD*) with a 488 nm laser and the filter options 533/30 or by FACS (*BD*) with a 488 nm laser and the filter options 533/40. The data was processed using either Accuri™ software (*BD*) for measurements performed with Accuri™ C6 (*BD*) (163) or the software Flowing software (version 2.5.1, *Turku Centre for Biotechnology of Turku*) for measurements performed with FACS (*BD*). Afterwards the data analysis was performed using Microsoft Excel (*Microsoft)* or Mathematica II software (*Wolfram*).

4.4.2. Single sample analysis after growth in a tube/flask

An overnight culture of the strain of interest was grown in 3-5 mL medium in a tube or 50 mL in a flask, respectively. The OD$_{600}$ was measured photometrically and 3-5 mL/50 mL of induction media were inoculated towards an OD$_{600}$ of 1 in a new tube or flask. The inoculated medium was selected depending on the experimental setup. The samples were incubated for 20 h at 25 °C and 180 rpm. For analysis 300-500 μL of the cell suspension were used. If necessary, the

cell suspension was centrifuged and cells and supernatant were stored and analyzed separately. Both, cells and supernatant were stored separately at 4 °C.

4.4.3. Multiple sample analysis in a 96-deep-well plate

For comparison of multiple samples, the incubation and induction were performed in a 96-deep-well plate. For incubation 500 μL of the desired medium was inoculated in a 96-deep-well plate. The cells were grown overnight at 30 °C using a plate incubator (Titramaxx 1000 and Incubator 1000 by *Heidolph*). For induction, most experiments were performed in biological triplicates. Therefore 450 μL of the selected medium was mixed with 50 μL of the overnight cultures. The induction was performed at 25 °C for 20 h and 1000 rpm. If necessary, the cell suspension was centrifuged and cells/supernatant were stored and analyzed separately.

4.4.4. Data collection for time dependent measurements

For time dependent measurements, induction was performed using a 50 ml Falcon™ tube. Therefore, 10 mL of the induction medium were inoculated with yeast cells as described above. The samples were grown at 25°C for 48 h. After each hour 200 μl of cells were transferred into a new reaction tube. The cell suspension was centrifuged at 13000 rpm, the supernatant was separated for ABTS assay (4.5.7) and the cells suspended in 500 μL PBS for flow cytometry measurement. In order to retain the total volume, 200 μl of the induction medium were replaced after each measurement.

4.5. Biochemical and -physical methods
4.5.1. Preparation of GOase and vNAR

Both reporter genes were secreted to the medium. Hence, after growth and induction the cell suspension was centrifuged at 3000 rpm for 5 min. The supernatant and the cells got separated and were stored separately. For verification of GOase and vNAR, the experimental setup is described in 4.5.2 and 4.5.3. For further experiments, the experimental setups described in 4.4 were used.

4.5.2. GOase purification using Viva flow

For GOase verification, the enzyme was purified. Therefore, cells were grown overnight in a 50 ml flask in SD drop-out medium at 30 °C. After growth cells were inoculated to a cell density of OD_{600} of 1 in 1000 ml SG-ura drop-out medium. The induction was completed by addition of 1000 μl of a 1 mM ES stock solution. Cells were induced at 25 °C for 20 h. The expression of the GOase-tGFP construct was checked by tGFP verification *via* flow cytometry. The cells were precipitated by centrifugation at 3000 rpm for 5 min. The supernatant was transferred into a

fresh flask and concentrated to 25 ml using a Vivaflow 200, 10.000 MWCO Hydrosart laboratory crossflow cassette (*Sartorius*). The purified and concentrated supernatant was stored at 4 °C. Meanwhile, the cell pellet was resuspended in PBS and disrupted using a cell disrupter (*Constant systems LTD*). The cell debris was removed by centrifugation and the suspension stored at 4 °C. Both supernatant and cell debris were analyzed using SDS-PAGE (4.5.4) as well as ABTS assay (4.5.7).

4.5.3. vNAR purification using IMAC

For vNAR verification, the shark antibody was purified. Therefore, cells were grown overnight in a 50 ml flask in SD drop-out medium at 30 °C. After growth cells were inoculated to a cell density of OD_{600} of 1 in 500 ml SG-ura drop-out medium. The induction was completed by addition of 500 μl of a 1 mM ES stock solution. Cells were induced at 30 °C for 20 h. The expression of the vNAR-tGFP construct was checked by tGFP verification via flow cytometry. The cells were precipitated by centrifugation at 3000 rpm for 5 min. The supernatant was transferred into a fresh flask and concentrated to 3 mL using Amicon Ultra-15 Centrifugal Filter Units (MWCO 3 kDa, *Merck Millipore*). Meanwhile, the cell pellet was resuspended in IMAC buffer A (10 mM imidazole) and disrupted using a cell disrupter (*Constant systems LTD*). The cell debris was removed by centrifugation.

The His-tagged vNAR was isolated by immobilized metal affinity chromatography (IMAC). IMAC allows the simple and efficient purification of proteins recombinantly fused to a hexahistidine affinity tag (6xHis-Tag). Purification is performed by the metal chelating agent nitrilotriacetic acid (NTA), which is coupled to the column matrix (164).

For IMAC 30 mL of the cell-lysate were applied to a 1 mL HisTrap HP column (*GE*), which was washed with 10 column volumes of buffer A. For elution, a linear gradient of 0-100 % IMAC buffer B (1 M imidazole) was applied over 20 column volumes. Fractions of 1 mL were collected and stored at 4 °C until further analysis by SDS-PAGE and Western-blot analysis.

4.5.4. SDS polyacrylamide gel electrophoresis

Sodium dodecyl sulphate-polyacrylamide gel electrophoresis (SDS-PAGE) allows to separate denatured proteins in an electric field depending on their molecular weight. Hence, this method was used to verify the presence and correct size of GOase and vNAR. SDS-PAGE was performed as described in (165).

For SDS PAGE, the protein samples were mixed with 17% volume of the 5x loading dye. The loading dye contained the reducing agent β-mercaptoethanol, which results in the disruption of protein disulphide bonds. The samples were denatured at 95 °C for 5 min. The SDS PAGE gel was prepared as a 15 % (w/v) SDS PAGE gel (Table 18), placed in an electrophoresis

chamber and covered with loading buffer, before 15 μL of each sample were applied. 5 μL of the Blue Prestained Protein Standard, Broad Range (11-190 kDa, *New England Biolab*) were applied as marker. Electrophoresis was performed at 40 mA for 1 h. To visualize the proteins, the SDS PAGE gels were stained with Coomassie (4.5.5).

Table 18 Mixture of 15 % SDS PAGE gel (w/v), consisting of separation and stacking gel. Volumes are calculated for five gels.

Stock solution	Separation gel	Stacking gel
30 % (w/v) acrylamid, 0,8 % bisacrylamid	18 mL	2.4 mL
4x separation gel buffer	9 mL	-
4x stacking gel buffer	-	3.6 mL
Water	9 mL	8.4 mL
APS-Stock 10 % (w/v)	270 μL	129.6 μL
TEMED	13.5 μL	10.8μL

4.5.5. Protein Coomassie staining

To visualize protein, SDS gels were stained with Coomassie staining solution containing Coomassie Brilliant Blue R-250 and G-250. The gel was placed in a small bowl, doused with the Coomassie solution and heated in a microwave for dyeing. To remove nonspecific staining, decolorization was carried out with a solution out of 10 % (v/v) acetic acid, 25 % (v/v) isopropanol. The gel was heated up again und destaining solution 1 was replaced with destaining solution 2 containing 10% (v/v) acetic acid in distilled water. The gel remained in this solution until background staining was sufficiently removed.

4.5.6. Western-blot analysis

Western-blot analysis is performed in order to visualize specific proteins. Therefore, SDS PAGE is used to separate the proteins, before being transferred to a nitrocellulose membrane. The protein on the membrane can be detected by a specific antibody, which either is directly labelled by an enzyme or a fluorescent tag, or can be recognized by a second visualization antibody. When labelled to an antibody-alkaline phosphatase (AP), the complex can be visualized by a mixture of Nitro-blue tetrazolium (NBT) and 5-bromo-4-chloro-3'-indolyphosphate (BCIP), which leads to an insoluble black-purple precipitate. This technique was utilized for vNAR detection.

After SDS-PAGE of selected fractions, the proteins were blotted onto a nitrocellulose membrane (Semi-dry Western Blot). Therefore, 12 Whatman filter papers were pre-wetted with Western blot transfer buffer. The SDS gel and the nitrocellulose membrane were also pre-wetted with Western blot transfer buffer for 5 min. The components were arranged on a semidry blotting

chamber in the following order: 6x Whatman filter papers, nitrocellulose membrane, SDS gel, 6x Whatman filter papers. The blot was run for 45 min at 12 V and 300 mA.

Afterwards, the membrane was washed with ddH$_2$O and blocked with 1.5% milk powder solution (PBS-TM) for 1 h at room temperature. The membrane was washed with PBS-T for 10 min. Afterwards incubation with constant shaking was performed with the primary antibody for 1 h. The membrane was washed three times in PBS-T for 10 min, followed by incubation with the second antibody for 1 h. The membrane was washed another three times with PBS-T for 10 min and afterwards equilibrated in AP buffer. For detection 50 μl NBT and 75 μl BCIP were added into the AP buffer and shaken constantly until the desired color intensity was reached. The membrane was washed with ddH$_2$O several times to stop the reaction.

4.5.7. ABTS assay

In order to verify GOase, ABTS (2,2′-azino-bis(3-ethylbenzothiazoline-6-sulphonic acid)) assay can be used to demonstrate its activity. GOase uses galactose as a substrate and oxidizes it, which leads to the production of H$_2$O$_2$. The coenzyme horse radish peroxidase (HRP) reduces H$_2$O$_2$ to H$_2$O. ABTS serves as electron acceptor and receives the electrons generated by HRP. This results in the green-colored radical cation ABTS$^{\bullet+}$, which allows to measure an absorption shift (166–168).

For the ABTS assay, cleared supernatant was utilized. The samples were diluted 1:10 in PBS. 180 μL of the solution were mixed with 10 μl HRP (0.1 mg/ml), 10 μl ABTS (10 mM) and 10 μl galactose as substrate (1 M). After 5 min the absorption of ABTS and ABTS$^{\bullet+}$ was measured at 405 nm with the INFINITE Tecan M-1000 (*Tecan*) reader. The absorption data was exported to and analyzed with MS Excel (*Microsoft*).

5. Results and Discussion

Multiple switches based on antibiotics like tetracycline, metabolists like glucose or steroid hormones like β-estradiol have been successfully established. All of those switches have their own specific advantages and disadvantages (46,57,74). In order to allow tightly controlled and targeted gene expression, this work delivers a strategy to combine different switches to a functional gate or circuit.

5.1. Implementation and characterization of a galactose dependent CRISPR/dCas9-based switch

5.1.1. Construction of the reporter gene setup

The basis for the different setups is a three component CRISPR/dCas9 system, which was already demonstrated to allow the targeted gene expression control in the yeast *S. cerevisiae* (5). For functional gene expression, three CRISPR/dCas9 components have to be implemented into the yeast cells:

- a dCas9 of type II from *S. pyogenes*
- an effector protein fused to a transcriptional activator
- a scRNA containing a hairpin loop for recruitment of the effector protein

This setup was chosen because of the high expression rates of a reporter gene and the modularity demonstrated by Zalatan *et al*. (5). According to their data, the combination of bacteriophage coat protein MS2 (MCP) fused to the transcription activator VP64 as effector protein and a scRNA containing two different MCP recruitment motifs delivers the highest expression levels. The utilized scRNA contained a mixed hairpin construct out of a MS2 wildtype hairpin and an aptamer hairpin named f6 (2x MS2 [WT + f6]) (5,169) (Figure 22).
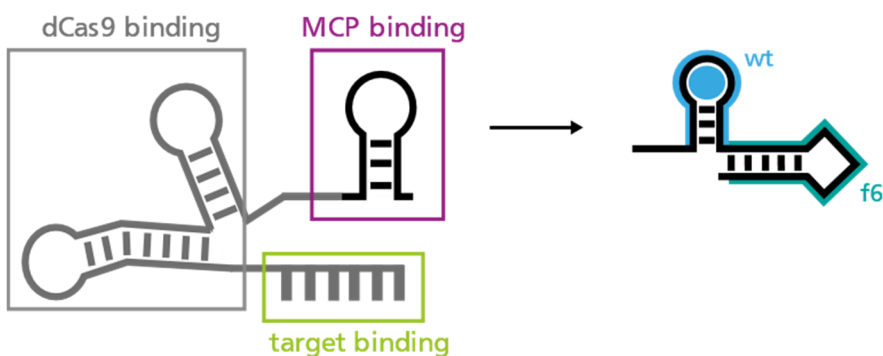

Figure 22 Structure of the utilized scRNA.

The scRNA is assembled from three subunits, the 20 bp long target binding site, the 76 bp long dCas9 recruiting hairpin and the 29 bp long MCP recruiting hairpins. Two different MCP recruitment hairpins are used, the MS2 wildtype hairpin and an aptamer hairpin named f6. (Figure adapted after (4))

Additionally, besides the CRISPR/dCas9 components, the implementation of a reporter gene construct is necessary. Following the setup of Zalatan *et al.*, a *tet*O sequence was used for scRNA binding and the yellow fluorophore Venus as reporter. The use of *tet*O as a binding sequence brings a crucial advantage. With the implementation of a Tet-On System, the testing of the inducibility of the reporter construct will be enabled. In total five strains were kindly provided by Jesse Zalatan containing the reporter gene Venus placed behind different *tet*O copy numbers. For the generation of the yeast strains, the *rtTA-msn2_hphR* gene was genetically integrated into the *HO* gene of the yeast strain SO992. The obtained clone was named cSLQ.sc002 and subsequently transformed with the reporter gene constructs, containing *Venus* as the reporter gene placed behind 1x, 2x, 3x and 7x *tet*O copies. The constructs were genomically integrated into the *trp1* locus, leading to the provided strains yJZC02 (1x *tet*O), yJZC03 (2x *tet*O), yJZC04 (3x *tet*O) and cSLQ.sc003 (7x *tet*O) (5).

5.1.2. Examination of the general inducibility of the reporter gene setup

As a first step, the newly constructed strains were tested for inducibility of the reporter constructs with the help of the implemented Tet-On system. Doxycycline is added to the growth medium, resulting in the binding of the constitutively expressed rtTA to dox and subsequently *tet*O, which induces Venus gene expression (74). This allows direct Venus fluorescence detection by flow cytometry (Figure 23A).

For the experiment, the strains cSLQ.Sc003, yJZC02, yJZC03 and yJZC04 were inoculated and induced in a 96-deep-well plate. The experiment was carried out according to paragraph 4.4.3. Cells were grown in full SD medium. Induction was performed using 100 μg/mL dox following a protocol for doxycycline-dependent target gene expression (170). Additionally, untreated samples were prepared as controls. For each sample triplicates were applied. Deviating from the protocol, induction was only performed for 4-5 h. Venus fluorescence was directly measured using *BD* Accuri™ C6 (*BD*). For analysis the Accuri™ software (*BD*) was used. A gate excluding cell debris and contaminations was applied (data not shown). The average of the mean fluorescence and the standard deviation of the gated triplets were calculated using Microsoft Excel (*Microsoft)* (Figure 23B).

SD medium was measured as a blank and did not show any fluorescence, as expected. Hence, this control could be neglected for future experiments. Analysis of the samples showed that the fluorescence increased according to the *tet*O copy numbers. For 7x *tet*O copy numbers, the fluorescence slightly decreased in comparison to 3x *tet*O copy numbers. This can be explained by Supplementary Figure 50, showing a decreased total number of induced cells for 7x *tet*O copy numbers. Due to the dox induction, it was demonstrated, that all reporter constructs are functional. Even though the Tet systems generally suffer from a high basal activity (73), it was

demonstrated, that in the absence of an inducer all switches were relatively tightly regulated. A low basal activity was crucial for further applications, since it was aimed to combine the CIRPSR/dCas9 platform with multiple switches to a tightly regulated toolbox. For the purposes of this work, the *tet*O-generated leakiness is acceptable and the approach can be used as a platform.
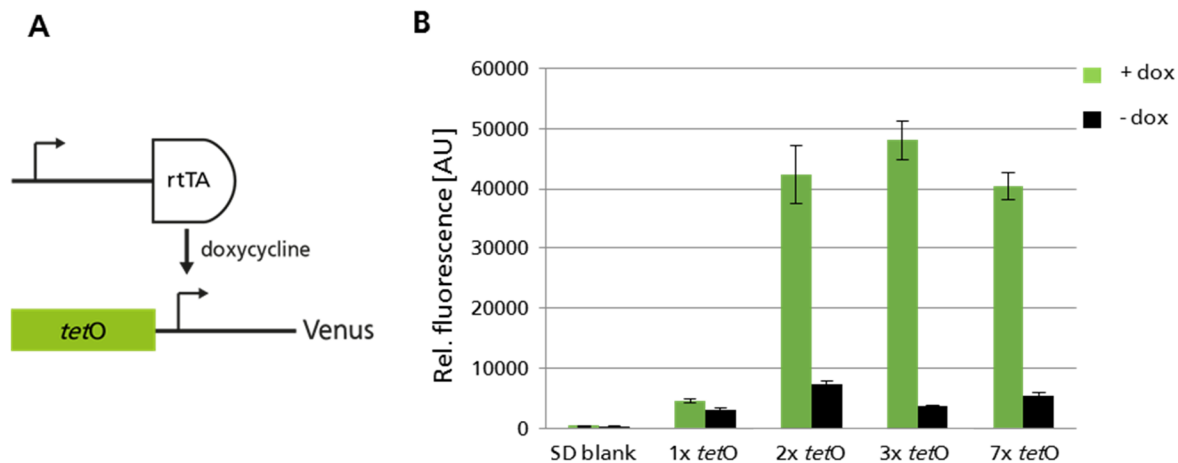

Figure 23 Verification of the functionality of the reporter gene constructs.

(A) Logic gate for the doxycycline induction of the Tet-On system. (B) The induction of the reporter gene constructs was successful. The expression range strongly depends on the tetO copy number. The fluorescence was measured with the 488 nm laser of BD Accuri™ C6 [533/30]. Error bars indicate the standard deviation of the biological triplicates.

### 5.1.3. Construction of a galactose-inducible switch

After demonstrating the general inducibility of the reporter constructs, the next objective was to implement and characterize a switch. Zalatan *et al.* implemented a galactose dependent switch in their approach by bringing dCas9 under the control of the *Gal10* promoter (Figure 24A). This chapter describes the building of a galactose-dependent switch and its characterization regarding suitability as part of complex genetic circuits.

To build a galactose-dependent CRISPR/dCas9-based single switch (Ssw), the three CRISPR/dCas9 components were integrated into the strains cSLQ.Sc003, yJZC02, yJZC03 and yJZC04, which already contained the *tet*O-Venus reporter gene constructs in the *trp1* gene. A type II dCas9 derived from *S. pyogenes* was placed behind the *Gal10* promoter, whereas MCP-VP64 and scRNA were expressed continuously (Figure 24B). MCP-VP64 was expressed by the strong constitutive *Adh1* promoter. The scRNA was expressed by the constitutive snoRNA *SNR52* promoter and contained a terminator from the 3′ region of the yeast SUP4 gene (159). Unless stated differently, this setup was retained for the following experiments. All plasmids with genes for the CRISPR/dCas9 complex were obtained from *addgene* (3.2).
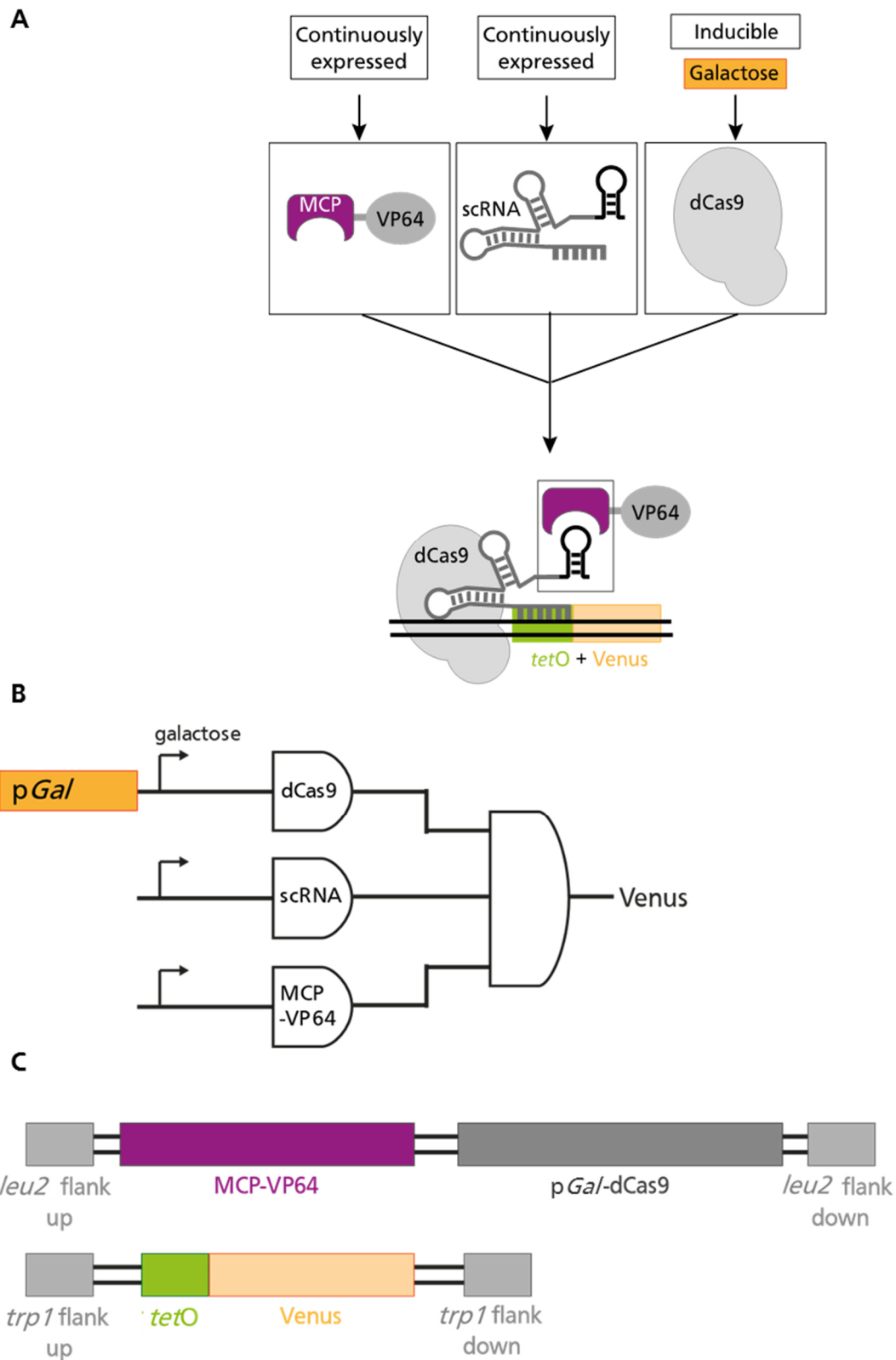
Figure 24 Schematic and genetic overview of the galactose-dependent single switch.

(A) Schematic overview and (B) logic gate for the single switch (Ssw). Both showing, that MCP-VP64 and the scRNA are continuously expressed, whereas the dCas9 is inducible by galactose. When all components are expressed, they bind to *tet*O and induce Venus expression. (C) Genomic overview for the Ssw including homologous flanks for genomic integration as well as the gene combinations, that were genomically integrated.

The *pGAL*-dCas9 and the effector protein fusion MCP-VP64 were genomically integrated, whereas the scRNA was transformed as a CEN/ARS plasmid (Figure 24C). Hence in a first transformation step, *dCas9* and *MCP-VP64* genes were integrated into the genome. It was decided for genomic integration, since genetic networks based on plasmids can be unstable (171). Thus, most metabolic engineering efforts for complex, multistep pathways rely on genomic integration (172). Traditionally genomic integration of heterologous genes into yeast is performed *via* integration into an integrative plasmid and subsequent integration of the plasmid into the genome (173). One option is to integrate the entire plasmid into the chromosome. Therefore, the vector only needs to be linearized to be integrated by a single cross-over event (174). It is possible, that this method results in multiple integrations or tandem duplication of the integration site (175). Hence, a second option is preferred, where the backbone is removed before integration. On those plasmids, the marker and the GOI are flanked by homologous sequences for the up- and downstream region of the integration site. To integrate the construct of upstream flank-marker-GOI-downstream flank, the plasmid needs to be double digested with two enzymes (173,175).

This backbone-free integration method was used for the integration of the MCP-VP64 and *GAL*-dCas9 genes. The plasmid pJZC638 contained both genes between *leu2* homology flanks. The plasmid was digested with the enzyme *Pme*I, which did cut directly outside of both homology flanks. The digestion was controlled by agarose gel electrophoresis and subsequently purified using the *Wizard*® SV Gel and PCR-Clean up System (*Promega*). The protocols can be found in (4.2.5). The digested DNA was integrated into the strains cSLQ.Sc003, yJZC02, yJZC03 and yJZC04 *via* electroporation (4.1.5). Selection was performed using SD-leu drop-out-plates. Due to the high effort of genetic integration for the cells, cells were grown for up to 120 h. Correct integration was verified by colony PCR (cPCR) using the oligonucleotides fw_genomic int._leu-dCas Plasmid, rv_genomic int._leu-dCas Plasmid, dCAS_fw_Colony PCR and rv_copy number_dCas-dCas Plasmid (3.4) (data not shown, but can be found in (176)).

In order to establish a functional CRISPR/dCas9 platform, the scRNA was added to the dCas9 and MCP-VP64 containing yeast cells. Therefore, the scRNA containing plasmid pJZC588 was obtained from *addgene*. The utilized shuffle plasmid pJZC588 contains the (2x MS2 [WT + f6])-scRNA under control of the constitutive snoRNA *SNR52* promoter. The plasmid pJZC588 is a shuttle vector containing both, the genes for reproduction in *E. coli* as well as for stable expression in *S. cerevisiae*. Therefore, it contains the auxotrophic marker for *ura3* (177) and a CEN6_ARS4 origin of replication (ori). The CEN6_ARS4 ori consist of an autonomously replicating sequence (ARS) and yeast centromere (CEN) and is a low copy ori, that allows relatively stable expression of a target gene (178).

In a second transformation step, the scRNA was genomically integrated with this plasmid. Transformation was performed *via* electroporation into the positively tested dCas9/MCP-VP64 clones. Selection was performed using SD-ura drop-out-plates. Cells were grown for 48 h and correct integration was verified by cPCR using the oligonucleotides gRNA_fw_Colony PCR and gRNA_rv_Colony PCR (3.4) (data not shown, but can be found in (176)).

As a control, the classical two component CRISPR/dCas9 system was integrated into the yeast strains as well. This allowed for the comparative analysis with the three components CRISPR/dCas9 system especially for the efficiency of transcriptional activation. For a functional complex a dCas9, which was fused to a transcription activator, and a gRNA targeting *tet*O were required. For dCas9-VP64 integration, the plasmid pJZC519 was used. The plasmid contained a gene for type II dCas9 derived from *S. pyogenes,* which was fused to the transcription activator VP64 and placed between *leu2* homology flanks. For backbone-free genome integration the plasmid was digested with *Pme*I. The digestion was controlled by agarose gel electrophoresis and subsequently purified using the *Wizard®* SV Gel and PCR-Clean up System (*Promega*). The digested DNA was integrated *via* electroporation into the strains cSLQ.Sc003, yJZC02, yJZC03 and yJZC04 already containing the *tet*O-Venus reporter gene constructs in the *trp1* gene. Selection was performed using SD-leu drop-out-plates. Cells were grown for up to 120 h and correct integration was verified by cPCR using the oligonucleotides fw_genomic int._leu-dCas Plasmid, rv_genomic int._leu-dCas Plasmid, dCAS_fw_Colony PCR and rv_copynumber_dCas-dCas Plasmid (3.4) (data not shown, but can be found in (176)).

In a second transformation step, the CEN/ARS plasmid pJZC523 was transformed into the positively tested dCas9-VP64 strains. The plasmid is a shuttle plasmid containing a gRNA under control of the constitutive snoRNA *SNR52* promoter, guiding the dCas9-VP64 to the *tet*O target site. The plasmid pJZC523 contained the auxotrophic marker *ura3* for selection. The transformation was performed *via* electroporation. Selection was performed using SD-ura drop-out-plates. Cells were grown for 48 h and the correct integration was verified by cPCR using the oligonucleotides gRNA_fw_Colony PCR and gRNA_rv_Colony PCR (3.4) (data not shown, but can be found in (176)).

To sum up, the following transformations were performed:

Table 19 Summary of the transformed clones for Ssw and control strains.

Name	Integrated genes	Origin
Ssw, 1x *tet*O	*trp1::TET01-Venus leu2::MCP-VP64_Gal10-dCas9*, scRNA (plasmid)	yJZC02
Ssw, 2x *tet*O	*trp2::TET01-Venus leu2::MCP-VP64_Gal10-dCas9*, scRNA (plasmid)	yJZC03
Ssw, 3x *tet*O	*trp3::TET01-Venus leu2::MCP-VP64_Gal10-dCas9*, scRNA (plasmid)	yJZC04
Ssw, 7x *tet*O	*trp7::TET01-Venus leu2::MCP-VP64_Gal10-dCas9*, scRNA (plasmid)	cSLQ.sc003
dC-VP64, 1x *tet*O	*trp1::TET01-Venus leu2::dCas9-VP64*, gRNA (plasmid)	yJZC02
dC-VP64, 2x *tet*O	*trp1::TET02-Venus leu2::dCas9-VP64*, gRNA (plasmid)	yJZC03
dC-VP64, 3x *tet*O	*trp1::TET03-Venus leu2::dCas9-VP64*, gRNA (plasmid)	yJZC04
dC-VP64, 7x *tet*O	*trp1::TET07-Venus leu2::dCas9-VP64*, gRNA (plasmid)	cSLQ.sc003

At least one clone was achieved for every transformation. For each strain a positively tested clone was cultivated and subsequently stored at -80 °C.

5.1.4. Function and inducibility of the utilized CRISPR/dCas9 approach and the Ssw

As demonstrated before, induction of Venus expression in the utilized *tet*O strains is possible due to addition of doxycycline. The successful integration of CRISPR genes will additionally enable the targeted gene expression of Venus by the two and three component CIRPSR/dCas9 systems. The CRISPR/dCas9 associated reporter gene expression as well as the galactose dependent reporter gene expression of the Ssw are examined in this chapter.

All strains described in Table 19 were inoculated and induced in flasks. The experiment was carried out according to paragraph 4.4.2. Cells were grown in -ura drop-out medium. The dC-VP64 clones were inoculated in SD medium only, whereas the Ssw clones were inoculated in both SD and SG medium. This setup allowed the comparison of induced and uninduced single switch cells. Strains only containing the *MCP-VP64_pGald-Cas9* or *dCas9-VP64* gene respectively were inoculated in SD medium. Additionally, the strain Ssw, 7x tetO was induced with 100 µg/mL dox in SD medium as positive control and the cSLQ.sc002 strain was inoculated in SD medium as negative control. Venus fluorescence was measured *via* Accuri™ (*BD*). An overlay histogram (A) and a single histogram for each *tet*O copy number (B) is shown in Supplementary Figure 51. For the comparative analysis of both approaches, the Accuri™ software (*BD*) was used. A gate including only fluorescent cells was applied. For the successful and comparable application of a gate, only 5 % of the cells of the negative control were included (Supplementary Figure 51). If not stated differently, this strategy was used for all gates applied. The mean fluorescence of the cells in the gate was compared in a diagram using Microsoft Excel (*Microsoft)* (Figure 25).

The samples dC_VP64, 1x, 2x and 3x *tet*O did not show any significant fluorescence. The sample dC_VP64, 7x *tet*O showed a slight increase in fluorescence, demonstrating the general functionality of the two component CRIPSR/dCas9 system. In comparison, the fluorescence expression achieved with the Ssw strains was distinctly higher. Already for Ssw, 1x *tet*O a significant fluorescence was detected. The fluorescence increased exponentially with the *tet*O copy number. Thus, fluorescence of Ssw, 3x *tet*O already increased around 20-fold in comparison to Ssw, 2x *tet*O, whereas the fluorescence of Ssw, 7x *tet*O increased around 40-fold. The florescence of the positive control 7x *tet*O, SD + dox was 20-fold lower than the corresponding fluorescence of the fluorescence of Ssw, 7x *tet*O, but around 2.5-fold stronger than the fluorescence of dC_VP64, 7x *tet*O. The fluorescence of the negative control was in range of the strains only containing the *MCP-VP64_pGald-Cas9* or *dCas9-VP64* gene respectively and the Ssw samples grown in SD only. In comparison to that, the fluorescence of the Ssw, 7x *tet*O was slightly increased.
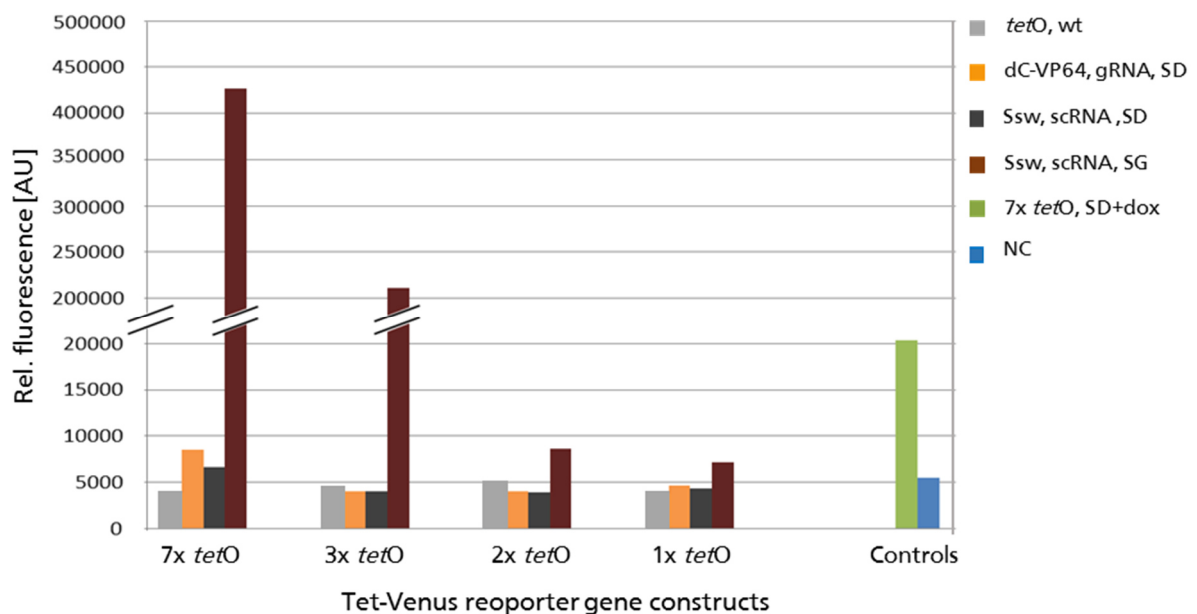

Figure 25 Relative fluorescence depending on the integrated CRISPR/dCas9 system and the *tet*O copy number.

Four different samples are shown for each of the *tet*O strains; 7x *tet*O, 3x *tet*O, 2x *tet*O and 1x *tet*O. Clones called wt contained only the dCas9 genes and are shown in grey; cells for the construct 519_523/dC-VP64 in orange; cells for the construct 638_588/Ssw grown in SD-ura drop-out medium in dark grey and induced with SG-ura drop-out medium in dark red. As controls cells of the strain Ssw, 7x *tet*O induced with 100 µg/mL dox in SD-ura drop-out medium are shown in green and in blue the cells of the strain cSLQ.sc002 = negative control, not containing any reporter or CRISPR genes.

The observation that the fluorescence increases with the number of *tet*O boxes can easily be explained. The increased number of scRNA binding sites exponentially increases the likelihood of MCP-VP64 binding and subsequent associated transcriptional activation. Moreover, it is possible that several scRNA/dCas9/MCP-VP64 complexes bind to the *tet*O binding sites

simultaneously. This finding fits the common practice to increase the copy number of a binding site, when high transcription rates are desired (45,79).

Interestingly, the induced Ssw, 1x *tet*O and dC_VP64, 7x *tet*O show approximately the same fluorescence. Thus, it can be stated that the three-component system activates transcription much stronger than the classical two-component system. A simple explanation is, that MCP binds to its RNA target as a dimer (179). Hence, for each scRNA hairpin loop, two MCP-VP64 are recruited, which allows the recruitment of up to four MCP-VP64 molecules per scRNA molecule. This effect strongly enhances the transcription activation, making the Ssw setup the perfect tool for high expression rates (5).

5.1.5. Leakiness of the galactose switch

An unfortunate side effect is that the basal activity also increases with the copy number of *tet*O. Further analysis was performed in order to verify the functionality of the approach for further circuit design. Therefore, the strain Ssw, 7x *tet*O, showing the highest basal activity, was inoculated in a flask and induced with SD and SG medium, respectively. As negative control the 7x *tet*O strain only containing the *MCP-VP64_pGald-Cas9* genes was inoculated in SD medium. Venus fluorescence was measured *via* Accuri™ (*BD*) and the Accuri™ software (*BD*) was used for analysis. The resulting histograms are shown in Figure 26. A gate was applied covering only cells that were showing fluorescence.

For the negative control, only a few cells were fluorescent, whereas for the galactose induced strain nearly all cells were fluorescent. Both results demonstrate, that the induction worked as intended. Furthermore, 34 % of the cells grown in SD medium were fluorescent. These results emphasize, that the galactose inducible Ssw system has the disadvantage of high basal activity. Due to the biological background (2.2.1.), a certain leakiness must be expected for galactose dependent promoters (57).

To sum up, the three-component CRISPR/Cas9 system allows the functional expression of the reporter gene Venus. Transcription activation thereby strongly depends on the copy number of *tet*O. In the Ssw setup, the addition of galactose allows targeted activation of transcription with the only necessity of a galactose dependent promoter in front of a GOI. Hence, beside the achieved high expression rates, the main advantage of the galactose switch is its simplicity. However, with an increase of transcriptional activation, the basal activity increases as well. Thus, the main disadvantage of the galactose switch is its natural leakiness.
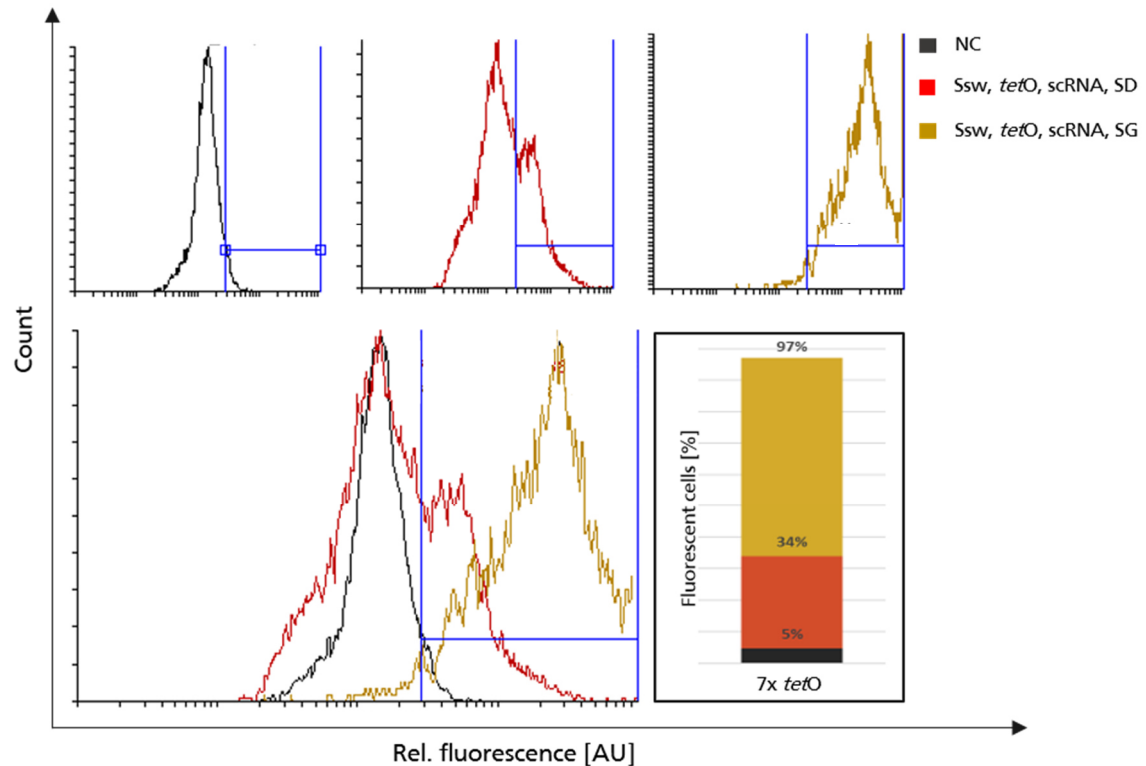
Figure 26 Leakiness of the Ssw, 7x tetO depending on the induction medium.

The Ssw, 7x *tet*O was either grown in SD (red) or induced by growth in SG (yellow). For comparison the 7x *tet*O clone only containing the *MCP-VP64_pGald-Cas9* gene was grown in SD (black). For each strain a histogram is given, showing the fluorescence for Venus measured by FACS with a 488 nm laser and the filter options 530/540. An overlay histogram was prepared. A gate was implemented containing 5 % of the wild type cells. The percentage of cells in the gate is shown as a diagram.

5.2. A hormonal transcription factor for a tight and dose-dependent AND gate

The aim of this thesis is to combine various genetic switches in order to remove disadvantages, while maintaining advantages. Furthermore, the goal of the following chapter is the addition of a second switch to the Ssw system, allowing the tight regulation of the whole genetic network, while maintaining the high expression rates of the galactose switch. Additionally, the second switch should enable the concentration-dependent induction of expression of the gene of interest. According to Ottoz *et al.*, their ES-inducible approach allows both, the tight and dose-dependent induction of a target GOI (45). Hence, the implementation of this approach into the galactose-dependent three-component CRIPSR/dCas9 system, to achieve a functional, tightly regulated and dose-dependent AND gate, was investigated and is described below.

5.2.1. Function of the hTF LexA-ER-B112

In order to establish a modular platform based on the three component CRISPR/dCas9 system, that is precisely tunable at low induction levels as well as tightly regulated, an ES-dependent switch, based on a heterologous transcription factor, was utilized. This heterologous

transcription factor consists of the bacterial LexA DNA-binding protein (92), the ES-binding domain of the human estrogen receptor (ER) (46,47,92) and the short unstructured acidic peptide B112 as activation domain (AD) (91,92) (Figure 27). In the absence of ES, the hTF is located in the cytoplasm and is bound to Hsp90 (47) and other molecular chaperone components like a p23 monomer (180). This complex represses the ER's transcriptional regulatory activities, while it maintains a receptor conformation that is able to bind ES with a high affinity (181). After addition of ES, the hormone diffuses through the cell membrane, binds to the hTF and the Hsp90 complex is released (46). The hTF-ES complex localizes to the nucleus, where it binds to *lexA* and strongly activates transcription through the activation domain B112 (45).
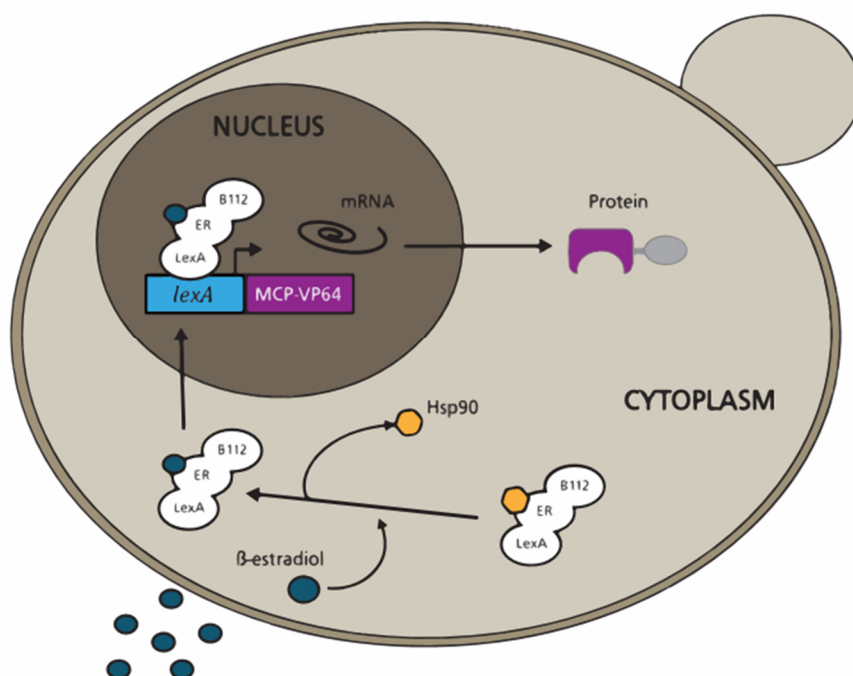

Figure 27 Induction of LexA-ER-B112 fusion protein transcription activation by ES.

The fusion protein containing the LexA binding domain, the human estrogenic receptor ER and the transcription activator B112 are bound to Hsp90 in absence of ES. After addition of ES Hp90 is displaced and is able to enter the nucleus, where it binds to the lexA boxes preceding the *MCP-VP64* gene. The gene is transcribed to mRNA, transits from the nucleus to the cytoplasm and is translated into a functional fusion protein. (Figure adapted after (4))

5.2.2. Construction of an AND gate with a single and double reporter system

In order to achieve a double switchable AND gate, MCP-VP64 was brought under the control of ES, whereas dCas9 remained under the control of galactose (Figure 28A). The scRNA was constitutively expressed from the constitutive snoRNA *SNR52* promoter. By combining the sensitive LexA based ES tunability with the modularity and low basal activity of CRISPR/dCas9 and the high expression levels of galactose promoters, an AND gate was designed depending on both galactose and ES.

Three different reporter gene setups were implemented (Figure 28B). For a single reporter setup, the successfully tested *tetO*-Venus setup was chosen (AND). As demonstrated before, this allows the direct and simple measurement of the reporter gene by flow cytometry. With regard to possible biotechnological applications, the aim was to establish an approach that enables the tight regulation of biologically relevant, but not directly detectable GOIs. Therefore, two double reporter setups were chosen, combining either the enzyme galactose oxidase (GOase) or the variable domain of new antigen receptors (vNAR) from sharks with a T2A-tGFP (green fluorophore turbo GFP).

After Grzeschik *et al.* the usage of T2A allows the monitoring of the expression of secreted or cell surface displayed proteins. Therefore, the fluorescence of a T2A coupled tGFP is measured, which remains in the cell cytoplasm (157). In general, picornaviral 2A peptides allow the generation of multiple proteins from one mRNA transcript by ribosomal skipping (182,183). For this work, the 18 amino acid T2A sequence derived from the *Thosea asigna* virus was utilized. Compared to other 2A variants, the T2A sequence results in the most efficient cleavage (184). Thus, once a GFP fluorescence can be detected, it is indicative of GOI expression. To investigate, whether the T2A-tGFP expression monitoring works, the double reporter systems were constructed as GOase-T2A-tGFP (AND, GO) and vNAR-T2A-tGFP (AND, vNAR) (Figure 28C). Due to the secretion signal app8 (185), the utilized GOase from *Fusarium spec.* as well as the vNAR were secreted in the medium, while the green fluorophore turbo GFP remained in the cell after ribosomal skipping.

In addition to the indirect measurement of tGFP fluorescence *via* flow cytometry, the properties of GOase allowed the direct measurement of the enzyme's expression. GOase mediates the oxidative conversion of D-galactose to D-galactohexodialdose, which leads to the side production of hydrogen peroxide (186,187). This hydrogen peroxide formation can be determined quantitatively by ABTS (2,2'-azinobis-(3-ethylbenzthiazoline-6-sulphonic acid) assay. When hydrogen peroxide is produced due to the GOase reaction, it oxidizes ABTS to produce a radical cation (ABTS$^{\bullet+}$) (166,167). This shift can be photometrically measured and the absorption can be compared in order to detect samples containing active GOase (4).

The AND, vNAR setup contained an anti-Matuzumab vNAR, which is a shark derived antibody domain. In order to examine different purification strategies, the vNAR was expanded with a C-terminal hexahistidine tag (vNAR-6His) that can be used for protein detection by western blot analysis. This setup should allow vNAR purification by IMAC chromatography followed by detection via ELISA assay (188). The reporter genes were genetically implemented after 7x *tet*O. The single reporter setup was additionally implemented after 3x *tet*O.

5.2.3. CasEMBLR for efficient genomic integration

The need of genomic integration of multiple genes required a method that is more efficient and less time consuming than genome integration by homologues recombination (HR). As described in (2.4.2), CasEMBLR should deliver a tool for the simple assembly and efficient integration of multiple parts into up to three genomic loci (99). To achieve a functional CasEMBLR integration, only an active Cas9 and a gRNA, which is targeting the integration locus, need to be integrated into a host strain. All CasEMBLR constructs were kindly provided by the Süß lab (*TU Darmstadt*).

In order to implement an ES- and galactose-dependent AND switch, the fusion protein MCP-VP64 was genetically placed behind four *lexA* boxes and the dCas9 was placed behind the P_{GAL10}. Both genes were integrated into the *ade2* locus. All reporter constructs described in 5.2.2 were integrated into the *his3* locus. To achieve a functionals ES-inducible switch, the LexA-ER-B112 hTF was implemented into the *his3* locus as well. The assembled genes are described in Figure 28C.

For the assembling the HR capacity of *S. cerevisiae* was used. To allow the successful assembly and integration *via* HR *in vivo*, 30 bp overlaps were added to the ends of each part when combined with another part and 120 bp when combined with the yeast genome. For the plasmid preparation, the *E. coli* strain DH5α or TOP10 were used. Those plasmids were used as templates for the desired parts. To amplify the parts with the required flanks, PCR was performed following the manufacturer's instructions using either Q5®High-Fidelity DNA Polymerase or Phusion® High-Fidelity DNA Polymerase (*New England Biolabs, Inc*.) (4.2.1). All parts used for the construction of the AND gate are listed in Table 20, of the AND, GO in Table 21 and of the AND, vNAR in Table 22.

Table 20 Parts utilized for the construction of the AND switch with 3x/7x *tet*O.

| Parts	Method	fw	rv	Template	Size [bp]	c [ng/μL]	pmol/μL
Ade2	PCR, Q5	A4	A5	pJZC638	530	68.7	0.39
Ade3	PCR, Q5	A6	A7	pJZC625	840	87.6	0.32
Ade5	PCR, Q5	A1, A11	A12	pFRP793	590	20.45	0.11
Ade6	PCR, Phu	A13	A3	pJZC638	7350	80.46	0.03
His1B2	RT PCR, Q5	H1, H2	H8	pJZC532	2100	85.27	0.12
His1B3	RT PCR, Q5	H1, H3	H8	pSLQ1119	2500	50.3	0.06
His2	RT PCR, Q5	H9	H6, H7	pFRP880	3100	42.7	0.04
pAH006	-	-	-	-	-	237.42	-
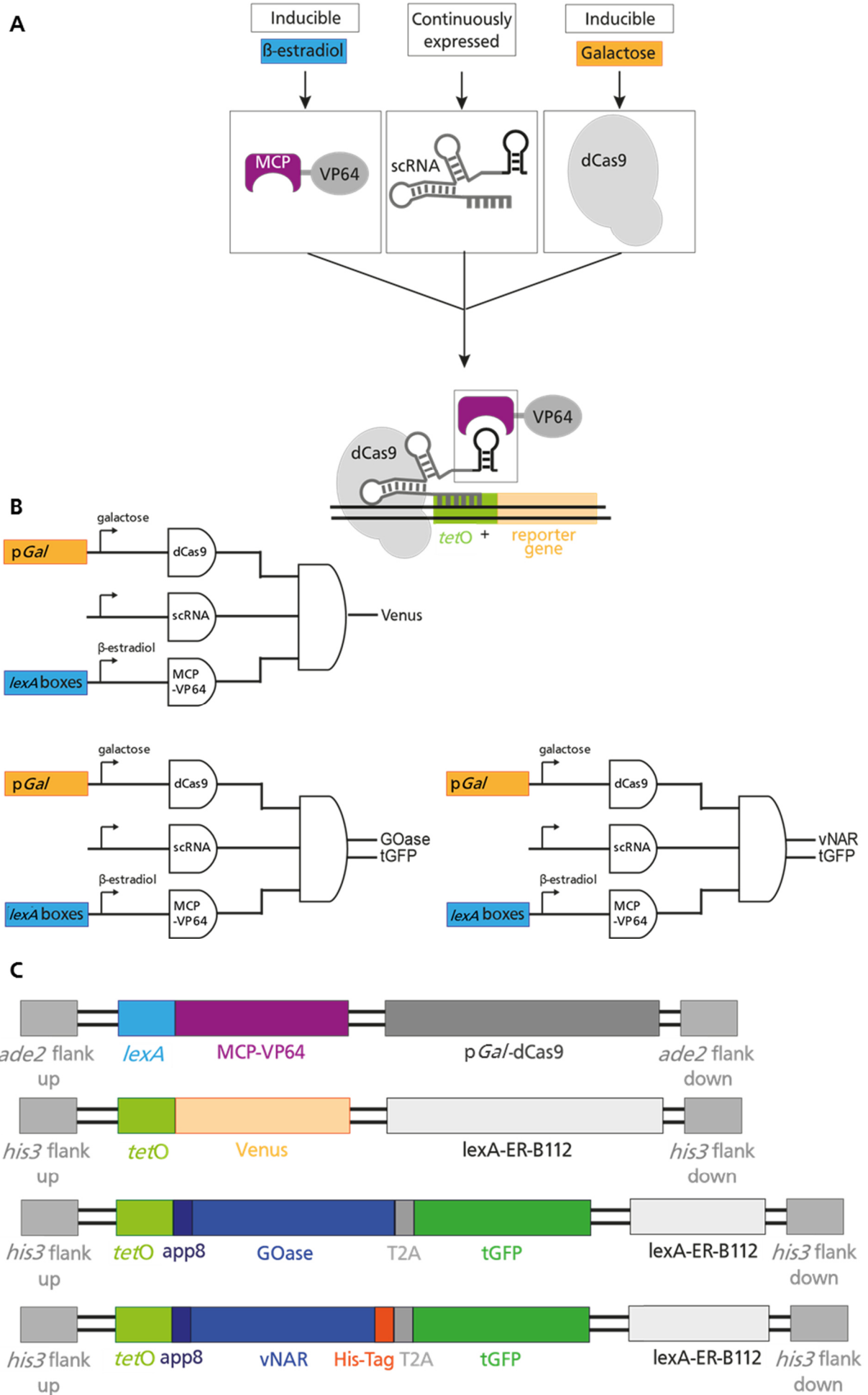
Figure 28 Schematic and genetic overview of the AND gate.

(A) Schematic overview and (B) logic gate for the AND gate. Both showing, that MCP-VP64 is inducible by ES and dCas9 is inducible by galactose, whereas the scRNA stays constitutively expressed. Only when all components are expressed, they bind to *tet*O and induce reporter gene expression. (B) Three different reporter gene setups were tested. First the AND gate with Venus as a single reporter gene. Second GOase and tGFP in a double reporter setup (AND, GO). Third a vNAR and tGFP also in a double reporter setup (AND, vNAR). (C) Genomic overview for the AND gates including homologous flanks for genomic integration as well as the reporter gene combinations, that were genomically integrated.

Table 21 Parts utilized for the construction of the AND, GO switch.

Fragment	Method	fw	rv	Template	Size [bp]	c [ng/μL]	pmol/μL
Ade1	RT PCR, Phu	A1, A11	A12	pJZC793	590	67.34	0.35
Ade2	RT PCR, Phu	A13	A20, A10	pJZC638	7451	84.58	0.03
His2	PCR, Q5	H17	H18	pYD_Leu_app8	315	38.33	0.37
His6	RT PCR, Q5	H1, H3	H16	pSLQ1119	895	230.42	0.78
His14	PCR, Q5	H19	H33	pET22b	2007	120.29	0.18
His15	PCR, Q5	H34	H35	PCT_2A-GFP	1110	39.36	0.11
His16	PCR, Q5	H36	H6, H7	pFRP880	3063	116.22	0.11
gRNA (H)	-	-	-	-	-	64.88	-
gRNA (A)	-	-	-	-	-	80.17	-

Table 22 Parts utilized for the construction of the AND, vNAR switch.

Fragment	Method	fw	rv	Template	Size [bp]	c [ng/μL]	pmol/μL
A1	RT PCR, Phu	A1, A11	A12	pFRP793	590	70.68	0.36
A2	RT PCR, Phu	A13	A20, A10	pJZC638	7451	74.33	0.03
H6	RT PCR, Q5	H1, H3	H16	pSLQ1119	895	68.69	0.23
H11	PCR, Q5	H17	H29	pYD_Leu_app8	315	48.59	0.47
H16	PCR, Q5	H36	H6, H7	pFRP880	3063	20.75	0.02
H20	PCR, Q5	H30	H41	pvNAR	403	135.87	1.02
H21	PCR, Q5	H42	H35	PCT_2A-GFP	1111	120.87	0.33
gRNA (H)				pA6	7612	93	0.04
gRNA (A)				p425-antiAde	7233	122.73	0.05

For the genetic integration, the strain cSLQ.Sc002 was utilized, especially since cSLQ.Sc002 does not contain reporter or CRISPR genes. Due to the high amount of desired DNA, electroporation would be difficult to perform. Hence, for CasEMBLR cells were made chemo competent using the Frozen-EZ Yeast Transformation II Kit (Zymo Research). The chemo competent cells were transformed with 2 μg of the Cas9 encoding plasmid p414 (99)(4.1.6). Transformants were selected by SD-trp agar plates and integration was checked by colony PCR using the oligonucleotides Cas1 and Cas2 (data not shown). The positively tested cSLQ.Sc002_p414 clones were picked, made chemo-competent again and frozen at -80 °C for the following chromosomal integrations.

For transformation 4 picomoles of each part were mixed with 1 μg of the corresponding gRNA plasmid. An exception was made for very large parts, *e.g.* the part encoding for dCas9. For these parts, 0.5 μg of DNA were used. After amplification, the correct size of the constructs was verified by agarose gel electroporation. The DNA was purified using the Wizard® SV Gel and PCR-Clean up System (*Promega*). The parts and plasmid(s) were precipitated and suspended in 5 μL nuclease free water (0). The utilized parts and plasmids for the genomic integrations as well as the concentrations used for precipitation, can be found in Table 23 for the AND gate, Table 24 for AND, GO and Table 25 for AND, vNAR.

Table 23 Used concentrations and parts for 3x/7x *tet*O AND gate transformation.

Part	for 4 pmol [μL]	for 1 μg [μL]	Use [μL]	T2B	T2C	total	V total [μL]
Ade2	10,18	14,56	10	X	X	2	20
Ade3	12,66	11,42	13	X	X	2	26
Ade5	38,08	48,90	40	X	X	2	80
Ade6	120,58	12,43	13	X	X	2	26
His1B2	32,51	11,73	12	X		1	12
His1B3	65,61	19,88	20		X	1	20
His2	95,83	23,42	25	X	X	2	50
pAH006	-	4,21	5	X	X	2	10

Table 24 Used concentrations and parts for the AND, GO transformation.

Part	for 4 pmol [μL]	for 1 μg [μL]	Use [μL]	T2B	T2C	total	V total [μL]
Ade1	11.57		10	X		1	10
Ade2	116.28	11.82	13	X		1	13
His2	10.85		11		X	1	11
His6	5.13		5		X	1	5
His14	22.02		22		X	1	22
His15	37.23		38		X	1	38
His16	34.79	8.60	10		X	1	10
gRNA (H)		15.41	15		X	1	15
gRNA (A)		12.47	15	X		1	15

Table 25 Used concentrations and parts for the AND, vNAR transformation.

Part	for 4 pmol [μL]	for 1 μg [μL]	Use [μL]	T2B	T2C	total	V total [μL]
A1	11.02	14.15	11	X		1	11
A2		13.45	17	X		1	17
H6	17.20	14.56	20		X	1	20
H11	8.56	20.58	9		X	1	9
H16		48.19	40		X	1	40
H20	3.92	7.36	4		X	1	4
H21	12.13	8.27	12		X	1	12
gRNA (H)		10.75	15		X	1	15
gRNA (A)		8.15	9	X		1	9

For the AND switch, a one-step integration for both, the reporter genes as well as the CRISPR/dCas9 gene was performed. In order to enable the integration in two loci, *ade2* and *his3*, during the same transformation step, a new gRNA plasmid was generated. This new gRNA plasmid pAH006 contained a gRNA for both loci and was constructed from the backbone of p425-αAde_gRNA. All utilized parts are listed in Table 26. The plasmid was obtained by ligation of the fragments gRNA1 and gRNA3a with T4 DNA Ligase (*NEB*) and produced in the *E. coli* strain DH5α. The plasmid was prepared using the *PureYield™* Plasmid Miniprep System Kit (*Promega*) and the correct sequence was verified by cPCR using the oligonucleotides gRNA7 and gRNA8 as well as by sequencing using the oligonucleotide gRNA7 (data not shown).

Table 26 Fragments utilized for the construction of pAH006 and the concentration used.

Fragment	Method	fw	rv	Template	Size [bp]	c [ng/μL]
gRNA1	digestion	*Sal*I	*Hind*III	p425-αAde	7233	estimated
gRNA3	PCR, Q5	gRNA5	gRNA6	p425-αHis	390	47.75
gRNA3a	digestion	*Sal*I	*Hind*III	gRNA3	390	estimated

After the successful generation of pAH006, one-step integration for the AND switch was performed using the chemo-competent cSLQ.Sc002_p414 cells. After transformation, cells were plated on SD-trp-leu drop-out agar plates and grown for up to 120 h. Correct part assembly and correct genomic integration was verified by cPCR. For verification of correct integration into the *ade2* locus the oligonucleotides A15, A18 (correct integration into the genome), A25, A26, A27 and A28 (correct assembly) were used. To proof correct integration into the *his3* locus the oligonucleotides H10, H11, H12, H14 (correct integration into the genome), fw_gene-gene_lexA FP and rv_gene-gene_lexA FP (correct assembly) were used (data not shown).

One-step transformation was demonstrated to be efficient. Almost all tested clones contained the target genes in the correct locus. However, only very few clones were obtained, which led to the decision for a two-step transformation. This two-step transformation was expected to be

as efficient regarding integration, but much more efficient regarding the obtained number of clones. Hence, the transformation for AND, GO and AND, vNAR were performed in a two-step transformation.

In the first transformation step, the CRISPR genes were integrated into the *ade2* locus of chemo-competent cSLQ.Sc002_p414 cells. Cells were plated on SD-trp-leu drop-out agar plates and grown for up to 120 h. This order allowed to keep the total number of transformations as low as possible. Additionally, the integration into the *ade2* locus allowed a red/white color screening. *S. cerevisiae* cells are normally white colored, but turn red when the *ade2* mutation in the adenine biosynthetic pathway leads to the accumulation of a cell-limited red pigment (189,190). Hence, after the successful integration of the CRISPR parts into the *ade2* locus, the colonies turned red. This effect allowed the easy selection of putative positively transformed clones. For these clones, the correct part assembly as well as correct genomic integration was verified by cPCR using the oligonucleotides A15, A18 (correct integration into the genome), A25, A26, A27 and A28 (correct assembly) (data not shown). In a second transformation step, the reporter genes were integrated into the *his3* locus. Cells positively tested on the integration of the CRISPR genes were made chemo-competent and transformed with the reporter gene part and plasmid mix. After transformation cells were plated on SD-trp-leu drop-out agar plates and grown for up to 120 h. Correct part assembly as well as correct genomic integration was verified by cPCR using the oligonucleotides H10, H11, H12, H14 (correct integration into the genome), fw_gene-gene_lexA FP and rv_gene-gene_lexA FP (correct assembly) (data not shown).

After successful genomic integration, the CasEMBLR plasmids were removed for both methods by growth in regular YPD medium and subsequent dilution of the culture to 5×10^5 cells/ml. For each strain, 100 μL of these cells were plated out on YPD agar plates and grown for 48 h. Single colonies were picked and transferred to YPD, SD-trp and SD-leu drop-out plates and grown for 48 h. One clone per AND switch was selected for further experiments, that only grew on YPD. This plasmid-free clone was subsequently transformed with 2 μg of the scRNA plasmid pJZC588 *via* electroporation. Cells were plated out on SD-ura drop-out agar plates and correct plasmid integration was verified by cPCR using the oligonucleotides gRNA_fw_Colony PCR and gRNA_rv_Colony PCR (data not shown).

To sum up, at least one clone per switch setup was obtained (Table 27). The tool CasEMBLR has repeatedly proven its suitability for genomic engineering in *S. cerevisiae*. As described by Jakociunas *et al.* (99), it is indeed possible to simply and efficiently assemble different genes *in vivo* from DNA parts. However, integration into multiple loci at the same time has not proved as effective as promised by the authors. After the integration into two loci, the number of colonies was very low. Thus, a two-step transformation was preferred and is recommended as method of choice for integration into several loci. In conclusion, CasEMBLR provides a reliable

tool for genomic integration in *S. cerevisiae* with the huge advantage that the parts do not have to be assembled beforehand.

Table 27 Summary of the transformed clones for the different AND gates.

Name	Integrated genes	Origin
AND, 3x *tet*O	*ade2::lexA-MCP-VP64_Gal10-dCas9 his3::TET03-Venus_lexA-ER-B112*, scRNA (plasmid)	cSLQ.sc002
AND, 7x *tet*O	*ade2::lexA-MCP-VP64_Gal10-dCas9 his3::TET07-Venus_lexA-ER-B112*, scRNA (plasmid)	cSLQ.sc002
AND, GO	*ade2::lexA-MCP-VP64 Gal10-dCas9 his3::TET07-app8-Goase-T2A-tGFP_ lexA-ER-B112*, scRNA (plasmid)	cSLQ.sc002
AND, vNAR	*ade2::lexA-MCP-VP64 Gal10-dCas9 his3::TET07-app8-vNAR-His-Tag-T2A-tGFP lexA-ER-B112*, scRNA (plasmid)	cSLQ.sc002

5.2.4. Examination of the functionality of the AND gate

After all transformations were successfully performed, the different switches were tested on their functionality and leakiness (5.2.4, 5.2.5 and 5.2.7), their tunability (5.2.6) and their time-dependency (5.2.8). As a first experiment, the general functionality of the double-inducible setup was verified by induction of the single reporter AND gate. Therefore both, the AND switch with Venus placed behind 3x *tet*O and the AND switch with Venus placed behind 7x *tet*O were used for an induction experiment. Additionally, the Ssw, 7x *tet*O was used as positive control and the strain cSLQ.sc002 as negative control.

The four strains were inoculated and induced in tubes following the protocol 4.4.2. The strain cSLQ.sc002 was grown in SD full medium, whereas the other strains were grown in -ura drop-out medium. For the induction experiment, cells of the Ssw, 7x *tet*O strain were grown in SD medium as a control and in SG medium for induction. Cells of the AND gate strains were grown in SD, SD + ES and SG as controls and in SG + ES for induction.

The utilized ES approach was adapted from Ottoz *et al.*, who detected that their ES-inducible approach is fully activated between 500 nM and 2000 nM ES (45). The ES concentration used for induction was chosen according to their findings. In order to ensure that the ES concentration in the induction medium is high enough to allow target gene expression, cells were induced using 500 μM ES. Moreover, to verify that the reporter construct is functional both strains were induced with 100 μg/mL Dox in SD medium. Venus fluorescence was measured *via* FACS (*BD*). For the comparative analysis of the strains, the Flowing software (*Turku Centre for Biotechnology of Turku*) was used. The Ssw, 7x *tet*O and the AND, 7x *tet*O strains were compared in Figure 29A and the AND gate with the different *tet*O copy numbers in Figure 29B. The data of the dox experiments is not shown, but Venus expression was successful.

In the comparative overlay histogram of Figure 29A it is shown, that the AND switch setup is functional. When grown in SG + ES, the reporter Venus is strongly expressed. In comparison to the Ssw, 7x *tet*O, both strains have an equally strong Venus reporter gene expression. When grown in SG only the AND gate is tightly regulated, whereas growth in SD + ES results in a significant leakiness. Likewise, both *tet*O strains strongly express Venus, when induced with galactose and ES (Figure 29B). Both are tightly regulated in SD and SG, but are leaky upon addition of ES. There was little difference between the *tet*O copy numbers concerning the leakiness. In comparison, the rate of expression for 7x *tet*O was slightly higher. Therefore, for further experiments only the clone AND, 7x *tet*O was used.
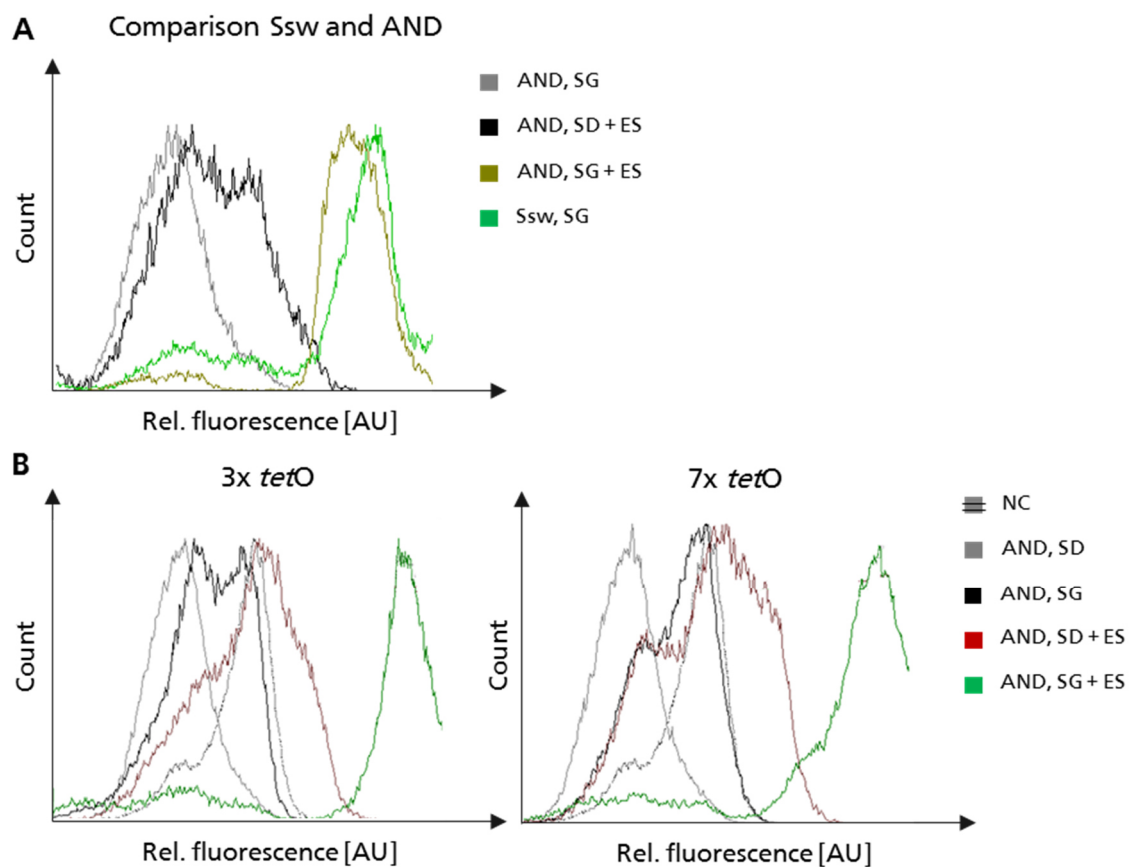
Figure 29 ES and galactose induction of the 3x *tet*O and 7x *tet*O AND switch.

(A) First induction experiment for the 7x *tet*O AND switch grown in SG (grey), SD + 500 µM ES (black) and SG + 500 µM ES (khaki). Additionally, the Ssw, 7x *tet*O was induced with SG (green). As NC the strain cSLQ.sc002 was grown in SD (dotted grey).

To sum up, two requirements of the AND gate have already been met. First, the AND switch design can generally be stated as functional, since the setup allows the ES and galactose inducible expression of a reporter gene. Second, the expression levels match those of the single galactose switch. The third requirement of tight regulation is not fulfilled yet.

The AND gate is tightly regulated in the presence of galactose only, but not in the presence of ES only. Even though, the disadvantage of high basal activity of the galactose switch seems to

be successfully compensated by the tight ES switch, the leakiness in the presence of ES was unexpected, since the ES system is described as being tightly regulated (45,46,191). Interestingly, it has been demonstrated, that in high concentrations ES can have a toxic effect on yeast cells (192,193). In comparison to the ES-induction concentrations of Ottoz *et al.*, this induction experiment was carried out with up to 250x higher concentrations (Ottoz *et al.* max. 2 μM, here 500 μM) (45).

To elucidate, which role ES played in the high basal expression, another experiment was conducted. To this end, cells of the strain AND, 7x *tet*O were grown in SD medium with different ES concentrations. Measurement of the cell distribution was performed using FACS (*BD*) and analysis was performed using the Flowing software (*Turku Centre for Biotechnology of Turku*). The cell distribution was represented by the ratio of forward (FSC) to sideward (SSC) scatter and can be found in Supplementary Figure 52. Depending on the ES concentration, the cell distribution changed significantly. At a low ES concentration, the population of cells displayed a narrower fluorescence distribution compared to cells that were subjected to high ES concentration. It can therefore be assumed that a high ES concentration causes an increased mortality and fluorescence distribution of the cells. Therefore, significantly lower ES concentrations were used in future experiments. Furthermore, it can be assumed that the desired tight regulation of the AND gate can be achieved with comparable low ES concentrations of 100 nM and below.

5.2.5. Examination of the functionality of the double reporter setup

After having demonstrated, that the single reporter AND setup is functional, the next step was to demonstrate the functionality of the double-reporter setup as well. To this end, the AND and AND, GO setups were compared *via* fluorescence measurements (Figure 30).

For the experiment cells were inoculated and induced in tubes following the protocol described in 4.4.2. All strains were grown in -ura drop-out medium. For the induction experiment, cells of the strains AND and AND, GO were grown in SD, SD + 100 nM ES as controls and SG + 100 nM ES for induction. For comparison, the strain Ssw, 7x *tet*O was grown in SD as a control and SG for induction. All samples were prepared as biological triplicates. The Venus and tGFP fluorescence were measured *via* Accuri™ (*BD*). For analysis, cytometry data was exported as FCS 3.0 files and kindly processed by Johannes Falk using Mathematica 11 software (*Wolfram*). This setup allowed the direct comparison of basal activity and expression levels. The comparison of the leakiness and the fold activation of the Ssw, 7x *tet*O, the AND gate and AND, GO are shown in Figure 30.
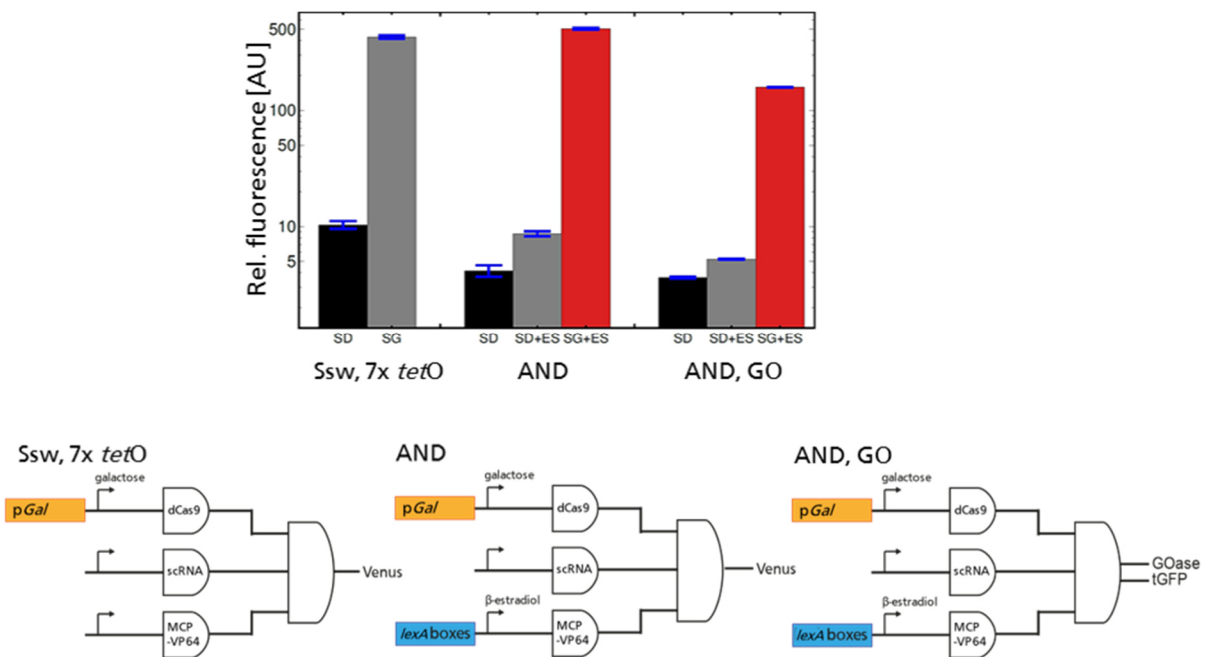
Figure 30 Comparative induction of Ssw, 7x *tet*O AND and AND, GO.

The AND gate and the AND, GO gate were grown in SD (black), SD + 100 nM ES (grey) and SG + 100 nM ES (red). Error bars indicate the standard deviation of the biological triplicates. The corresponding logic gate is shown at the bottom for all three setups.

First, it can be stated that 100 nM ES are sufficient to achieve maximum induction. At an induction concentration of 100 nM ES, only a slight impact on cell distribution for the AND switch was detected (Supplementary Figure 52). Additionally, induction with 100 nM ES had no effect on cell growth of the AND strain and only a slight impact of the AND, GO strain (Supplementary Figure 53). Hence, for following experiments a concentration of 100 nM was set as the maximum ES induction concentration.

In Figure 29 it was shown, that the expression level of the AND switch corresponds to that of the Ssw, 7x *tet*O, which was confirmed hereby. In comparison to these expression levels, the expression level of the double reporter AND, GO was slightly lower. This effect may be due to different fluorophore properties (Venus and tGFP), like slightly different excitation and emission wavelength (194), but at least partially may also be caused by the T2A setup. Due to the properties of ribosomal skipping, the transcript behind the T2A signal is not always completely translated (157). As a result, slightly less fluorophore is produced compared to a classical expression scheme lacking T2A. Nevertheless, the GOI-T2A-tGFP double reporter setup worked as intended.

The basal activity for the strain AND, GO corresponds to the one of the single reporter AND gate for both SD and SD + ES. For both strains, the basal expression of cells grown in SD only is slightly lower, than when grown in SD + ES. Hence, the gate is still not completely tightly regulated. However, when compared to the Ssw, 7x *tet*O, the basal expression is significantly lower for all AND switch controls. Thus, by implementing the ES switch to build a double

switchable AND gate, it was possible to reduce the basal expression significantly. Even in the presence of the inducer ES, the switch is so tightly regulated, that the level of basal expression remains under the level of basal expression of Ssw, 7x *tet*O in SD only. A fold-activation of 111-fold for the AND switch and 99-fold for the AND, GO were observed.

5.2.6. Concentration-dependent analysis

In the previous chapter, the general functionality of the single and double reporter setups was demonstrated. In this paragraph, a concentration-dependent induction experiment was performed. Therefore, the dose-dependent ES induction was examined for the AND, GO and AND, vNAR in Figure 31A.

To compare the strains AND, GO and AND, vNAR, both strains were inoculated and induced in tubes following the protocol described in 4.4.3. For the controls, cells were grown in SD, SD + 100 nM ES and SG medium. To verify dose-dependency, cells of both strains were induced in SG with the ES concentrations 1 nM, 10 nM and 100 nM. The tGFP fluorescence was measured *via* Accuri™ (*BD*). For analysis, cytometry data were exported as FCS 3.0 files and kindly processed by Johannes Falk using Mathematica 11 software (*Wolfram*).

Both strains show a very similar ES concentration-dependent induction behavior. Even the sample, which was induced with only 1 nM ES, showed significant fluorescence. This is especially interesting, since the ES system published by Ottoz *et al.* containing the hTF LexA-ER-B112 showed first induction only around 30 nM ES (45). These results demonstrate, that the AND switch setup did not only enable a very sensitive induction, but also allows ES concentration-dependent induction.

To verify those results and to gain more information about the dose-dependency, two further experiments were performed using the strains AND and AND, GO. First, a detailed ES dose-dependent experiment (Figure 31B), and second, a galactose dose-dependent experiment were performed (Figure 31C).

For both experiments the same procedure was used as described in the paragraph above. For the first experiment induction was performed with SG and multiple concentrations of ES between 0.1 nM and 100 nM ES: 0.1 nM, 0.5 nM, 1 nM, 5 nM, 10 nM, 15 nM, 20 nM, 30 nM, 50 nM, 100 nM. For the AND gate fluorescence could be detected beginning at 5 nM ES and a maximum fluorescence was reached at approximately 30 nM ES. For AND, GO an increase in fluorescence could already be measured at 0.1 nM ES reaching a maximum value at 20 nM concentration. Interestingly, for AND, GO maximum cellular fluorescence was reached at a lower ES concentration compared to AND, whereas the mean fluorescence signal was weaker. This leads to the assumption, that the double reporter design lead to an increased sensitivity, so the ES concentration resolution was refined at lower concentrations. In conclusion, the AND

gate setup in principle enables the fine adjustable expression of different GOI at low nanomolar ES concentration.
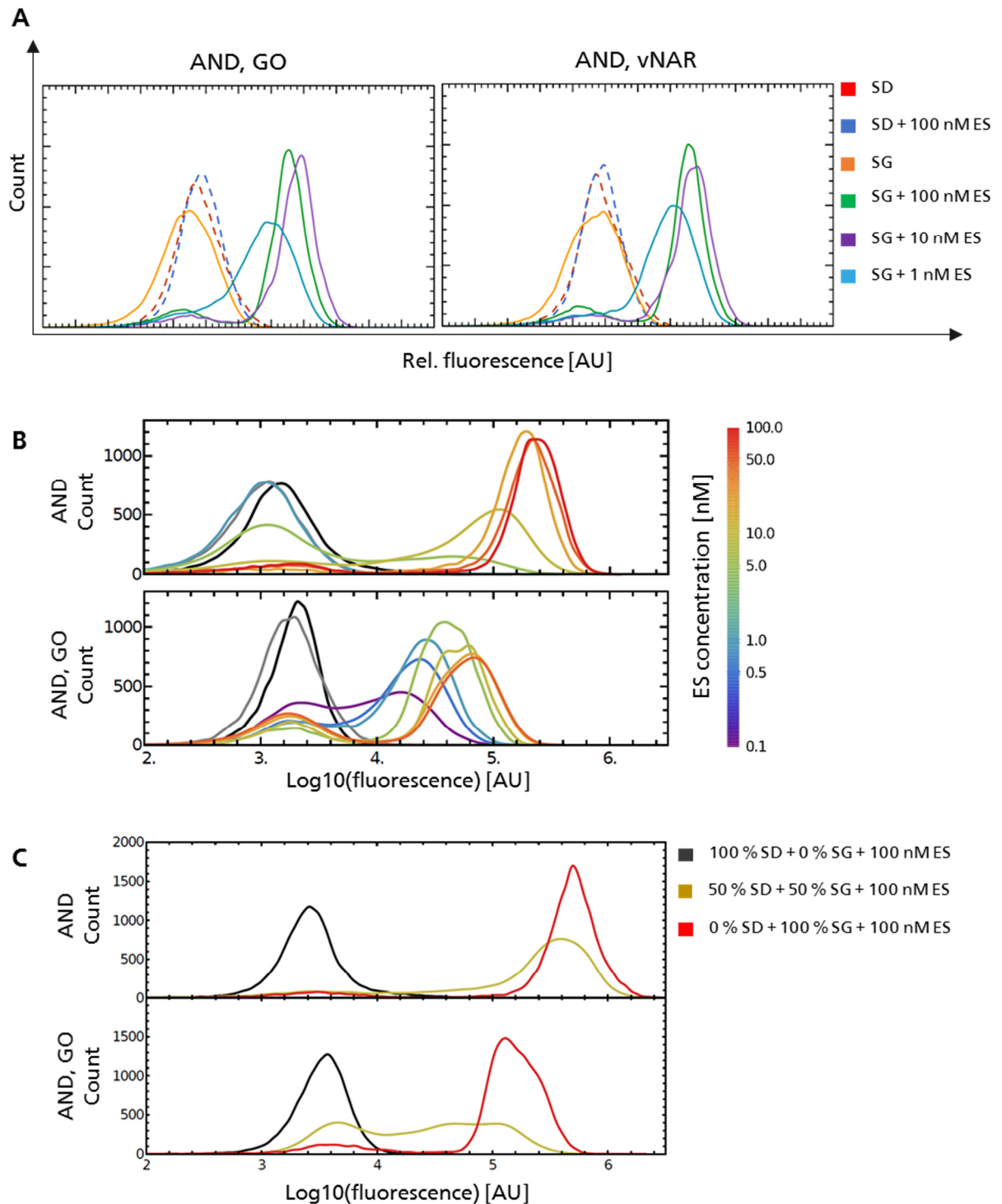

Figure 31 Dose–response induction of the single and dual reporter gene setup.

(A) Dose-response histograms of the AND, GO (left) and the AND, vNAR (right) gate. (B) Dose-Response histograms of the single-reporter system (top) and the dual reporter AND, GO setup (bottom). The black histogram indicates the control, where cells were grown in SD only, the gray histogram indicates, where cells were grown in SG without ES. (C) Test for Galactose tunability of the AND (top) and AND, GO clone (bottom). The clones were induced with a constant amount of ES, but different SG concentrations.

For the second experiment, induction was performed with 100 nM Es and different ratios of SD and SG. This experimental setup was performed in order to determine, whether a dose-dependent galactose induction is also possible. Therefore, the cells were inoculated into medium with three different SD to SG ratios: 100/0, 50/50 and 0/100. For both strains no induction at 0 % SG, a smooth induction for 50 % SG and a strong induction at 100 % SG were detected (Figure 33C). Hence, dose-dependent galactose switching was demonstrated, but resulted in a fluorescence distribution of Venus and tGFP producing cells over a broad range rather than a distinct off/on switch. Switching with galactose was not further investigated.

From these results, it can be summarized that not only the single reporter AND setup, but also the double reporter setups AND, GO and AND, vNAR are functional. At ES concentrations of 100 nM all AND gates are tightly regulated, whereas a high fold-activation was achieved. Hence, the already fulfilled requirements for double-dependent functionality and high expression levels were also fulfilled. Additionally, the third requirement of tight regulation is fulfilled by adjustment of the applied ES concentration. Even the requirement for a concentration-dependent AND gate is fulfilled, which was demonstrated in Figure 31. To sum up, four requirements for the AND gate design were fulfilled. In order to be certain about the functionality of the double-reporter setup, further experiments were performed to specifically verify the expression of GOase and vNAR.

5.2.7. Verification of the expression of GOase and vNAR

First, the expression of GOase had to be verified by SDS PAGE and ABTS assay. Therefore, the expression of reporter construct GOase-T2A-tGFP was induced in order to determine if GOase is actually secreted. GOase expression and purification were performed according to the protocol described in 4.5.1 and 4.5.2. Induction of GOase-T2A-tGFP expression was checked by flow cytometry (data not shown). After successful verification of tGFP fluorescence, the cells were precipitated and the supernatant was concentrated to 25 ml using a Vivaflow 200, 10.000 MWCO Hydrosart laboratory crossflow cassette (*Sartorius*). Until further usage, the supernatant was stored at 4 °C. Meanwhile, the cell pellet was resuspended in 1x PBS, disrupted using a cell disrupter (*Constant systems LTD*) and cell debris was removed by centrifugation. Both supernatant and cell debris were analyzed using ABTS assay (Figure 32A) as well as SDS-PAGE (Figure 32B).

For ABTS assay, 180 μl of cell suspension or supernatant (sample diluted 1:10 in PBS) were mixed with 10 μl Horseradish peroxidase (0.1 mg/ml), 10 μl ABTS (10 mM) and 10 µl galactose substrate (1 M). After 5 min the absorption of ABTS was measured at 405 nm with INFINITE Tecan M-1000 (Tecan). The absorption was exported to MS Excel (*Microsoft*) and the analysis was kindly performed by Johannes Falk using Mathematica 11 software (*Wolfram*). As negative

control supernatant of uninduced cells was used. ABTS assay revealed, that GOase was only present in the supernatant. This result was confirmed by SDS PAGE analysis of the concentrated supernatant.

In a second setup, the concentration-dependent expression of GOase was examined (Figure 32C). Therefore, the AND, GO strain was grown in tubes according to the protocol described in 4.4.2. Cells were grown in SD, SD + 100 nM ES and SG for controls and in SG with ES concentrations of 1 nM, 10 nM and 100 nM for induction. After growth, cells and supernatant were separated by centrifugation. The supernatant was replaced and stored at 4 °C in a 96-well plate until analysis. Analysis was performed using ABTS assay. 0.25 % H_2O_2 were added as positive control. The error bars indicate the standard deviation of the biological triplicates, except for SG + 100nM ES, where only a duplicate was available. Even though ABTS assay is really sensitive, no GOase activity was detected for the negative controls. For the samples a dose dependent GOase expression was detected.
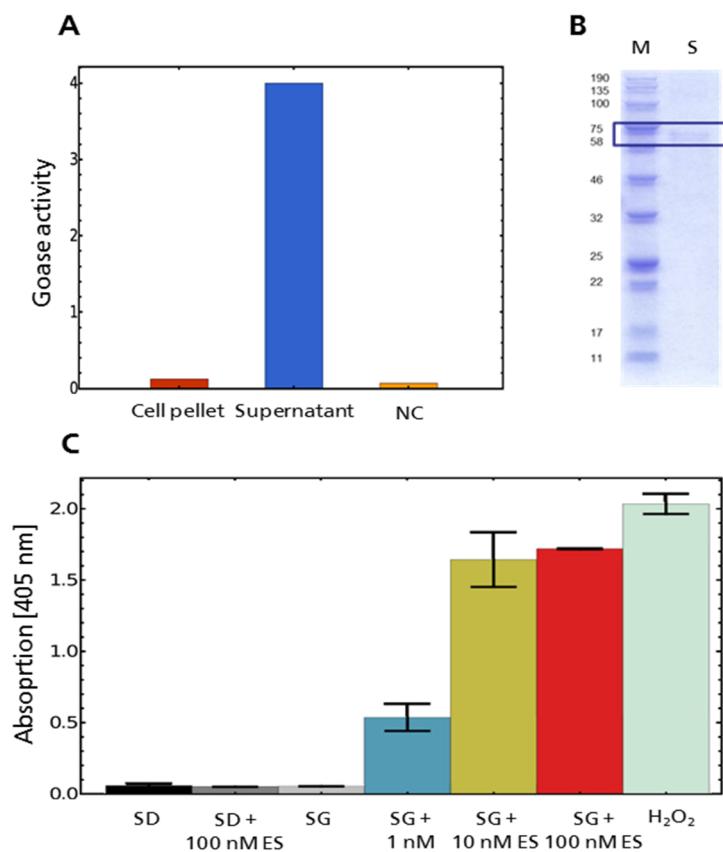
Figure 32 Detection and verification of GOase activity.

(A) Localization of GOase activity. ABTS assay of the GOase-tGFP reporter strain after induction of 1 l of yeast culture. The supernatant was concentrated by cross-flow filtration with a Viva flow 200, 10.000 MWCO Hydrosart (Sartorius) from 1 l to 50 ml. As negative control supernatant of uninduced cells was used. (B) SDS PAGE analysis of concentrated supernatant. M = Blue Prestained Protein Standard, Broad Range (*NEB*) and S = supernatant. (C) ABTS assay for determination of GOase activity in cell supernatants upon induction of gene expression at varying ES concentrations. H_2O_2: PC, 0.25 % H_2O_2 were added to the ABTS assay. Error bars indicate the standard deviation of the biological triplicates. For SG + 100nM ES only a duplicate was available.

Therefore, the results of the tGFP measurement were verified. Thus, the AND gate design allows the concentration-dependent expression of one or multiple reporter genes when combined with a T2A setup.

Second, the expression of vNAR had to be verified by SDS PAGE, Western blot and ELISA. Therefore, vNAR expression and purification was performed according to the protocol described in 4.5.1 and 4.5.3. vNAR-tGFP expression was verified by flow cytometry (data not shown). After successful verification of tGFP fluorescence, the cells were precipitated and the supernatant was concentrated to 3 mL using Amicon Ultra-15 Centrifugal Filter Units (*MWCO 3 kDa, Merck Millipore*). The cell pellet was suspended in IMAC buffer A, disrupted using a cell disrupter (*Constant systems LTD*) and cell debris was removed by centrifugation. For purification of the His-tagged vNAR construct, IMAC was used. During elution 1 mL fractions were collected and applied on SDS-PAGE. Gels were either stained with Coomassie Blue for visualization of the whole protein content (Figure 33A) or blotted onto nitrocellulose membrane (Semi-dry Western Blot) for specific immunostaining (Figure 33B). For western blot analysis, the membrane was blocked with 1.5% milk powder solution, and incubated with monoclonal Penta-His antibody followed by Anti-Mouse IgG (whole molecule)-Alkaline Phosphatase antibody (*Sigma Aldrich*). Addition of the detection reagent resulted in a purple-black precipitate only in presence of alkaline phosphatase activity, which enabled indirect detection of His-tagged proteins.
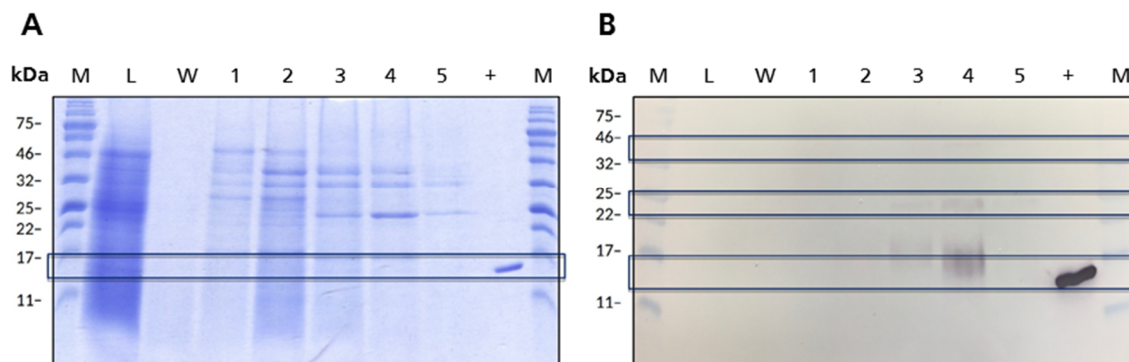
Figure 33 Purification and analysis of vNAR.

(A) and (B) both show the results of the purification of the AND, vNAR cell lysate with immobilized metal ion affinity chromatography (IMAC). (A) Samples were collected and applied to on an SDS PAGE. (B) Western blot analysis of the samples, which were immunostained with α-His antibody (mouse) and anti-mouse IgG-AP (goat). L = filtrated cell lysate, W = IMAC wash, 1-5 = IMAC elution/peak fractions, + = PC vNAR His-tag. Expected sizes for the constructs are vNAR = 13.256 kDa, vNAR+app8 = 22.045 kDa, vNAR+T2A+tGFP=39,726 kDa, vNAR+app8+T2A+tGFP=48,512 kDa, tGFP=24,676 kDa. For SDS PAGE and Western blot Blue Prestained Protein Standard, Broad Range (*NEB*) was used.

For SDS-PAGE multiple bands were detected for all samples. Hence, IMAC was not sufficient for complete purification of the vNAR construct. By contrast, Western blot was able to specifically detect the vNAR and a vNAR-app8 construct in two fractions. Thus, the expression

of vNAR was verified and the functionality of the double reporter AND, vNAR gate was demonstrated. However, the purified supernatant still contained to many other proteins in order to perform ELISA. ELISA was intended to demonstrate functionality and dose-dependency of the double-reporter setup. Both have already been demonstrated by fluorophore analysis of AND, GO and vNAR in Figure 30 and for GOase in Figure 32. Functionality has also been demonstrated by Western blot analysis. Hence, no further purification steps were performed for vNAR purification and ELISA detection was not further pursued.

With this paragraph the specific expression of GOase and vNAR was demonstrated. Hence, the double reporter setup allows the expression and indirect verification of any GOI in the T2A setup. For complete characterization of the switching behavior, in a last experiment the time-dependent induction of the single and double reporter setup was analyzed. Because of the simple and quick detection methods of GOase, for this experiments the AND, GOase strain was used.

5.2.8. Time-dependent analysis

Time-dependent analysis was performed to achieve information about the length of the time period needed, until the first reporter gene expression can be measured as well as how long it takes to reach maximum induction. For time-dependent measurement, the single reporter AND gate and the double reporter AND, GO gate were utilized. For both gates flow cytometry analysis was performed on cells incubated with 10 nM ES and galactose (Figure 34A+B) and additionally with 100 nM ES for the double reporter system (Figure 34C).

For the time dependent measurements, the strains were inoculated and induced according to the protocol described in 4.4.4. Induction was performed using either 10 μL or 100 μL of a 10 μM ES stock solution, leading to a concentration of 10 or 100 nM, respectively. After each hour 200 μL of the cell suspension were removed and replaced by 200 μL of SG medium containing 10 nM/100 nM ES. The extracted cell suspension was centrifuged and the cells were suspended in PBS for flow cytometry measurement. For the AND, GO samples the supernatant was used for ABTS. Data analysis was kindly performed by Johannes Falk using Mathematica 11 software (*Wolfram*).

A first increase of fluorescence was measured after approximately 6 h for the single reporter setup and after 2 h for the double reporter setup, regardless of the ES concentration. After 15 h both gates were fully activated and no further increase of the fluorescence was detected. In comparison, the fluorescence for both AND, GO concentrations increased approximately to the same extent, but for the higher concentration it has reached an overall higher maximum. The same effect was demonstrated for GOase activity.
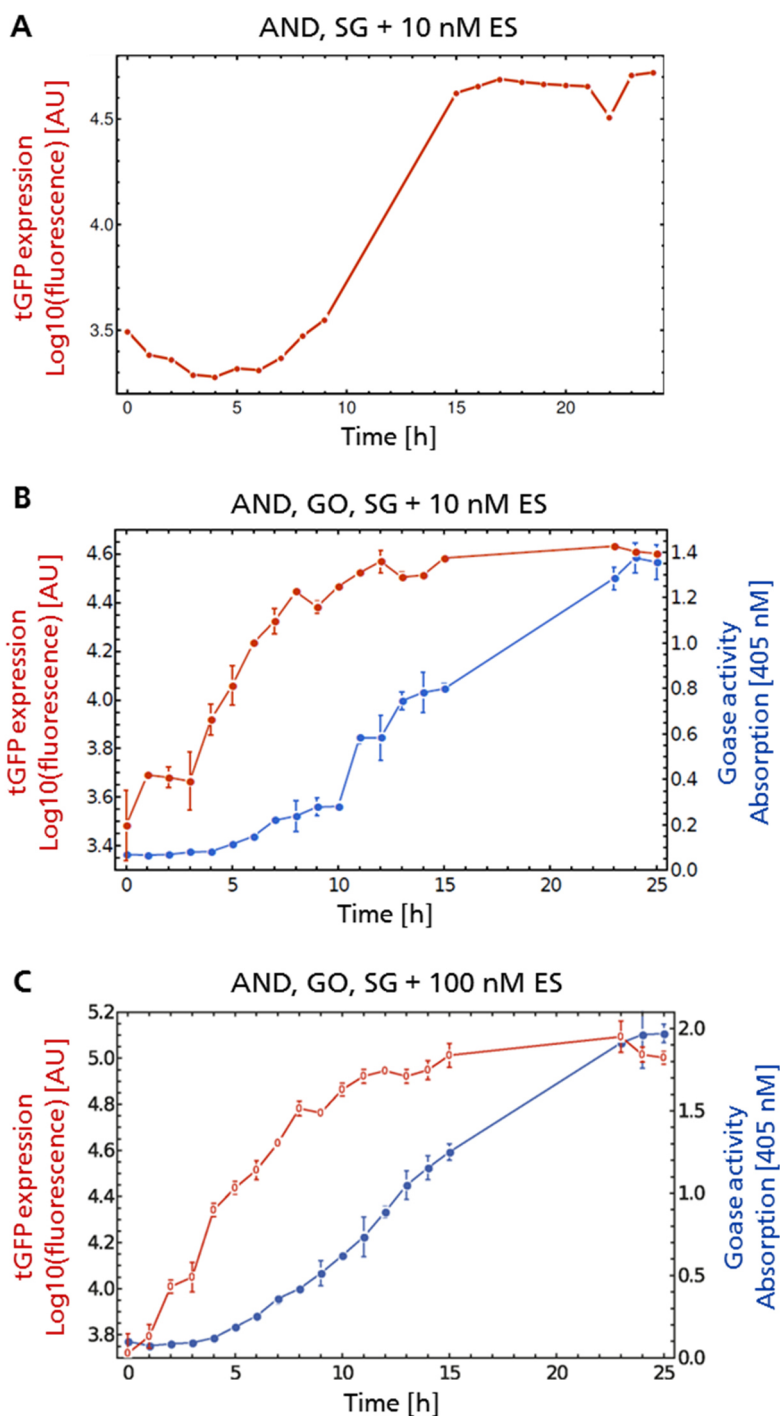
Figure 34 Time-dependent measurement of gene expression for the dual reporter system.

(A) Time dependent measurement of single reporter system. Induction was performed with 10 nM ES and galactose. (B) + (C) Time dependent measurement of gene expression for the dual reporter system. Induction was performed with 10 nM ES (B) or 100 nM ES (C) and galactose, (blue) time dependent measurement of GOA activity examined by ABTS assay, (red) time dependent measurement of tGFP by flow cytometry. The error bars indicate the standard deviation of the biological triplicates.

GOase activity was determined by ABTS assay for AND, GO. For both induction concentrations, first GOase activity was observed after 6 h and continued to increase until the hour 23. As expected, GOase activity correlated well with cellular fluorescence. However, measurement of GOase activity was delayed for approximately 4 h. This delay may be explained by the different

synthesis pathways: cytoplasmic expression of tGFP versus secretion of GOase. For secretion, a protein has to pass through the endoplasmic reticulum and the Golgi apparatus prior to be packaged into secretory vesicles, which fuse with the plasma membrane to release the fully processed protein into the surrounding medium (195). This process takes time, which leads to a decreased detection. Additionally, GOase is with a size of 65 kDa (168) larger than tGFP with a size of 26 kDa (196). Since the time needed for protein folding among others depends on its length (197), GOase requires more time for folding so that the detection is delayed. Nevertheless, our data indicates that co-translation *via* T2A ribosomal skipping can be used as a tool to follow time-dependent expression of a GOI and to quantitate its accumulation.

5.3. Further analysis of the AND gate by collaborations with other scientific fields

This work has been performed in the context of synthetic biology, making numerous opportunities for collaboration with other scientific disciplines available. In the course of further analysis of the AND setup, it was decided to work together with two different disciplines. The collaborations included both, computer-based modeling conducted by Johannes Falk from the group of Prof. Drossel (Physics Department of TU Darmstadt) and microfluidic measurements carried out by Tim Prangemeier from the group of Prof. Koeppl (Department of Electrical Engineering and Information Technology at TU Darmstadt). The results of the collaborations have been published, hence some parts of the following section were taken and adapted from Hofmann *et al.* Additional material and methods also can be found in Hofmann *et al.* and in the dissertation of Johannes Falk (4,198).

5.3.1. Mathematical modeling to rebuild the experimental setup

In order to understand the underlying principles that account for the observed dose dependency, a minimalistic dynamical mathematical model was developed in collaboration with Johannes Falk. The model comprises three important processes:

- the diffusion of the transcription factor (hTF)
- the expression of mRNA regulated by the hTF
- the degradation of the fluorescent reporter proteins Venus or tGFP

The established minimal model allowed, to capture most biological processes while still being capable of covering all important results of the experiment. Based on different reaction equations, a model was generated based on two ordinary differential equations that describe the time dependent concentrations of the ES-hTF complex in the nucleus and the tGFP mRNA. The corresponding formulas and derivations can be found in (4). The concentration of ES in the medium was given by the experimental conditions and was held constant during the

---

experiment. To be able to compare the model and the data, a scaling factor was introduced. This scaling factor accounts for the translation process and additionally maps the number of fluorescent proteins to the measured fluorescence value. The obtained values can be found in (4). For the model it was taken into account, that two reporter systems based on different fluorescent proteins were used. The AND gate was simulated using the Stochastic Simulation Algorithm (199) of the Dizzy Software Package (200).
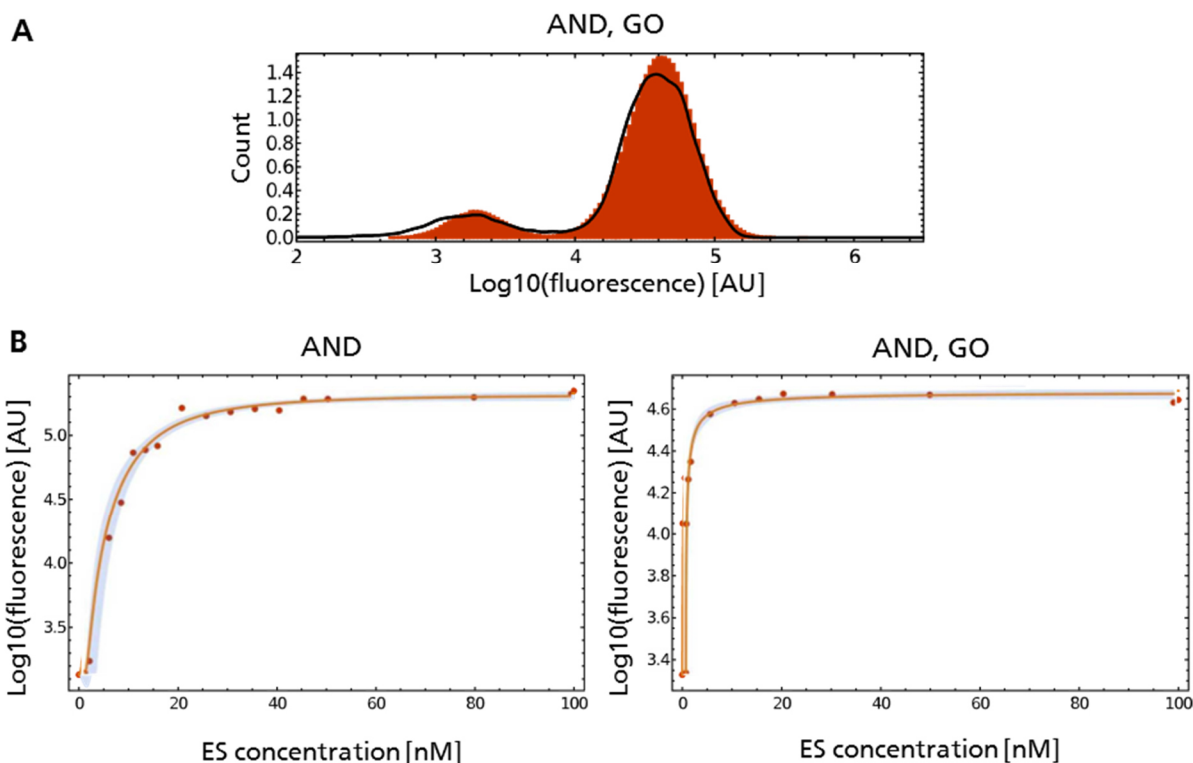

Figure 35 Comparison of model data with the real data.

(A) Comparison of the stochastic model (red histogram) with the experiment (black solid line) for AND, GO at an ES concentration of 5 nM. (B) Dose–response curves of single reporter (left) and double reporter (right) setup. Markers indicate experimental results; the solid line indicates the expectation according to the mathematical model. The blue band denotes the 90% confidence interval of the mean of the model. The standard-error bars of the experimental data are smaller than the markers.

First results using the minimal model predicted maximum reporter gene expression of both, the single and double-reporter setups at a concentration above approximately 35 nM ES after 20 h of induction. An exemplary comparison between the experimental data and the data obtained from the stochastic model is given in Figure 35A. A detailed comparison for the single and double reporter setup can be found in (4). In Figure 35B the mean of the dose-respond histograms for AND and AND, GO are shown together with the fitted model. The model accurately predicted the fluorescence behavior of the AND gates. Thus, the established computational model could be used to obtain further results *in silico*. For example, it would be possible to exactly quantify the ES concentration that is necessary to reach a desired fluorescence or other target gene expression. In this context, it is important to note that the

model is by purpose not designed as a complex model that tries to capture all ongoing processes in full detail. The intention of the model is rather to describe universal principles that can lead to the observations made by the experimental data.

In conclusion, the AND gate enables the fine adjustable expression of different GOI at low nanomolar ES concentration. Outside this rather small range GOI expression is broadly binary.

5.3.2. Microfluidic enables time-lapse single-cell experiments

After the concentration dependency had been examined more closely with the help of the mathematical model, the time-dependent induction was further analyzed using microfluidics. Flow cytometry, which was performed to gain the results shown above, can only provide snapshots into the distribution of fluorescence across a population of cells. Hence, to gain a deeper insight into dynamics of individual cells, time-lapse measurements were recorded for the dual reporter setup. Time-lapse single-cell experiments were carried out on a microfluidic chip using a platform inspired by ALCATRAS (201) in cooperation with Tim Prangemeier.

For the experiments, cells of the AND, GO gate were utilized. Cells were grown over night and freshly inoculated into SD-ura medium. These cells were grown at 30 °C for 5 h before they were induced at t = 0 with SG-ura and 20 nM or 100 nM ES, respectively. Cells were loaded on the microfluidic chip and exposed to a controlled environment at 30 °C with continuous flow of the respective inducer medium. This continuous flow ensures that daughter cells are flushed away, while the mother cells are confined. For analysis a microscope image was recorded every 10 min. The resulting single traces were extracted with a FiJi/Matlab script. The results can be seen in Figure 36.

Distinctive differences were observed for single-cell traces of the two ES concentrations. For the relatively high induction concentration of 100 nM ES, the cells demonstrated a homogeneous dynamic without a phase shift. Already 7 h after induction the maximum fluorescence was reached, after 12 h the cells arrested their growth and no further budding events were detected. The production of tGFP stopped as well, leading to a rapid decrease of detected fluorescence. The main reasons for this decrease might be photobleaching and potential bleaching due to presence of protein damaging H_2O_2. The arrested cell growth might be the result of a combination of detrimental effects, such as metabolic overload and potential toxicity of GOase-mediated generation of H_2O_2. In comparison, for the lower induction concentration of 20 nM ES, the cells behave more heterogeneously: some of the cells remained switched off and the cells that switch on, did so with an intermittent phase shift. For some cells even an oscillation between the off and on state was detected. Some of the cells reached an arrested state as well, while others remained budding and continuously increased the expressed fluorescence. Hence, the arrest of growth seemed to be dose dependent.
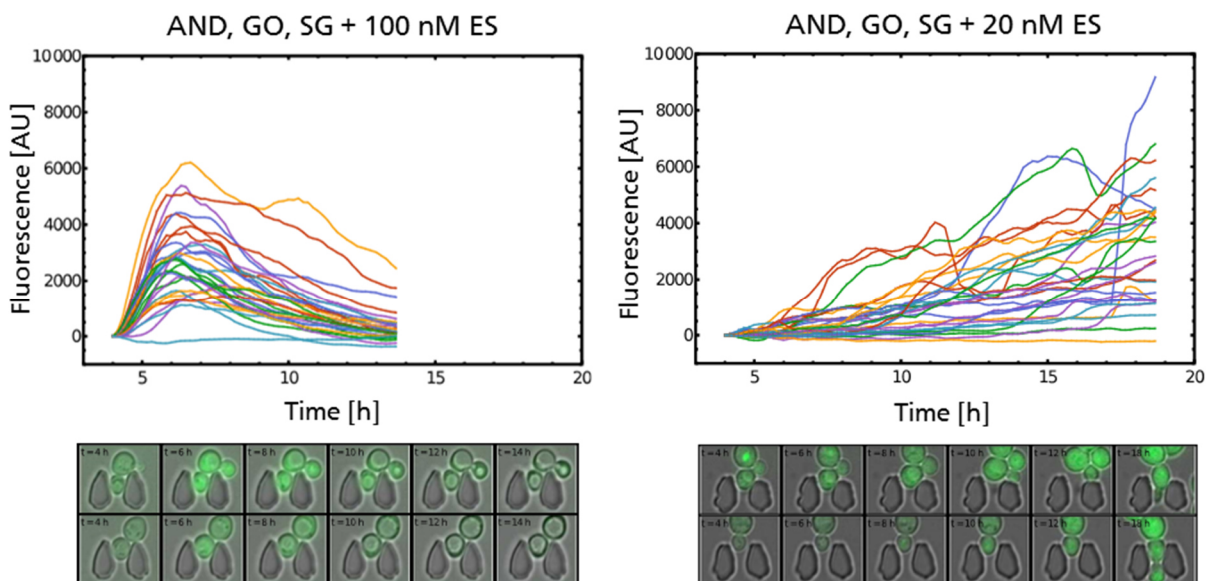
Figure 36 Microfluidic measurements for time-dependency.

Single-cell traces from 30 cells, each for 100 nM ES (left) and 20 nM ES (right), respectively. Below are corresponding fluorescence microscope images of selected cells for a given time-point. The cells are trapped in micro-patterned traps in continuous flow.

While there is no conclusive evidence as to a single cause, it is deemed to be a combination of metabolic overload, increased sensitivity of the AND gate to ES and also the production of potentially toxic H_2O_2. For further experiments, this may be a key limiting factor in protein production. However, it cannot be excluded, that the different growth conditions in the microfluidic device had an impact as well, since ES-dependent cell growth arrest was not detected upon bulk cell cultivation in 96-deep-well plates, tubes or flasks (Supplementary Figure 53).

Nevertheless, in combination all three, the experimental results, mathematic modeling and microfluidic single cell measurements supported the finding of a tightly regulated AND gate with no measurable basal transcription activation. Since the AND gate was satisfactorily characterized, no further attempts were made to this purpose.

5.4. A positive feedback loop allowing removal of galactose after first induction

The AND switches presented in section 5.2 and 5.3 demonstrated the successful combination of three different systems to one tightly regulated and dose-dependent double switch setup. Namely as the basis for switch designs a three component CRISPR/dCas9 system was used, allowing a modular and complex gate design. As the first switch, the well-established galactose inducible promoter *GAL*, leading to high expression rates, and as the second switch the ES inducible complex, enabling a dose-dependent and tight regulation, were implemented.

Many positive features of each switch have been combined. Nevertheless, some disadvantages remained. One of the major disadvantages is that the required change from glucose to galactose triggers a change in metabolism. Because of the high consumption of energy for the cell metabolism, this change limits the energy for the production of the reporter/target proteins (202,203). Additionally, cell growth often is slowed down. Hence, it may be helpful to switch back to glucose medium after a short induction in galactose containing medium. In the following paragraph a positive feedback loop is described, that allows one to remove galactose from the medium after only a short induction time. The feedback loop further enabled significantly higher expression rate than the already high ones achieved with the previous setups.

5.4.1. Construction of the positive feedback loop based on the AND, GO setup

For the positive feedback loop, the well characterized AND, GO strain was utilized. Hence, MCP-VP64 is under the control of ES and dCas9 is under the control of galactose, whereas the scRNA is constitutively expressed (Figure 37A). After induction with ES and galactose CRISPR/dCas9 can bind to the *tet*O binding region, leading to the expression of GOase and tGFP (Figure 37B). As visualized in Figure 37A, only tGFP fluorescence was measured for evaluation of the feedback loop. It was already demonstrated in 5.2.5 and 5.2.7, that tGFP expression is analogous to that of GOase. Since no further preparation is needed for the detection of tGFP *via* flow cytometry, it was decided to only use tGFP fluorescence to analyze the feedback loop. Since cells of the AND, GO strain were utilized, no further integration of the CRIPSR/dCas9, reporter genes or scRNA was necessary. Therefore, only a gene allowing a positive feedback had to be designed, cloned and integrated into the AND, GO strain (Figure 37C).

For the positive feedback loop design, a setup was chosen that allows for the quick switch back to glucose after a short addition of galactose, mainly because galactose induction leads to unwanted side effects like slow growth rates. For the utilized setup, dCas9 expression was under control of galactose. Once induced with galactose, dCas9 was intended to be continuously expressed without further addition of galactose. To this end, dCas9 was placed under the control of *tet*O. After induction, the CRISPR/dCas9 complex did not only bind to the *tet*O preceding tGFP, but also to the *tet*O preceding dCas9. As a consequence, dCas9 should be constitutively expressed and the addition of galactose would be no longer necessary.
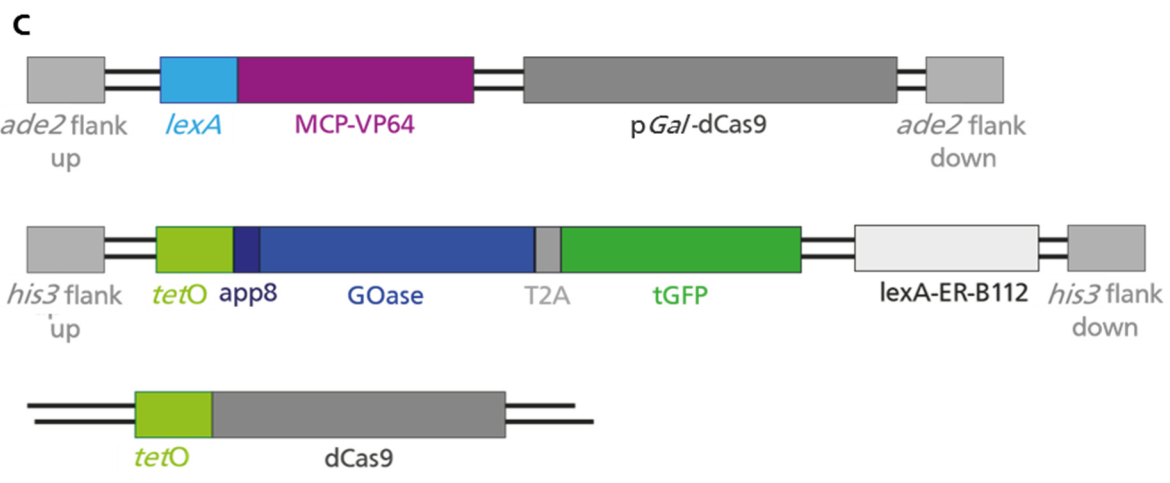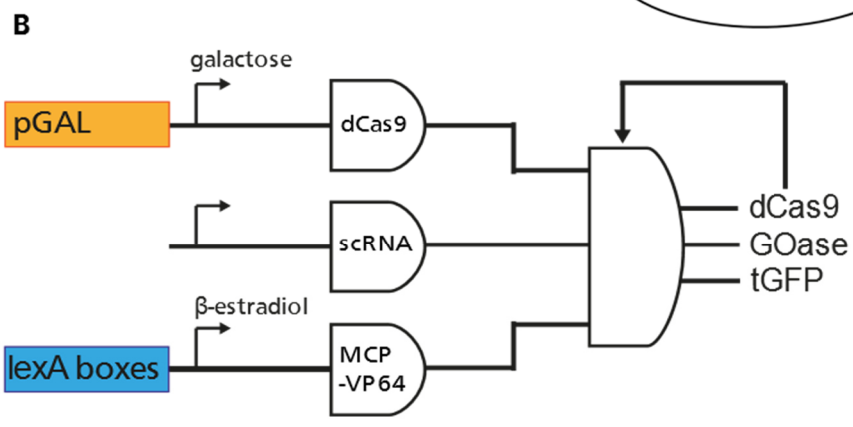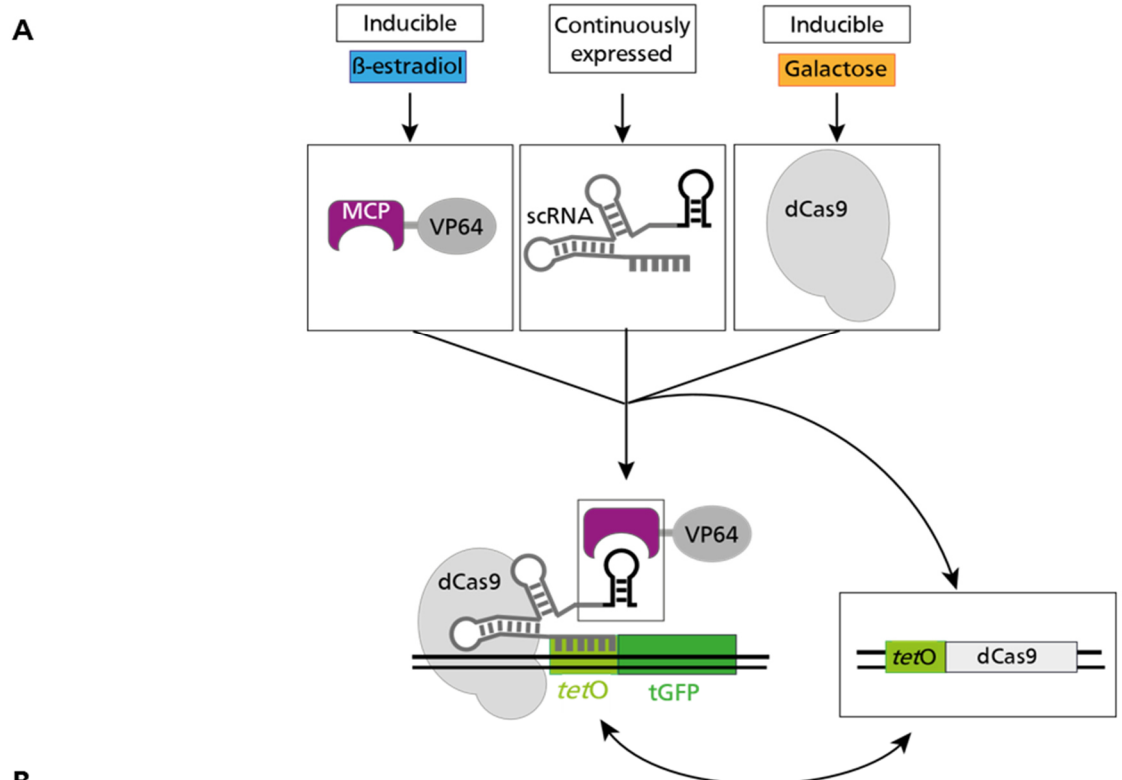
Figure 37 Schematic and genetic overview of the positive feedback loop.

(A) Schematic overview and (B) logic gate for the positive feedback loop. Both showing, that MCP-VP64 is inducible by ES and dCas9 is inducible by galactose, whereas the scRNA stays constitutively expressed. Only when all components are expressed, they bind to *tet*O and induce tGFP expression. Additionally, a dCas9 placed behind *tet*O as well, will be expressed. Thus, dCas9 will be produced without further induction and galactose can be removed. (B) The AND, GO setup was utilized for the feedback loop implementation. (C) Genomic overview for the feedback loop including homologous flanks for genomic integration as well as the reporter gene combination, that was genomically integrated. The *tet*O-dCas9 plasmid is shown as well.

To allow for the implementation of the feedback loop into different strains, the gene *tet*O-dCas9 complex was integrated into a plasmid backbone. The backbone of p425 containing a 2μ ori was used and combined with a *tet*O sequence in front of dCas9 and a tryptophan auxotrophic marker amplified from the plasmid p414. To keep the cellular burden by overexpression of dCas9 as small as possible, only 3 copies of *tet*O were used. All utilized fragments, that were needed to build the new plasmid pAH019, are listed in Table 28.

Table 28 Fragments and concentrations utilized for the construction of pAH019.

Fragment	Method	fw	rv	Template	Size [bp]	c [ng/μL]	Use [μL]
fAH001	PCR, Phu	Cas13	Cas14	p425_aAde	3676	15.75	50
fAH002	PCR, Q5	Cas15	Cas8	p414	1016	36.52	20
fAH004	PCR, Q5	Cas9	Cas10	pJZC532	377	54.53	20
fAH005	PCR, Phu	Cas11	Cas12	pJZC638	4973	70.02	50

The fragments were combined by HR in yeast after PCR amplification with 30 bp overlaps on both ends of the fragment. A concentration of approximately 4 picomolar of the small fragments was mixed with 0.5 μg of the bigger fragments. The mixture was precipitated, suspended in 5 μL of nuclease free water and subsequently used for transformation into chemo competent cSLQ.Sc002 cells prepared with the Frozen-EZ Yeast Transformation II Kit (*Zymo Research*). Cells were selected using SD-trp drop-out agar plates and were grown for 48 h. Correct plasmid assembly was verified by cPCR using the oligonucleotides oAH003 and oAH004. A correct clone was chosen and after growth overnight the plasmid was isolated using the *Zymoprep*™ Yeast Plasmid Miniprep II Kit (*Zymoresearch*). The isolated plasmid was subsequently transformed into freshly prepared competent *E. coli* cells. After transformation, selection was performed using dYT+Amp agar plates and cells were grown overnight. Correct transformation was checked by cPCR using the oligonucleotides oAH003 and oAH004 (data not shown). A correct clone was chosen and after growth overnight the plasmid was isolated using the *PureYield*™ Plasmid Miniprep System Kit (*Promega*). The correct plasmid sequence was verified by sequencing using the oligonucleotides lexA FP 8 and oAH004 (data not shown).

After the successful generation of pAH019, transformation of the plasmid into electrocompetent AND, GO cells was performed. Cells were selected using SD-trp-ura drop-out agar plates and were grown for 48 h. Correct plasmid integration was verified by cPCR using the oligonucleotides oAH003 and oAH004 (data not show). The newly generated strain was named AND, GO, pFL (positive Feedback Loop).

5.4.2. Examination of the functionality of the positive feedback loop

After the general functionality of the positive feedback loop was demonstrated (data not shown), the positive feedback loop was tested in a setup, where the cells were precultured in

SD medium, induced for a fixed time span with galactose and ES and subsequently transferred back to SD medium containing ES.

For the experiment cells of the strains AND, GO and AND, GO, pFL were utilized. Both strains were inoculated in 10 mL and induced in 96-deep-well plates according to the protocol described in 4.4.3. Cells containing the pFL were grown in -trp-ura drop-out medium, others in -ura drop-out medium. For every strain a cell suspension with an OD_{600} of 1was prepared and subsequently used for induction. 475 μL of this cell mixture were pipetted into a 96-deep-well plate and mixed with 25 μL of medium or an ES stock leading to a concentration of 10 nM ES. For control cells were grown in SD, SD + 10 nM ES or SG. Cells constantly grown in SG + 10 nM ES were used as positive control. For induction cells were induced with SG + 10 nM ES. After 30 min or 120 min, respectively, 200 μL of each sample were transferred to a fresh 96-well plate and stored at 4 °C until measurement. The remaining cells were centrifuged, suspended in 500 μL SD + 10 nM ES and further grown at 25 °C. After 20 h, again 200 μL of each sample were transferred to the 96-well plate and stored at 4 °C until measurement. The samples were refilled with the corresponding medium and further grown for 76 h. Again 200 μL of each sample were transferred to the 96-well plate. The tGFP fluorescence was directly measured with Accuri™ C6 (*BD*) using the 96-well plate. The mean fluorescence and the percentage of fluorescent cells were exported to Microsoft Excel (*Microsoft)*. For each sample the percentage of fluorescent cells was compared (Figure 38, bright colors). For the comparison of the samples the mean fluorescence of the positive control (corresponding strain grown for 20 h in medium containing both inducers, namely SG + 10 nM ES) was set to 100 % and the respective percentage fluorescence in comparison to the positive control was calculated for the controls and samples (Figure 38, light colors). All time-points were applied for the samples. For the controls data was only applied for growth of 20 h. No significant change was obtained for further growth (data not shown).

For both samples, the PC was clearly induced with around 85 % of fluorescent cells and a strong mean fluorescence. The negative controls were tightly regulated for the AND, GO. For AND, GO, pFL the controls SD and SG showed a slight increase in the number of fluorescent cells, but not for the mean fluorescence. Hence, more cells did show basal activity, but only at a low level. For the negative control SD + ES a significant increase of both, mean fluorescence and percentage of fluorescent cells, can be detected for AND, GO, pFL. Once more, the mean fluorescence did not increase as much as the percentage of fluorescent cells. It can therefore be assumed that due to the incorporation of the feedback loop the threshold for untargeted gene expression has dropped, but the general basal fluorescence has not increased to a great extent.

Legend:
- AND, GO, fluorescent cells [%]
- AND, GO, mean fluorescence [%]
- AND, GO, pFL, fluorescent cells [%]
- AND, GO, pFL, mean fluorescence [%]
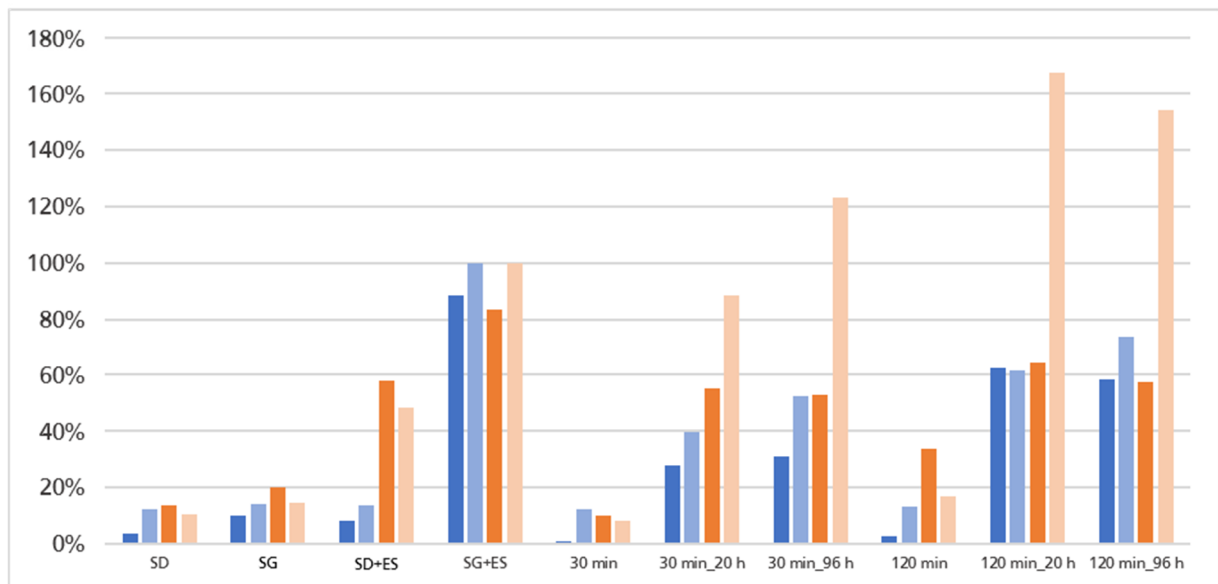
Figure 38 Induction experiment for the positive feedback loop.

For the experiment cells of the AND, GO (blue) and AND, GO, pFL (orange) were used. As negative controls cells were grown in SD, SD + 50 nM ES and SG. As positive control cells were grown in SG + 10 nM ES. For the samples cells were induced with 10 nM ES and galactose, with galactose being removed after 30 min and 120 min. For both, fluorescence was measured directly, after growth for 20 h and 96 h, respectively. For all controls and samples, the percentage of fluorescent cells (dark color) and mean fluorescence (light color) was applied.

The same results were obtained for the samples, which were only briefly incubated with galactose and then directly provided for measurement. For induction with galactose for 30 min, nearly no fluorescent cells were detected for AND, GO, but some for AND, GO, pFL. For induction with galactose for 120 min, again nearly no fluorescent cells were detected for AND, GO, but more than 30 % of the cells already expressed tGFP for AND, GO, pFL.

When induced with galactose for 30 min and grown for 20 h, a significant difference between the two strains was obtained. The fluorescent pFL cells were about twice the number of cells from AND, GO. Only 25 % of the AND GO cells showed fluorescence, whereas 55 % of the pFL did. These numbers remained roughly constant even after growth for 96 h. Only the mean fluorescence did increase between 20 h and 96 h of induction. For the AND, GO strain after 20 h 40 % and after 96 h 55 % of the PC fluorescence were obtained. In comparison for the pFL strain 85 % were already obtained after 20 h of induction, whereas 120 % were obtained after 96 h. Due to the integration of the pFL, the percentage of the mean fluorescence has therefore increased more than twice.

When induced with galactose for 120 min, for both strains and both timepoints the number of cells showing fluorescence was roughly 60 %. After growth of 20 h, a percentage of 165 % mean

fluorescence for the pFL was obtained, which slightly decreased after further growth. Hence, the maximum fluorescence was reached after 20 h and according to the microfluidic measurements, cells seemed to have reached an arrested state and stopped the production of tGFP. The ratio of the fluorescence of AND, GO to pFL roughly doubled after growth for 20 h, which was similar to the previous result. After growth for 96 h the mean fluorescence of AND, GO slightly increased, but remained with 70 % under the fluorescence of the PC.

To sum up, the implementation of a positive feedback loop led to an increase of number of fluorescent cells as well as the maximum fluorescence, especially when galactose induction was only performed for a short period. In detail, the implementation of the positive feedback loop resulted in an increased number of fluorescent cells for both, controls and samples. For the control SD+ES this may be explained by the leakiness of the galactose switch (57). As long as no ES is added, the ES switch tightly regulated the expression of the transcription activator complex MCP-VP64. Hence, even in the presence of dCas9 and scRNA, the CIRPSR/dCas9 can only bind to *tet*O, but did not activate tGFP or dCas9 expression. As soon as ES is added and the basal expression of the galactose switch has led to the expression of a few dCas9 molecules, the AND gate is able to constantly produce more dCas9. The two-hairpin design of the scRNA was already demonstrated to achieve high expression rates, hence it can be assumed that a significantly higher number of dCas9 molecules will be produced than it was the case with the galactose switch only. The induction of MCP-VP64 by ES thus triggered a chain reaction, which activated the reporter gene expression to a certain degree even without the addition of galactose.

However, the same chain effect is responsible for a quick induction and the achievement of high induction values. Even though a short induction with galactose and subsequent growth in SD + ES is sufficient for the AND, GO to achieve a certain degree of tGFP expression, the number of cells showing fluorescence and especially the achieved mean fluorescence are much weaker, than for AND, GO, pFL. The higher number of AND, GO, pFL cells that are fluorescent may be explained by the circumstances, that dCas9 is a relatively large protein and the galactose-inducible switching behavior is rather slow. As a result, for AND, GO the short galactose induction may only be sufficient to induce synthesis of a few dCas9 proteins per cell. These in turn might be insufficient to promote full activation of the CRISPR system. In comparison, for the AND, GO, pFL already a single dCas9 molecule may be sufficient to produce more dCas9 proteins and hence start the already described chain reaction.

On the other hand, the significantly increased mean fluorescence is more difficult to explain. Upon positive feedback loop mediated overexpression of dCas9, a significant increase of maximum reporter gene expression was observed. Hence, the experimental results suggest, that dCas9 had been the limiting factor for the further increase of the expression rate. Earlier

research, however, does not support this hypothesis (106,204). Instead Jinek *et al.* demonstrated, that gRNA expression and/or assembly of the gRNA into Cas9 are the limiting factors of CRISPR/(d)Cas9 mediated gene expression (204). According to this idea, it is conceivable that due to the significantly higher number of dCas9 molecules achieved due to the integration and activation of the positive feedback loop, the assembly of the scRNA with dCas9 is no longer a limiting factor. As a consequence, a significantly higher maximal expression of the reporter gene would be possible. To further investigate this hypothesis, another feedback approach was designed aimed at generating a fast degrading tGFP variant that would allow one to precisely investigate, at which time point how much tGFP is expressed.

Nevertheless, the pFL was demonstrated to be functional and the anticipated requirements of a reduction of galactose induction to a short period as well as a high reporter gene expression rate were completely fulfilled.

5.4.3. Construction of a positive feedback loop containing a fast-degrading tGFP

With the clone AND, GO, pFL a positive feedback loop was established. Nevertheless, due to the long half-life of tGFP (196,205), a time-dependent induction of tGFP expression could not be measured. Hence, after tGFP has been first expressed, it will remain in the cell and after some time it cannot be easily determined whether further tGFP is produced. In order to solve this problem, tGFP should be combined with a protein degradation tag, leading to a fast degradation and more precise analysis of the feedback loop.

A new clone was designed using CasEMBLR. Following the AND switch design, MCP-VP64 expression was controlled by ES, dCas9 expression was controlled by galactose and scRNA was continuously expressed from a plasmid (Figure 39A). After induction with ES and galactose, the CRISPR/dCas9 system binds to the *tet*O binding region, leading to the expression of Ubi-tGFP and dCas9 (Figure 39B). To achieve a fast degrading tGFP a degradation tag was fused to the *N*-terminus. It was decided to use Ubi-Y, which was classified as a medium strong degradation tag (206). Ubi-Y was already used in yeast, resulting in detectable levels of fluorescence only at high expression levels (42). Since the utilized AND gate results in high tGFP levels, the Ubi-Y tag was chosen to allow tGFP detection only when the reporter gene expression is strongly activated. This setup should also reduce the relatively high basal activity of the positive feedback loop design. As before, the CRISPR genes were integrated into the *ade2* locus, the reporter genes and the hTF in the *his3* locus and *tet*O-dCas9 as well as the scRNA as a plasmid (Figure 39C).
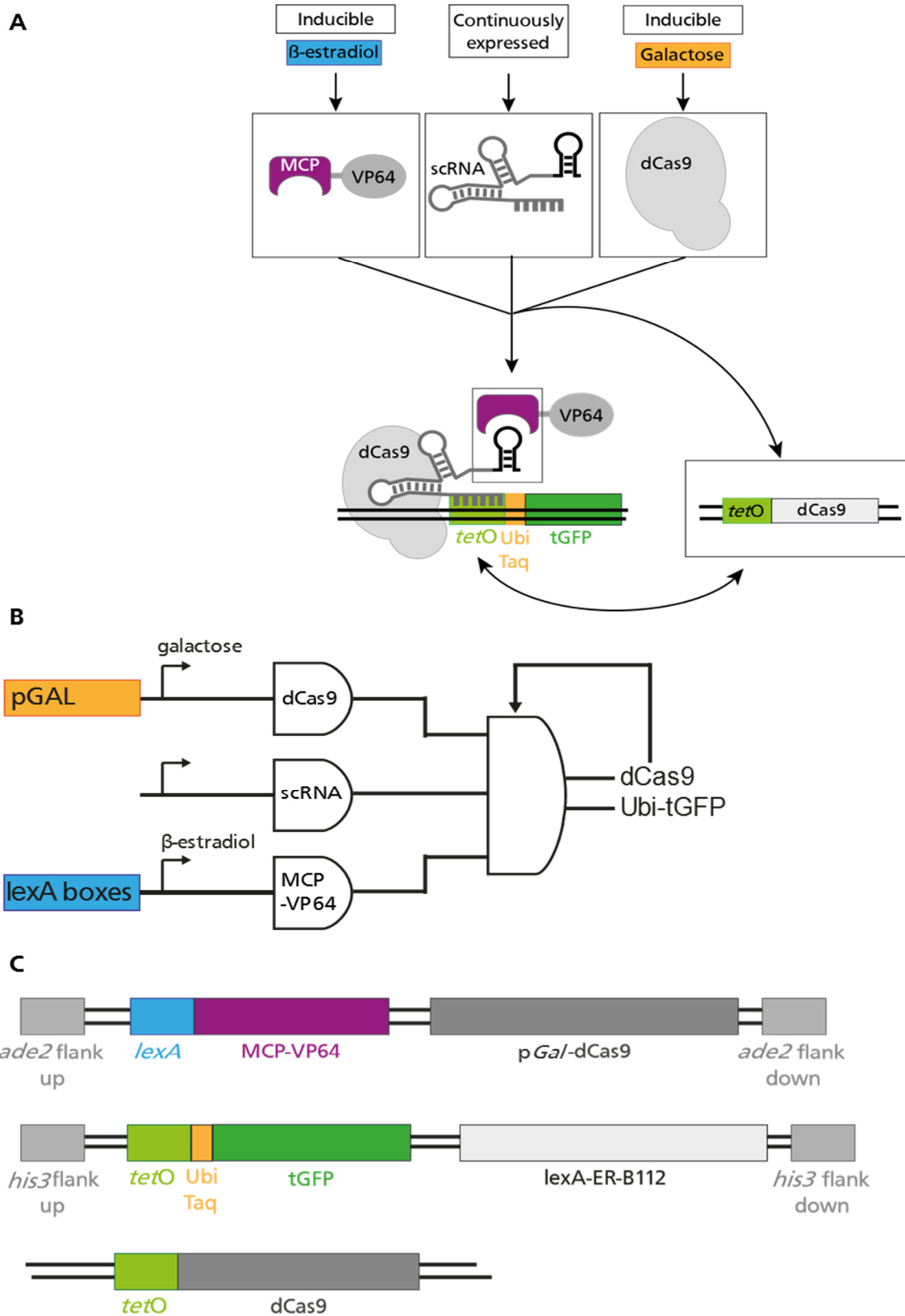
Figure 39 Schematic and genetic overview of the positive feedback loop with a Ubi-tGFP.

(A) Schematic overview and (B) logic gate for the positive feedback loop with a Ubi-tGFP. Both showing, that MCP-VP64 is inducible by ES and dCas9 is inducible by galactose, whereas the scRNA stays constitutively expressed. Only when all components are expressed, they bind to *tet*O and induce Ubi-tGFP expression. Additionally, a dCas9 placed behind *tet*O, will be expressed. Thus, dCas9 will be produced without further induction and galactose can be removed. (B) The AND, GO setup was utilized for the feedback loop implementation. (C) Genomic overview for the feedback loop including homologous flanks for genomic integration as well as the reporter gene combination containing the Ubi-tGFP, that was genomically integrated. The *tet*O-dCas9 plasmid is shown as well.

In order to implement an ES- and galactose-dependent AND switch, the fusion protein MCP-VP64 was genetically placed behind four *lexA* boxes. The dCas9 was placed behind the P$_{GAL10}$ and both genes were integrated into the *ade2* locus. The 7x *tet*O-Ubi-Y-tGFP reporter and the LexA-ER-B112 hTF were integrated into the *his3* locus. To amplify the parts with the required flanks, PCR was performed following the manufacturer's instructions using either Q5® High-Fidelity DNA Polymerase or Phusion® High-Fidelity DNA Polymerase (*New England Biolabs, Inc.*). All parts used for the construction of the Ubi-tGFP AND gate are listed in Table 29. After amplification, the correct size of the constructs was verified by agarose gel electrophoresis. The DNA was purified using the Wizard® SV Gel and PCR-Clean up System (*Promega*).

Table 29 Parts utilized for the construction of the Ubi-tGFP AND gate.

Part	Method	fw	rv	Template	Size [bp]	c [ng/μL]	pmol/μL
fAH025	PCR, Q5	A1, A11	A12	pFRP793	590	22.00	0.11
fAH027	RT PCR, Phu	A13	A20, A10	pJZC638	6746	22.30	0.01
fAH032	RT PCR, Phu	H33	H6, H7	pFRP880	3063	39.46	0.04
fAH048	PCR, Q5	H1, H3	oAH066	pSLQ.119	895	53.39	0.18
fAH049	PCR, Q5	oAH067	oAH068	pYTK042	405	77.19	0.58
fAH050	PCR, Q5	oAH069	H35	PCT_2A-GFP	1110	111.90	0.31
gRNA (H)	-	-	-	-	-	53	-
gRNA (A)	-	-	-	-	-	80.17	-

For *in vivo* assembling of the parts, 4 picomoles of each part were mixed with 1 μg of the corresponding gRNA plasmid. An exception was made for very large parts. For these parts, 0.5 μg of DNA were used. The parts and plasmid were precipitated and suspended in 5 μL nuclease free water (0). The utilized parts and plasmids for the genomic integrations as well as the concentrations used for precipitation, can be found in Table 30.

Table 30 Used concentrations and parts for Ubi-tGFP AND gate transformation

Part	for 4 pmol [μL]	for 1 μg [μL]	Use [μL]	T2B	T2C	total	V total [μL]
fAH025	35.40	15.26	35	X		1	35
fAH027	399.31	26.09	22	X		1	22
fAH032	102.46	25.34	25		X	1	25
fAH048	22.13	18.73	22		X	1	22
fAH049	6.93	12.96	7		X	1	7
fAH050	13.09	8.94	13		X	1	13
gRNA (H)		9.42	10		X	1	10
gRNA (A)		12.47	15	X		1	15

For the genetic integration, the chemo competent strain cSLQ.Sc002_p414 was used for a two-step CasEMBLR transformation. The *ade2* parts were transformed, plated on SD-trp-leu drop-out agar plates and grown for up to 120 h. After the successful integration of the CRISPR parts into the *ade2* locus, the colonies turned red. For those cells, correct part assembly and correct genomic integration were verified by cPCR using the oligonucleotides A15, A18 (correct integration into the genome), A25, A26, A27 and A28 (correct assembly) (data not shown).

In a second transformation step, the 7x *tet*O-Ubi-Y-tGFP reporter gene and the hTF were integrated into the *his3* locus. Cells positively tested on the integration of the CRISPR genes were made chemo-competent and transformed with the parts for *his3*. Cells were plated on SD-trp-leu drop-out agar plates and grown for up to 120 h. Correct part assembly as well as correct genomic integration were verified by cPCR using the oligonucleotides H43, H44, H12, H14 (correct integration into the genome), fw_gene-gene_lexA FP and rv_gene-gene_lexA FP (correct assembly) (data not shown). The successful transformed clone was named Ubi, wt.

After successful genomic integration, the CasEMBLR plasmids were removed as described in 5.2.2. One plasmid-free clone per AND switch was selected for further experiments and subsequently transformed via electroporation with 2 μg of the scRNA plasmid pJZC588 (Ubi, scRNA) or 1 μg of both, pJZC588 and pAH019 (Ubi, pFL). Cells were plated out on SD-ura drop-out agar plates or SD-trp-ura drop-out agar plates and correct plasmid integration was verified by cPCR.

5.4.4. Examination of the functionality of the Ubi-tGFP positive feedback loop

In this chapter the general functionality and inducibility of the new setup was verified. Therefore, five clones were inoculated: the AND, GO gate; the AND, GO, pFL; the Ubi wt, containing the ES inducible MCP-VP64 and the galactose inducible dCas9, but no scRNA; the Ubi, scRNA, inserting the constitutively expressed *tet*O-binding scRNA; the Ubi, pFL, containing both, the scRNA and the positive feedback loop.

All clones were inoculated in 10 mL and induced in a 96-deep-weel-plate following the protocol described in 4.4.3. Cells containing the pJZC588 and pFL were grown in -trp-ura drop-out medium, cells containing only pJZC588 in -ura drop-out medium and Ubi, wt in full SD. Induction was performed in biological triplicates in 96-deep-well plates. For every strain a cell suspension with an OD_{600} of 1 was prepared and subsequently used for induction. 475 μL of this cell mixture were pipetted into a 96-deep-well plate and mixed with 25 μL of medium or an ES stock leading to a concentration of 50 nM ES. For controls, cells were grown in SD and for induction in SG + 50 nM ES. After 20 h of growth at 25 °C, 200 μL of each sample was transferred to a 96-well plate and stored at 4 °C until measurement. The remaining sample volume was filled up to 450 μL with the corresponding medium and cells further grown for

24 h. Again 200 μL of each sample were transferred to the 96-well plate. The tGFP fluorescence was directly measured with Accuri™ C6 (*BD*) using the 96-well plate. The average of the mean fluorescence and the standard deviation of the gated triplets were calculated for 20 h (Figure 40) and 48 h (Supplementary Figure 54) of induction using Microsoft Excel (*Microsoft*).
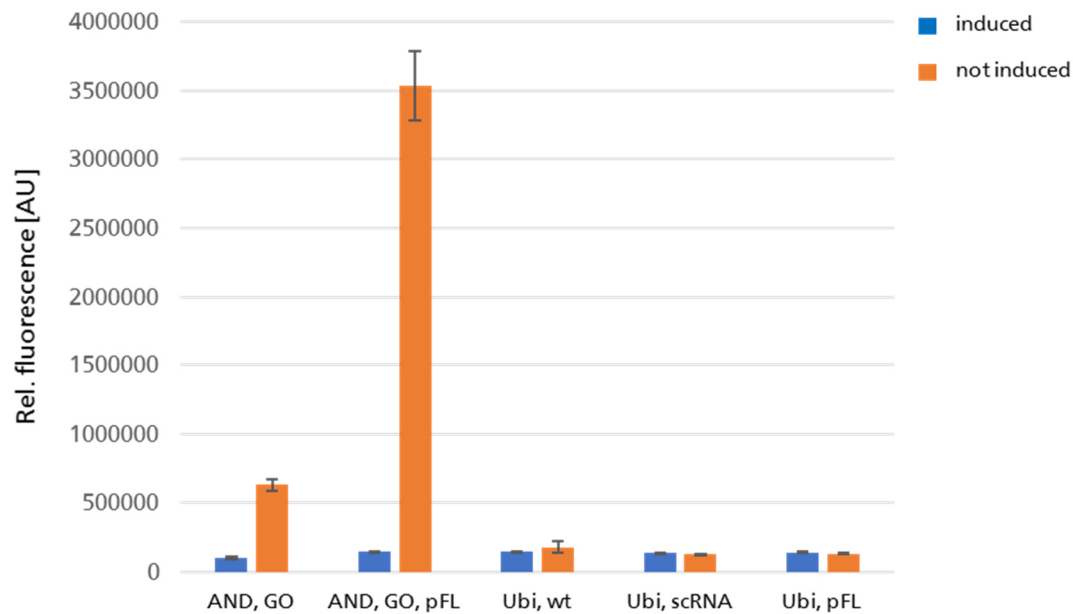

Figure 40 Induction experiment for the positive Ubi-tGFP feedback loop.

For the experiment cells of the AND, GO, AND, GO, pFL, Ubi wt (not containing a scRNA), Ubi, scRNA and Ubi, pFL were used. As negative control cells were grown in SD. As positive control cells were grown in SG + 10 nM ES for 24 h. Error bars indicate the standard deviation of the biological triplicates

None of the new Ubi clones showed fluorescence at any time point, whether induced or not. The fluorescence of those samples corresponded to that of the non-induced AND, GO and AND, GO, pFL. Induction was generally successful, since AND, GO and AND, GO, pFL were strongly activated. It can be assumed, that the Ubi strains are either generally not inducible or, more likely, the Ubi-Y tag induces tGFP degradation so efficiently that the accumulation in the cell is negligible. For further experiments another degradation sequence could be considered such as the degradation domain of mouse ornithine decarboxylase that was already successfully used to reduce the half-life of tGFP (205,207).

Nevertheless, this measurement demonstrated how strongly tGFP expression is increased by the positive feedback loop. As can be seen from Figure 42, the fluorescence of pFL is about 7x stronger than the one of the normal AND gate. Since with this experiment and the one described in 5.4.2, the criteria for the positive feedback loop are fulfilled, no further experiments with a less effective degradation tag were performed.

5.5. Transfer of the AND setup to achieve an inducible scRNA

In the previous chapters it was shown, that both, the fusion protein MCP-VP64 as well as dCas9, are excellently suited for inducible expression. However, the inducible expression of the scRNA was not yet investigated. Therefore, this chapter deals with the design and implementation of an inducible scRNA into a functional CRISPR/dCas9 system.

5.5.1. Self-cleaving ribozymes for a functional scRNA

There is a major challenge for the design of an inducible scRNA switch: the scRNA gene has to be transcribed into a functional scRNA. Therefore, conventionally promoters transcribed by RNA polymerase III (pol III) like *U3*, *U6* or *SNR52* are used (103,129). The physiological function of RNA pol III is to transcribe small nuclear RNA genes such as *U6* and *U3 snRNA* as well as ribosomal genes like *5S rRNA* or *tRNA* (208). Hence, RNA pol III is optimally suited for the transcription of a gRNA or scRNA, respectively. However, there are multiple limitations to RNA III-based gene expression. Due to the constitutive and ubiquitous expression of *U6* and *U3 snRNA* genes, it is not possible to express a gene cell or tissue specific (158,208). Additionally, in many organisms those promoters have not been characterized yet, making it even more challenging to design a functional CRISPR system (158). RNA Pol III also has a limited capacity to yield long RNA transcripts, making it difficult to express larger genes. The most restraining limitation in the scope of this work was the limitation of tightly regulated inducible RNA pol III promoters (209–211).

In comparison, for RNA polymerase II (pol II), which has the physiological function to transcribe the majority of mRNA, there are already multiple inducible promoters available. mRNAs expressed from these promoters undergo extensive processing and modification at both ends, like capping or polyadenylation (212). Additionally, mRNAs expressed by RNA pol II promoters are actively transported out of the nucleus into the cytoplasm. Since the CIRPSR complex has to form in the nucleus to be able to target the genomic DNA, this transport would lead to an unfunctional CRISPR system (158).

To sum up, the utilized RNA pol III promoter *SNR52* is sufficient for constitutive and cell/tissue unspecific expression, but does not allow inducible scRNA expression (Figure 41A). Instead inducible scRNA expression by RNA pol II promoters like the inducible *lexA*-minimal promoter region is generally possible, but will lead to the processing of the scRNA and its transport out of the nucleus, resulting in a non-functional scRNA (Figure 41B). Thus, the simple exchange of the RNA pol III promoter *SNR52* by the RNA pol II *lexA*-minimal promoter region is not possible. Nevertheless, in 2014 Gao and Zhao demonstrated the successful transcription of a gRNA by the RNA pol II promoter *Adh1* (158). To this end, they took advantage of the nuclease activity of ribozymes (213,214) and designed a setup, where the gRNA was genetically flanked by two

ribozymes resulting in the construct Ribozyme-gRNA-Ribozyme. They used a ribozyme of the type Hammerhead (HH) (215) at the 5'-end of the gRNA and hepatitis delta virus (HDV) ribozyme (216) at the 3'-end. After transcription the ribozymes undergo precise self-catalyzed cleavage, followed by the release of a functional gRNA (158). Following this setup, the design of a ribozyme flanked scRNA should allow the inducible expression by RNA pol II (Figure 41C).
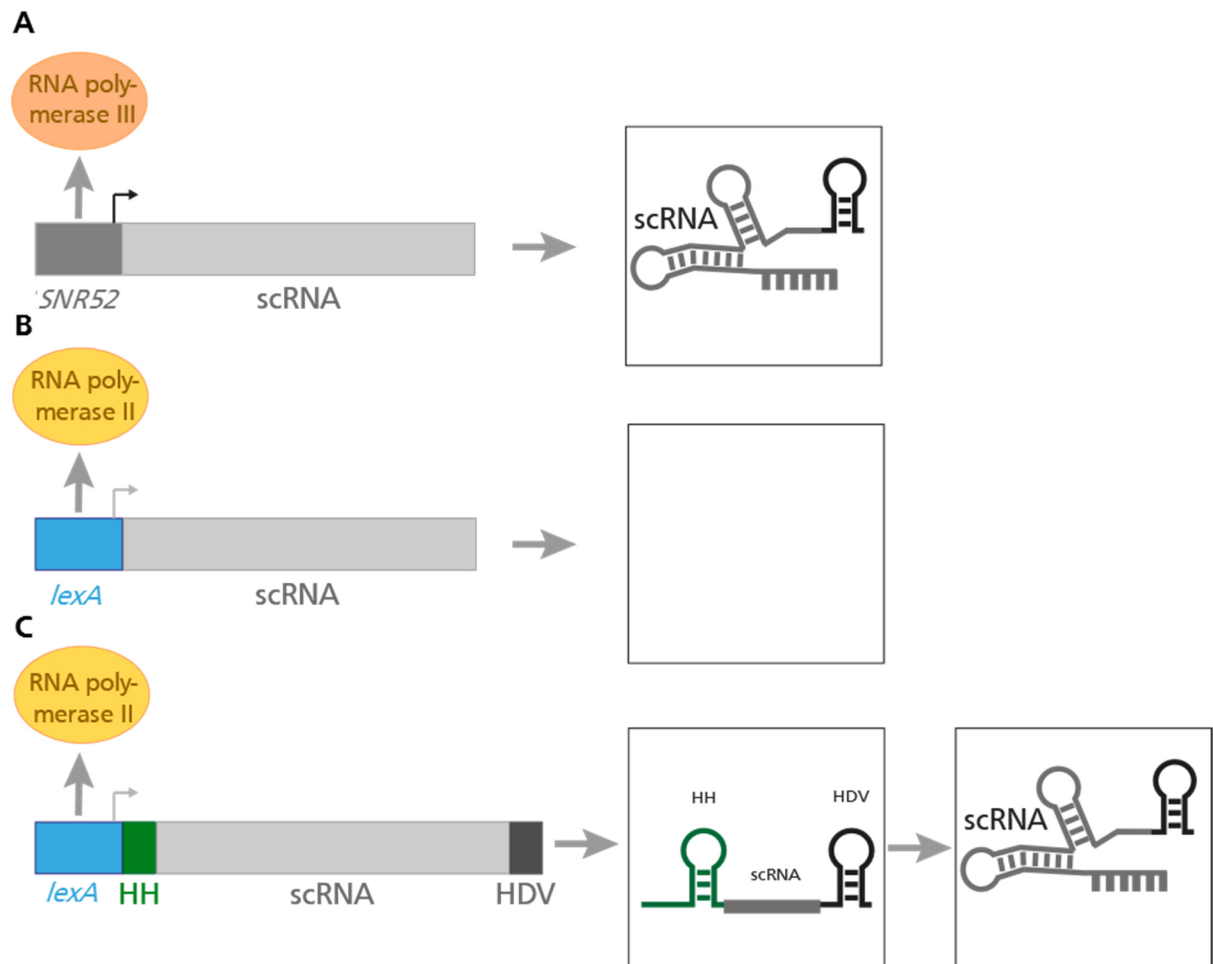

Figure 41 Promoter change leading to the recruitment of a different RNA polymerase.

The different promoter setups are shown for (A) the RNA polymerase recruiting *SNR52* promoter and (B) + (C) the RNA polymerase recruiting and ES inducible *lexA* minimal promoter. (A) results in a functional scRNA. (B) does not result in a functional scRNA. (C) results in a ribozyme flanked mRNA transcript, whom is subsequently cleaved off and a functional scRNA is achieved.

5.5.2. Construction of a CRISPR/dCas9 system using a ribozyme flanked scRNA

Following the design of Gao and Zhao, the HH ribozyme was placed at the 5'-end and the HDV ribozyme at the 3'-end of the *tet*O-binding scRNA. The HH-scRNA-HDV construct was expressed from the strong constitutive RNA pol II promoter *Adh1*. To find out, whether the ribozyme setup was applicable to the CRIPSR/dCas9 system and functional even when transcribed by RNA pol II, it was integrated into the galactose inducible Ssw, 7x *tet*O (Figure 42A). In this construct, dCas9 is inducible by galactose and both, MCP-VP64 and the scRNA as HH-scRNA-

HDV construct, are constitutively expressed (Figure 42B). This setup does not only allow one to verify the functionality of scRNA expression by RNA pol II expression, but it also enables one to test, whether the construct leads to an enhanced leakiness or reduction of reporter gene expression. Furthermore, this setup could be used to test, whether the scRNA-ribozyme construct works with the galactose switch in order to build an AND switch in further experiments. As reporter gene the fluorophore Venus was used (Figure 42C).

For the HH-scRNA-HDV construct, the plasmid pJZC625 was utilized (3.2) (5). The plasmid already contained the HH-scRNA-HDV construct under control of *Adh1*. Hence, pJZC625 could be used directly for transformation into the target strain Ssw, 7x *tet*O. For transformation, cells of the strain Ssw, 7x *tet*O were freshly inoculated and grown overnight. Cells were made electrocompetent and transformed with 2 μg of the plasmid pJZC625. After transformation, selection was performed using SD-ura drop-out agar plates. The cells were grown for 48 h at 30 °C. Correct plasmid integration was verified by cPCR using the oligonucleotides scRNA31 and scRNA32 (data not shown). One correct clone was cultivated and stored at -80 °C.

5.5.3. Examination on the functionality of the ribozyme setup

After successful transformation, the growth, induction and analysis of the Ssw, 7x *tet*O, HH-scRNA-HDV strain was performed. As a control the Ssw, 7x *tet*O containing the plasmid pJZC588 was used. This plasmid contained the *SNR52* promoter, constitutively expressing the scRNA trough RNA pol III. Cells of both strains were inoculated and induced in -ura drop-out medium in tubes according to the protocol described in 4.4.2. Both strains were grown in SD medium as a negative control and in SG for induction. The Venus fluorescence was measured *via* Accuri™ (*BD*) and analysis was performed using the Accuri™ software (*BD*). The resulting histograms were applied to Figure 43.

For the Ssw, 7x *tet*O, HH-scRNA-HDV strain a clear Venus expression was obtained, when induced with SG. In comparison, no fluorescence was detected for the negative control. When compared with the strongly Venus expressing strain Ssw, 7x *tet*O, no significant difference was detected. In both cases, the expression pattern of the strains was very similar. When grown in SD only, both strains demonstrated the same basal expression. When grown in the galactose containing induction medium SG, the strains equally strong expressed Venus.
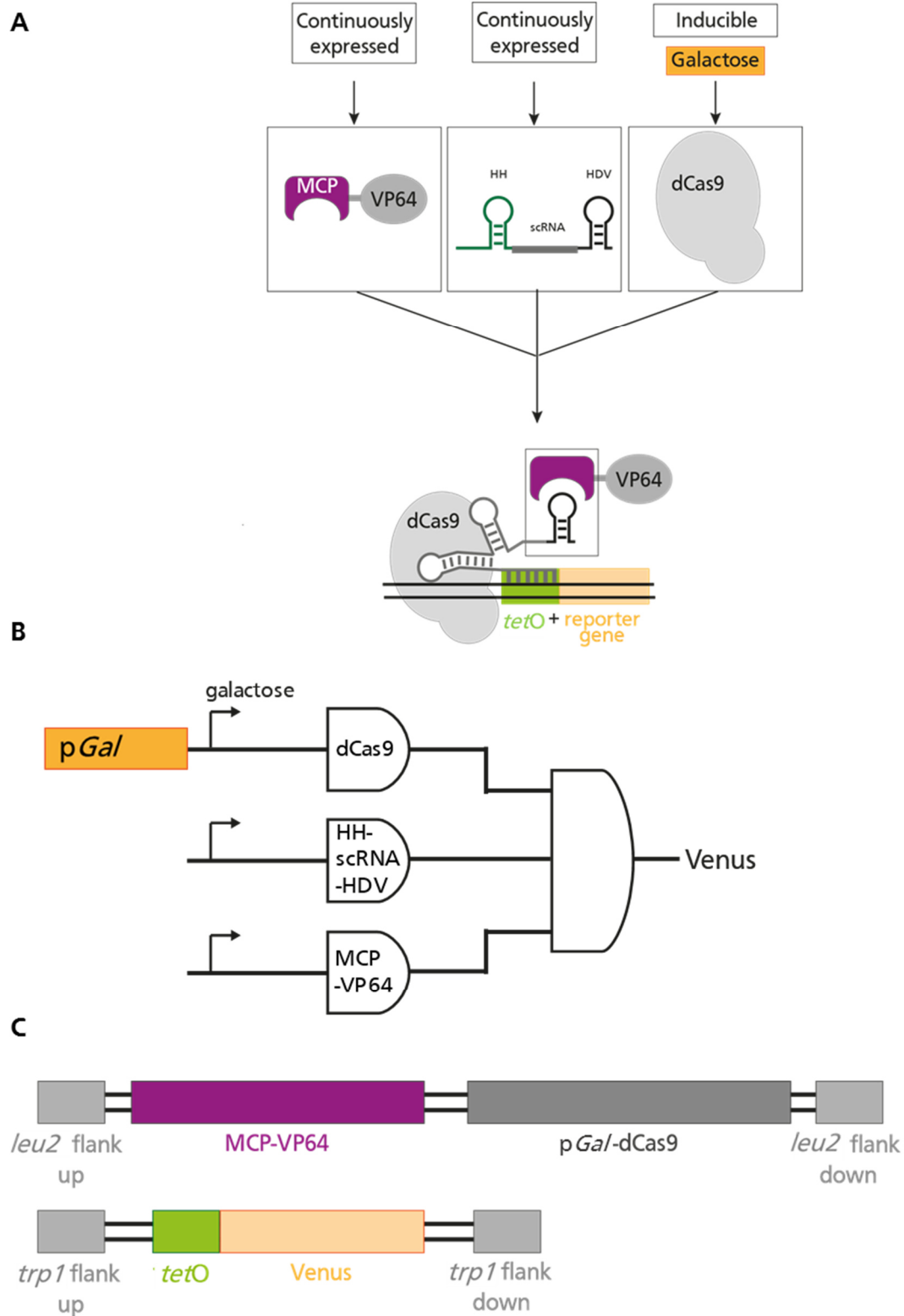
Figure 42 Schematic and genetic overview of the Ssw combined with a ribozyme flanked scRNA.

(A) Schematic overview and (B) logic gate for the Ssw combined with a ribozyme flanked scRNA and a constitutive RNA polymerase II promoter. Both showing, that MCP-VP64 and the HH- scRNA-HDV are continuously expressed, whereas the dCas9 is inducible by galactose. When all components are expressed, they bind to *tet*O and induce Venus expression. (C) Genomic overview for the Ssw including homologous flanks for genomic integration as well as the gene combinations, that were already genomically integrated.
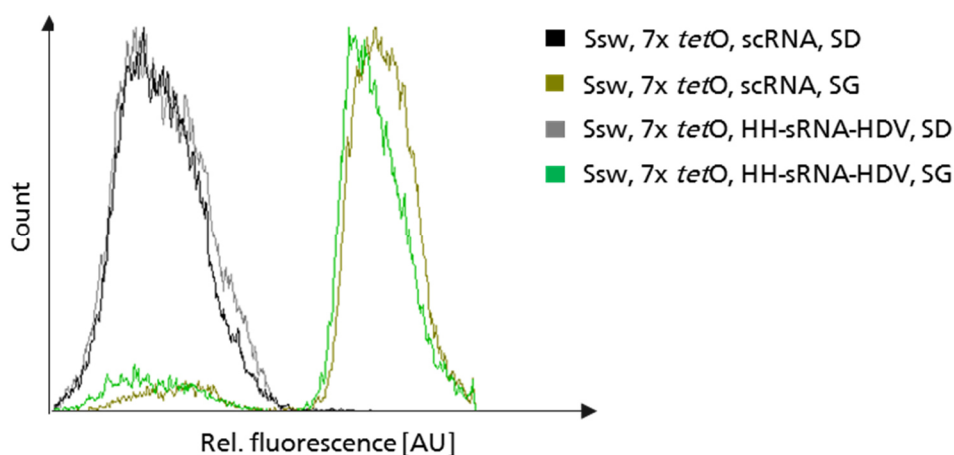
Figure 43 Galactose induction of the Ssw, 7x *tet*O, HH-scRNA-HDV strain.

Comparative induction experiment for the strains Ssw, 7x *tet*O and Ssw, 7x *tet*O, HH-scRNA-HDV. Both clones were grown in SD-ura medium (Ssw black, Ssw HH-scRNA-HDV grey) as a negative control and in SG-ura medium (Ssw khaki, Ssw HH-scRNA-HDV green) for induction.

From these results, it can be assumed that the ribozyme setup is functional in the utilized three component CRIPSR/dCas9 system. The scRNA ribozyme construct expressed by RNA pol II works as well as the plain scRNA does which is expressed by RNA pol III. Therefore, the HH-scRNA-HDV setup can successfully be used for scRNA transcription from RNA pol II promoters. As a next step, the inducible *lexA*-minimal promoter construct should be tested with the HH-scRNA-HDV setup.

5.5.4. Construction of an ES inducible scRNA and assembly to an AND gate

The general functionality of the HH-scRNA-HDV setup was verified using the constitutive RNA pol II promoter *Adh1*. Since the setup proved to be functional, it was used to build an AND gate based on an ES inducible scRNA and a galactose inducible dCas9 (Figure 44A+B). In order to build such an AND gate, the galactose-inducible strain Ssw, 7x *tet*O was transformed with the necessary genes for ES inducibility. Since the strain Ssw, 7x *tet*O already contained two genomic integrations, the hTF LexA-ER-B112 was implemented as a plasmid named pAH015 (Figure 44C). The *lexA*_HH-scRNA-HDV construct was also implemented as a plasmid, namely pAH021. For the design and construction of the plasmid pAH015 containing the hTF LexA-ER-B112, the backbone of p425_αAde was combined with the hTF insert amplified from the plasmid pFRP880. The backbone contained a 2μ ori and LEU as selection marker. The fragments and utilized concentrations for the new plasmid pAH015 are listed in Table 31.

Table 31 Fragments and concentrations utilized for the construction of pAH015.

Fragment	Method	fw	rv	Template	Size [bp]	c [ng/μL]	Use [μL]
FP1	PCR, Phu	FP9	FP10	p425_aAde	6822	22,24	50
FP2	PCR, Phu	FP11	FP12	pFRP880	3017	23,82	50
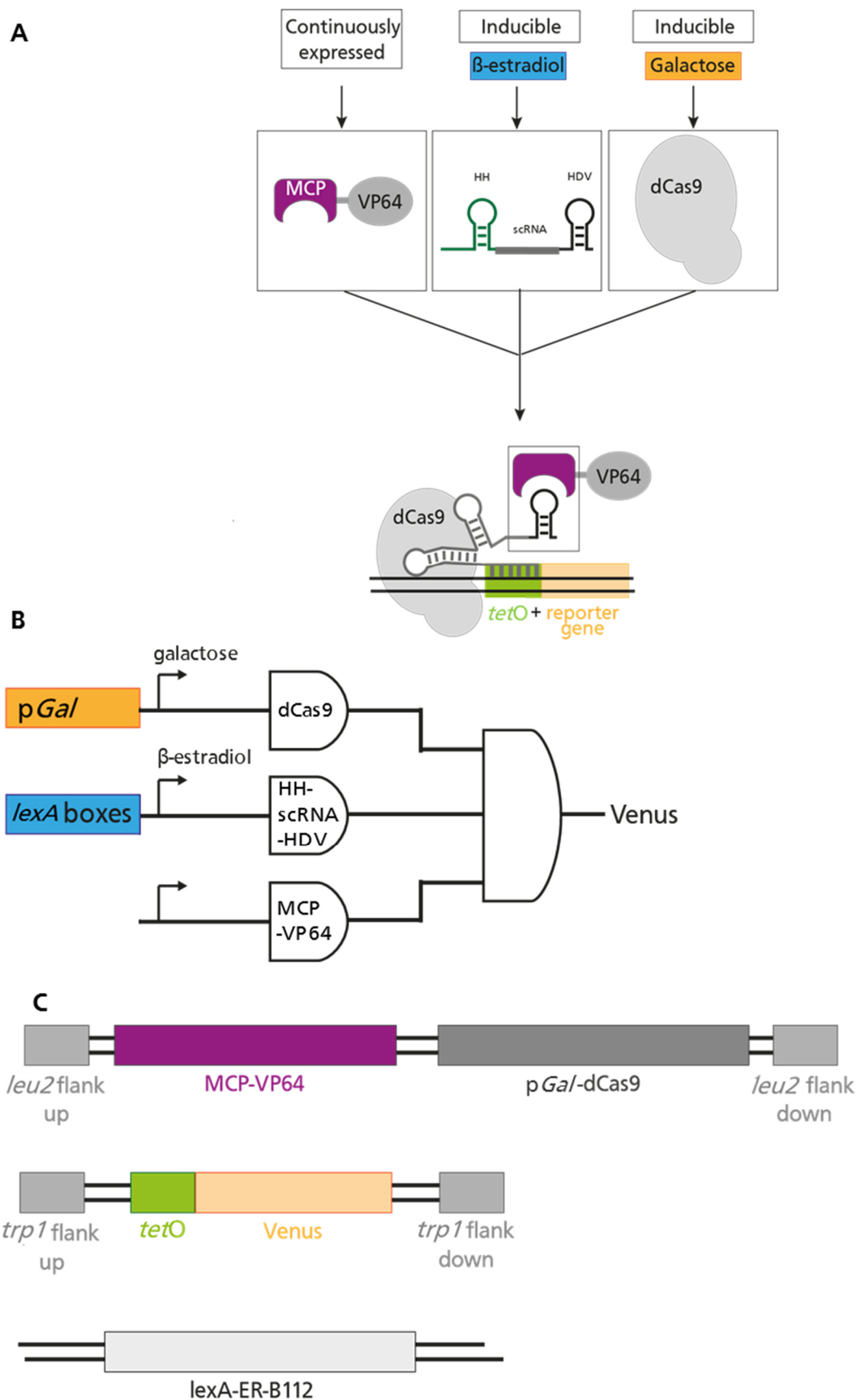
Figure 44 Schematic and genetic overview of the AND gate achieved by an inducible scRNA.

(A) Schematic overview and (B) logic gate for the Ssw combined with an inducible scRNA. Both showing, that MCP-VP64 is continuously expressed, whereas the dCas9 is inducible by galactose and the HH-scRNA-HDV is inducible by ES. When all components are expressed, they bind to *tet*O and induce Venus expression. (C) Genomic overview for the Ssw including homologous flanks for genomic integration as well as the gene combinations, that were already genomically integrated. Additionally, the plasmid based hTF lexA-ER-B112 is shown.

In order to perform gap repair, the DNA was prepared according to the protocol described in 4.1.7. After gap repair in chemo competent yeast cells, correct plasmid assembling was verified by cPCR using the oligonucleotides lexA FP 7 and lexA FP 13. A correct clone was chosen, isolated using the *Zymoprep™* Yeast Plasmid Miniprep II Kit (*Zymoresearch*), transformed into electrocompetent *E. coli* cells and isolated using the *PureYield™* Plasmid Miniprep System Kit (*Promega*). The correct plasmid sequence was verified by sequencing using the oligonucleotide lexA FP 7 (data not show).

For design and construction of the inducible scRNA plasmid pAH021, multiple cloning steps were necessary. In total three different plasmids were generated to integrate all required parts. Each plasmid was generated as described for pAH015. Hence, only the cPCR and sequencing primers are noted without further experimental explanations. The plasmid cards for the intermediate plasmids pJZC588/lexA and pAH013 are not shown.

In a first step the intermediate plasmid pJZC588/lexA was generated by gap repair. The backbone of the plasmid pJZC588, containing a CEN/ARS ori and an URA selection marker, was combined with the 4x *lexA* boxes from the plasmid pFRP793. The fragments and utilized concentrations for the new plasmid pJZC588/lexA are listed in Table 32. For cPCR the oligonucleotides fw_lexA+scRNA_ColonyPCR and rv_lexA+scRNA_ColonyPCR were used and for sequencing the oligonucleotide fw_lexA+scRNA_ColonyPCR (data not shown).

Table 32 Fragments and concentrations utilized for the construction of pJZC588/lexA.

Fragment	Method	fw	rv	Template	Size [bp]	c [ng/μL]	Use [μL]
scRNA1	digestion	*Xba*I	*Eco*RI	pJZC588	5255	-	8
scRNA2	PCR, Q5	lexA up	lexA lo1	pFRP793	489	-	10

After successful integration of the *lexA* boxes into the scRNA-plasmid backbone, in the second transformation step, the HH-scRNA-HDV construct was implemented into the new plasmid pH013. Therefore, the backbone of the plasmid pJZC588/lexA was digested and fused *via* gap repair to the HH-scRNA-HDV insert amplified from the plasmid pJZC625. The fragments and utilized concentrations for the new plasmid pJZC588/lexA are listed in Table 33. For cPCR the oligonucleotides fw_lexA+scRNA_ColonyPCR and scRNA32 were used. For sequencing the oligonucleotide fw_lexA+scRNA_ColonyPCR was used (data not shown).

Table 33 Fragments and concentrations utilized for the construction of pAH013.

Fragment	Method	fw	rv	Template	Size [bp]	c [ng/μL]	Use [μL]
V5	digestion	*Bam*HI	*Eco*RI	pJZC588/lexA	5353	23,86	40
scRNA6	PCR, Q5	scRNA33	scRNA34	pJZC625	776	62,76	16,3

In a control experiment, the plasmid pAH013 was able to partially induce Venus expression in absence and fully in the presence of ES (data not shown). Since the directly attached URA selection marker did not possess a terminator, translational read-trough lead to the transcription of (some) HH-scRNA-HDV mRNAs (217). Due to the self-catalyzed cleavage of the ribozymes, functional scRNA could be produced from any transcript. Nevertheless, the plasmid already contained the *lexA*_HH-scRNA-HDV construct, which was used for the construction of the final plasmid pAH021. The plasmid pAH021 was built from a pJZC588 backbone containing a CEN/ARS ori and an URA selection marker, the *lexA*_HH-scRNA-HDV construct amplified from pAH013 and the CYC1 terminator placed behind the URA selection marker amplified from pFRP793. The assembled plasmid is shown in 3.2. The fragments and utilized concentrations for the new plasmid pAH021 are listed in Table 34. For cPCR the oligonucleotides oAH007 and rv_lexA+scRNA_ColonyPCR and for sequencing the oligonucleotide oAH011 and rv_lexA+scRNA_ColonyPCR were used (data not shown).

Table 34 Fragments and concentrations utilized for the construction of pAH021.

Fragment	Method	fw	rv	Template	Size [bp]	c [ng/μL]	Use [μL]
fAH010	PCR, Q5	oAH005	oAH006	pAH013, I	1212	24,72	50
fAH011.1	digestion	KpnI	NsiI	pJZC588	4025	34,26	25
fAH012	PCR, Q5	oAH009	oAH010	pFRP793	250	11,42	25

After the successful generation of pAH015 and pAH021, transformation of both plasmids was performed into electrocompetent Ssw, 7x *tet*O cells. Selection was performed using SD-leu-ura drop-out agar plates. Cells were grown for 48 h at 30 °C. Correct plasmid integration was verified by cPCR using the oligonucleotides lexA FP 7 and lexA FP 13 for pAH015 and oAH007 and rv_lexA+scRNA_ColonyPCR for pAH021 (data not show). The strain now contained all genes for a functional AND gate based on the ES inducible scRNA and hence is called AND, scRNA.

As a control the plasmid pAH021 was transformed into electrocompetent Ssw, 7x *tet*O cells as well. Without the plasmid pAH015 the hTF LexA-ER-B112 is missing, which is necessary to allow ES dependent induction, hence this strain served as negative control. After transformation, selection was performed using SD-ura drop-out agar plates. Cells were grown for 48 h at 30 °C. Correct plasmid integration was verified by cPCR using the oligonucleotides oAH007 and rv_lexA+scRNA_ColonyPCR for pAH021 (data not show). This strain is named NC in the following experiment.

5.5.5. Examination on the functionality of the ES inducible ribozyme-flanked scRNA

After the successful generation of the strains AND, scRNA and NC, a first comparative experiment was performed. Therefore, the cells were inoculated and induced in tubes according to the protocol described in 4.4.2. The AND, scRNA cells were grown in medium with the dropout mixture -ura-leu, whereas the NC was grown in medium with the drop-out mixture -ura. Cells were induced by growth in SG + 1 nM ES, 10 nM ES and 100 nM ES. This setup allows one to check whether ES dose-dependent inducibility was achieved. As control the cells were grown in SD, SD + 100 nM ES and SG. The tGFP fluorescence was measured *via* Accuri™ (*BD*) and analysis was performed using the Accuri™ software (*BD*). The mean fluorescence and the percentage of fluorescent cells were exported to Microsoft Excel (*Microsoft*). The percentage of fluorescent cells was calculated from Accuri flow cytometry measurements (Figure 45, bright colors). For the comparison of the mean fluorescence the sample AND, scRNA SG + 100 nM ES was set as 100 % and the respective percentage fluorescence in comparison to this sample was calculated for the controls and samples (Figure 45, light colors).

The NC did show approximately the same percental mean fluorescence of only 5 % and fraction of fluorescent cells of 20 % for all samples. In comparison, the AND, scRNA did show an increased tGFP expression when induced with ES. Hence, the strain NC was suited to serve as a negative control and the AND, switch was demonstrated to be functional. The number of fluorescent cells and the mean fluorescence correlated well. Hence, it is sufficient to analyze only one of the parameters in future experiments.
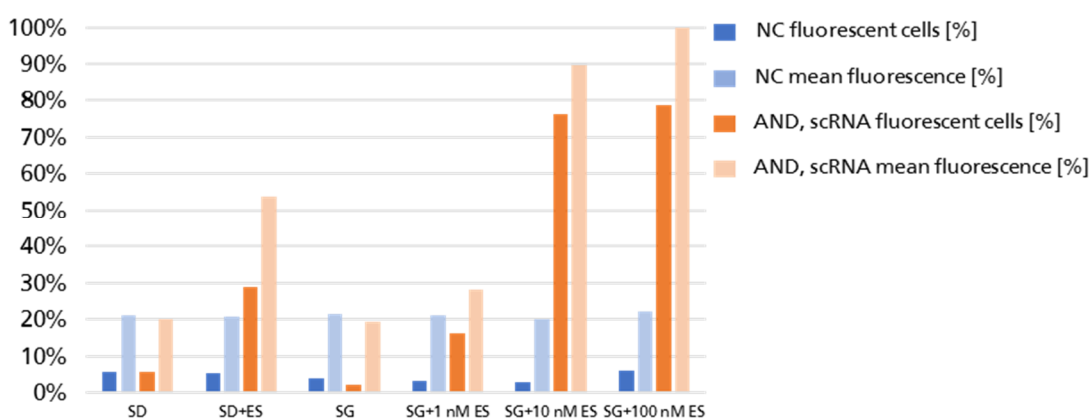
Figure 45 Induction experiment for the inducible scRNA based AND gate.

For the experiment cells of the strains Ssw, 7x *tet*O, HH-scRNA-HDV (NC, blue) and AND, scRNA (peach) were used. Both strains were grown in SD, SD + 100 nM ES, SG, SG + 1 nM ES, SG + 10 nM ES and SG + 100 nM ES. For all samples the percentage of fluorescent cells (dark color) and percentual mean fluorescence (light color) was applied.

For the control cells grown in SD or SG, no difference between NC and AND, scRNA was detected. Hence, the ES inducible scRNA is tightly regulated. A significant difference between the strains was visible for the control SD + 100 nM ES, where the AND, scRNA did show an increased number of fluorescent cells as well as an increased mean fluorescence. To investigate the effect of the HH-scRNA-HDV complex, an analysis on RNA (5.5.6) and DNA level was performed (5.5.7).

After induction of the strain AND, switch with 1 nM ES a slight increase in the number of fluorescent cells and in the mean fluorescence was observed. But when induced with 10 nM ES or 100 nM ES, nearly 80 % of the cells did show fluorescence and a bright mean fluorescence was achieved. As a matter of fact, the difference between 1 nM and 10 nM ES was significantly greater than that for 10 nM to 100 nM ES. Therefore, it can be assumed that 10 nM ES is already close to the smallest concentration for maximum induction. This dose-dependency was investigated in further experiments (5.5.8).

5.5.6. Analysis of the HH-scRNA-HDV construct on RNA level

For the analysis of the HH-scRNA-HDV construct, it was important to examine the actual ribozyme self-cleavage capacity. Therefore, the RNA was extracted from the cells, purified and reverse transcribed into cDNA. This cDNA was then used for PCR to determine, if none, one or both ribozymes were attached to the scRNA (Figure 46A).

Therefore, five different strains were utilized. Four of the five strains contained a scRNA, three the HH-scRNA-HDV setup. The AND, scRNA strain was used twice, once induced and once not induced. The strain cSLQ.sc002 was used as negative control, since it did not contain any scRNA genes. The utilized strains and the growth/induction media are described in Table 35.

Table 35 Strains utilized for RNA analysis with the gene of interest and growth/induction medium.

Number	GOI	Strain	Medium
1	NC	cSLQ.sc002	SD
2	scRNA	Ssw, 7x *tet*O scRNA	SD-ura
3	HH-scRNA-HDV	Ssw, 7x *tet*O HH-scRNA-HDV	SD-ura
4	*lexA_* HH-scRNA-HDV	AND, scRNA	SD-ura-leu
5	Ind. *lexA_* HH-scRNA-HDV	AND, scRNA	SG-ura-leu + 50 nM ES

For scRNA expression, the strains were freshly inoculated in 5 mL of the corresponding medium and grown overnight. The cell density was determined and 5 mL of the corresponding medium were inoculated towards an OD_{600} of 1. The cells were grown for 20 h at 25 °C. Afterwards the cells were pelleted and both, RNA and DNA extracted as described in 4.3.1. The DNA was removed by addition of TURBO-DNase and subsequent RNA purification. The concentration of the extracted RNA was determined using the ND-1000 Spectrophotometer and adjusted to

100 ng/μL for further experiments. For quality control, 500 ng of the RNA samples were applied on a 1 % agarose gel (Figure 46B). As marker, the 1kb DNA-ladder (*vwr*) was used. Extraction was successful for all five samples, even though the bands for the NC were faint.

The extracted RNA was used for cDNA synthesis as described in 4.3.2. Reverse transcription was performed using the reverse transcriptase M-MuLV (*New England Biolabs*). As a control, the same experiment was performed without the addition of the reverse transcriptase, hence no cDNA was produced. The obtained cDNA was used for PCR amplification with four different oligonucleotide pairs. First a pair of the oligonucleotides oAH019 and oAH21 was used, that amplified HH-scRNA (HH-scRNA), the second pair oAH020 and oAH22 amplified scRNA-HDV (scRNA-HDV) and the third pair oAH20 and oAH21 amplified the scRNA only (scRNA). As a control the oligonucleotide pair ura3 204 and ura3 205 was used, that amplified a 200 bp long fragment from the yeast *ura3* gene (PC), which is present in all yeast strains. This sample served as a positive control. After PCR with the *Taq* polymerase (*New England Biolabs*), the samples were applied to a 3 % agarose gel. As marker, the Ultra Low Range DNA-Leiter II, peqGOLD (*vwr*) was used. The results of the experiment are shown in Figure 46C. The experiment was performed twice in order to verify the results. The results for the second experiment are shown in Supplementary Figure 55.

For the control experiment, in which no reverse transcriptase was added, no PCR product was obtained. Hence, no off-target binding to *e.g.* remaining RNA did occur. When reverse transcriptase was added, the correct sized PCR product was obtained for the ura gene for all five strains. Hence, the RNA extraction, reverse transcription into cDNA and amplification *via* PCR did generally work. The oligonucleotides to amplify the scRNA were used to verify the expression of the scRNA. The detection of scRNA was possible for the strains 2 - 5. The sample 2 and 3 expressed the scRNA gene constitutively. For the samples of the AND, scRNA strain, only the ES induced sample 5 should lead to a PCR fragment. For samples 2, 3 and 5, the scRNA fragment was confirmed, but a slight band was also visible for sample 4. Due to the sensitivity of the method PCR, already small amounts of DNA are sufficient for amplification and achievement of a PCR fragment (218). Additionally, as described in 5.5.4, after read-trough of other genes on the plasmid, the HH-scRNA-HDV construct allows the successful expression of the scRNA. It can be assumed, that a small amount of functional scRNA was either achieved by basal expression, which is rather low for the ES switch (4,46,45), or by read-trough of the plasmid (217), which led to the weak band detectable for sample 4.
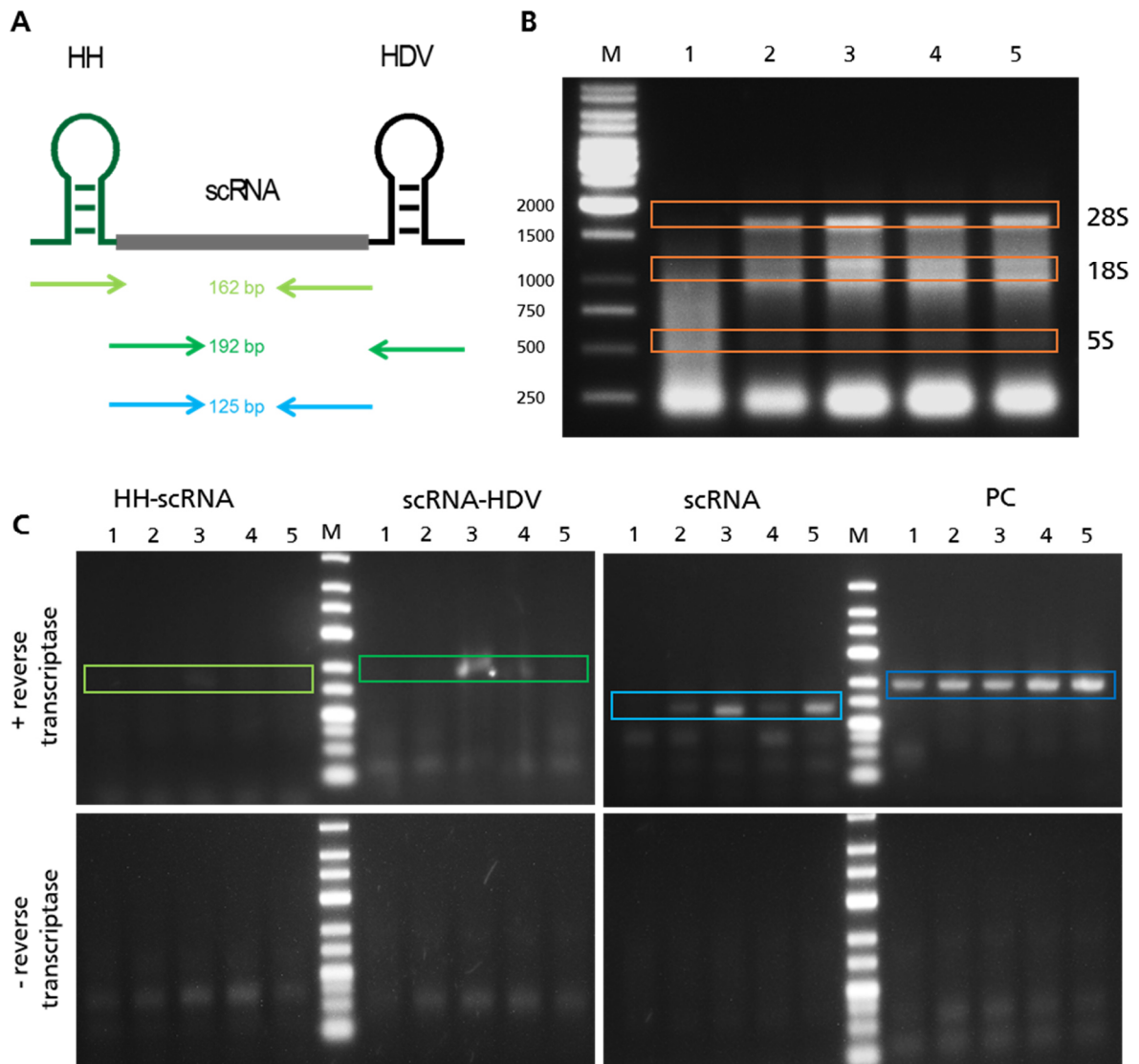
Figure 46 RNA extraction and cDNA analysis for the HH-scRNA-HDV construct.

(A) The planned PCR strategy, in which three different fragments should be tested. (B) Isolated RNA applied on a 1 % agarose gel. As marker, the 1kb DNA-ladder (*vwr*) was used. (C) PCR of the reverse transcribed cDNA showing which fragment could be amplified. On the top, cDNA was reverse transcribed using the M-MuLV reverse transcriptase (*New England Biolabs*). On the bottom the control is shown, where no -MuLV reverse transcriptase was added. Samples were applied to a 3 % agarose gel. As marker, the Ultra Low Range DNA-Leiter II, peqGOLD (*vwr*) was used.

After successfully demonstrating that the scRNA is expressed, the other two oligonucleotide pairs were used to investigate whether the ribozymes were cleaved off. If the ribozymes had successfully performed auto-cleavage, amplification with these primers should not be possible and no band should be detectable. Only the strains 3 to 5 contained the HH-scRNA-HDV construct and thus only bands could occur here. After PCR, no fragments were detected for any of the samples. Hence, auto-cleavage of the HH ribozyme was successfully performed. For scRNA-HDV no fragments were detected for sample 4 and 5. However, a band was amplified for sample 3, which expressed the HH-scRNA-HDV construct from the strong constitutive *Adh1* promoter. This leads to the assumption that due to the high expression rate, at the time of the

RNA isolation of the sample, not all HDV ribozymes were cleaved off eventually leading to the generation of a cDNA/PCR product.

To sum up, the expression of the scRNA on RNA level as well as the successful and complete auto-cleavage of the ribozyme HH and the mostly complete auto-cleavage of the ribozyme HDV were demonstrated. The results were confirmed by the Supplementary Figure 55. In a next step, it should be investigated to what extent the ribozymes are actually necessary to express a functional scRNA by the *lexA*-minimal promoter.

5.5.7. Analysis of the HH-scRNA-HDV construct on DNA level

To analyze, if none, one or both ribozymes are necessary and/or sufficient for functional scRNA expression, three new plasmids were designed, build and implemented into the S*sw*, 7x *tet*O strain together with pAH015. The plasmids pAH024, containing *lexA*_scRNA, the plasmid pAH025, containing *lexA*_HH-scRNA, and the plasmid pH026, containing *lexA*_scRNA-HDV were built by gap repair after 4.1.7. For all plasmids the backbone was generated by digestion of pAH021, bringing in a CEN/ARS ori, an URA selection marker and the *lexA*_minimal promoter. The inserts were amplified from the plasmids pJZC588 and pJZC625. The fragments and utilized concentrations for the new plasmids pAH024, pAH025 and pAH026 are listed in Table 36.

Table 36 Fragments and concentrations utilized for the construction of pAH024-26.

For plasmid	Fragment	Method	fw	rv	Template	Size [bp]	c [ng/µL]	Use [µL]
pAH024-26	fAH018	digestion	PstI	AleI-v2	pAH021	5236	29,97	12
pAH024	fAH019	PCR, Q5	oAH025	oAH026	pJZC588	212	14,00	20
pAH025	fAH020	PCR, Q5	oAH027	oAH028	pJZC625	230	20,00	15
pAH026	fAH021	PCR, Q5	oAH025	oAH029	pJZC625	277	15,00	25

In order to perform gap repair, the DNA was prepared according to the protocol described in 4.1.7. After gap repair in chemo competent yeast cells, correct plasmid assembly was verified by cPCR using the oligonucleotides fw_lexA+scRNA_ColonyPCR and oAH031. A correct clone was chosen, the plasmid isolated using the *Zymoprep*™ Yeast Plasmid Miniprep II Kit (*Zymoresearch*), transformed into electrocompetent *E. coli* cells and isolated using the *PureYield*™ Plasmid Miniprep System Kit (*Promega*). The correct plasmid sequence was verified by sequencing using the oligonucleotide fw_lexA+scRNA_ColonyPCR (data not show).

The successfully generated plasmids were transformed into electrocompetent S*sw*, 7x *tet*O cells together with the plasmid pAH015 containing the hTF LexA-ER-B112 enabling ES inducibility. Selection was performed using SD-leu-ura drop-out agar plates. Cells were grown for 48 h at 30 °C. Correct plasmid integration was verified by cPCR using the oligonucleotides lexA FP 7

and lexA FP 13 for pAH015 and fw_lexA+scRNA_ColonyPCR and oAH031 for pAH024-26 (data not shown).

For the comparative analysis of the AND, scRNA gate with the strains containing the newly generated plasmids, all strains were freshly inoculated into a deep-well plate and grown shaking overnight at 30 °C. Induction was performed in biological triplicates in a 96-deep-well plate. Therefore, 50 μL of the precultured cells were mixed with either 450 μL of SD medium or SG medium + 50 nM ES. If desired, 2.5 μL of an ES stock solution were added to the cell suspension. The Venus fluorescence was measured *via* Accuri™ (*BD*) with a 488 nm laser and the filter options 533/30. For analysis the Accuri™ software (*BD*) was used. The percentage of fluorescent cells was exported to Microsoft Excel (*Microsoft)* and applied to Figure 47.

Induction was successful for the AND, scRNA strain. In the absence of galactose and ES, the fluorophore expression was tightly regulated, whereas in presence of both nearly 80 % of the cells showed fluorescence beyond the arbitrarily set 5% threshold of control cells. As expected, neither the uninduced nor the induced NC showed an increased cellular fluorescence. The strains containing the plasmids pAH024-26 showed approximately the same fraction of fluorescent cells as the NC when uninduced. Interestingly, the fraction of fluorescent cells even decreased for those clones, when induced with galactose and ES. Hence, for neither of the three constructs scRNA only, HH-scRNA and scRNA-HDV an induction was achieved. As are result, both ribozymes flanking the scRNA are necessary to achieve a functional scRNA generation.
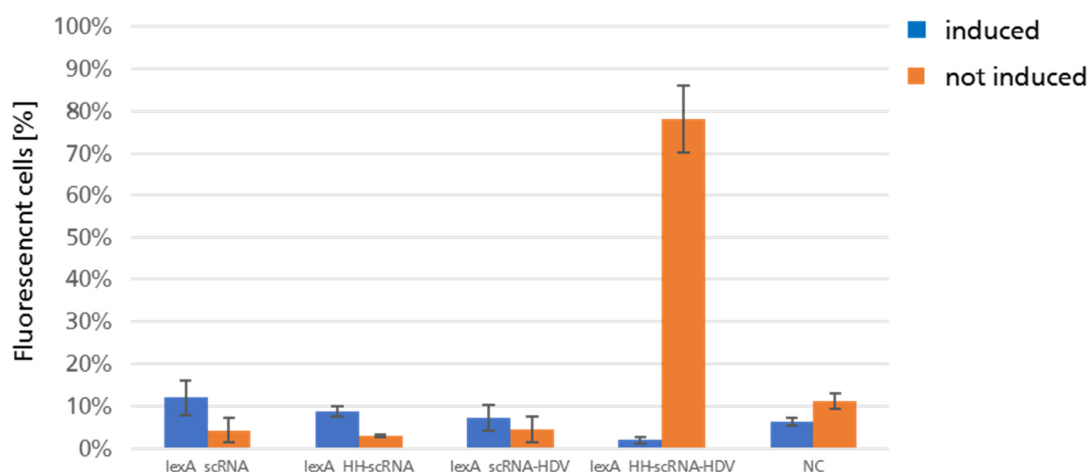
Figure 47 Comparative induction of different *lexA*_scRNA-Ribozyme constructs.

For the experiment cells of the strains containing the constructs *lexA*_scRNA, *lexA*_HH-scRNA, *lexA*_scRNA-HDV, *lexA*_HH-scRNA-HDV (AND, scRNA) and a NC. The strains were grown in SD for not induced (orange) or SG + 50 nM ES for induction (blue). Y-axis showing fluorescent cells beyond the 5 % threshold. Error bars indicate the standard deviation of the biological triplicates.

Summing up the results of the RNA and DNA analysis, it can be concluded that the expression of the scRNA by an RNA pol II promoter is possible only with the help of the flanking ribozyme setup and that the auto-cleaving properties of the utilized ribozymes work sufficiently well.

5.5.8. Dose-dependent analysis of the AND, scRNA gate

In a last experiment, the dose-dependency of the AND, scRNA gate should be determined. Therefore, the AND, scRNA strain was induced with different ES concentrations between 0.005 nM ES and 100 nM ES. Induction was performed in a 96-deep well plate in triplicates following the protocol described in 4.4.3. For induction, cells were freshly inoculated in 15 mL SD-ura-leu medium and grown at 30 °C overnight. The cell density was measured and a cell suspension was obtained by inoculation of different media towards an OD_{600} of 1. Subsequently, 475 μL of this cell mixture were pipetted into a 96-deep-well plate and mixed with 25 μL of medium or an ES solution. For the controls, cells were grown in SD, SD + 100 nM ES or SG. For induction cells were grown in SG and different ES solutions. For the ES solutions, two serial dilutions in PBS were performed. One starting at 100 nM and ending at 0.1 nM ES and one starting at 50 nM ES and ending at 0.005 nM ES. During the analysis it has to be considered, that through the two dilution series, the applied concentrations do not decrease proportionally. Additionally, as controls the strains NC and Ssw, 7x *tet*O, pAH015 + pAH024-26 were grown and induced the same way. The Venus fluorescence was directly measured with *BD* Accuri™ C6 (*BD*) using the 96-well plate. The mean fluorescence and the percentage of fluorescent cells were exported to Microsoft Excel (*Microsoft*). The mean fluorescence of the AND, scRNA was applied to Figure 48. The number of fluorescent cells of the AND, scRNA and the controls as well as the percentage of fluorescent cells for the controls were applied to the Supplementary Figure 56.
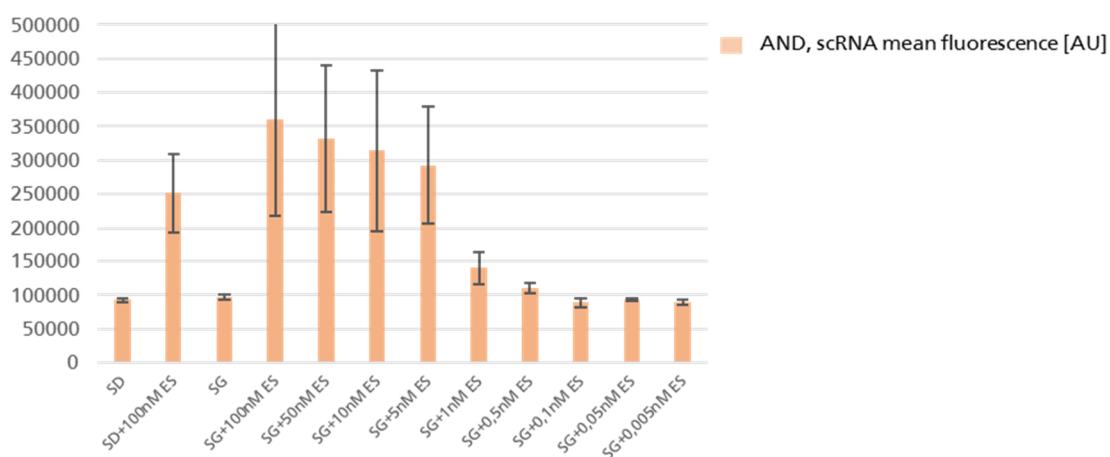
Figure 48 ES dose-dependent induction experiment for the inducible scRNA based AND gate.

For the experiment cells of AND, scRNA were used. Cells were grown in SD, SD + 100 nM ES and SG for controls. The samples were grown in SG plus decreasing concentrations of ES. Error bars indicate the standard deviation of the biological triplicates.

For the controls, the same results were obtained as before. Both, mean fluorescence and the number of fluorescent cells did not increase due to induction with galactose and any ES concentration. For the AND, scRNA strain, the control growth in SD and SG did show the expected negative results. For the samples, the fraction of fluorescent cells beyond threshold of the AND, scRNA strain was about the same for all concentrations of 5 nM and above. This raises the assumption that the maximum shift of mean fluorescence resulting from induced cells in this setup is already reached at an ES concentration of 5 nM. Afterwards the fraction of fluorescence decreased fast to nearly 0 %. A similar decrease was obtained for the shift of mean fluorescence. From 100 nM to 5 nM ES a slight decrease of the mean fluorescence was detected. For concentrations below 5 nM ES, a strong decrease was observed and reached at 0.1 nM ES the level of the SD only control. Hence, a dose-dependent behavior similar to the AND, AND, GO and AND, vNAR gates (5.2) was obtained.

However, in contrast for the previously tested AND gates, for the AND, scRNA gate again high basal activity was observed for the control SD + ES. It is generally possible, that the leakiness of the galactose-inducible switch led to a relatively high basal dCas9 expression that in combination with high level synthesis of scRNA accounts for this finding. In recent work, the limiting factor of a CRISPR/(d)Cas9 system was demonstrated to be the gRNA expression and/or the assembly of the gRNA into Cas9 (204). When expressed from a RNA pol II promoter the excess of scRNA may aid assembly of a transcription activator complex.

In conclusion, these experiments showed that a dose-dependent induction of the AND, scRNA gate is possible. Hence, a functional and dose-dependent AND gate was built not only for dCas9 and MCP-VP64, but also for dCas9 and scRNA. It is likely, that the AND gate setup can also be applied to other systems and thus can be understood as a synthetic toolbox for targeted gene expression.

6. Conclusion and Outlook

Within the presented work, different routes for targeted gene expression were applied to the yeast *S. cerevisiae* and a genetic toolbox was established. An AND gate was developed that allows a modular and tightly regulated gene expression. To this end, a CRISPR/dCas9 system was utilized, which allows for targeted gene expression with the help of the three components dCas9, MCP-VP64 and scRNA (5). All components were implemented into *S. cerevisiae* cells along with the scRNA *tet*O-binding site preceding the reporter gene Venus. This setup offered the possibility to efficiently and quickly test the reporter gene using the Tet-On system (74). Different *tet*O copy numbers were used. Gene expression of the reporter gene construct was successfully induced by doxycycline addition.

With the implementation of a *GAL* promoter in front of the dCas9 coding sequence, the dCas9 expression was placed under control of galactose addition and a first switch was implemented. To achieve this, strains were generated containing different *tet*O copy numbers preceding reporter gene Venus. The established single switch strains were compared with the conventionally used two component CRISPR/dCas9-VP16 transcription activator (141). The galactose-dependent single switch was not only functional, but also reached significantly higher expression levels compared to the conventional CRISPR/dCas9-VP16 system. This effect is likely to be mainly caused by the two MCP-VP64 hairpin loops (179) attached to the scRNA. In combination with up to seven scRNA binding sites, the recruitment of multiple transcription activation molecules at the same time is possible. Unfortunately, these high expression rates lead to an increased basal expression level. Particularly due to the inherent leakiness of the *GAL* promoter (57), a certain amount of dCas9 is expressed even in the absence of galactose. dCas9 builds a complex with the constitutively expressed MCP-VP64 and scRNA and especially when a high *tet*O copy number was used, a small amount of Venus was unintentionally produced.

To solve this problem, and also to allow dose-dependent induction, a second switch reliant on ES as an inducer was added to the CRISPR/dCas9 system. After integration of the hTF LexA-ER-B112 and 4x *lexA* boxes in front of MCP-VP64 (45), a functional AND gate was generated. Only when induced with galactose and ES at the same time, Venus expression was detectable. The AND gate showed the expected concentration and time-dependent behavior while being tightly regulated. In addition to the reporter Venus, a more biologically relevant setup was investigated in which a GOI was linked to a tGFP by the ribosomal skipping sequence T2A (157). With the help of this setup, the enzyme GOase and the shark antibody fragment vNAR were successfully produced and verified by SDS-PAGE or ABTS assay. To allow simple and quick analysis a signal sequence was N-terminal fused to GOase and vNAR, and for vNAR additionally a *C*-terminal hexahistidine tag. Due to this setup it was possible to simply centrifuge

the cells suspension and to detect GOase directly in the supernatant. No further purification steps were needed allowing quick and easy purification as well as analysis of GOase expression. In contrast, the His tag containing vNAR needed to be purified by IMAC after expression. Despite this additional purification step, the vNAR was insufficiently purified and thus could not be detected by ELISA. However, the verification of vNAR expression succeeded with SDS gel and western blot analysis. For all samples successful co-verification of induction was performed by measurement of the tGFP fluorescence in the cells. Thanks to a collaboration with Johannes Falk from the group of Prof. Drossel (Physics Department of TU Darmstadt), it was possible to develop a simple model that perfectly reproduced the AND gate data. In the future, the model will make it possible to predict target gene expression/AND gate output based on the ES concentration (4,198). Thus, with the help of the T2A setup, the AND gate enables the tightly regulated expression of any target gene and the level of target gene expression can be precisely adjusted by the ES concentration used.

The AND gate is based on the assembly of two switches; one depending on galactose and the other on ES as inducer. However, growth in galactose is known to be a burden to *S. cerevisiae* strains (202,203). In order to reduce this burden, a positive feedback loop was designed and built which, after a short induction with galactose, should allow growth and reporter gene expression in glucose. A plasmid was established, which contained the dCas9 gene behind 3x *tet*O binding sites and transformed to the AND gate clone. The established strain contained both, the genes for a functional CRISPR/dCas9 system and the plasmid for the positive feedback loop. After induction of the CRISPR system, not only the reporter gene tGFP, but also the dCas9 can be expressed. Thus, galactose does not have to be further added to maintain a sufficient dCas9 concentration. After induction with galactose was performed for 30 or 120 min, respectively and ES was constantly added to the medium, the strain was demonstrated to be functional even after removal of the galactose inducer by transfer to glucose containing medium. In addition, unexpectedly high expression values were achieved with the help of the positive feedback loop. Among others, the assembly of the gRNA/scRNA into dCas9 is the limiting factor of a CRISPR/dCas9 system (204). Hence, the overexpression of dCas9 may have resolved this expression limitation of the AND gate. To get a deeper understanding of how the feedback loop works, a degradation tag was added to the *N*-terminus of the tGFP reporter, which should allow a more precise analysis of the feedback process. However, the degron used was too efficient and no tGFP fluorescence was detectable. To allow more precise analysis of the functionality of the positive feedback loop and time-dependent tGFP expression, a weaker degradation mechanism would have to be used in further experiments. If this degradation mechanism would demonstrate to be functional, the construction of a negative feedback loop

would be conceivable. A negative feedback loop would allow for even more precise tuneability, as well as a further reduction in basal activity (219,220).

To demonstrate that the AND gate setup is modular, the ES switch was transferred to the scRNA synthesis. In order to achieve an ES inducibility of the scRNA transcription, the utilized RNA polymerase III promoter first had to be replaced by the ES inducible RNA polymerase II *lexA* minimal promoter construct. In order to circumvent problems with processing of the scRNA by RNA pol II (212), a ribozyme-scRNA-ribozyme setup was implemented (158). This construction proved to be successful for scRNA expression from the constitutive *Adh1* promoter as well as from the ES inducible *lexA* minimal promoter construct. Thus, a dose-dependent AND gate was constructed based on a galactose inducible dCas9 and an ES inducible scRNA. The AND gate was tightly regulated, except when grown in ES containing medium. A possible explanation is basal level dCas9 expression, which in combination with high ES-induced scRNA expression may allow for facile assembling of scRNA and dCas9 at low concentration of dCas9. A possible experiment to prove/disprove this model would be to determine the exact amount of scRNA as a function of time by RT-qPCR (221) and to further reduce the dCas9 basal level of expression. For future work, it will be interesting to see whether more sophisticated genetic switches and circuits can be implemented using the toolbox of strains and DNA constructs developed in this work. For example, it might be interesting to investigate, whether expression of two reporters can be individually controlled by two different dCas9/scRNA constructs, each addressing a different operator (Figure 49A+B). Likewise, positive and negative feedback loops could be implemented in a single cell as well as oscillators (222–224). Further work is required to investigate whether the complexity of this type of dCas9/scRNA derived switches, gates and circuits can be expanded and whether the behavior of such type of complicated integrated systems can be modeled and predicted.

In summary, in this work it was successfully demonstrated that the AND gate operates in a modular fashion, maintaining computable features, such as concentration dependency, independent of the setup used. Therefore, the AND gate setup designed, assembled and extensively characterized in this work can be considered as a contribution to the SynBio toolboxes for yeast.
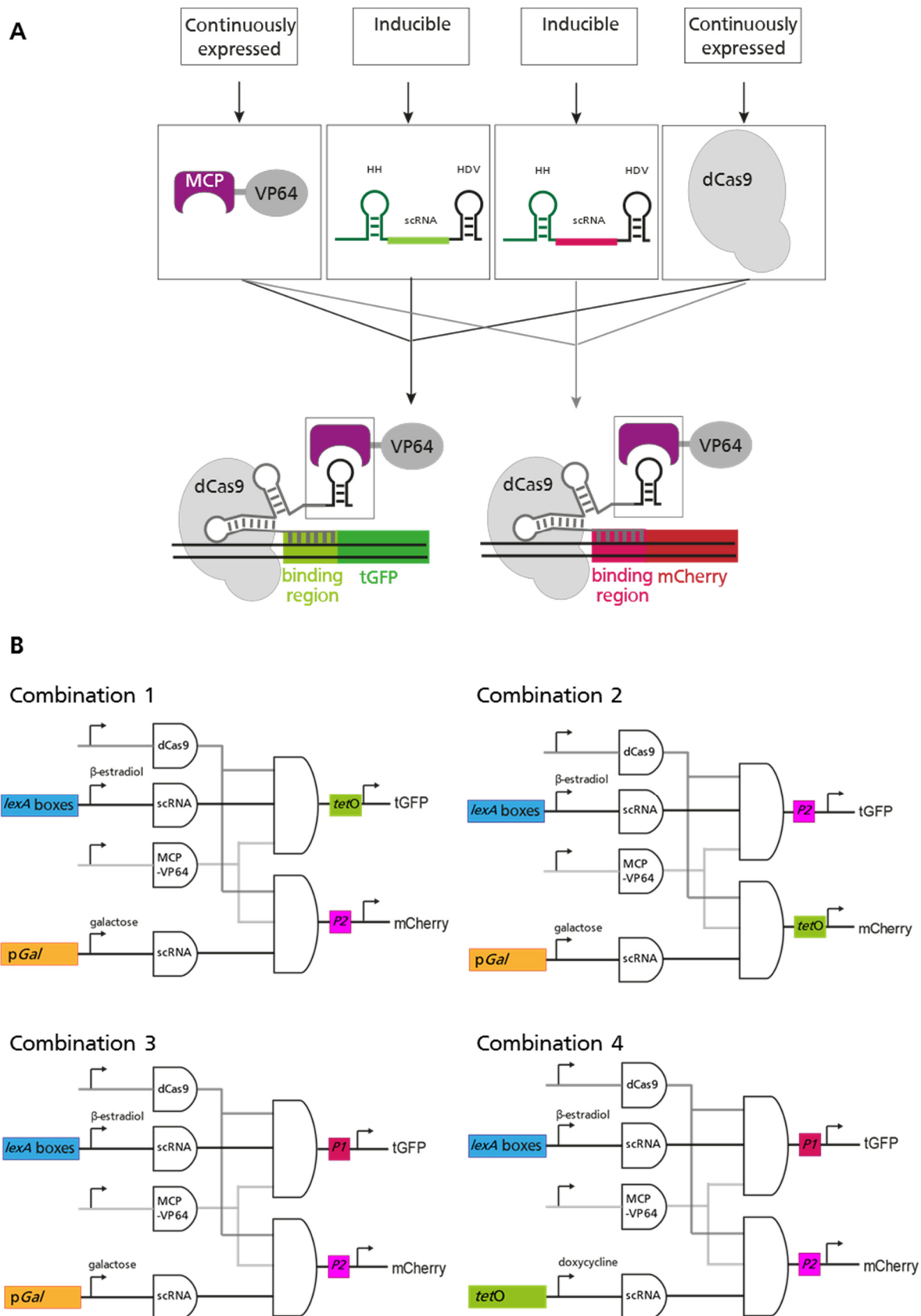
Figure 49 Schematic idea for expression of two reporters, individually controlled by two different dCas9/scRNA constructs, each addressing a different operator.

(A) Strain design for the double gene expression control. (B) scheme of the corresponding genetic switches. *tet*O, P1 and P2 indicate individual operator sequences that can be addressed with complementary scRNAs.

7. References

1. Lorenzo, V. de, Prather, K.L., Chen, G.-Q., O'Day, E., Kameke, C. von, Oyarzún, D.A., Hosta-Rigau, L., Alsafar, H., Cao, C. and Ji, W. *et al.* (2018) The power of synthetic biology for bioproduction, remediation and pollution control: The UN's Sustainable Development Goals will inevitably require the application of molecular biology and biotechnology on a global scale, *EMBO reports,* **19**.

2. Jensen, M.K. and Keasling, J.D. (2015) Recent applications of synthetic biology tools for yeast metabolic engineering, *FEMS yeast research,* **15**, 1–10.

3. Kavšček, M., Stražar, M., Curk, T., Natter, K. and Petrovič, U. (2015) Yeast as a cell factory: current state and perspectives, *Microb Cell Fact,* **14**, 1–10, https://microbialcellfactories.biomedcentral.com/track/pdf/10.1186/s12934-015-0281-x.

4. Hofmann, A., Falk, J., Prangemeier, T., Happel, D., Köber, A., Christmann, A., Koeppl, H. and Kolmar, H. (2019) A tightly regulated and adjustable CRISPR-dCas9 based AND gate in yeast, *Nucleic acids research,* **47**, 509–520.

5. Zalatan, J.G., Lee, M.E., Almeida, R., Gilbert, L.A., Whitehead, E.H., La Russa, M., Tsai, J.C., Weissman, J.S., Dueber, J.E. and Qi, L.S. *et al.* (2015) Engineering Complex Synthetic Transcriptional Programs with CRISPR RNA Scaffolds, *Cell,* **160**, 339–350, http://www.sciencedirect.com/science/article/pii/S0092867414015700.

6. König, H., Frank, D., Heil, R. and Coenen, C. (2013) Synthetic genomics and synthetic biology applications between hopes and concerns, *Current genomics,* **14**, 11–24.

7. Purnick, P.E.M. and Weiss, R. (2009) The second wave of synthetic biology: from modules to systems, *nrm,* **10**, 410–422, https://www.nature.com/articles/nrm2698.pdf.

8. Lorenzo, V. de and Danchin, A. (2008) Synthetic biology: discovering new worlds and new words, *EMBO reports,* **9**, 822–827.

9. Leduc, S. (1911) The Mechanism Of Life. Rebman.

10. Katz, L., Chen, Y.Y., Gonzalez, R., Peterson, T.C., Zhao, H. and Baltz, R.H. (2018) Synthetic biology advances and applications in the biotechnology industry: a perspective, *Journal of industrial microbiology & biotechnology,* **45**, 449–461.

11. Gleason, N.W. (ed.) (2018). *Higher Education in the Era of the Fourth Industrial Revolution.* Springer Singapore, Singapore.

12. Johnson, I.S. (1983) Human insulin from recombinant DNA technology, *Science (New York, N.Y.),* **219**, 632–637.

13. Cases, I. and Lorenzo, V. de (2005) Genetically modified organisms for the environment: stories of success and failure and what we have learned from them, *International microbiology : the official journal of the Spanish Society for Microbiology,* **8**, 213–222.

14. Antunes, M.S., Ha, S.-B., Tewari-Singh, N., Morey, K.J., Trofka, A.M., Kugrens, P., Deyholos, M. and Medford, J.I. (2006) A synthetic de-greening gene circuit provides a reporting system that is remotely detectable and has a re-set capacity, *Plant biotechnology journal,* **4**, 605–622.

15. Savage, D.F., Way, J. and Silver, P.A. (2008) Defossiling fuel: how synthetic biology can transform biofuel production, *ACS chemical biology,* **3**, 13–16.

16. Kitada, T., DiAndreth, B., Teague, B. and Weiss, R. (2018) Programming gene and engineered-cell therapies with synthetic biology, *Science (New York, N.Y.),* **359**.

17. Keating, K.W. and Young, E.M. (2019) Synthetic biology for bio-derived structural materials, *Current Opinion in Chemical Engineering,* **24,** 107–114, http://www.sciencedirect.com/science/article/pii/S2211339818300856.

18. Basu, S., Mehreja, R., Thiberge, S., Chen, M.-T. and Weiss, R. (2004) Spatiotemporal control of gene expression with pulse-generating networks, *Proceedings of the National Academy of Sciences of the United States of America,* **101,** 6355–6360.

19. Atkinson, M.R., Savageau, M.A., Myers, J.T. and Ninfa, A.J. (2003) Development of genetic circuitry exhibiting toggle switch or oscillatory behavior in Escherichia coli, *Cell,* **113,** 597–607.

20. Bashor, C.J. and Collins, J.J. (2018) Understanding Biological Regulation Through Synthetic Biology, *Annual review of biophysics,* **47,** 399–423.

21. Wang, S., Li, T., Chen, C., Kong, W., Zhu, S., Dai, J., Diaz, A.J., Hitz, E., Solares, S.D. and Li, T. *et al.* (2018) Transparent, Anisotropic Biofilm with Aligned Bacterial Cellulose Nanofibers, *Adv. Funct. Mater.,* **28,** 1707491.

22. Wu, H., Williams, G.R., Wu, J., Wu, J., Niu, S., Li, H., Wang, H. and Zhu, L. (2018) Regenerated chitin fibers reinforced with bacterial cellulose nanocrystals as suture biomaterials, *Carbohydrate Polymers,* **180,** 304–313, http://www.sciencedirect.com/science/article/pii/S0144861717311682.

23. Kaern, M., Blake, W.J. and Collins, J.J. (2003) The engineering of gene regulatory networks, *Annual review of biomedical engineering,* **5,** 179–206.

24. Lutz, R. and Bujard, H. (1997) Independent and tight regulation of transcriptional units in Escherichia coli via the LacR/O, the TetR/O and AraC/I1-I2 regulatory elements, *Nucleic acids research,* **25,** 1203–1210.

25. Brenner, M.J., Cho, J.H., Wong, N.M.L. and Wong, W.W. (2018) Synthetic Biology: Immunotherapy by Design, *Annual review of biomedical engineering,* **20,** 95–118.

26. Larroude, M., Rossignol, T., Nicaud, J.-M. and Ledesma-Amaro, R. (2018) Synthetic biology tools for engineering Yarrowia lipolytica, *Biotechnology Advances,* **36,** 2150–2164, http://www.sciencedirect.com/science/article/pii/S0734975018301678.

27. Chu, L. and Robinson, D.K. (2001) Industrial choices for protein production by large-scale cell culture, *Current opinion in biotechnology,* **12,** 180–187, http://www.sciencedirect.com/science/article/pii/S095816690000197X.

28. Nikel, P.I., Martínez-García, E. and Lorenzo, V. de (2014) Biotechnological domestication of pseudomonads using synthetic biology, *nrmicro,* **12,** 368–379, https://www.nature.com/articles/nrmicro3253.pdf.

29. Penprase, B.E. (2018) The Fourth Industrial Revolution and Higher Education. In Gleason, N.W. (ed.), *Higher Education in the Era of the Fourth Industrial Revolution.* Springer Singapore, Singapore, pp. 207–229.

30. Khalil, A.S. and Collins, J.J. (2010) Synthetic biology: applications come of age, *Nature reviews. Genetics,* **11,** 367–379.

31. Hong, K.-K. and Nielsen, J. (2012) Metabolic engineering of Saccharomyces cerevisiae: a key cell factory platform for future biorefineries, *Cellular and Molecular Life Sciences,* **69,** 2671–2690, https://doi.org/10.1007/s00018-012-0945-1.

32. Buchholz, K. and Collins, J. (2013) The roots--a short history of industrial microbiology and biotechnology, *Applied microbiology and biotechnology,* **97,** 3747–3762.

33. Li, M. and Borodina, I. (2015) Application of synthetic biology for production of chemicals in yeast Saccharomyces cerevisiae, *FEMS yeast research,* **15,** 1–12.

34. van Dien, S. (2013) From the first drop to the first truckload: commercialization of microbial processes for renewable chemicals, *Current opinion in biotechnology,* **24,** 1061–1068.

35. Lan, E.I. and Liao, J.C. (2013) Microbial synthesis of n-butanol, isobutanol, and other higher alcohols from diverse resources, *Bioresource technology,* **135,** 339–349.

36. Shin, S.-Y., Jung, S.-M., Kim, M.-D., Han, N.S. and Seo, J.-H. (2012) Production of resveratrol from tyrosine in metabolically engineered Saccharomyces cerevisiae, *Enzyme and microbial technology,* **51,** 211–216.

37. Nielsen, A.A.K., Segall-Shapiro, T.H. and Voigt, C.A. (2013) Advances in genetic circuit design: novel biochemistries, deep part mining, and precision gene expression, *Current opinion in chemical biology,* **17,** 878–892.

38. Annaluru, N., Muller, H., Mitchell, L.A., Ramalingam, S., Stracquadanio, G., Richardson, S.M., Dymond, J.S., Kuang, Z., Scheifele, L.Z. and Cooper, E.M. *et al.* (2014) Total synthesis of a functional designer eukaryotic chromosome, *Science (New York, N.Y.),* **344,** 55–58.

39. Brochado, A.R. and Patil, K.R. (2013) Overexpression of O-methyltransferase leads to improved vanillin production in baker's yeast only when complemented with model-guided network engineering, *Biotechnology and bioengineering,* **110,** 656–659.

40. Ellis, T., Wang, X. and Collins, J.J. (2009) Diversity-based, model-guided construction of synthetic gene networks with predicted functions, *Nature biotechnology,* **27,** 465–471.

41. Lee, M.E., Aswani, A., Han, A.S., Tomlin, C.J. and Dueber, J.E. (2013) Expression-level optimization of a multi-enzyme pathway in the absence of a high-throughput assay, *Nucleic acids research,* **41,** 10668–10678.

42. Lee, M.E., DeLoache, W.C., Cervantes, B. and Dueber, J.E. (2015) A Highly Characterized Yeast Toolkit for Modular, Multipart Assembly, *ACS synthetic biology,* **4,** 975–986.

43. Weinhandl, K., Winkler, M., Glieder, A. and Camattari, A. (2014) Carbon source dependent promoters in yeasts, *Microb Cell Fact,* **13,** 1–17, https://microbialcellfactories.biomedcentral.com/track/pdf/10.1186/1475-2859-13-5.

44. Da Silva, N.A. and Srikrishnan, S. (2012) Introduction and expression of genes for metabolic engineering applications in Saccharomyces cerevisiae, *FEMS yeast research,* **12,** 197–214.

45. Ottoz, D.S.M., Rudolf, F. and Stelling, J. (2014) Inducible, tightly regulated and growth condition-independent transcription factor in Saccharomyces cerevisiae, *Nucleic acids research,* **42,** e130.

46. McIsaac, R.S., Silverman, S.J., McClean, M.N., Gibney, P.A., Macinskas, J., Hickman, M.J., Petti, A.A. and Botstein, D. (2011) Fast-acting and nearly gratuitous induction of gene expression and protein depletion in Saccharomyces cerevisiae, *Molecular biology of the cell,* **22,** 4447–4459.

47. Louvion, J.-F., Havaux-Copf, B. and Picard, D. (1993) Fusion of GAL4-VP16 to a steroid-binding domain provides a tool for gratuitous induction of galactose-responsive genes in yeast, *Gene,* **131,** 129–134, http://www.sciencedirect.com/science/article/pii/037811199390681R.

48. Triezenberg, S.J., Kingsbury, R.C. and McKnight, S.L. (1988) Functional dissection of VP16, the trans-activator of herpes simplex virus immediate early gene expression, *Genes & development,* **2,** 718–729.

49. Koller, A., Valesco, J. and Subramani, S. (2000) TheCUP1 promoter ofSaccharomyces cerevisiae is inducible by copper inPichia pastoris, *Yeast,* **16,** 651–656.

50. Li, N., Zhang, L.-M., Zhang, K.-Q., Deng, J.-S., Prändl, R. and Schöffl, F. (2006) Effects of heat stress on yeast heat shock factor-promoter binding in vivo, *Acta biochimica et biophysica Sinica,* **38,** 356–362.

51. Carlson, M. (1999) Glucose repression in yeast, *Current Opinion in Microbiology,* **2,** 202–207.

52. Wilson, W.A., Hawley, S.A. and Hardie, D.G. (1996) Glucose repression/derepression in budding yeast: SNF1 protein kinase is activated by phosphorylation under derepressing conditions, and this correlates with a high AMP:ATP ratio, *Current Biology,* **6,** 1426–1434.

53. Gancedo, J.M. (1998) Yeast Carbon Catabolite Repression†, *Microbiol. Mol. Biol. Rev.,* **62,** 334–361.

54. Conrad, M., Schothorst, J., Kankipati, H.N., van Zeebroeck, G., Rubio-Texeira, M. and Thevelein, J.M. (2014) Nutrient sensing and signaling in the yeast Saccharomyces cerevisiae, *FEMS microbiology reviews,* **38,** 254–299.

55. Walther, K. and Schüller, H.J. (2001) Adr1 and Cat8 synergistically activate the glucose-regulated alcohol dehydrogenase gene ADH2 of the yeast Saccharomyces cerevisiae, *Microbiology (Reading, England),* **147,** 2037–2044.

56. Ostergaard, S., Olsson, L., Johnston, M. and Nielsen, J. (2000) Increasing galactose consumption by Saccharomyces cerevisiae through metabolic engineering of the GAL gene regulatory network, *Nature biotechnology,* **18,** 1283–1286.

57. Kang, H.A., Kang, W.K., Go, S.-M., Rezaee, A., Krishna, S.H., Rhee, S.K. and Kim, J.-Y. (2005) Characteristics of Saccharomyces cerevisiae gal1 Delta and gal1 Delta hxk2 Delta mutants expressing recombinant proteins from the GAL promoter, *Biotechnology and bioengineering,* **89,** 619–629.

58. Gossen, M. and Bujard, H. (1992) Tight control of gene expression in mammalian cells by tetracycline-responsive promoters, *Proceedings of the National Academy of Sciences of the United States of America,* **89,** 5547–5551.

59. Benjamin, I.J., Kröger, B. and Williams, R.S. (1990) Activation of the heat shock transcription factor by hypoxia in mammalian cells, *Proceedings of the National Academy of Sciences of the United States of America,* **87,** 6263–6267.

60. Fuerst, T.R., Fernandez, M.P. and Moss, B. (1989) Transfer of the inducible lac repressor/operator system from Escherichia coli to a vaccinia virus expression vector, *Proceedings of the National Academy of Sciences of the United States of America,* **86,** 2549–2553.

61. Brown, M., Figge, J., Hansen, U., Wright, C., Jeang, K.-T., Khoury, G., Livingston, D.M. and Roberts, T.M. (1987) Lac repressor can regulate expression from a hybrid SV40 early promoter containing a lac operator in animal cells, *Cell,* **49,** 603–612, http://www.sciencedirect.com/science/article/pii/0092867487905368.

62. Wyborski, D.L. and Short, J.M. (1991) Analysis of inducers of the E.coli lac repressor system in mammalian cells and whole animals, *Nucleic acids research,* **19,** 4647–4653.

63. Hillen, W. and Wissmann, A. (1989) Tet repressor-tet operator interaction. InSaenger, W. and Heinemann, U. (eds.), *Protein-Nucleic Acid Interaction.* Macmillan Education UK, London, s.l., pp. 143–162.

64. Yamaguchi, A., Udagawa, T. and Sawai, T. (1990) Transport of divalent cations with tetracycline as mediated by the transposon Tn10-encoded tetracycline resistance protein, *J. Biol. Chem.,* **265,** 4809–4813, http://www.jbc.org/content/265/9/4809.full.pdf.

65. Berg, C.M., Liu, L., Wang, B. and Wang, M.D. (1988) Rapid identification of bacterial genes that are lethal when cloned on multicopy plasmids, *Journal of bacteriology,* **170,** 468–470.

66. Hillen, W. and Berens, C. (1994) Mechanisms underlying expression of Tn10 encoded tetracycline resistance, *Annual review of microbiology,* **48,** 345–369.

67. Lederer, T., Kintrup, M., Takahashi, M., Sum, P.E., Ellestad, G.A. and Hillen, W. (1996) Tetracycline analogs affecting binding to Tn10-Encoded Tet repressor trigger the same mechanism of induction, *Biochemistry,* **35,** 7439–7446.

68. Takahashi, M., Altschmied, L. and Hillen, W. (1986) Kinetic and equilibrium characterization of the Tet repressor-tetracycline complex by fluorescence measurements: Evidence for divalent metal ion requirement and energy transfer, *Journal of Molecular Biology,* **187,** 341–348, http://www.sciencedirect.com/science/article/pii/0022283686904377.

69. Orth, P., Schnappinger, D., Hillen, W., Saenger, W. and Hinrichs, W. (2000) Structural basis of gene regulation by the tetracycline inducible Tet repressor–operator system, *Nat Struct Mol Biol,* **7,** 215–219, https://www.nature.com/articles/nsb0300_215.pdf.

70. McMurry, L., Petrucci, R.E. and Levy, S.B. (1980) Active efflux of tetracycline encoded by four genetically different tetracycline resistance determinants in Escherichia coli, *Proceedings of the National Academy of Sciences of the United States of America,* **77,** 3974–3977.

71. Hanson, S., Berthelot, K., Fink, B., McCarthy, J.E.G. and Suess, B. (2003) Tetracycline-aptamer-mediated translational regulation in yeast, *Molecular Microbiology,* **49,** 1627–1637, https://onlinelibrary.wiley.com/doi/full/10.1046/j.1365-2958.2003.03656.x.

72. Das, A.T., Tenenbaum, L. and Berkhout, B. (20) Tet-On Systems For Doxycycline-inducible Gene Expression, *Current Gene Therapy,* **16,** 156–167.

73. Berens, C. and Hillen, W. (2003) Gene regulation by tetracyclines. Constraints of resistance regulation in bacteria shape TetR for application in eukaryotes, *European journal of biochemistry,* **270,** 3109–3121.

74. Gossen, M., Freundlieb, S., Bender, G., Müller, G., Hillen, W. and Bujard, H. (1995) Transcriptional activation by tetracyclines in mammalian cells, *Science (New York, N.Y.),* **268,** 1766–1769.

75. Urlinger, S., Baron, U., Thellmann, M., Hasan, M.T., Bujard, H. and Hillen, W. (2000) Exploring the sequence space for tetracycline-dependent transcriptional activators: novel mutations yield expanded range and sensitivity, *Proceedings of the National Academy of Sciences of the United States of America,* **97,** 7963–7968.

76. Wishart, J.A., Hayes, A., Wardleworth, L., Zhang, N. and Oliver, S.G. (2005) Doxycycline, the drug used to control the tet-regulatable promoter system, has no effect on global gene expression in Saccharomyces cerevisiae, *Yeast,* **22,** 565–569.

77. Zhou, X., Vink, M., Klaver, B., Berkhout, B. and Das, A.T. (2006) Optimization of the Tet-On system for regulated gene expression through viral evolution, *Gene Ther,* **13,** 1382–1390, https://www.nature.com/articles/3302780.pdf.

78. Loew, R., Heinz, N., Hampf, M., Bujard, H. and Gossen, M. (2010) Improved Tet-responsive promoters with minimized background expression, *BMC Biotechnol,* **10,** 1–13, https://bmcbiotechnol.biomedcentral.com/track/pdf/10.1186/1472-6750-10-81.

79. Bellí, G., Garí, E., Piedrafita, L., Aldea, M. and Herrero, E. (1998) An activator/repressor dual system allows tight tetracycline-regulated gene expression in budding yeast, *Nucleic acids research,* **26,** 942–947.

80. Saez, E., No, D., West, A. and Evans, R.M. (1997) Inducible gene expression in mammalian cells and transgenic mice, *Current opinion in biotechnology,* **8,** 608–616, http://www.sciencedirect.com/science/article/pii/S0958166997800377.

81. Pfahl, M. (1981) Characteristics of tight binding repressors of the lac operon, *Journal of Molecular Biology,* **147,** 1–10, http://www.sciencedirect.com/science/article/pii/0022283681900759.

82. Beato, M. (1993) Gene Regulation by Steroid Hormones. In Karin, M. (ed.), *Gene expression. General and cell-type-specific.* Birkhäuser, Boston, pp. 43–75.

83. O'Malley, B. (1990) The steroid receptor superfamily: more excitement predicted for the future, *Molecular endocrinology (Baltimore, Md.),* **4,** 363–369.

84. Catelli, M.G., Binart, N., Jung-Testas, I., Renoir, J.M., Baulieu, E.E., Feramisco, J.R. and Welch, W.J. (1985) The common 90-kd protein component of non-transformed '8S' steroid receptors is a heat-shock protein, *The EMBO Journal,* **4,** 3131–3135.

85. Eilers, M., Picard, D., Yamamoto, K.R. and Bishop, J.M. (1989) Chimaeras of Myc oncoprotein and steroid receptors cause hormone-dependent transformation of cells, *Nature,* **340,** 66–68, https://www.nature.com/articles/340066a0.pdf.

86. Metzger, D., Losson, R., Bornert, J.M., Lemoine, Y. and Chambon, P. (1992) Promoter specificity of the two transcriptional activation functions of the human oestrogen receptor in yeast, *Nucleic acids research,* **20,** 2813–2817.

87. Sadowski, I., Ma, J., Triezenberg, S. and Ptashne, M. (1988) GAL4-VP16 is an unusually potent transcriptional activator, *Nature,* **335,** 563–564, https://www.nature.com/articles/335563a0.pdf.

88. Brent, R. and Ptashne, M. (1985) A eukaryotic transcriptional activator bearing the DNA specificity of a prokaryotic repressor, *Cell,* **43,** 729–736, http://www.sciencedirect.com/science/article/pii/0092867485902466.

89. Little, J.W. and Hill, S.A. (1985) Deletions within a hinge region of a specific DNA-binding protein, *Proceedings of the National Academy of Sciences of the United States of America,* **82,** 2301–2305.

90. Little, J.W. and Mount, D.W. (1982) The SOS regulatory system of Escherichia coli, *Cell,* **29,** 11–22, http://www.sciencedirect.com/science/article/pii/009286748290085X.

91. Ma, J. and Ptashne, M. (1987) A new class of yeast transcriptional activators, *Cell,* **51,** 113–119, http://www.sciencedirect.com/science/article/pii/0092867487900158.

92. Ruden, D.M., Ma, J., Li, Y., Wood, K. and Ptashne, M. (1991) Generating yeast transcriptional activators containing no yeast protein sequences, *Nature,* **350,** 250–252, https://www.nature.com/articles/350250a0.pdf.

93. Ma, J. and Ptashne, M. (1987) Deletion analysis of GAL4 defines two transcriptional activating segments, *Cell,* **48,** 847–853, http://www.sciencedirect.com/science/article/pii/009286748790081X.

94. Capecchi, M.R. (1989) The new mouse genetics: Altering the genome by gene targeting, *Trends in Genetics,* **5,** 70–76, http://www.sciencedirect.com/science/article/pii/0168952589900292.

95. Capecchi, M.R. (1989) Altering the genome by homologous recombination, *Science (New York, N.Y.),* **244,** 1288–1292.

96. Thomas, K.R., Folger, K.R. and Capecchi, M.R. (1986) High frequency targeting of genes to specific sites in the mammalian genome, *Cell,* **44,** 419–428, http://www.sciencedirect.com/science/article/pii/0092867486904630.

97. Addgene (2017) CRISPR 101: A Desktop Resource.

98. Orr-Weaver, T.L., Szostak, J.W. and Rothstein, R.J. (1981) Yeast transformation: a model system for the study of recombination, *Proceedings of the National Academy of Sciences of the United States of America,* **78,** 6354–6358.

99. Jakočiūnas, T., Rajkumar, A.S., Zhang, J., Arsovska, D., Rodriguez, A., Jendresen, C.B., Skjødt, M.L., Nielsen, A.T., Borodina, I. and Jensen, M.K. *et al.* (2015) CasEMBLR: Cas9-Facilitated Multiloci Genomic Integration of in Vivo Assembled DNA Parts in Saccharomyces cerevisiae, *ACS synthetic biology,* **4,** 1226–1234.

100. Gaj, T., Gersbach, C.A. and Barbas, C.F. (2013) ZFN, TALEN, and CRISPR/Cas-based methods for genome engineering, *Trends in Biotechnology,* **31,** 397–405, http://www.sciencedirect.com/science/article/pii/S0167779913000875.

101. Urnov, F.D., Rebar, E.J., Holmes, M.C., Zhang, H.S. and Gregory, P.D. (2010) Genome editing with engineered zinc finger nucleases, *Nat Rev Genet,* **11,** 636–646, https://www.nature.com/articles/nrg2842.pdf.

102. Wyman, C. and Kanaar, R. (2006) DNA double-strand break repair: all's well that ends well, *Annual review of genetics,* **40,** 363–383.

103. Mali, P., Yang, L., Esvelt, K.M., Aach, J., Guell, M., DiCarlo, J.E., Norville, J.E. and Church, G.M. (2013) RNA-Guided Human Genome Engineering via Cas9, *Science,* **339,** 823–826, https://science.sciencemag.org/content/sci/339/6121/823.full.pdf.

104. Wiedenheft, B., Sternberg, S.H. and Doudna, J.A. (2012) RNA-guided genetic silencing systems in bacteria and archaea, *Nature,* **482,** 331–338, https://www.nature.com/articles/nature10886.pdf.

105. Jinek, M., Chylinski, K., Fonfara, I., Hauer, M., Doudna, J.A. and Charpentier, E. (2012) A programmable dual-RNA-guided DNA endonuclease in adaptive bacterial immunity, *Science (New York, N.Y.),* **337,** 816–821.

106. Gilbert, L.A., Larson, M.H., Morsut, L., Liu, Z., Brar, G.A., Torres, S.E., Stern-Ginossar, N., Brandman, O., Whitehead, E.H. and Doudna, J.A. *et al.* (2013) CRISPR-Mediated Modular RNA-Guided Regulation of Transcription in Eukaryotes, *Cell,* **154,** 442–451, http://www.sciencedirect.com/science/article/pii/S009286741300826X.

107. Sander, J.D. and Joung, J.K. (2014) CRISPR-Cas systems for editing, regulating and targeting genomes, *nbt,* **32,** 347–355, https://www.nature.com/articles/nbt.2842.pdf.

108. Breitbart, M. and Rohwer, F. (2005) Here a virus, there a virus, everywhere the same virus?, *Trends in Microbiology,* **13,** 278–284, http://www.sciencedirect.com/science/article/pii/S0966842X05001083.

109. Barrangou, R., Fremaux, C., Deveau, H., Richards, M., Boyaval, P., Moineau, S., Romero, D.A. and Horvath, P. (2007) CRISPR provides acquired resistance against viruses in prokaryotes, *Science (New York, N.Y.),* **315,** 1709–1712.

110. Horvath, P. and Barrangou, R. (2010) CRISPR/Cas, the immune system of bacteria and archaea, *Science (New York, N.Y.),* **327,** 167–170.

111. Jansen, R., van Embden, J.D.A., Gaastra, W. and Schouls, L.M. (2002) Identification of genes that are associated with DNA repeats in prokaryotes, *Molecular Microbiology,* **43,** 1565–1575.

112. Sorek, R., Kunin, V. and Hugenholtz, P. (2008) CRISPR — a widespread system that provides acquired resistance against phages in bacteria and archaea, *Nat Rev Microbiol,* **6,** 181–186, https://www.nature.com/articles/nrmicro1793.pdf.

113. van der Oost, J., Jore, M.M., Westra, E.R., Lundgren, M. and Brouns, S.J.J. (2009) CRISPR-based adaptive and heritable immunity in prokaryotes, *Trends in Biochemical Sciences,* **34,** 401–407, http://www.sciencedirect.com/science/article/pii/S0968000409001200.

114. Makarova, K.S., Wolf, Y.I., Alkhnbashi, O.S., Costa, F., Shah, S.A., Saunders, S.J., Barrangou, R., Brouns, S.J.J., Charpentier, E. and Haft, D.H. *et al.* (2015) An updated evolutionary classification of CRISPR–Cas systems, *nrmicro,* **13,** 722–736, https://www.nature.com/articles/nrmicro3569.pdf.

115. Gesner, E.M., Schellenberg, M.J., Garside, E.L., George, M.M. and MacMillan, A.M. (2011) Recognition and maturation of effector RNAs in a CRISPR interference pathway, *Nat Struct Mol Biol,* **18,** 688–692, https://www.nature.com/articles/nsmb.2042.pdf.

116. Deltcheva, E., Chylinski, K., Sharma, C.M., Gonzales, K., Chao, Y., Pirzada, Z.A., Eckert, M.R., Vogel, J. and Charpentier, E. (2011) CRISPR RNA maturation by trans -encoded small RNA and host factor RNase III, *Nature,* **471,** 602–607, https://www.nature.com/articles/nature09886.pdf.

117. Brouns, S.J.J., Jore, M.M., Lundgren, M., Westra, E.R., Slijkhuis, R.J.H., Snijders, A.P.L., Dickman, M.J., Makarova, K.S., Koonin, E.V. and van der Oost, J. (2008) Small CRISPR RNAs guide antiviral defense in prokaryotes, *Science (New York, N.Y.),* **321,** 960–964.

118. Westra, E.R., van Erp, P.B.G., Künne, T., Wong, S.P., Staals, R.H.J., Seegers, C.L.C., Bollen, S., Jore, M.M., Semenova, E. and Severinov, K. *et al.* (2012) CRISPR Immunity Relies on the Consecutive Binding and Degradation of Negatively Supercoiled Invader DNA by Cascade and Cas3, *Molecular Cell,* **46,** 595–605, http://www.sciencedirect.com/science/article/pii/S1097276512002250.

119. Ishino, Y., Shinagawa, H., Makino, K., Amemura, M. and Nakata, A. (1987) Nucleotide sequence of the iap gene, responsible for alkaline phosphatase isozyme conversion in Escherichia coli, and identification of the gene product, *Journal of bacteriology,* **169,** 5429–5433.

120. Haft, D.H., Selengut, J., Mongodin, E.F. and Nelson, K.E. (2005) A guild of 45 CRISPR-associated (Cas) protein families and multiple CRISPR/Cas subtypes exist in prokaryotic genomes, *PLoS computational biology,* **1,** e60.

121. Kleinstiver, B.P., Prew, M.S., Tsai, S.Q., Topkar, V.V., Nguyen, N.T., Zheng, Z., Gonzales, A.P.W., Li, Z., Peterson, R.T. and Yeh, J.-R.J. *et al.* (2015) Engineered CRISPR-Cas9 nucleases with altered PAM specificities, *Nature,* **523,** 481–485, https://www.nature.com/articles/nature14592.pdf.

122. Makarova, K.S., Haft, D.H., Barrangou, R., Brouns, S.J.J., Charpentier, E., Horvath, P., Moineau, S., Mojica, F.J.M., Wolf, Y.I. and Yakunin, A.F. *et al.* (2011) Evolution and classification of the CRISPR–Cas systems, *Nat Rev Microbiol,* **9,** 467–477, https://www.nature.com/articles/nrmicro2577.pdf.

123. Garneau, J.E., Dupuis, M.-È., Villion, M., Romero, D.A., Barrangou, R., Boyaval, P., Fremaux, C., Horvath, P., Magadán, A.H. and Moineau, S. (2010) The CRISPR/Cas bacterial immune system cleaves bacteriophage and plasmid DNA, *Nature,* **468,** 67–71, https://www.nature.com/articles/nature09523.pdf.

124. Cho, S.W., Kim, S., Kim, J.M. and Kim, J.-S. (2013) Targeted genome engineering in human cells with the Cas9 RNA-guided endonuclease, *nbt,* **31,** 230–232, https://www.nature.com/articles/nbt.2507.pdf.

125. Yoder, K.E. and Bundschuh, R. Host Double Strand Break Repair Generates HIV-1 Strains Resistant to CRISPR/Cas9, *srep,* **6,** 29530, https://www.nature.com/articles/srep29530.pdf.

126. Barrangou, R. (2014) Cas9 Targeting and the CRISPR Revolution, *Science,* **344,** 707–708, https://science.sciencemag.org/content/sci/344/6185/707.full.pdf.

127. Wu, Y., Liang, D., Wang, Y., Bai, M., Tang, W., Bao, S., Yan, Z., Li, D. and Li, J. (2013) Correction of a Genetic Disease in Mouse via Use of CRISPR-Cas9, *Cell Stem Cell,* **13,** 659–662, http://www.sciencedirect.com/science/article/pii/S1934590913004621.

128. Zhang, J.-P., Li, X.-L., Li, G.-H., Chen, W., Arakaki, C., Botimer, G.D., Baylink, D., Zhang, L., Wen, W. and Fu, Y.-W. *et al.* (2017) Efficient precise knockin with a double cut HDR donor after CRISPR/Cas9-mediated double-stranded DNA cleavage, *Genome Biol,* **18,** 1–18, https://genomebiology.biomedcentral.com/track/pdf/10.1186/s13059-017-1164-8.

129. Le Cong, Ran, F.A., Cox, D., Lin, S., Barretto, R., Habib, N., Hsu, P.D., Wu, X., Jiang, W. and Marraffini, L.A. *et al.* (2013) Multiplex genome engineering using CRISPR/Cas systems, *Science (New York, N.Y.),* **339,** 819–823.

130. Wach, A., Brachat, A., Pöhlmann, R. and Philippsen, P. (1994) New heterologous modules for classical or PCR-based gene disruptions inSaccharomyces cerevisiae, *Yeast,* **10,** 1793–1808.

131. Jakočiūnas, T., Bonde, I., Herrgård, M., Harrison, S.J., Kristensen, M., Pedersen, L.E., Jensen, M.K. and Keasling, J.D. (2015) Multiplex metabolic pathway engineering using CRISPR/Cas9 in Saccharomyces cerevisiae, *Metabolic Engineering,* **28,** 213–222, http://www.sciencedirect.com/science/article/pii/S1096717615000105.

132. Park, J., Bae, S. and Kim, J.-S. (2015) Cas-Designer: a web-based tool for choice of CRISPR-Cas9 target sites, *Bioinformatics (Oxford, England),* **31,** 4014–4016.

133. Park, J., Kim, J.-S. and Bae, S. (2016) Cas-Database: web-based genome-wide guide RNA library design for gene knockout screens using CRISPR-Cas9, *Bioinformatics (Oxford, England),* **32,** 2017–2023.

134. Fu, Y., Sander, J.D., Reyon, D., Cascio, V.M. and Joung, J.K. (2014) Improving CRISPR-Cas nuclease specificity using truncated guide RNAs, *nbt,* **32,** 279–284, https://www.nature.com/articles/nbt.2808.pdf.

135. Mali, P., Aach, J., Stranges, P.B., Esvelt, K.M., Moosburner, M., Kosuri, S., Yang, L. and Church, G.M. (2013) CAS9 transcriptional activators for target specificity screening and paired nickases for cooperative genome engineering, *nbt,* **31,** 833–838, https://www.nature.com/articles/nbt.2675.pdf.

136. Ran, F.A., Hsu, P.D., Lin, C.-Y., Gootenberg, J.S., Konermann, S., Trevino, A.E., Scott, D.A., Inoue, A., Matoba, S. and Zhang, Y. *et al.* (2013) Double Nicking by RNA-Guided CRISPR Cas9 for Enhanced Genome Editing Specificity, *Cell,* **154,** 1380–1389, http://www.sciencedirect.com/science/article/pii/S0092867413010155.

137. Cho, S.W., Kim, S., Kim, Y., Kweon, J., Kim, H.S., Bae, S. and Kim, J.-S. (2014) Analysis of off-target effects of CRISPR/Cas-derived RNA-guided endonucleases and nickases, *Genome Res.,* **24,** 132–141, http://genome.cshlp.org/content/24/1/132.full.

138. Slaymaker, I.M., Gao, L., Zetsche, B., Scott, D.A., Yan, W.X. and Zhang, F. (2016) Rationally engineered Cas9 nucleases with improved specificity, *Science (New York, N.Y.),* **351,** 84–88.

139. Casini, A., Olivieri, M., Petris, G., Montagna, C., Reginato, G., Maule, G., Lorenzin, F., Prandi, D., Romanel, A. and Demichelis, F. *et al.* (2018) A highly specific SpCas9 variant is identified by *in vivo* screening in yeast, *nbt,* **36,** 265–271, https://www.nature.com/articles/nbt.4066.pdf.

140. Esvelt, K.M., Mali, P., Braff, J.L., Moosburner, M., Yaung, S.J. and Church, G.M. (2013) Orthogonal Cas9 proteins for RNA-guided gene regulation and editing, *Nature methods,* **10,** 1116–1121.

141. Qi, L.S., Larson, M.H., Gilbert, L.A., Doudna, J.A., Weissman, J.S., Arkin, A.P. and Lim, W.A. (2013) Repurposing CRISPR as an RNA-Guided Platform for Sequence-Specific Control of Gene Expression, *Cell,* **152,** 1173–1183, http://www.sciencedirect.com/science/article/pii/S0092867413002110.

142. Kim, Y.B., Komor, A.C., Levy, J.M., Packer, M.S., Zhao, K.T. and Liu, D.R. (2017) Increasing the genome-targeting scope and precision of base editing with engineered Cas9-cytidine deaminase fusions, *Nat Biotechnol,* **35,** 371–376, https://www.nature.com/articles/nbt.3803.pdf.

143. Komor, A.C., Kim, Y.B., Packer, M.S., Zuris, J.A. and Liu, D.R. (2016) Programmable editing of a target base in genomic DNA without double-stranded DNA cleavage, *Nature,* **533,** 420–424, https://www.nature.com/articles/nature17946.pdf.

144. Landrum, M.J., Lee, J.M., Benson, M., Brown, G., Chao, C., Chitipiralla, S., Gu, B., Hart, J., Hoffman, D. and Hoover, J. *et al.* (2016) ClinVar: public archive of interpretations of clinically relevant variants, *Nucleic acids research,* **44,** D862-8.

145. Hilton, I.B., D'Ippolito, A.M., Vockley, C.M., Thakore, P.I., Crawford, G.E., Reddy, T.E. and Gersbach, C.A. (2015) Epigenome editing by a CRISPR-Cas9-based acetyltransferase activates genes from promoters and enhancers, *nbt,* **33,** 510–517, https://www.nature.com/articles/nbt.3199.pdf.

146. Vojta, A., Dobrinić, P., Tadić, V., Bočkor, L., Korać, P., Julg, B., Klasić, M. and Zoldoš, V. (2016) Repurposing the CRISPR-Cas9 system for targeted DNA methylation, *Nucleic Acids Res,* **44,** 5615–5628, https://academic.oup.com/nar/article-pdf/44/12/5615/17436386/gkw159.pdf.

147. Chen, B., Gilbert, L.A., Cimini, B.A., Schnitzbauer, J., Zhang, W., Li, G.-W., Park, J., Blackburn, E.H., Weissman, J.S. and Qi, L.S. *et al.* (2013) Dynamic Imaging of Genomic Loci in Living Human Cells by an Optimized CRISPR/Cas System, *Cell,* **155,** 1479–1491, http://www.sciencedirect.com/science/article/pii/S0092867413015316.

148. Hartenian, E. and Doench, J.G. (2015) Genetic screens and functional genomics using CRISPR/Cas9 technology, *The FEBS Journal,* **282,** 1383–1393, https://febs.onlinelibrary.wiley.com/doi/full/10.1111/febs.13248.

149. Doench, J.G., Fusi, N., Sullender, M., Hegde, M., Vaimberg, E.W., Donovan, K.F., Smith, I., Tothova, Z., Wilen, C. and Orchard, R. *et al.* (2016) Optimized sgRNA design to maximize activity and minimize off-target effects of CRISPR-Cas9, *nbt,* **34,** 184–191, https://www.nature.com/articles/nbt.3437.pdf.

150. Koike-Yusa, H., Li, Y., Tan, E.-P., Velasco-Herrera, M.D.C. and Yusa, K. (2014) Genome-wide recessive genetic screening in mammalian cells with a lentiviral CRISPR-guide RNA library, *nbt,* **32,** 267–273, https://www.nature.com/articles/nbt.2800.pdf.

151. Vanegas, K.G., Lehka, B.J. and Mortensen, U.H. (2017) SWITCH: a dynamic CRISPR tool for genome engineering and metabolic pathway control for cell factory construction in Saccharomyces cerevisiae, *Microb Cell Fact,* **16,** 1–12, https://microbialcellfactories.biomedcentral.com/track/pdf/10.1186/s12934-017-0632-x.

152. Jensen, N.B., Strucko, T., Kildegaard, K.R., David, F., Maury, J., Mortensen, U.H., Forster, J., Nielsen, J. and Borodina, I. (2014) EasyClone: method for iterative chromosomal integration of multiple genes Saccharomyces cerevisiae, *FEMS Yeast Res,* **14,** 238–248, https://academic.oup.com/femsyr/article-pdf/14/2/238/26050600/14-2-238.pdf.

153. Church, G.M., Elowitz, M.B., Smolke, C.D., Voigt, C.A. and Weiss, R. (2014) Realizing the potential of synthetic biology, *Nat Rev Mol Cell Biol,* **15,** 289–294, https://www.nature.com/articles/nrm3767.pdf.

154. Gander, M.W., Vrana, J.D., Voje, W.E., Carothers, J.M. and Klavins, E. Digital logic circuits in yeast with CRISPR-dCas9 NOR gates, *Nat Commun,* **8,** 1–11, https://www.nature.com/articles/ncomms15459.pdf.

155. Lee, T.C. and Ziff, E.B. (1999) Mxi1 Is a Repressor of the c-myc Promoter and Reverses Activation by USF, *J. Biol. Chem.,* **274,** 595–606, http://www.jbc.org/content/274/2/595.full.

156. Schreiber-Agus, N., Chin, L., Chen, K., Torres, R., Rao, G., Guida, P., Skoultchi, A.I. and DePinho, R.A. (1995) An amino-terminal domain of Mxi1 mediates anti-myc oncogenic activity and interacts with a homolog of the Yeast Transcriptional Repressor SIN3, *Cell,* **80,** 777–786, http://www.sciencedirect.com/science/article/pii/0092867495903569.

157. Grzeschik, J., Hinz, S.C., Könning, D., Pirzer, T., Becker, S., Zielonka, S. and Kolmar, H. (2017) A simplified procedure for antibody engineering by yeast surface display: Coupling display levels and target binding by ribosomal skipping, *Biotechnology journal,* **12.**

158. Gao, Y. and Zhao, Y. (2014) Self-processing of ribozyme-flanked RNAs into guide RNAs in vitro and in vivo for CRISPR-mediated genome editing, *Journal of integrative plant biology,* **56,** 343–349.

159. DiCarlo, J.E., Norville, J.E., Mali, P., Rios, X., Aach, J. and Church, G.M. (2013) Genome engineering in Saccharomyces cerevisiae using CRISPR-Cas systems, *Nucleic Acids Res,* **41,** 4336–4343, https://academic.oup.com/nar/article-pdf/41/7/4336/25342046/gkt135.pdf.

160. Bessa, D., Pereira, F., Moreira, R., Johansson, B. and Queirós, O. (2012) Improved gap repair cloning in yeast: treatment of the gapped vector with Taq DNA polymerase avoids vector self-ligation, *Yeast (Chichester, England),* **29,** 419–423.

161. Mullis, K., Faloona, F., Scharf, S., Saiki, R., Horn, G. and Erlich, H. (1986) Specific enzymatic amplification of DNA in vitro: the polymerase chain reaction, *Cold Spring Harbor symposia on quantitative biology,* **51 Pt 1,** 263–273.

162. New England Biolabs Tm calculator. New England Biolabs.

163. BD Biosciences (2014) BD Accuri™ C6 Flow Cytometer: Optical Filter Guide.

164. Block, H., Maertens, B., Spriestersbach, A., Brinker, N., Kubicek, J., Fabis, R., Labahn, J. and Schäfer, F. (2009) Chapter 27 Immobilized-Metal Affinity Chromatography (IMAC). In Burgess, R. (ed.), *Guide to protein purification.* Elsevier, Amsterdam. Vol. 463, pp. 439–473.

165. Sambrook, J. and Russell, D.W. (2006) SDS-Polyacrylamide Gel Electrophoresis of Proteins, *CSH protocols,* **2006.**

166. Miller, N.J. and Rice-Evans, C.A. (1997) Factors influencing the antioxidant activity determined by the ABTS.+ radical cation assay, *Free radical research,* **26,** 195–199.

167. Re, R., Pellegrini, N., Proteggente, A., Pannala, A., Yang, M. and Rice-Evans, C. (1999) Antioxidant activity applying an improved ABTS radical cation decolorization assay, *Free Radical Biology and Medicine,* **26,** 1231–1237, http://www.sciencedirect.com/science/article/pii/S0891584998003153.

168. Baron, A.J., Stevens, C., Wilmot, C., Seneviratne, K.D., Blakeley, V., Dooley, D.M., Phillips, S.E., Knowles, P.F. and McPherson, M.J. (1994) Structure and mechanism of galactose oxidase. The free radical site, *The Journal of biological chemistry,* **269,** 25095–25105.

169. Hirao, I., Spingola, M., Peabody, D. and Ellington, A.D. (1998) The limits of specificity: An experimental analysis with RNA aptamers to MS2 coat protein variants, *Molecular Diversity,* **4,** 75–89, https://doi.org/10.1023/A:1026401917416.

170. Becskei, A., Kaufmann, B.B. and van Oudenaarden, A. (2005) Contributions of low molecule number and chromosomal positioning to stochastic gene expression, *Nat Genet,* **37,** 937–944, https://www.nature.com/articles/ng1616.pdf.

171. (1996) Plasmid stability in recombinant Saccharomyces cerevisiae, *Biotechnology Advances,* **14,** 401–435.

172. Özaydın, B., Burd, H., Lee, T.S. and Keasling, J.D. (2013) Carotenoid-based phenotypic screen of the yeast deletion collection reveals new genes with roles in isoprenoid production, *Metabolic Engineering,* **15,** 174–183, http://www.sciencedirect.com/science/article/pii/S109671761200081X.

173. David, F. and Siewers, V. (2015) Advances in yeast genome engineering, *FEMS Yeast Res,* **15,** 1–14, https://academic.oup.com/femsyr/article-pdf/15/1/1/10745856/12200.pdf.

174. Sikorski, R.S. and Hieter, P. (1989) A system of shuttle vectors and yeast host strains designed for efficient manipulation of DNA in Saccharomyces cerevisiae, *Genetics,* **122,** 19–27.

175. Taxis, C. and Knop, M. (2006) System of centromeric, episomal, and integrative vectors based on drug resistance markers for Saccharomyces cerevisiae, *BioTechniques,* **40,** 73–78.

176. Hofmann, A. (2016) Towards genetic circuits in the yeast S. cerevisiae applying the CRISPR/dCas9, Darmstadt.

177. Rose, M. and Winston, F. (1984) Identification of a Ty insertion within the coding sequence of the S. cerevisiae URA3 gene, *Molecular and General Genetics MGG,* **193,** 557–560, https://doi.org/10.1007/BF00382100.

178. Karim, A.S., Curran, K.A. and Alper, H.S. (2013) Characterization of plasmid burden and copy number in Saccharomyces cerevisiae for optimization of metabolic engineering applications, *FEMS yeast research,* **13**.

179. Chao, J.A., Patskovsky, Y., Almo, S.C. and Singer, R.H. (2008) Structural basis for the coevolution of a viral RNA–protein complex, *Nat Struct Mol Biol,* **15,** 103–105, https://www.nature.com/articles/nsmb1327.pdf.

180. Nair, S.C., Toran, E.J., Rimerman, R.A., Hjermstad, S., Smithgall, T.E. and Smith, D.F. (1996) A pathway of multi-chaperone interactions common to diverse regulatory proteins: estrogen receptor, Fes tyrosine kinase, heat shock transcription factor Hsf1, and the aryl hydrocarbon receptor, *Cell Stress & Chaperones,* **1,** 237–250.

181. Knoblauch, R. and Garabedian, M.J. (1999) Role for Hsp90-Associated Cochaperone p23 in Estrogen Receptor Signal Transduction, *Molecular and Cellular Biology,* **19,** 3748–3759.

182. Luke, G.A., Escuin, H., Felipe, P. de and Ryan, M.D. (2009) 2A to the Fore – Research, Technology and Applications, *Biotechnology and Genetic Engineering Reviews,* **26,** 223–260.

183. Ryan, M.D., King, A.M. and Thomas, G.P. (1991) Cleavage of foot-and-mouth disease virus polyprotein is mediated by residues located within a 19 amino acid sequence, *The Journal of general virology,* **72 (Pt 11),** 2727–2732.

184. Chng, J., Wang, T., Nian, R., Lau, A., Hoi, K.M., Ho, S.C.L., Gagnon, P., Bi, X. and Yang, Y. (2015) Cleavage efficient 2A peptides for high level monoclonal antibody expression in CHO cells, *mAbs,* **7,** 403–412.

185. Rakestraw, J.A., Sazinsky, S.L., Piatesi, A., Antipov, E. and Wittrup, K.D. (2009) Directed evolution of a secretory leader for the improved expression of heterologous proteins and full-length antibodies in Saccharomyces cerevisiae, *Biotechnology and bioengineering,* **103,** 1192–1201.

186. Ito, N., Phillips, S.E.V., Stevens, C., Ogel, Z.B., McPherson, M.J., Keen, J.N., Yadav, K.D.S. and Knowles, P.F. (1991) Novel thioether bond revealed by a 1.7 Å crystal structure of galactose oxidase, *Nature,* **350,** 87–90, https://www.nature.com/articles/350087a0.pdf.

187. Spadiut, O., Olsson, L. and Brumer, H. (2010) A comparative summary of expression systems for the recombinant production of galactose oxidase, *Microb Cell Fact,* **9,** 1–13, https://microbialcellfactories.biomedcentral.com/track/pdf/10.1186/1475-2859-9-68.

188. Könning, D., Rhiel, L., Empting, M., Grzeschik, J., Sellmann, C., Schröter, C., Zielonka, S., Dickgießer, S., Pirzer, T. and Yanakieva, D. *et al.* Semi-synthetic vNAR libraries screened against therapeutic antibodies primarily deliver anti-idiotypic binders, *Sci Rep,* **7,** 1–13, https://www.nature.com/articles/s41598-017-10513-9.pdf.

189. Ugolini, S. and Bruschi, C.V. (1996) The red/white colony color assay in the yeast Saccharomyces cerevisiae: epistatic growth advantage of white ade8-18, ade2 cells over red ade2 cells, *Current Genetics,* **30,** 485–492, https://doi.org/10.1007/s002940050160.

190. Kokina, A., Kibilds, J. and Liepins, J. (2014) Adenine auxotrophy--be aware: some effects of adenine auxotrophy in Saccharomyces cerevisiae strain W303-1A, *FEMS yeast research,* **14,** 697–707.

191. Gao, C.Y. and Pinkham, J.L. (2000) Tightly regulated, beta-estradiol dose-dependent expression system for yeast, *BioTechniques,* **29,** 1226–1231.

192. Hamblen, E.L., Cronin, M.T.D. and Schultz, T.W. (2003) Estrogenicity and acute toxicity of selected anilines using a recombinant yeast assay, *Chemosphere,* **52,** 1173–1181, http://www.sciencedirect.com/science/article/pii/S0045653503003333.

193. Chen, M.-Y., Ike, M. and Fujita, M. (2002) Acute toxicity, mutagenicity, and estrogenicity of bisphenol-A and other bisphenols, *Environmental Toxicology,* **17,** 80–86, https://onlinelibrary.wiley.com/doi/pdf/10.1002/tox.10035.

194. Piston, D., Patterson, G., Lippincott-Schwartz, J., Claxton, N. and Davidson, M. Introduction to Fluorescent Proteins.

195. Zsebo, K.M., Lu, H.S., Fieschko, J.C., Goldstein, L., Davis, J., Duker, K., Suggs, S.V., Lai, P.H. and Bitter, G.A. (1986) Protein secretion from Saccharomyces cerevisiae directed by the prepro-alpha-factor leader region, *The Journal of biological chemistry,* **261,** 5858–5865.

196. evrogen Green fluorescent protein TurboGFP.

197. Wolynes, P.G., Onuchic, J.N. and Thirumalai, D. (1995) Navigating the folding routes, *Science (New York, N.Y.),* **267,** 1619–1620.

198.   Falk, J. Stochastische Modelle und Umgebungseffekte im Kontext der Synthetischen Biologie. Technische Universität, Darmstadt.

199.   Gillespie, D.T. (1977) Exact stochastic simulation of coupled chemical reactions, *J. Phys. Chem.,* **81,** 2340–2361.

200.   RAMSEY, S., ORRELL, D. and BOLOURI, H. (2005) DIZZY: STOCHASTIC SIMULATION OF LARGE-SCALE GENETIC REGULATORY NETWORKS, *J. Bioinform. Comput. Biol.,* **03,** 415–436.

201.   Crane, M.M., Clark, I.B.N., Bakker, E., Smith, S. and Swain, P.S. (2014) A Microfluidic System for Studying Ageing and Dynamic Single-Cell Responses in Budding Yeast, *PLOS ONE,* **9,** e100042, https://journals.plos.org/plosone/article/file?id=10.1371/journal.pone.0100042&type=printable.

202.   Demir, O. and Aksan Kurnaz, I. (2006) An integrated model of glucose and galactose metabolism regulated by the GAL genetic switch, *Computational Biology and Chemistry,* **30,** 179–192, http://www.sciencedirect.com/science/article/pii/S1476927106000120.

203.   Platt, A. and Reece, R.J. (1998) The yeast galactose genetic switch is mediated by the formation of a Gal4p-Gal80p-Gal3p complex, *The EMBO Journal,* **17,** 4086–4091.

204.   Jinek, M., East, A., Cheng, A., Lin, S., Ma, E. and Doudna, J. (2013) RNA-programmed genome editing in human cells, *eLife,* **2,** e00471.

205.   Evdokimov, A.G., Pokross, M.E., Egorov, N.S., Zaraisky, A.G., Yampolsky, I.V., Merzlyak, E.M., Shkoporov, A.N., Sander, I., Lukyanov, K.A. and Chudakov, D.M. (2006) Structural basis for the fast maturation of Arthropoda green fluorescent protein, *EMBO reports,* **7,** 1006–1012.

206.   Hackett, E.A., Esch, R.K., Maleri, S. and Errede, B. (2006) A family of destabilized cyan fluorescent proteins as transcriptional reporters in S. cerevisiae, *Yeast,* **23,** 333–349.

207.   Li, X., Zhao, X., Fang, Y., Jiang, X., Duong, T., Fan, C., Huang, C.C. and Kain, S.R. (1998) Generation of destabilized green fluorescent protein as a transcription reporter, *The Journal of biological chemistry,* **273,** 34970–34975.

208.   He, Y., Zhang, T., Yang, N., Xu, M., Yan, L., Wang, L., Wang, R. and Zhao, Y. (2017) Self-cleaving ribozymes enable the production of guide RNAs from unlimited choices of promoters for CRISPR/Cas9 mediated genome editing, *Journal of genetics and genomics = Yi chuan xue bao,* **44,** 469–472.

209.   Zhou, H., Huang, C. and Xia, X.G. (2008) A tightly regulated Pol III promoter for synthesis of miRNA genes in tandem, *Biochimica et biophysica acta,* **1779,** 773–779.

210.   Ohkawa, J. and Taira, K. (2000) Control of the functional activity of an antisense RNA by a tetracycline-responsive derivative of the human U6 snRNA promoter, *Human gene therapy,* **11,** 577–585.

211.   Lin, X., Yang, J., Chen, J., Gunasekera, A., Fesik, S.W. and Shen, Y. (2004) Development of a tightly regulated U6 promoter for shRNA expression, *FEBS letters,* **577,** 376–380.

212.   Sims, R.J., Mandal, S.S. and Reinberg, D. (2004) Recent highlights of RNA-polymerase-II-mediated transcription, *Current Opinion in Cell Biology,* **16,** 263–271, http://www.sciencedirect.com/science/article/pii/S0955067404000559.

213. Nakano, S., Chadalavada, D.M. and Bevilacqua, P.C. (2000) General acid-base catalysis in the mechanism of a hepatitis delta virus ribozyme, *Science (New York, N.Y.),* **287,** 1493–1497.

214. Scott, W.G., Murray, J.B., Arnold, J.R., Stoddard, B.L. and Klug, A. (1996) Capturing the structure of a catalytic RNA intermediate: the hammerhead ribozyme, *Science (New York, N.Y.),* **274,** 2065–2069.

215. Pley, H.W., Flaherty, K.M. and McKay, D.B. (1994) Three-dimensional structure of a hammerhead ribozyme, *Nature,* **372,** 68–74.

216. Ferré-D'Amaré, A.R., Zhou, K. and Doudna, J.A. (1998) Crystal structure of a hepatitis delta virus ribozyme, *Nature,* **395,** 567–574.

217. Dabrowski, M., Bukowy-Bieryllo, Z. and Zietkiewicz, E. (2015) Translational readthrough potential of natural termination codons in eucaryotes--The impact of RNA sequence, *RNA biology,* **12,** 950–958.

218. Hopert, A., Uphoff, C.C., Wirth, M., Hauser, H. and Drexler, H.G. (1993) Specifity and sensitivity of polymerase chain reaction (PCR) in comparison with other methods for the detection of mycoplasma contamination in cell lines, *Journal of Immunological Methods,* **164,** 91–100.

219. Nissim, L., Perli, S.D., Fridkin, A., Perez-Pinera, P. and Lu, T.K. (2014) Multiplexed and Programmable Regulation of Gene Networks with an Integrated RNA and CRISPR/Cas Toolkit in Human Cells, *Molecular Cell,* **54,** 698–710, http://www.sciencedirect.com/science/article/pii/S1097276514003554.

220. Vigouroux, A., Oldewurtel, E., Cui, L., van Teeffelen, S. and Bikard, D. (2017) Engineered CRISPR-Cas9 system enables noiseless, fine-tuned and multiplexed repression of bacterial genes.

221. Pfaffl, M.W. (2001) A new mathematical model for relative quantification in real-time RT-PCR, *Nucleic acids research,* **29,** e45.

222. Avendaño, M.S., Leidy, C. and Pedraza, J.M. Tuning the range and stability of multiple phenotypic states with coupled positive–negative feedback loops, *Nat Commun,* **4,** 1–8, https://www.nature.com/articles/ncomms3605.pdf.

223. Pigolotti, S., Krishna, S. and Jensen, M.H. (2007) Oscillation patterns in negative feedback loops, *Proceedings of the National Academy of Sciences of the United States of America,* **104,** 6533–6537.

224. Tsai, T.Y.-C., Choi, Y.S., Ma, W., Pomerening, J.R., Tang, C. and Ferrell, J.E. (2008) Robust, tunable biological oscillations from interlinked positive and negative feedback loops, *Science (New York, N.Y.),* **321,** 126–129.

8. Register

8.1. List of tables

8.2. List of figures

8.3. List of Abbreviations

Table 37 List of abbreviations used within the scope of this thesis.

Abbreviation	Long term
A	
aa	amino acid
AD	activation domain
AND	AND gate with Venus as reporter gene
AND, GO	AND gate with GOase and tGFP as reporter genes
AND, vNAR	AND gate with vNAR and tGFP as reporter genes
Amp	ampicillin
Aq	aqueous solution
ARS	autonomously replicating sequence
B	
bp	base pairs
C	
°C	Degree
Cas	CRISPR-associated
Cas9	CRISPR-associated protein 9
CEN	yeast centromere
CHO cells	Chinese hamster ovary cells
CRISPR	clustered regularly interspaced short palindromic repeats
CRISPRa	CRISPR activation
CRISPRi	CRISPR interference
cPCR	colony PCR
crRNA	CRISPR RNA
cTF	chimeric transcription factor
D	
dbd	DNA binding domain
dCas9	catalytically dead Cas9 mutant
dc-VP64	strains containing dCas9 fused to VP64
ddH2O	distilled water
DMSO	dimethyl sulfoxide
DNA	deoxyribonucleic acid
dNTP	desoxiribonucleotide phosphate
dox	doxycycline
DS	double strand
DSB	double strand break
DTT	dithiotreitol
dYT	double concentrated Yeast Tryptone medium
E	
E. coli	*Escherichia Coli*
e.g.	*exempli gratia*
ES	β-estradiol
eSpCas9	"enhanced specificity" SpCas9

ER	human estrogen receptor
evoCas9	evolved Cas9
F	
FACS	fluorescence-activated cell sorting
G	
g	gramm
Gal	galactose
Glu	glucose
GOase	galactose oxidase
GOI	gene of interest
gRNA	guide RNA
H	
HCl	hydrochloric acid
HDR	homology-directed repair
His	histidine
HR	homologous recombination
hTF	heterologous transcription factor
L	
L	liter
LD	loading dye
L/Leu	leucine
lexA	*lexA* operator
M	
μg	microgramm
μL	microliter
μM	micromolar
M	Molar
mg	milligramm
mL	milliliter
mM	millimolar
N	
NaCl	sodium chloride
NC	negative control
NHEJ	non-homologous end-joining
nm	nanometer
nM	nanomolar
nTF	natural transcription factor
O	
OD	optical density
ori	origin of replication
P	
P	promoter
PAM	protospacer adjacent motif

|	
PBS	phosphate buffered saline
PC	positive control
PCR	polymerase chain reaction
POI	protein of interest
R	
RNA	ribonucleic acid
Rpm	rounds per minute
RT PCR	roof tile PCR
rtTA	reverse tetracycline-controlled transactivator
S	
S. cerevisiae	*Saccharomyces cerevisiae*
scRNA	scaffold RNA
sgRNA	single guide RNA
Ssw	single switch
SpCas9	*Streptococcus pyogenes* Cas9
SynBio	synthetic biology
T	
TALE	Transcription Activator-like Effector
TALEN	Transcription Activator-like Effector Nucleases
tc	tetracycline
TetR	Tet repressor
tetO	tetracycline-controlled operator
TF	transcription factor
tGFP	turbo GFP
tracrRNA	trans-acting RNA
TRIS	tris(hydroxymethyl)aminomethane
tTA	tetracycline-controlled transactivator
V	
vNAR	variable domain of new antigen receptors
v/v	volume per volume
W	
W/Trp	tryptophan
w/v	weight per volume
Z	
ZF	Zinc-finger
ZFN	Zinc-finger nucleases

9.1. Supplementary figures
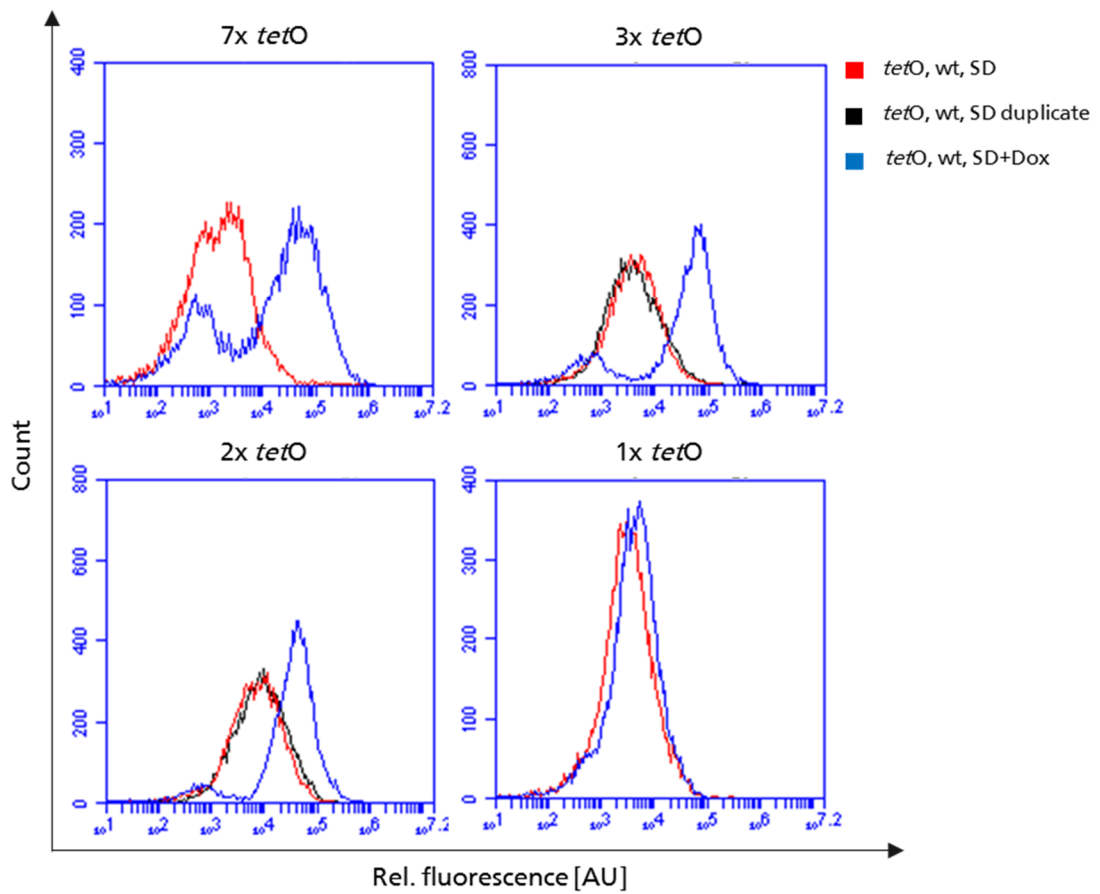
Figure 50 Histograms for doxycycline induction for the different *tet*O clones.

The histograms show Venus fluorescence after induction with 100 µg/mL dox. The fluorescence strongly depends on the *tet*O copy number. The fluorescence was measured with the 488 nm laser of *BD* Accuri™ C6 [533/30].
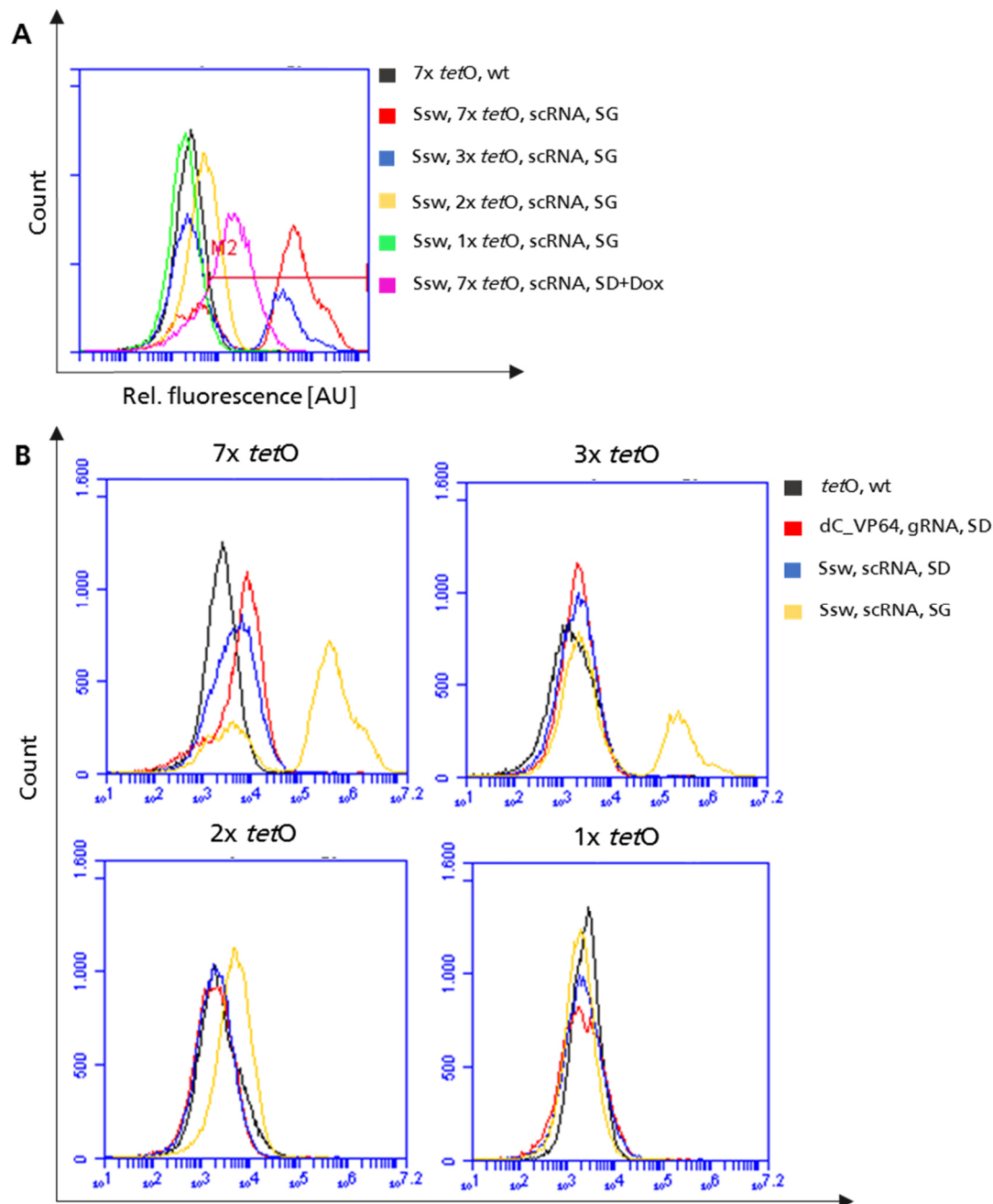
Figure 51 Histograms for galactose induction for the different Ssw, *tet*O clones.

The histograms show Venus fluorescence after induction with galactose or 100 µg/mL dox. The fluorescence strongly depends on the *tet*O copy number. The fluorescence was measured with the 488 nm laser of *BD* Accuri™ C6 [533/30].
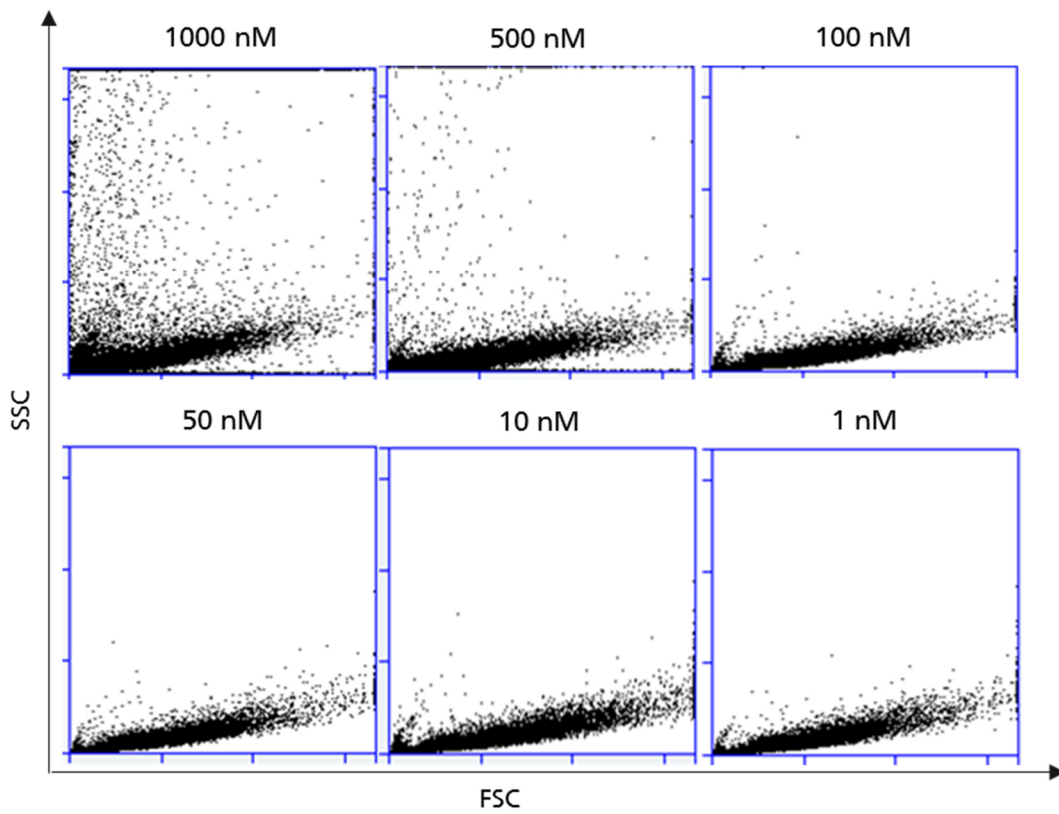
Figure 52 ES concentration-dependent cell distribution.

Single reporter AND gate, 7x *tet*O cells were grown in SD-ura and different ES concentrations. Depending on the ES concentration the cell distribution changed. Hence, cell distribution directly correlates with the amount of ES.
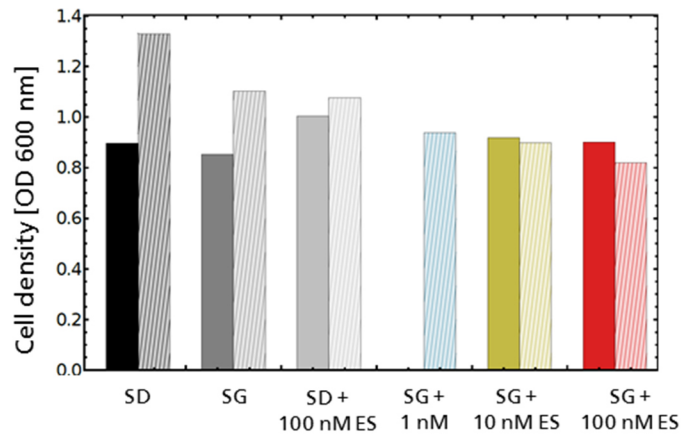
Figure 53 Influence of induction of reporter gene expression on cell growth.

Cells of the strains AND, 7x *tet*O (solid) and AND, GO (hatched) were grown in different media. Therefore, cells were inoculated to an OD_{600} of 1 in SD-ura medium and grown over night in SD-ura medium, SG-ura medium or induction medium containing SG-ura and 1 nM, 10 nM or 100 nM ES, respectively. Cell growth was determined photometrically. For the AND switch no significant influence in growth could be detected, whereas with increasing amount of ES the cell density of the AND, GO switch decreased slightly.
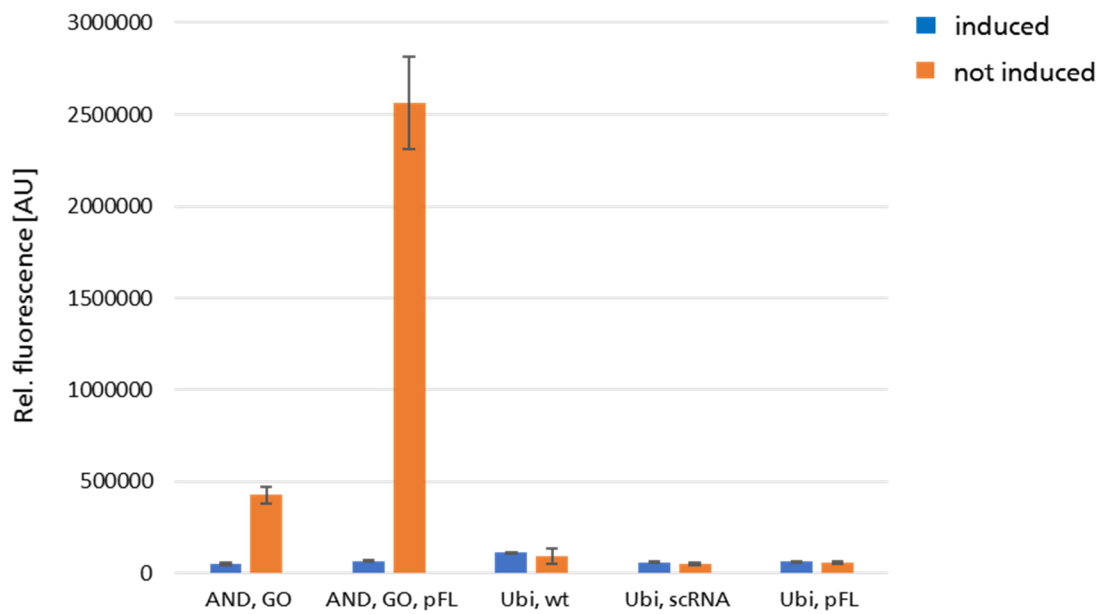
Figure 54 Induction experiment for the positive Ubi-tGFP feedback loop.

For the experiment cells of the AND, GO, AND, GO, pFL, Ubi wt (not containing a scRNA), Ubi pJZC588 and Ubi pJZC588 + pAH019 were used. As negative control cells were grown in SD. As positive control cells were grown in SG + 10 nM ES for 48 h. Error bars indicate the standard deviation of the biological triplicates.
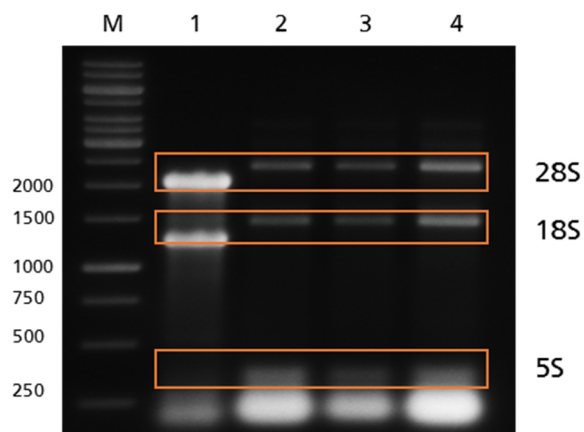
| No.	Properties
1	NC
2	scRNA
3	HH-scRNA-HDV
4	lexA_HH-scRNA-HDV
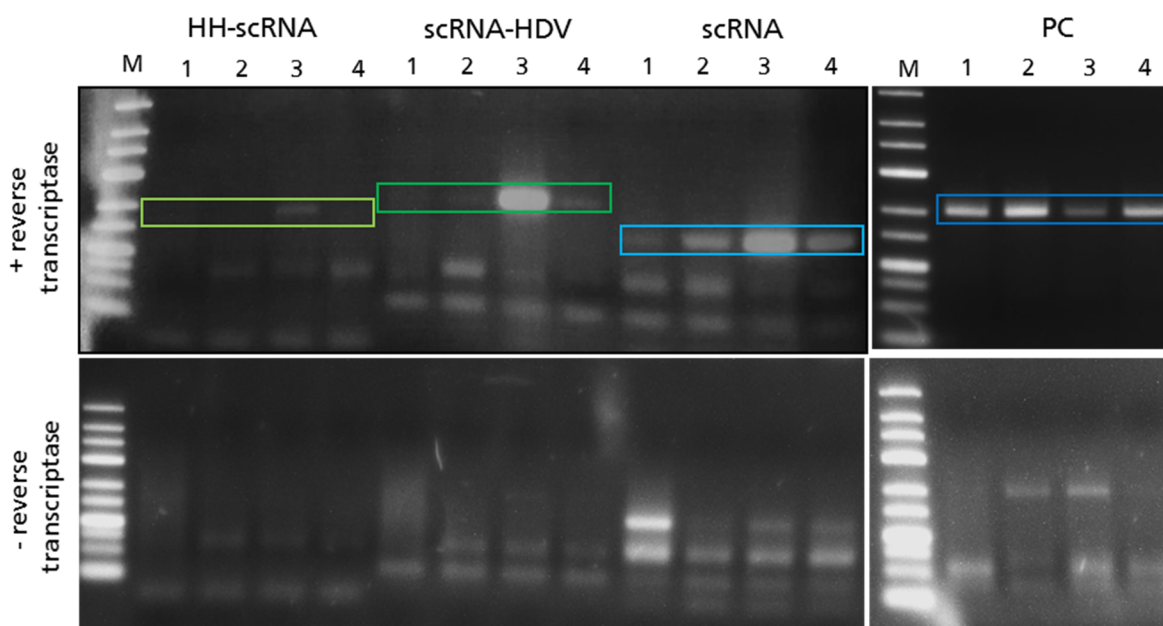
Figure 55 RNA extraction and cDNA analysis for the HH-scRNA-HDV construct, repetition of the experiment.

(A) The planned PCR strategy, in which three different fragments should be tested. (B) Isolated RNA applied on a 1 % agarose gel. As marker, the 1kb DNA-ladder (*vwr*) was used. (C) PCR of the reverse transcribed cDNA showing which fragment could be amplified. On the top, cDNA was reverse transcribed using the M-MuLV reverse transcriptase (*New England Biolabs*). On the bottom the control is shown, where no -MuLV reverse transcriptase was added. Samples were applied to a 3 % agarose gel. As marker, the Ultra Low Range DNA-Leiter II, peqGOLD (*vwr*) was used.
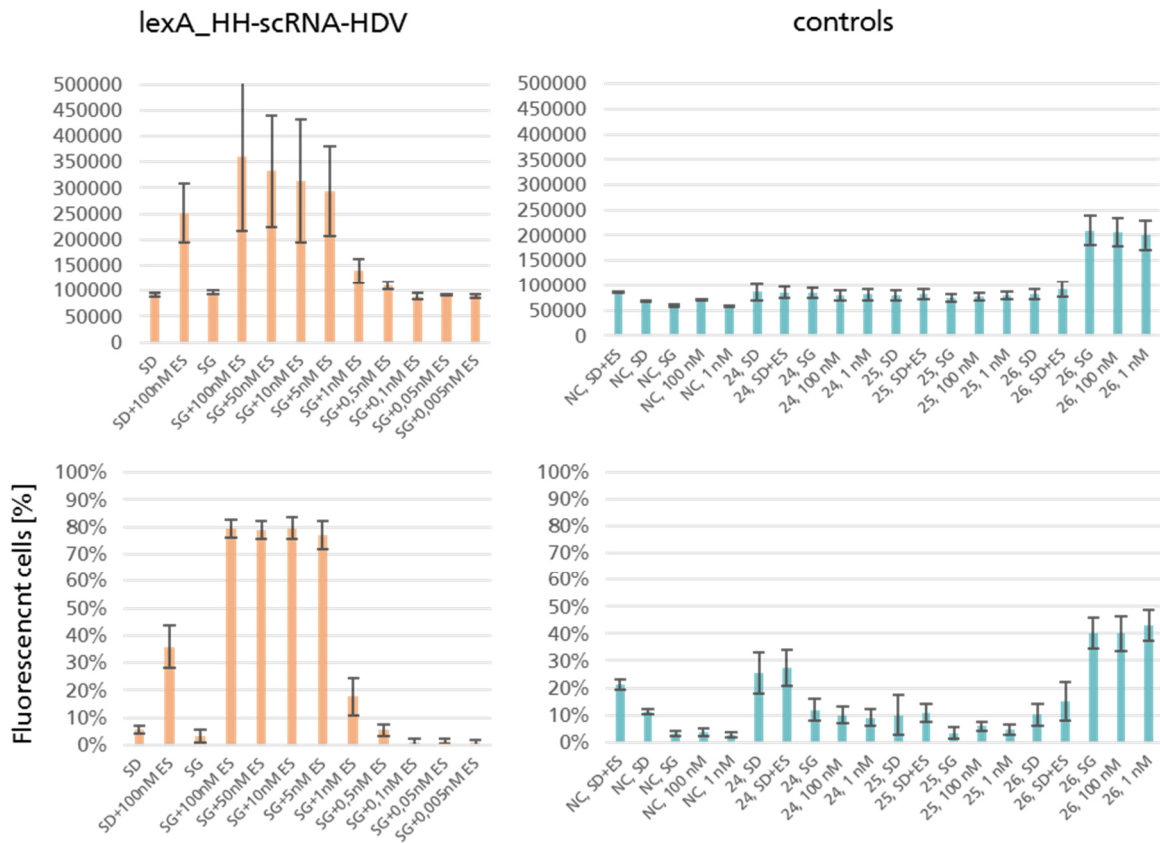
Figure 56 ES dose-dependent induction experiment for AND, scRNA gate and controls containing pAH024-26.

For the experiment cells of AND, scRNA, Ssw, 7x*tet*O, PAH024-26 and NC were used. Cells were grown in SD, SD + 100 nM ES and SG for controls. The samples were grown in SG plus decreasing concentrations of ES. Error bars indicate the standard deviation of the biological triplicates.

9.2. Danksagung

An dieser Stelle möchte ich allen danken, ohne deren Unterstützung diese Doktorarbeit nicht zustande gekommen wäre:

Zunächst danke ich **Herrn Prof. Dr. Harald Kolmar** für die Möglichkeit zur Anfertigung dieser Arbeit in seiner Arbeitsgruppe und die Bearbeitung dieses interessanten Themas. Außerdem danke ich ihm für das stets entgegengebrachte Vertrauen und die Möglichkeiten immer wieder Neues zu lernen. In besonderem Maße danke ich ihm für die Unterstützung und Freistellung für mein Fachpraktikum in den USA.

Frau Prof. Dr. Beatrix Süß danke ich für die Übernahme des Korreferates, sowie für die Möglichkeit in ihrer Arbeitsgruppe einen Teil der Versuche durchzuführen. Außerdem danke ich Frau Süß für die vielen persönlichen und fachlichen Gespräche, die mich stets motivierten und neue Wege und Ideen aufbrachten.

Herrn Prof. Dr. Siegfried Neumann und **Herrn Prof. Dr. Johannes Kabisch** danke ich für die Übernahme der Rolle als erster und zweiter Fachprüfer. Auch danke ich Ihnen für die fachlichen Gespräche während der letzten drei Jahre.

Herrn Dr. Andreas Christmann möchte ich für seine Unterstützung und Zeit danken, um mit mir über Ergebnisse und das weitere Vorgehen zu sprechen. Außerdem danke ich ihm für seine professionelle Hilfe am FACS.

Lara Neureiter möchte ich herzlichst für ihr offenes Ohr und die netten Gespräche beim Mittagessen danken, die den ein oder anderen Arbeitstag bereicherten. Außerdem danke ich ihr sehr für die gemeinsame, aufregende USA Rundreise.

Dominic Happel danke ich für seine unermüdliche Hilfe und die Arbeit, die er investiert hat, um die Fertigstellung des gemeinsamen Papers auch in meiner Abwesenheit zu ermöglichen.

Dr. Johannes Falk möchte ich herzlichst für die gemeinsamen Versuche, die vielen inspirierenden Gespräche und die Nachhilfe in punkto Modeling danken. Ebenso möchte ich **Tim Prangemeier** für die inspirierende Zusammenarbeit danken.

Jan Habermann danke ich für seine Hilfe am FACS, auf die ich stets zählen konnte.

Bei **Dr. Brigitte Held** möchte ich mich ganz besonders für die vielen aufbauenden Worte und die Unterstützung in allen Belangen von CompuGene bedanken.

Aileen Ebenig möchte ich für die zahlreichen, interessanten morgendlichen Gespräche danken, sowie für das Korrekturlesen dieser Arbeit.

Dr. Marc Vogel danke ich für die Hiflsbereitschaft, sowie für die Einweisung in verschiedene RNA-basierte Techniken.

Allen nicht namentlich genannten ehemaligen und aktuellen Mitgliedern der AG Kolmar möchte ich für die gemeinsame Zeit und die Unterstützung danken. Ebenso danke ich allen nicht namentlich genannten ehemaligen und aktuellen Mitgliedern des LOEWE Schwerpunktes CompuGene. Den nicht namentlich genannten Mitgliedern, welche ebenfalls Anteil am Gelingen dieser Arbeit tragen, gilt mein besonderer Dank.

Der Arbeitsgruppe Süß (Biologie) danke ich für die gemeinsamen Mittagessen, in denen immer viel gelacht wurde, sowie für die Erlaubnis zur Nutzung ihrer Geräte.

Sehr dankbar bin ich für die mentale Unterstützung meines Freundes **Emir Ahmetbegovic**, die mir trotz vieler Rückschläge immer wieder die Kraft gab weiter zu machen. Ebenfalls danke ich ihm für die intensive Korrektur dieser Arbeit.

Lisa Hofmann, **Niclas Fester** und **Johanna Borchert** möchte ich herzlichst für die Unterstützung bei der Korrektur dieser Arbeit danken.

Ein besonderer Dank geht an meine Eltern, **Heike und Bernd**, die mich bereits mein ganzes Leben in all meinen Entscheidungen unterstützt und so diese Doktorarbeit erst ermöglicht haben. Danke für eure Geduld und euren Glauben an mich! Danke auch an meine kleine Schwester, für deine Unterstützung, auf die man sich immer verlassen kann!

9.3. *Curriculum Vitae*

Personal infromation

Name:	Anja Hofmann
Date of birth:	15.09.1992 in Offenbach am Main
Adress:	Gründenseestraße 31, 60386 Frankfurt am Main, Germany

Experience

10/2016 – 10/2019	Doctoral candidate at Technische Universität Darmstadt
	Working Group Kolmar, CompuGene, Department of Biochemistry
04/2018 – 06/2018	Specialist internship at the University of Washington
	The Zalatan Lab, Department of Biochemistry, Washington, USA
09/2015 – 11/2015	Working student at Merck Serono, Darmstadt
	Protein Engineering & Antibody Technologies
10/2013 – 04/2014	Working student at Fresenius KABI, Oberursel
	CF Global Sourcing/Transparency & Processes, Pharmaceuticals Division
11/2013	Internship at the Paul-Ehrlich-Institut, Langen
	Molecular Allergology
10/2011 – 09/2013	Scientific support at the Technische Universität Darmstadt
	Working group Buxmann, Department of Business informatics
07/2011 – 08/2011	Internship at the Paul-Ehrlich-Institut, Langen
	Division of Allergology

Education

10/2013 - 01/2016	Technische Universität, Darmstadt
	Degree: Master of Science in Technical Biology (Final grade: 1,13)
	Thesis completed in the working group of Prof. Dr. Kolmar,
	title: "Towards genetic circuits in the yeast S. cerevisiae applying the CRISPR/dCas9"
10/2010 - 07/2013	Technische Universität, Darmstadt
	Degree: Bachelor of Science in Biology (Final grade: 1,55)
	Thesis completed at the Paul-Ehrlich-Institut in Langen,
	title: "Comparative investigation of TLR7-mediated activation of reporter and antigen presenting cells"
09/2001 - 07/2010	Friedrich-Ebert-Gymnasium, Mühlheim
	General university entrance qualification (A-level) (Final grade: 1,5)

9.4. Affirmations

9.4.1. Erklärung zur selbstständigen Bearbeitung der Dissertation

Darmstadt, den ....

Erklärung

Ich erkläre hiermit, dass meine Dissertation selbstständig und nur mit den angegebenen Hilfsmitteln angefertigt wurde. Zudem erkläre ich, dass ich noch keinen Promotionsversuch unternommen habe.

....
(Anja Hofmann)

9.4.2. Erklärung zur Übereinstimmung

Darmstadt, den …………………

Erklärung zur Übereinstimmung

Ich erkläre hiermit, dass die elektronische Version der Doktorarbeit mit der schriftlichen Verion übereinstimmt. Die elektronische Version liegt dem Prüfungssekretariat vor.

…………………………………

(Anja Hofmann)